Symposium on

MATERIALS FOR RADIO-ISOTOPE HEAT SOURCES

Thomas
Harms
Huntoon

Nuclear Metallurgy Committee
Institute of Metals Division
The Metallurgical Society of AIME

NUCLEAR METALLURGY, VOLUME 14

NUCLEAR METALLURGY, VOLUME 14

SYMPOSIUM ON

MATERIALS FOR RADIO-ISOTOPE HEAT SOURCES

Edited by D. E. Thomas,
W. O. Harms,
R. T. Huntoon.

Proceedings of the 1968 Nuclear Metallurgy Symposium held in Gatlinburg, Tennessee on October 2 - 4, 1968.

Sponsored by
Nuclear Metallurgy Committee,
Institute of Metals Division,
The Metallurgical Society,
American Institute of Mining,
Metallurgical, and Petroleum Engineers, Inc.

Hosted by
Oak Ridge National Laboratory

Jack V. Richard, Executive Publisher

345 East 47th Street
New York, New York 10017

Printed in the United States of America.

FOREWORD

The Symposium on Materials for Radioisotope Heat Sources was presented at the Mountain View Hotel and Motor Lodge in Gatlinburg, Tennessee. The symposium, consisting entirely of invited papers, began with a review of both space and terrestrial applications and requirements, followed by papers on properties and fabrication of fuel forms, encapsulation materials and processes, environmental effects, and compatibility effects. The Symposium Chairman was D. E. Thomas, Westinghouse Astronuclear Laboratory; W. O. Harms, Oak Ridge National Laboratory and R. T. Huntoon, Savannah River Laboratory served as co-chairmen. They were assisted in chairing the various sessions by E. Lamb, Oak Ridge National Laboratory and A. J. Clark, Sandia Corporation.

The fifth and last session of the symposium was held at the Oak Ridge National Laboratory on a classified basis, hence these papers are not reproduced in this volume.

THE METALLURGICAL SOCIETY*

Michael Tenenbaum, President
J. Harry Jackson, Past President
Paul Queneau, Vice President
Carleton C. Long, Treasurer
Jack V. Richard, Secretary

INSTITUTE OF METALS DIVISION - NUCLEAR METALLURGY COMMITTEE*

W. F. Sheely, Chairman
J. L. Klein, Past Chairman
James Waber, Vice Chairman
A. N. Holden, Secretary

E. N. Aqua
P. Chiotti
W. O. Harms
K. E. Horton
R. T. Huntoon
H. M. Klepfer
G. A. Last
R. E. Machery
S. Marshall
D. E. Thomas
J. Watson
J. R. Weeks
R. A. Wolfe

CONFERENCE COMMITTEE

D. E. Thomas, Chairman
W. O. Harms, Co-Chairman
R. T. Huntoon, Co-Chairman

CONFERENCE SESSION CHAIRMEN

D. E. Thomas; Applications and Requirements
E. Lamb; Properties and Fabrication of Fuel Forms
W. O. Harms; Encapsulation - Materials and Processes
A. J. Clark; Environmental Effects
R. T. Huntoon; Compatibility of Fuels and Capsule Materials

*Officers at the time of the conference.

TABLE OF CONTENTS

APPLICATIONS OF RADIOISOTOPE SPACE POWER SYSTEMS

Joseph D. Lafleur, Jr.

Abstract

In the 1970's, the National space program will include several categories of missions which will require new technical considerations in the design for on-board supply of electrical power. In several categories, the competitiveness of nuclear power systems depends on new factors relating to the new mission environments involved and the technology that could be available in the coming years. It is essential that power system development objectives be realistic in view of the likely missions and the probable competition. The mission categories are examined, competitive power concepts are compared, and development objectives for various isotopic power systems are derived.

Joseph D. Lafleur, Jr., is the Assistant for Applications and Requirements to the Director of the Atomic Energy Commission's Space Electric Power Office.

APPLICATIONS OF RADIOISOTOPE SPACE POWER SYSTEMS

by

Joseph D. Lafleur, Jr.

PROCEDURE

An analysis of likely applications of radioisotope power systems consists of three main parts: First, a survey must be made of missions being proposed for the future by the agencies which are responsible for conducting missions in space. Second, the characteristics of these likely future missions, and of alternative power systems, must be considered to see what potential benefits might be realized by the use of isotopic power systems. Finally, certain classes of missions must be identified within which there are likely to be enough important applications that power system technology specially suited to the requirements of those classes should be developed. The criteria of these classes of power systems can then be used in the planning of a power systems development program.

MISSION ANALYSIS AND APPLICABLE NUCLEAR CONCEPTS

During 1968, a detailed analysis was made of proposed future missions of the National Aeronautics and Space Administration, the Department of Defense, the Communications Satellite Corporation, and the Environmental Science Service Administration. Project officers and others aware of the importance and special requirements of various missions were consulted wherever the analysis suggested a block of more likely applications.

A catalog of available information on all likely missions has been compiled. These data are being updated as better information is received. The system is capable of retrieving data in various forms, usable in planning and reporting progress.

The use of this approach in a search for firm mission requirements is of limited value, chiefly because of the uncertainty of future mission plans. It is possible, nevertheless, by this procedure to learn much about the classes of missions and the likely power system requirements of each. With this large bank of characteristics of projected missions, a matrix of the type shown in Figure 1 can be filled in, using data current at any given time. The choice of power ranges is explained below. This chart then can be used to show groupings in which (1) isotope opportunities occur, and (2) it is believed such missions will be performed in the national space program. For purposes of power system technology planning, a general appreciation of the existence of likely power requirements in the various boxes of this chart and the performance requirements

of each, are of more value than a current prediction of the exact number of power systems required.

Figure 2 shows the categories of nuclear power systems and technology that appear to be applicable for various power levels. (Ref. 1). The categories range in decade increments from a few watts to 100 kw and above, for all nuclear systems. The dividing lines between these categories are not exact and inflexible. There is considerable power level overlap; however, there are special development problems which characterize each of these ranges. The isotope systems are attractive up to about 10 kw, and reactors are attractive from a few kilowatts up. There is an overlap of these two concepts in the 1-10 kw region.

In the lowest power range, the spacecraft tend to be small, so that the small, self-contained radioisotope-thermoelectric generator (RTG) is indicated. Within this low-power region, fuel cost is a small enough part of the overall mission cost that the currently-available 5 percent thermoelectric efficiency seems to be acceptable. Also, long lifetime is important. For example, if the useful lifetime of a satellite can be doubled by use of an isotopic power system, launch costs required to keep the satellite system operating may be significantly reduced. In this 100-1000 watt category, certain short-lived earth orbit missions have been suggested by the Department of Defense, the use of the cheaper fuel, Po-210 (half-life 138 days), for these missions is possible because of the short mission life. For longer-lived missions (years) at these power levels, or above these power levels, a more economical approach is required than the Pu-238 (half-life 87 years) - one-stage thermoelectric concept. At 5 percent efficiency, fuel costs are large and the fuel loading for one generator becomes a significant percentage of total fuel availability. Therefore, we need technology that promises either cheaper, more readily available fuel, the capability of fuel re-use, or improved efficiency which will allow better utilization of available fuels.

Wherever possible, it is desirable to define system designs which are modular in nature, so that the needs of individual missions can be accommodated without major development in each case. We must try to avoid the expense of developing a new system for each new mission that comes along. At the same time, it is important to recognize that this objective may not always be realizable when unusual mission needs are present and also as technological advances occur. A large part of the current high cost of nuclear power systems results from the requirement to assure that these units can be used safely, regardless of the type of mission aborts or malfunctions that may occur. This factor, coupled with the need for technological advancements to achieve performance goals, requires that extensive qualification testing and analysis be performed in order to obtain flight approval. Much of this expense should be eliminated in future missions if standard, pre-qualified components

and inherently safe fuel forms and heat sources are developed.

In the 1-10 kw range, there are two types of systems that are of interest. For manned missions (or any missions that require radiation-sensitive payloads), Pu-238 fuel will be acceptable if the fuel can be recovered and re-used and if high-efficiency power conversion is available, such as the Brayton or organic Rankine cycle. For unmanned missions, permitting low payload shielding, the SNAP-10A class of zirconium hydride reactors at temperatures of 1000-1300°F with thermoelectric conversion is available.

COMPETITIVE PERFORMANCE FACTORS

The next step in defining development objectives is to analyze the current and anticipated future capabilities of competitive power systems. In this review, many current non-nuclear designs and projections of future capabilities were considered. Often, complete current designs are difficult to use unless all the particulars of the power system design are accounted for. For example, a large part of the weight of a solar cell array may be in the structural substrate on which the individual cells are mounted. However, this substrate may serve also as the skin of the satellite, and it is almost impossible to know what part of the weight of this skin to charge to the solar power system. Additional information on competitive systems is contained in Reference 2. The findings are discussed below under the subjects of lifetime, area (or size), cost, and weight. The general case is examined; then the requirements of various classes of missions are considered.

Although some references are given, much of the data on specific missions and unpublished studies of advanced spacecraft are unsubstantiated in this paper. Some additional references on classified and unclassified missions can be obtained through the author.

AREA CONSIDERATIONS

Figure 3 illustrates certain essential facts relating to the comparison of the sizes of solar cell and radioisotope generators. The curve designated "5% RTG" indicates the specific area, in square feet-per-electrical kilowatt, of any power system operating at a system efficiency of 5%, as a function of effective radiator fin temperature. The dashed lines indicate the specific area of solar arrays today. The solar constant at 1 a.u. (the mean distance between Earth and the sun) is 130 watts per square foot, or about 7.7 square feet per kilowatt. Practical cell efficiencies of 8-11 percent are obtainable today, and when such factors as the blank spaces between cells are accounted for, about 110 square feet electrical kilowatt are usually required for an array while it is oriented directly toward the sun, at 1 a.u. Improvements of 20-30 percent are anticipated during the 1970's; and the specific areas shown could improve roughly by this factor. In low earth

orbit, where about 27 percent of the orbital time is spent in total darkness, the solar array must be enlarged to allow it to produce increased power during the sunlight periods. Practical values to ensure the availability of adequate power for battery charging usually are about twice the 1 a.u., full sunlight area, or as indicated by the middle dashed horrizontal line. Day and night operation of the solar array in synchronous orbit, where there is less shadow time, results in specific areas somewhere between 110 and 200 square feet per average electrical kilowatt. Where the complexity of orienting the solar cells is unacceptable, an all-around array must be mounted. On an ideal spherical shell an increase of a factor of 4 in area would result, indicated by the dashed line at 400 square feet-per-electrical-kilowatt.

It is shown in the following pages that the required dimensions of solar arrays increase with distance from the sun. It is seen that the minimum solar cell arrays are larger than isotopic system radiators, for radiator temperatures above about 350°F. It should be noted also that the solar cell area shown is a planar array; whereas, the nuclear radiator can assume various convenient shapes. The radiator can be wrapped around in a cylindrical shape, for which the frontal area is only $1/\pi$ times the total area. Looking at it from this point of view, it might be more informative to compare the isotopic system area to some solar area between the 1 a.u. full sun and the unoriented solar array cases, depending on whether average effective drag area, solar wind interference area, launch shroud packing volume, or some other limiting factor is involved.

At this point, it is desirable to examine the advisability of increasing radiator temperature in order to reduce radiator area. It might be noted that the "5% RTG" curve is for a system of the indicated heat rejection temperature. The thermoelectric hot junction temperature would depend on other conditions. For example, a system with a 200°F radiator temperature might have an 800°F hot junction temperature; but on the right end of the curve, for the 800°F radiator, the hot junction temperature obviously would have to be higher than 800°F. Otherwise, the Carnot efficiency would be zero and the electrical output would be zero.

We cannot examine the effect of increasing radiator temperature unless we make assumptions about hot junction temperatures and thermoelectric materials efficiencies. However, we can simplify this question by examining only a limited region. We do know that there are several practical generators operating in the 5% efficiency, 200°-400°F radiator temperature region, with hot junction temperatures (T_h) around 1100°F. If such a generator is re-designed (by reducing thermoelectric element length) to keep the 1100°F hot junction temperature and simply reduce the temperature drop through the thermoelectric legs, the system efficiency

can be reduced to 4%. (This assumes a constant thermoelectric material efficiency over the whole temperature drop).

The short curve designated "4% RTG, T_h=1100F" shows the resultant specific area for a generator previously operating in the 200^{o}-300^{o}F radiator temperature region. That same generator, with the shortened legs, will now require more fuel per electrical watt; but because of the better heat transfer from the radiator, radiator area is reduced from about 300 to about 140 square feet per electrical kilowatt. Of course, improvements can also be made by increasing hot junction temperatures, or by improving the power conversion efficiency; but this requires improved technology.

The conclusion is that solar arrays will almost always be larger than radioisotope system radiator areas, and usually much larger in the important area considerations, such as explosed area, frontal area, or packing volume. Also, at a modest sacrifice in other performance factors such as cost, and possibly weight, significant isotopic system area reductions can be achieved, if low area is needed.

These area observations are for solar arrays operating at about 1 a.u., that is, approximately the distance of earth from the sun. As spacecraft go closer to or farther from the sun, the increased or decreased solar energy flux will reduce or increase the size of solar cell arrays required for a given power level. Because of high-temperature operating problems, solar cell performance at Venus (0.72 a.u.) is not very different from that at earth (1 a.u.); although some improvement is to be expected for near-sun missions. Figure 4 illustrates the increase in solar array areas that are required at distances of greater than 1 a.u. This is a simple function of the square of the distance. It is seen that the nominal 100 ft^2 per kw would increase to about 1,000-2,000 ft^2 at Jupiter, and 20,000 ft^2 at Pluto. This effect is augmented by the fact that much of the power need is for communications back to earth. Since radio energy reception intensity also is reduced by the square of the distance, this leads to a fourth power disadvantage factor for solar cell area for communications power from spacecraft, as they go farther from the sun.

SOLAR CELL-BATTERY WEIGHTS

The Minimum Weight Cases - The conditions relating to shadow time, power and orientation, which were discussed under "Area Considerations", are also useful in estimating solar power system weights; although the multiplication factors for weight and area will not be the same. Figure 5 shows the past and projected future progress of solar array weights, in terms of total weight of the structural substrate, frame, cells and cover filters. This weight is based on direct orientation toward the sun at 1 a.u., and does not include orientation devices or expendables, batteries, voltage regulators and other components. The weights of the arrays of the

Ranger, Mariner, and (proposed) Voyager solar cell systems are shown; and the 0.4-lb/ft^2 (approximately 40 lbs per kw) objective of several NASA and DOD development programs is shown as the projection of weight capability for the early 1970's. (References 3, 4). A projection of secondary battery (rechargeable) capability is given in References 4 and 5 as 0.14 lbs/whr for either NiCd (1-3x10^4 cycles) or Ag Cd batteries (about 6,000 cycles) for 1968 and 0.14 for NiCd and 0.10 for Ag Cd in 1975. It is informative to consider the weights of "idealized" typical minimum-weight systems which could be designed using these weight objectives. Later, we will examine real design weights of systems planned for this period. Figure 6 shows these and other typical weights of solar cell-battery systems for the conditions of an oriented array at 1 a.u.; and 40 minutes of shadow per orbit (low earth orbit).

It is seen that for this typical minimum-weight case, complete systems could weigh as little as about 0.23 lbs per electrical watt (ew) today and about 0.17 lbs per ew in 1975. Using the 1975 objective weights of 40 lbs per kw (1 a.u., oriented array, without batteries), assuming no additional structural weights are needed for large arrays, and applying the multiplication factors of Figure 4, this array alone would weigh about 1,040 lbs per kw at Jupiter and about 60,000 lbs per kw at Pluto. Solar cell-battery or solar cell-fuel cell systems for the lunar surface suffer in weight due to the high-temperature daylight conditions and the long (350 hours), cold, lunar night. These will be discussed below. Figure 6 (line D) also shows a rough weight estimate for unoriented arrays plus batteries in low earth orbit. Several developments, now in progress, of "roll-up" or other flexible arrays, could reduce the array weight of these systems a few pounds below the 40 lbs-per-kw mentioned above.

Weight and Radiation Vulnerability - The importance of radiation vulnerability is illustrated in a gross way in Figure 6, line E. In order to increase by a factor of 10 the fluence of trapped electrons in space that the solar cells can endure (for example, in the Van Allen Belts), the equivalent of about 116 mils of transparent fuzed silica must be bonded to the face of the solar cells. This factor of ten may be much too small in many applications, such as for those systems which must withstand environment resulting from a nuclear detonation. Nuclear systems are inherently less vulnerable to radiation damage, by several orders of magnitude. The weights which result if this much silica is added to the arrays of Lines C and D are shown in Line E. Since even this protection would appear to be inadequate for defense satellites, it appears that nuclear systems will provide one important option to spacecraft planners who are concerned about radiation vulnerability. Figure 7 shows weights of several solar cell power systems that have already been launched. This chart was published in Reference

6 and is revised here by inclusion of Mariner 64 data. Specific weights on this table are based on the maximum power produced, and hence would correspond roughly to weights slightly less than Line C, Figure 6. It is seen that most of these real 1969-1970 systems fall between 0.4 and 2.0 lb per electrical watt, on this basis.

This has been an oversimplified treatment of the weight of future solar cell systems. Such simplified description is of course of limited value for specific real space systems. Current and predicted weights of actual systems will be discussed within later treatments of each of the various mission classes.

SOLAR CELL SYSTEM COSTS

A brief survey of solar cell system costs was conducted and is summarized in Figure 8. In this table the total power system development and procurement cost is divided by the number of actual flights to get the cost per flight in millions of dollars. This figure is divided by the average power of the system to get the final line, in dollars per average watt. Several remarks are called for concerning this tabulation:

a. The numbers are rough estimates at best. In each case the reporter believes the costs represent an attempt to allocate power system costs objectively; however, for each project, different accounting systems are used. In many cases, it is impossible to estimate the proper share of NASA in-house costs to charge against the power system. In no case are charges for spacecraft development included. For example, no charge against the Nimbus B system is made for the complications in spacecraft development brought about by the orientation requirements which the solar array places on the craft.

b. It is seen that the earlier models of "custom made" systems incur the largest costs (NIMBUS 1 & 2, Mariner 64). This probably reflects the higher development costs of the first models. Also, as might be expected, the lowest costs occur when a follow-on system is purchased immediately after an earlier unit (Mariner 65) or when several craft are bought of the same design (Lunar Orbiter).

c. No conclusion is possible yet for the manned station systems. The lower figure of the range includes only contract costs, which is only a small percentage of the whole effort.

d. Finally, one important conclusion appears to be warranted, even from such rough data: With Pu-238 at about $12,000 per electrical watt, for 5% efficient thermoelectric systems, it appears that the fuel cost of RTG's alone, will probably be higher than solar cell system costs, unless either (1) some way can be found to reduce isotopic fuel costs, (2) some other important

saving or greater measure of effectiveness of the mission is obtained or (3) some other environment such as the lunar surface or deep planetary space reverses this cost comparison.

Current isotopic system cost estimates assume use of Pu-238 fuel, which is valid for systems of the early 1970's. Beyond 1975, curium-244 fuel may become available as a byproduct of the operation of commercial nuclear power reactors. It appears that Cm-244 may be producible at about $100 per thermal watt, compared to about $600 per thermal watt for Pu-238. It is evident that this cost reduction, plus some increases in efficiency (which would also serve to reduce fuel cost by requiring less fuel per electrical watt), could completely alter this cost comparison during the late 1970's.

COMPETITORS OF VARIOUS MISSION CLASSES

Since the mission environment has such an important effect on solar cell power system characteristics, the competitive performance requirements of each class must be analyzed. The following is a summary of the present and expected future performance capabilities of solar power systems by mission class.

Earth Orbit

Many space systems will continue to be flown in low earth orbit; although applications satellites planners including those of many DOD systems tend to prefer synchronous orbits for operational simplicity and economics. All of the isotope systems launched to date have been for use in low earth orbits. As noted above, because of the fairly high fraction of earth orbit spent in the shadow of the earth and the fact that this sun-shade cycle recurs every 90 minutes or so, a solar array in this orbit must be large enough to supply power for battery charging; and batteries capable of several thousands of charge-discharge cycles per year must be provided. As noted in Figure 6, this leads to 1968 nominal weights of 0.23 (oriented) - 0.65 (unoriented) pounds per watt, plus other components and any additional cover glass desired to reduce vulnerability to radiation in space. It is also noted in Figure 7 that actual practical systems vary in weight from about 0.5-1.6 lbs-per-watt. Figure 9 shows that for some missions this weight range is also applicable to current and expected 1975 solar power systems for manned stations in the 3-10 kw region.

Because of limitations in life expectancy of secondary batteries, a major contribution can be made in power system technology for low earth orbits if isotope systems having a lifetime of several years can be developed. The resulting reduction in launch costs of those missions that have to operate on a continuous basis could

defray a small weight penalty or the costs of the isotopic fuel; however, the cost of long-lived isotopic fuel may be limiting at high power for the early and mid 1970's.

Short-Lived Satellites - A special case is the short-lived satellites for certain possible sattelite missions. Figure 10 includes a brief description of the fuel cell system being developed by the DOD to meet this need as an alternative to solar cells and isotopes. Since this fuel cell system is to attain about 550 watt-hours-per-pound, it will weigh about 1 lb-per-watt for missions which last only 550 hours, or about 23 days. The weight would go up from that value roughly linearly with time, and it is seen that fuel cells become considerably heavier than 1 lb-per-watt for lifetimes greater than about a month. The 1 lb-per-watt weight objective of SNAP 29 corresponds to a combination of the capabilities of fuel cells and solar cells. The cost goals, radiator area, and other SNAP 29 specifications are also based on competitive factors for 3-5 month space missions.

High Orbits - The same factors apply in synchronous or other high earth orbits as in lower orbits except that there is only one period of shadow during each 24-hour period and then only during the days before and after the equinox, with a minimum of about 23 hours of trickle charge for each period. This means the battery goes through only about 100 cycles per year. Although these discharge periods are about twice as long as in low earth orbit, because of the fewer cycles and longer charge periods, deeper discharge is possible, battery weights are lower, and less solar cell area is required for charging. Also, the batteries can be designed to have longer life due to fewer cycles. Figure 10 includes a brief description of a solar cell system similar to the one being used on the DOD "TAC SAT COM" tactical communications satellite, which was launched on February 9, 1969. "Nominal" system weights of the future can be estimated from Figure 6, and would be about like Line C.

Radiation Vulnerability - One of the most difficult factors to assess for the sattelite missions is the desirability of "hardening" spacecraft, especially the DOD satellites, to resist damage by charged particles in the radiation belts around the earth, and possibly in other locations in space. A series of studies of the desirability and feasibility of hardening is now being conducted. Certain DOD and NASA satellites will continue to inhabit a low earth orbit, within the lowest Van Allen Belt. RTG power systems would avoid the fairly high solar cell degradation problem in this environment, and would reduce power system vulnerability to the effects of nuclear weapons events in space. Because of the greater inherent invulnerability of nuclear systems than that of solar cells, a decision by DOD or NASA to demand survivability obviously could significantly increase the relative

attractiveness and the number of likely applications of isotopic power systems. Residual particle flux in synchronous orbit is considerably lower than within the lower Van Allen belts. Unless hardened, satellites in synchronous orbit would be more vulnerable to deliberate nuclear weapons attacks than to Van Allen Belt damage.

Lunar Surface and Orbit

The lunar applications are NASA missions. Nuclear systems enjoy a special advantage on the lunar surface due to the long (350-hour) lunar night (which requires high weights of batteries or rechargeable fuel cells) and the high daylight temperature (which reduce solar cell efficiency). This is the reason for the SNAP 27 requirement for the Apollo Lunar Surface Experiments Package (ALSEP), the follow-on SNAP 27 units for later Apollo missions, and the proposed nuclear-powered Advanced ALSEP missions. An illustration of these solar power system weight effects is given in Figure 10 wherein the weights of a solar cell-rechargeable fuel cell system are shown to be about 2.7 lb-per-watt. A recent paper by Smith and Schulman (Reference 7) indicates 2.0 lbs-per-watt is a good rough weight estimate, for power systems of the kilowatt range. For a few tens of watts, because of the long periods of darkness, non-nuclear systems tend toward daytime power only, probably requiring isotope heaters to keep instruments warm during darkness.

In lunar orbit the distance from the sun is about 1 a.u., and approximately the same weights and areas (sizes) will apply as for earth orbit. If the lunar orbit is at low altitude, almost half the time will be spent in shadow, and the low earth orbit parameters will apply, although the radiation damage problem is low due to the absence of radiation belts.

Planetary

Planetary Vehicles - As spacecraft go farther from the sun than 1 a.u., local solar energy intensity is reduced. As noted above, at Mars, the solar cell area for a given power level is about twice what it is at earth; at Jupiter, 27 times; and at Pluto, 1550 times. Nuclear systems are independent of solar intensity. Solar cell area requirements for missions to the various planets are shown in Figure 4. The result is that even with almost no battery requirements, isotope systems, at 0.8-1.0 lb-per-watt, are lighter than solar cell systems for any locations farther out than about 3-5 a.u. (somewhere between Mars and Jupiter). Several user studies have led to this same conclusion. Figure 11 shows a typical set of tradeoffs for a Jupiter Flyby mission. For a Jupiter spacecraft, which in early flights could have a total of about 50 pounds of scientific instruments, another study has shown that about 50 pounds of power system weight can be saved if an RTG is used instead of solar cells, for a 70-watt capability. In recent meetings, NASA JPL engineers who are planning unmanned flights to planets beyond Jupiter, including

the "Grand Tour" of four planets in 1976, indicated an isotopic power system would be required for these missions. The toughest development requirement for the spacecraft of these missions is probably the long-life reliability requirement. Mission times of 8-12 years are required for the Grand Tour, for example. Verification of such long-life capability must be started as soon as possible in order to get useful endurance data by the mid 1970's launch dates. This schedule is especially critical because of the unusually favorable alignment of planets for the Grand Tour launches in the 1976-1979 period. This favorable alignment will not reoccur for 176 years.

Planetary Landers - NASA plans show several planetary "probes" and "landers" starting about the mid-1970's. Probes are small instrument packages which enter the atmosphere of a planet and do not survive atmospheric heating; whereas, landers are packages which continue to send data on planet surface conditions after landing intact. The earliest landers will be primary battery-powered, operating for only a few hours after landing. Solar cell weights estimated using the above guides are not accurate due to differing atmospheric conditions and durations of days on various planets and the problems of packaging solar systems to survive re-entry. A critical factor is the capability of the entire lander package to be sterilized without damage to essential functions. Since isotopic systems operate well above sterilization temperatures, no difficulties with isotopic power systems are foreseen in this regard. A critical development problem will be the long-life reliability required for the period of travel from the earth to the planet to be visited. As with planetary vehicle power, long-life demonstration will be required, and should be undertaken as early as possible.

CONCLUSIONS

Missions

Figure 12 presents a summary of classes of missions considered to be likely to require isotopic power sources during the next 10-15 years. The remarks column includes a brief statement of key mission factors stated in the preceeding sections.

The Navy Navigation satellite is the stated requirement of the Department of Defense. The unmanned satellites class includes operational defense missions in the 1970's. Many of these satellites would operate in synchronous orbits. Cost effectiveness on a multiple launch basis would be an important factor in power system selection; cost competitiveness would be achievable if a lower-cost RTG or isotope thermionic generator were developed, or if important savings due to longer life of isotope systems were involved. If DOD decides to make its satellites as invulnerable as possible to nuclear weapons effects,

the relative invulnerability of nuclear systems could be the essential element in power systems selection. For NASA Planetary missions, nuclear systems are clearly superior for all locations farther from the sun than 3-5 a.u. This includes missions to Jupiter and all the planets farther out than Jupiter. In view of the fact that there is no alternative to nuclear power for these missions, and they will require higher power than now available, it is clear that nuclear systems must be developed to meet this need. The number of planetary missions shown is based on judgement and on the launch rate experience of the last few years. The Planetary Landers have a somewhat different class of problems. Based on discussions with NASA project personnel, past experience with the planetary program, and forecasts in NASA planning documents it appears that the program will include lander instrument packages some of which would be "hard landers" and some "soft". Because of uncertainties about the planetary surface condition and because of the inhospitability of these conditions to solar cells, isotope systems will be required for almost any lander packages designed to operate more than a few hours after landing. The comparison to solar cell-battery systems is at least as favorable on the planetary surface as in space in the vicinity of the planet. Because of the shadow time effects and the hostility and unknowns of the atmospheres, the use of isotopic systems in long-life missions of this category is almost certain, if the development of the isotopic system is accomplished.

The Short-Lived Unmanned missions are the class for which the SNAP 29 is being developed. Specifications are similar to SNAP 29 specifications. The Lunar Surface missions will need isotopic systems in order to provide continuous power at any reasonable weight. NASA received 5 SNAP 27 units (each 66 watts) by the end of CY 1968. A new 500-watt system to power manned and unmanned roving vehicles, and possibly more unmanned scientific packages will be required if lunar exploration is seriously pursued. As noted above, it appears that isotope-dynamic systems will be advantageous for manned stations. Either military or NASA manned stations during the mid-1970's could use an isotopic system which meets the specifications set up by NASA for the isotope-Brayton power system.

These are the apparent isotopic system requirements. Others will arise as new missions or mission modifications are planned.

Development Objectives

Based on the above considerations, the following should be the goals of the technology program of each of the isotopic power categories listed (Figure 13):

0-100 watts - In this power range, it appears that a modular system meeting the specifications of the DOD Navigational Satellite would find uses in earth orbit and planetary vehicles in the early 1970's. As a longer-range technology objective, it appears that a specific weight of 0.25 lb-per-watt would break into the range of capability of solar cell-battery systems in synchronous orbit. This capability would clearly meet the needs of many DOD and NASA satellites of the mid-1970's, especially if invulnerability to nuclear weapons were to become an important criterion.

100-1000 watts - For 90-150 day missions, the SNAP 29 specifications will be valid during the 1970's; the objective of the SNAP 29 program is to demonstrate on the ground a generator capable of meeting these specifications. Long-life missions seem to consist of two sub-categories. Those that will require cheap fuel in order to be attractive, and those that will probably be attractive to users even using Pu-238 and 5-percent-efficient thermoelectrics. Because of the pressing need of the planetary missions, a multi-hundred watt modular system using Pu-238 and thermoelectric power conversion should be developed as soon as possible. An early start is necessary in order to demonstrate system lifetime capability on a schedule needed by NASA. It appears that 0.5-1.0 lb-per-watt is an acceptable specific weight. For the long range, however, greater economy is needed; and, as an advanced technology goal, the capability to produce cheaper systems must be developed. Invulnerability to nuclear weapons, a specific weight of 0.25 lb-per-watt, and a 5-year lifetime should be developed.

1-10 kw - For those missions requiring manned shielding, the development of a large isotope heat source to power the NASA isotope-Brayton cycle system with a system weight of 0.5-1.0 lb-per-watt is needed — especially for missions which will allow recovery and re-use of the Pu-238 fuel. The high efficiency of the Rankine or Brayton cycle will be needed to reduce fuel inventory and to achieve these weight objectives. For unmanned systems, it is possible that a reusable-fuel scheme cannot be accepted. Isotope systems are in competition with reactor thermoelectric systems, in these missions. However, it is possible that a cheap fuel such as Cm-244, Co-60 or Sr-90 may prove to be useful, if a 0.5-1.0 lb-per-watt technology can be demonstrated.

REFERENCES

1. Milton Klein, Director, Space Nuclear Systems, AEC, in testimony before the Committee on Aeronautical and Space Sciences, U. S. Senate, April 1968.

2. "Radioisotopes, Production and Development of Large Scale Uses," WASH 1095, U. S. Atomic Energy Commission, 1968. Available through Supt. of Documents, U. S. Government, Washington, D. C.

3. DOD Space Power Study, LMSC-B095176, Final Technical Brochure, Contract AF 04 (695)-954, Lockheed Missiles and Space Co., Sept. 1966.

4. W. H. Woodward, Director, NASA Division of Nuclear Power and Electrical Propulsion, in private communications.

5. Solar Cell Modules and Charges/Battery/Regulatory Modules, Preliminary Design, MSFC-R-ASTR-EP, 3/6/67.

6. Szego, George, Space Power Systems State of the Art, AIAA Paper No. 64-525, First AIAA Annual Meeting, June 29-July 2, 1964, Wash. D. C.

7. Schulman, F., and Smith, AH, Lunar Power Systems, AIAA Paper # 67-902, AIAA Annual Meeting, Anaheim California, October 1967.

8. Harootyan, L., Wright Patterson AFB, Private communication, Feb. 3, 1969.

Figure 1

POSSIBLE ISOTOPIC POWER REQUIREMENTS

Category	Low Earth	Synch	Lunar	Planetary	Planetary Lander
1. 1-100 w					
2. 100 w-1 kw					
a. 3-5 mos					
b. years					
(1) Pu-238					
(2) Low-Cost					
3. 1-10 kw					
a. Pu-238					
b. Low-Cost					

FIGURE 2

CATEGORIES OF NUCLEAR SYSTEMS AND TECHNOLOGY

CATEGORY	SYSTEM CHARACTERISTICS	ESTABLISHED SYSTEMS	PRINCIPAL TECHNOLOGY GOALS
0-100 W	Self-Contained Isotope-Thermo-Electric (TE)	SNAP 3A, 9A, 19, 27	Increase Fuel and Capsule Temperature
100-1000 W	Modular Isotope TE		
a. Short Life (2-5 Mos.)	Short Half-Life	--	Increase Power Conversion Efficiency
b. Long-Life	Reusable Fuel and or Higher Efficiency Power Conversion		Increase TE Life
1-10 KW			
a. Recoverable Fuel	Modular, Reusable Isotopes and High-Efficiency Power Conversion	--	Reduce Power Conversion System Weight
b. Unrecovered Fuel, Unmanned	Partly Shielded Reactor	SNAP 10A	Develop Higher Temperature to Reduce Specific Weight and Radiator Area
10-100 KW	Reactor-TE (10-25 KW)	--	
	Reactor-Rankine (25-100 KW)		Develop More Efficient Power Conversion
100 KW AND ABOVE	Reactor-Thermionic or Reactor Rankine	--	Increase Power Conversion System Life

FIGURE 3

AREA OF POWER SYSTEMS, 1968

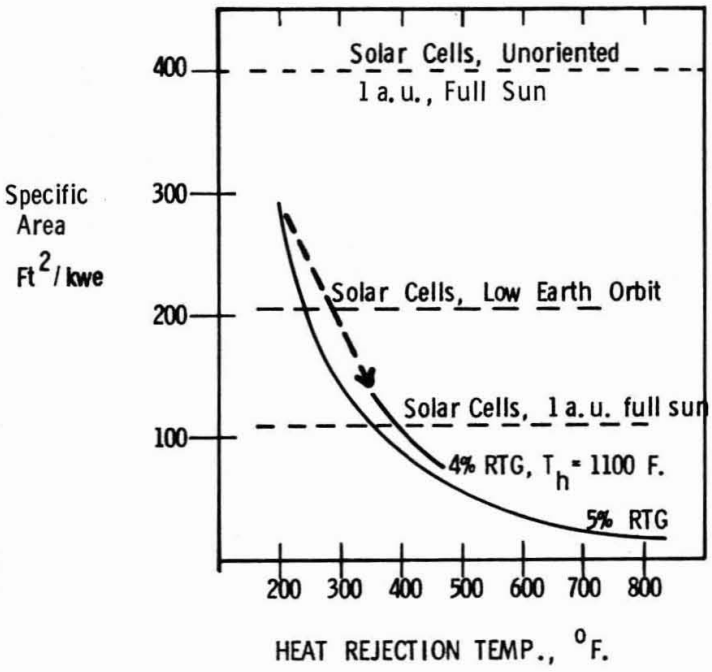

FIGURE 4

SOLAR CELL AREA AS A FUNCTION OF DISTANCE FROM THE SUN (FULL SUNLIGHT)

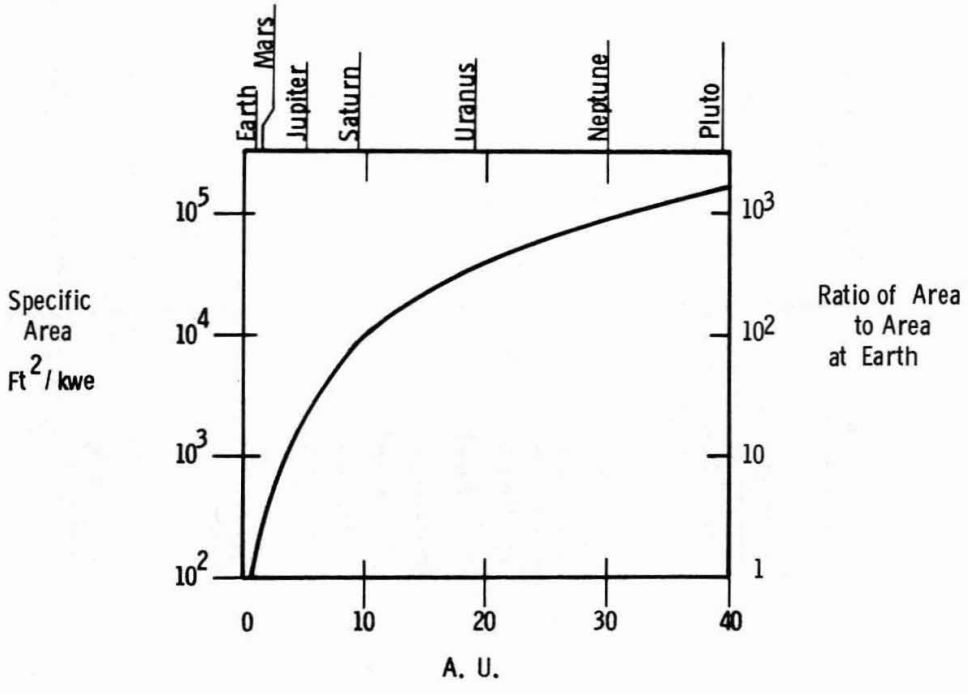

FIGURE 5

SOLAR CELL WEIGHT PROJECTION
FULL SUN, ORIENTED, 1 a. u.

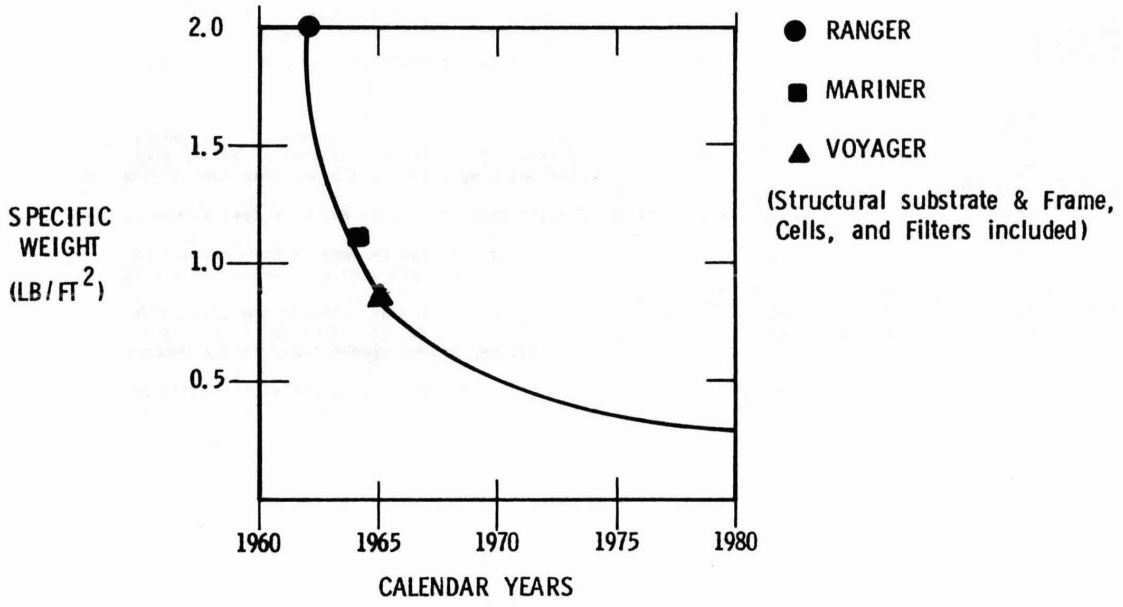

FIGURE 6

WEIGHT OF EARTH ORBIT SOLAR CELL-BATTERY SYSTEMS

Application Case	1968	1975
A. Arrays, including structural assembly, cells and minimum filters-lbs/ew (In full sun) (1)	.07	.04
B. Secondary batteries, usable energy density (2,3)		
NiCd (1-3x10^4 cycles) lb/whr	.14	.14
Ag Cd (~6,000 cycles) lb/whr	.14	.10
C. At 1 a.u., array plus batteries for 40 minutes shadow, several years, lb/ew	.23	.17
D. If unoriented, 8X array wt + 40 minutes battery, lb/ew	.65	.37
E. Weight including cover glass to reduce radiation belt damage by factor of 10 (116 mils silica) lb/ew (4) Case C above	.5	.4
Case D above	1.5	1.4

(1) LMSC-B095176 and several current arrays

(2) Solar Cell & Modular & Change/Battery/Regulator Modules, Prelim. Design, MSFC-R-ASTR-EP, 3/6/67; AI chart 66-8162-73-7.

(3) W. H. Woodward Presentation to Space Council Staff, Fall, 1967.

(4) Lafleur Memo, 3/16/67, Survivability of Solar Cells in Radiation Fields

FIGURE 7

SPACECRAFT SOLAR POWER SYSTEM CHARACTERISTICS

	Nimbus B	OSO 1	OAO	UK-1	Explorer XIV	IMP A	Relay 1	Mariner IV b
Orientation a	0	0	NO	NO	NO	NO	NO	0
Cell Mounting	Panels	Panels	Paddles	Paddles	Paddles	Paddles	Body	Panels
Max. Power Watts	470	31	980	11.7	34.7	74.3	35	325
Array lb/watt	0.17	0.17	0.28	0.77	0.38	0.36	0.71	0.23
Storage lb/watt	0.24	1.0	0.17	1.2	.18	0.09	0.8	--
Array ft^2/watt	0.1	.13	0.24	0.9	0.43	0.38	0.5	0.22
System lb/watt	0.4	1.1	0.45	2.0	0.56	0.45	1.7	0.27
Array Effic. %	7.5	5.9	8.8	0.8	1.8	2.0	1.5	7.5

[a] "O" oriented - "NO" oriented

[b] at Mars

Figure 8 Solar Cell-Battery System Costs

	Actual Mariner			Actual Nimbus			Actual	Estimated (1970's)
	1964 Mars	1965 Venus	1969 Mars	1 & 2	B	D	Lunar Orbiter	Manned Station
Cost Per Flight (Unit (10^6)	7.0	1.01	3.0	6.3	2.4	1.0	1.36	
Average Power (watts at 1 a.u.)	700	700	700	225	225	225	380	
No. of Flight Units	1	1	2	2	1	1	5	
No. of Spares	1	1 3/4	1	1	1	1	6	
Other Test Sub-System Included	Yes	No	Yes	Yes	Yes	Yes	Yes	
Unit Cost for Flight ($/avg watt)	10,000	1,440	4,280	28,000	10,700	4,440	3,680	1,000-10,000

Figure 9
Solar Cell-Battery Systems Being Designed for Manned Stations

	Advanced RCA	ATM System (Ref. 5)
Weight, lbs.		
Array	1393	1766
Boom, etc. & Orientation Apparatus	164	2000
Batteries	2178	1234
Electronics	1005	2226
Propellant to Overcome Drag	1868	--
Total Weight	6608	7226*
Specific Weight, lbs/Kwe avg	940	1900*
Cell Efficiency, percent	10.5	10
Cover glass thickness, mils of fused silica	6	20
Batteries		
Watts hrs/pound	353	
Type	NiCd	NiCd
Depth of Discharge	0.50	0.25
Costs to develop, millions of dollars	33.8	
Cost per additional copy	9.3	
Array area, ft^2	1720	
Specific area ft^2 Kwe avg	245	240
Orbit Altitude, nm	200	260
Lifetime yrs	1	1
Output, kw avg	about 7.1	3.48

* Weight does not include propellant to overcome drag.

Figure 10

TYPICAL SYNCHRONOUS ORBIT SOLAR ARRAY

Geometry - right cylinder

Substrate Weight	175 lbs.
Solar Cells Weight	100 lbs.
Total	275 lbs.

Battery Weight

If no operation during 80 hrs/year of darkness required - 52 lbs. For full, 3-yr operation, 24 hrs per day - 400 lbs.

Area of cylinder - 300 ft^2

Power Level BOL - 910 ew

EOL (3 yrs) 800 ew

The full weight of the substrate should not be charged to the power system, since it serves as the skin of the satellite.

Based on report in journals. 5/6/68

AIR FORCE DEVELOPMENTAL UNMANNED FUEL CELL

Power, nominal	500 watts
Energy	750 kwh
System Energy Density	545 whr/lb
Operating Life	60 days

Weight Breakdown:

4 cells	140 lbs.
H_2+O_2	675 lbs.
Plumbing	10 lbs.
Tanks	550 lbs.
Total	1375 lbs.

Based on discussions with project officers, 2/3/69 (Ref. 8)

LUNAR SURFACE SOLAR CELL-FUEL CELL SYSTEM
Specific Weights for 5.5 kwe Avg.

Electrolysis Dry	Sp.Wt. -	1.16 lb/w
Solar Array	Sp.Wt. -	0.75
Fuel Cell	Sp.Wt. -	0.30
Reactant	Sp.Wt. -	0.46
Total (1-yr.)	Sp.Wt. -	2.67 lb/w

Based on Prelin Report, Contract NAS8-21190, Sept. 1967

Figure 11

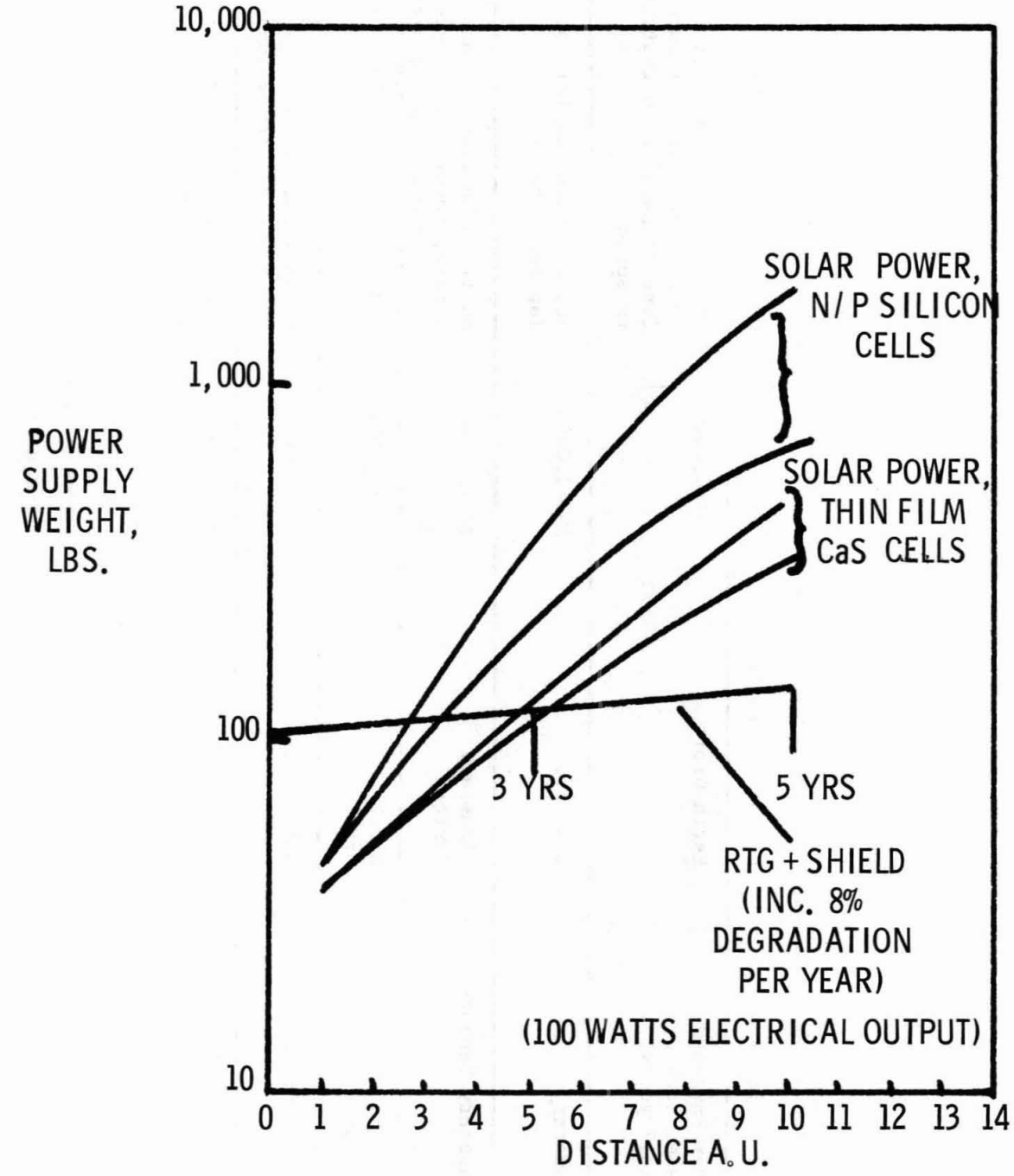

POWER SUPPLY WEIGHT vs DISTANCE FROM THE SUN,

JUPITER MISSION

Figure 12

LIKELY ISOTOPE ELECTRIC POWER MISSIONS OF THE 1970's

MISSION	ENVIRONMENT	POWER	REMARKS
Navy Navigation	Low Earth Orbit	20 w	Development in progress
Other Unmanned Satellites (1-12 years)	Earth Orbit	100-2,000w	Competitive weight difficult to achieve. Nuclear much less vulnerable to radiation in space.
Planetary	3-40 a.u.	100-1,000w	Nuclear much lighter for Jupiter & beyond
Planetary Landers	Planetary Surface	20-1,000w	Surfaces hostile to solar arrays; uncertain. Rugged, sun-independent power needed.
Unmanned Satellites (90-150 days)	Earth Orbit	400-1,000w	SNAP 29 under development
Lunar Surface	350-hr Night	65-1,000w	Nuclear much lighter if day and night power needed
Manned Stations	Low Earth Orbit	5.5-25kw	Design studies show nuclear lighter and solar power impractical; fuel cells too heavy for long life.

Figure 1 3 Isotopic System Development Objectives

0-100 Watts

By 1970 - NAVSAT System Objectives
By 1975 - 1. Reduce weight to 0.25 lb-per-watt
2. Increase lifetime to 11 years

100 w-1 kw

90 day Life - SNAP 29 System Objectives

Long-Life Planetary and Other High Priority (By 1974)

1. Demonstrate long-life capability of 5% Pu-238, TE system.
2. 0.5-1.0 lb-per-watt weight OK.

Long-Life Earth Orbit (By early 1970's)

1. Demonstrate radiation invulnerability
2. Demonstrate 5-year lifetime
3. Reduce weight to 0.25 lb-per-watt
4. Develop lower fuel costs

1-10 Kw (Long Life)

Recoverable Fuel, Pu-238

1. Develop Large Heat Source for Isotope-Brayton
2. Demonstrate 0.5-1.0 lb-per-watt

Unmanned, Unreusable Fuel

1. Develop cheap fuel cycle
2. Demonstrate 0.5-1.0 lb-per-watt

TERRESTRIAL ISOTOPE POWER SYSTEMS IN PERSPECTIVE

Stanley J. Seiken[1]
CDR. William A. Bair, CEC, USN[2]

Paper investigates history, present status and projected future of terrestrial isotopic power sources for energy ranges from microwatts to kilowatts. Current and potential applications, along with economic considerations, of these interesting power sources are discussed. British and Russian efforts in the field of terrestrial isotopic power sources are briefly mentioned. The Atomic Energy Commission's basic developmental precepts and program philosophy are defined, and the relative priorities of technological effort are identified. Paper summarizes areas of technological weakness, and suggests that public and official acceptance of widespread deployment of radioisotope power sources may require careful control and international regulation.

1. Branch Chief (Acting), Isotopic Auxiliary Power
Division of Reactor Development and Technology
U. S. Atomic Energy Commission
Washington, D. C.

2. Project Engineer, Isotopic Auxiliary Power
Division of Reactor Development and Technology
U. S. Atomic Energy Commission
Washington, D. C.

Terrestrial Isotope Power Systems in Perspective

A. Introduction

The purpose of this paper is to present for your consideration, the historical highlights of terrestrial isotopic power system development; current and planned program activities; technological objectives; and an assessment of problem areas--present and projected. In addition, I shall attempt to cover such related subjects as the economics of radioisotope power sources in regard to specific applications in an oceanographic environment; current and predicted uses for these unique power producing devices; safety considerations; various comparative and competitive electrical conversion systems; government and industrial participation in both technological and financial contributions to the "state-of-the-art"; and lastly my assessment of the future of radioisotopic power systems in both the short and long term outlook.

B. Background

Nuclear power became a reality on December 2, 1942, when the first self-perpetuating chain reaction occurred in a squash court beneath the stands of Stagg Field on the campus of the University of Chicago. This date is memorable for yet another reason since it represents, for the first time, a capability not only for the release of large amounts of energy in a controllable form, but also marks the beginning of a capacity for large scale production of radioisotopes. I am certain that Dr. Fermi at that time did not recognize the full significance of this second benefit of his experiment.

As the field of nuclear knowledge advanced, two factors concerning radioisotope production utilizing a nuclear reactor source became apparent. The first of these was the realization that the fission fragment debris from split uranium atoms contained some fascinating properties; secondly, that entirely new radioisotopes (and for that matter, new elements) could be produced in quantity by irradiating target materials in a reactor.

In time, fission fragments were chemically separated from spent reactor fuel, their radioactive properties and relative quantities catalogued. In common with any industrial enterprise, it was only natural that someone was soon at work investigating ways to utilize the interesting by-products of the main reactor endeavor. It was shortly recognized that certain isotopes--both the "refuse" from the fission reaction, and specific isotopes produced by irradiation had just the right combination of power density, favorable half-lifes, and chemical properties to provide a long lived, low weight, reliable heat source whose energy could be ultimately converted power. In 1956, the Atomic Energy Commission began the development of a series of these isotopic power source generators for space and terrestrial uses.

On January 16, 1959, a device that transformed the heat from radioactivity into electricity was demonstrated publicly for the first time on the desk of the President of the United States. The device was the size of a grapefruit. It weighed four pounds and was capable of delivering 11,600 watt-hours of electricity for about 280 days. This is equivalent to the energy produced by nearly 700 pounds of nickel-cadmium batteries. It was fueled with Polonium-210, and was designated SNAP-3.*

The feasibility of reliable low power, unattended, isotopic power sources was demonstrated in August of 1961 when a radio-isotope powered weather station was installed on Canada's remote Axel Heiberg Island--only 700 miles from the North Pole. The test, which ran for two years, was completely successful.

The follow-on program to the SNAP-3 and the Axel Heiberg unit was the SNAP-7 series of thermoelectric generators. This program, again highly successful, culminated in the production of three (3) 60-watt devices (SNAP's 7B, D, and F), two (2) 10-watt power sources, (SNAP-7A and C) and one 7.5 watt ocean bottom beacon (SNAP-7E). All of the SNAP-7 isotopic powered thermo-electric devices utilized strontium-90 titanate as a fuel source. With the exceptions of SNAP-7A (10 watt) and SNAP-7F (60 watt) which were removed from service, disassembled, and inspected after failures in the thermoelectric power conversion systems, the remainder of the devices are still undergoing actual operational testing under adverse encironmental conditions. (See Figure 1.)

SNAP-7B (a 60-watt device) powered an unattended fixed light station for the U. S. Coast Guard in Baltimore Harbor from 1963-1966. In 1966 it was transferred to an oil platform operated by the Phillips Petroleum Company in the Gulf of Mexico. SNAP-7B there replaced SNAP-7F which had been operating from this same platform powering a fixed navigational light station since 1965. SNAP-7B continues to operate this facility at present.

SNAP-7C has been powering an unattended weather station on Minna Bluff, Antarctica, since February 1962. Minna Bluff is located only 700 miles from the South Pole. SNAP-7C will be returned to the U. S. in early 1969, be refurbished, and placed in the Smithsonian Institute.

SNAP-7D is mounted on a floating barge moored in the Gulf of Mexico. This device, a part of the Navy's NOMAD (Navy Oceanographic and Meteorological Automatic Device) system, powers an

* Systems for Nuclear Auxiliary Power. Models fueled with radio-isotopes are designated with odd numbers; those with small nuclear reactors are designated with even numbers.

unattended weather station and a navigational beacon. It was placed in service during January 1964 and continues to operate in a satisfactory manner despite having weathered two major hurricanes with no adverse effects.

SNAP-7E, a 7.5 watt device is a unique thermoelectric generator that has been operating in 15,000 feet of water in the Atlantic Ocean some 750 miles east of Jacksonville, Florida. Its purpose is to power an experimental underwater navigational beacon. It has operated without interruption or repair since July of 1964.

In this brief historical development, I should be remiss if I did not mention that the British Atomic Energy Research Establishment (AERE) has been quite active in the development of their RIPPLE* generators. The British began serious development of their radioisotopic power sources in about 1963 (some seven years after the first AEC efforts) and to date have produced ten devices that range in power output from a few milliwatts to about two watts. Three of these devices (RIPPLES V, VI, and VII), installed in 1967, are currently being evaluated as sources of power for navigational lights in Sweden, Denmark, and off the Kent Coast of the United Kingdom. Two additional units are under construction, RIPPLE IV, a 2-watt generator will power a transistorized submerged telecommunication repeater, and RIPPLE IX, a 6-watt device will be evaluated as civil aviation radio beacon installation in the outer Hebrides Islands. In addition, a series of RIPPLE X generators of a power range of 8 - 50 watts are currently under development by the AERE. All RIPPLE generators are fueled with strontium-90 titanate, and employ direct thermoelectric conversion. Operating periods of five years are anticipated, with the RIPPLE X series planned for a 5 - 10 years expected lifetime.

The Russian endeavors in the field of terrestrial isotopic power generator development are not well publicized. Occasionally, a news release will be issued indicating that some developmental effort is being expended but the amounts of information provided is terse and usually explained in relatively unsophisticated language. For example, last May 20, the Prague CTK International Service, under a Moscow dateline, announced that a 1-watt, thermoelectric generator fueled with Pu-238 had been developed as a power source for experimental laboratory instruments. Unattended life expectancy was stated as 10 years. It was called a "small table atomic power station." Details of construction and design were not provided. About all we can say is that the Russians are working in this field, but we cannot say to what extent--nor can we measure their relative progress.

* RIPPLE (Radio Isotope Powered Prolonged Life Equipment.)

Thus far, I've considered only AEC effort on devices in the low watt range to about 60 watts electrical output. I should also mention that some work and developmental effort in the milliwatt range has been conducted. The SNAP-15A and -15C programs were initiated by the AEC to provide reliable, long-lived prototype power sources for specialized weapons and communications applications. These classified programs, at present largely completed, have yielded considerable technical information that has been added to the unclassified literature. SNAPs-15A and -15C utilized Pu-238 as a fuel and employed direct thermoelectric conversion.

The relative success of the SNAP-7 program--with appropriate additional technical and engineering inputs from the space isotopic power programs, plus technological advancements in material sciences, resulted in an important change in the Atomic Energy Commission's terrestrial isotopic power source program philosophy. The early systems (developed as "proof-of-principle" devices) demonstrated conclusively that isotopic power sources have the capability for unattended, safe operation for long periods of time under environmental extremes. The early developmental effort, however, also highlighted those areas where significant technological advancements were still required. In addition, the wide variety of potential applications of radioisotope power sources that became immediately apparent indicated to the Atomic Energy Commission that the power sources should be further developed--independent of any one specific application or requirement.

This rationale resulted in a plan of continuous assessment of potential needs in order that meaningful design and performance criteria could be established. Utilizing this broad approach, we would then be in a position to initiate development of families of all purpose power devices, within a number of discrete output levels, that would have maximum potential applications. We would likewise then be able to direct out R&D efforts toward the attainment of a technological base that is readily adaptable to this large number of potential applications. Further extensions of the "state-of-the-art" for specific applications and unusual environmental conditions, beyond this broad technological base, could easily be accomplished in a straight forward engineering manner.

With the above program philosophy in mind, the AEC in 1966 began developmental consideration of four families of terrestrial (and oceanographic) isotopic power sources--roughly two-three orders of magnitude apart in energy output levels. The incremental output steps began at the hundreds of micro-watt level and extended to the 1-10 kw range. It is to be noted that the overall power output levels span some 8 orders of magnitude and are designed for wide divergence of potential applications and environmental extremes and, of course, the problems associated with each family of devices are not capable of direct scaling from one level to

another. This scaling anomaly is due to nonlinear physical property characteristics of materials, efficiency of conversion techniques, and safety considerations.

It was therefore determined that future R&D effort should be expended in three general areas. (Figure (2))

1. Immediate initiation of prototype development.

2. Conceptual and parametric studies, and

3. Supporting technology.

Development priority and level of financial support accorded to each catagory was dependent upon both status of technology and timing of application requirements.

I should like to emphasize again that the efforts of the space isotopic power source programs are closely followed. Space application problems are different (e.g., stringent weight limitations, more sophisticated heat rejection mechanisms and lower sink temperatures, higher shock and vibration levels, launch and reentry safety problems, etc.); however, there are sufficient similarities that cross-fertilization of ideas and concepts in several common areas of interest warrant close liaison (e.g.,, insulation system development, thermoelectric material technology, dynamic conversion system improvements, and device safety considerations when in a terrestrial environment). In addition, certain related studies and developmental work have been independently financed by industry and other governmental agencies. This data has significantly added to our storehouse of knowledge. All these factors are considered as inputs to the overall terrestrial isotopic power developmental effort.

C. Present Status

1. Active Developmental Effort

This now brings us to our present status of technology and development. Let me first begin with a brief discussion of those isotopic power sources that are undergoing active prototype hardware development.

a. Microwatt

A microwatt, Pu-238 fueled, thermoelectric device intended for use as a surgically implantable cardiac pacemaker has been undergoing active development since FY-1967. While the R&D effort for this power range has been concentrated on the Pacemaker, the basic engineering concept is expected to provide important data for other biomedical stimulation applications.

The design of this isotopic-powered Pacemaker, as shown in Figure (3), incorporates metallic thermocouple wire interwoven into a glass tape. The tape is spirally wound about a heavy encapsulated Pu-238 heat source which provides a temperature differential of 360°F across the thermocouples. Titanium-zirconium foils are used to thermally insulate the heat source from the other case. Power from the generator is 162 microwatts. Effort to date has resulted in the development of an electrical "proof-of-principle" mockup that has (1) demonstrated the fabrication and complex assembly techniques and (2) verified electrical design characteristics of the thermopile. Heavy R&D effort is presently being concentrated upon (1) minimizing total fuel inventory necessary to reduce external radiation to medically acceptable levels; (2) developing efficient heat rejection techniques and (3) selection of electronic components of proven reliability to assure attainment of the 10-year minimum operating lifetime objective. The basic R&D phase of this program will be completed in the fall of 1969. Subsequent effort will involve an extensive fabrication and statistical test effort, and will include animal "in-vivo" testing.

b. 10-100 Watt Power Levels

R&D effort in this power range class has been centered in the development of two, "second generation" devices-- the SNAP-21, underseas power system, and the SNAP-23A, remote terrestrial power source. These isotopic power generators are currently developed to the point where experimental electrically heated mockup systems have been fabricated, subcomponents tested, and prototype design either recently completed or in process. It is planned that these devices will possess the required reliability, operating lifetime and economic advantages necessary to insure widespread applicability in marine and remote terrestrial environments.

(1) SNAP-21

SNAP-21 is a 2-phase project to develop a series of compact strontium-90 power systems for deep-sea and ocean-bottom application. The first phase design and component development effort on the basic 10-watt system has been successfully completed. A second phase systems development and test effort has been underway since July 1966 and will extend through 1970. The 3M Company has primary responsibility for both project phases. A series of 10 and 20 watt fueled prototype power systems will be fabricated, assembled and environmentally tested to demonstrate attainment of all performance objectives. Commonality of material, components and design is a major objective.

The design of the SNAP-21 system 10-watt device is illustrated in Figure (4). The 10-watt unit contains a single pellet (33,000 curies) of strontium titanate encased in a Hastelloy-C fuel capsule. This heavy-walled capsule is designed to contain the fuel under all operational and credible accident conditions and as such represents an important safety design feature. Biological shielding is accomplished by use of a depleted uranium-8 w/o Mo shield. This heat source assembly (capsule and shield) is insulated by a high vacuum (10 microns) insulation canister consisting of numerous thin metal reflective foils interspaced with fibrous spacers. Test data of the prototype vacuum insulation canister have verified thermal design requirements. Heat loss through the insulation canister measured 12 watts excluding structural support losses. The heat source assembly is supported within the insulation canister by means of a Hastelloy X neck tube coupled with a bottom mounted spider-tension rod assembly.

Heat is conducted from the heat source assembly into a hermetically sealed thermoelectric converter. This converter contains 48 segmented PbTe couples operating at a hot junction temperature of approximately 1100°F. Initial conversion efficiency of the prototype converters measured close to 8 percent. Heat is rejected through spring loaded beryllium oxide followers and a copper cold frame. A spring loaded segmenting ring serves as a converter mounting plate and heat transfer path to the BeCu pressure vessel. A solid state power conditioner provides for specified voltage output and regulation.

A summary of SNAP-21 characteristics is shown in Figure (5) together with schedule information. Although we are pleased with initial SNAP-21 data it should be emphasized that there are several important problems yet to be resolved particularly concerning dynamic capability, materials compatibility and long-term stability.

(2) SNAP-23A

The SNAP-23 project involves the development of a series of economically-attractive strontium-90 power systems for remote terrestrial application. This project will result in the fabrication of 25, 60 and 100 watt units, and is being jointly managed by Westinghouse and 3M Company; Westinghouse being responsible for the systems development and 3M responsible for the thermoelectric converter.

The 60-watt SNAP-23 system currently under development is illustrated in Figure (6).

The heat source assembly consists of a single Hastelloy C fuel capsule containing strontium-titinate fuel pellets, a tantalum diffusion barrier, a radiation shield of Uranium-8 w/o Mo, a copper heat accumulator and a heat source jacket. The hermetically sealed heat source jacket, protects the copper from oxidation. Thermal energy from the heat accumulator is conducted to the 252 couple thermoelectric converter at a temperature of 1100°F. The heat source, converter, radiator, and power conditioner form an integral structure with the removable thermoelectric converter bolted to the heat source. A thin mica sleeve is fitted over the heat source stud at the stud-converter interface to avoid binding and galling of the mating parts during converter removal.

The heat source is supported in the downward vertical and horizontal directions by a steel insulation can which forms the inner surface of the insulation assembly. Upward vertical support is accomplished by a stainless steel retaining ring which bolts to the container. The insulation can is positioned by an eight-legged truss system fastened between the can and the container. The truss system is sized to accommodate dynamic loads of 5 g's, over and above any static loading. The insulation assembly contains Min-K 2000 filled with krypton gas at a pressure of 0.9 atmosphere.

An insulating cap of Min-K 2000 covers the heat source between the converter and the insulation assembly. Heat loss from the heat source stud is minimized by an insulating plug of Min-K 200 which fits into the top of the converter hot frame. Waste heat from the converter is dissipated to ambient air by a finned radiator which also acts to support the power conditioner.

In the design of an unattended power supply with a long operating lifetime such as SNAP-23, the underlying consideration must be reliability. In view of the 1400°F heat source inner temperature, material selection is probably the single most important factor of the items contributing to overall reliability. As such heavy emphasis is being placed upon material properties evaluation and compatibility testing prior to design finalization.

A summary of major SNAP-23 performance characteristics are shown in Figure (7).

2. Engineering Applications and Conceptual Design Studies

Two of the families of terrestrial power levels are not, at present, in the actual prototype hardware developmental stage. The milliwatt level isotopic power output is considered to be sufficiently developed technologically, to meet application requirements for the next few years. The large kilowatt heat source involves unique problems of concept, economics, and safety that have not heretofore been investigated. The status of these two isotopic power source levels is as follows:

a. Milliwatt Power Levels

An extensive applications engineering and parametric design study was completed in FY-1966. From the data obtained in this study, developmental programs were scheduled to be initiated in FY-1970. (Budget considerations, however, may delay this start until FY-1971.) The programs will culminate in the fabrication, testing and demonstration of proven prototype systems in areas where they are expected to find greatest use. As mentioned earlier, considerable data and engineering experience has been gained in this power range from the SNAP-15A and -15C programs, which devices were developed for usage in classified weapons and communications applications. It is anticipated that further work in these energy output levels will continue to utilize thermoelectric conversion systems and either Pu-238 or Sr-90 fuels.

b. Kilowatt Systems

In regard to kilowatt level isotopic power sources, the AEC has become increasingly aware of the potential needs for the development of terrestrial systems in the 1-10 kw range. The Navy's deep ocean technology (DOT) program and a top-priority ASW active surveillance network are but two of the near-term applications where in fact, an isotopic fueled generator provides the only feasible type of power source for extended mission duration. Efforts in this regard have been modest to date, with primary emphasis being placed on engineering design and cost effectiveness studies to determine system concepts, fuel selection, operating environments and power conversion capabilities. Present efforts in the field of large kilowatt sources (FY-1969) are limited to work being accomplished by the AEC to further the previous preliminary engineering studies as related to specific Navy applications.

Initial design criteria relating to these large isotope systems are shown in figure (8). You will note that the isotopic fuels of interest are limited to Sr-90, Co-60, and Ce-144--primarily due to cost and availability considerations.

As I indicated, these engineering studies will parametrically evaluate alternate isotope fuels and power conversion techniques to be used as a basis for conceptual design studies. In the course of this study, liaison will be conducted with potential users in order to match alternate concepts with broad areas of application. The final objective of this initial effort, once the parametric, conceptual design, and cost effectiveness studies are completed, is to define and assess the technological advancements required to develop the various power systems that offer greatest promise, and to determine the resources and time required to pursue this development. This assessment will form the basis for preparation of detailed development plans relating to the implementation of the required base technology programs. These plans will delineate the advancements required in terms of materials development, power conversion technology, fuel form development and containment, shielding and handling, and fabrication technology. The combined capabilities and experiences of technical experts in the national laboratories and industry will be utilized in assessing the adequacy of these plans.

Upon development and acceptance of these plans, a base technology program will be implemented.

Funding limitations have precluded further AEC effort on the large kilowatt program in FY-1969. It is planned to resume development in FY-1970.

3. Summary and Plan

I should now like to call your attention to a summary of Program Elements for the four families (i. e., power output levels) of isotopic power sources currently under development and investigation by the AEC (figure 9). You will note that the figure likewise includes an assessment of potential applications that the isotopic generators may serve--some of the applications I have previously discussed, some of the uses are projections of our "best guesses" at this time.

D. Economics and Competitive Conversion Systems

Considerations of potential applications of isotopic power sources must, of necessity, include an economic and logistical

analysis of the installation under consideration. The unique features of an isotopic power source; i. e., long unattended life, high reliability, low weight, small size, may be determining factors in favor of the selection of isotopic powered energy systems regardless of economics (e.g., remote polar locations accessible only with difficulty during certain periods of the year). In many more common applications, however, competitive power sources such as batteries, fuel cells and conventional liquid hydrocarbon generators may offer significant advantages. I must, of course, mention that total cost--including initial purchase price, implantment, servicing and maintenance, operating costs including fuel, and salvage value at end of life, must be included in any economic comparison.

I will cite three examples:

1. Power is sold to operators of offshore oil and gas platforms in the Gulf of Mexico at an average cost of $10-$12 per kilowatt hour. The cost is significantly higher in other areas of the world. The 60-watt SNAP-23 generator has as its objective an operating cost of less than $10 per kilowatt-hour--exclusive of any fuel buy-back considerations. As oil operations extend further offshore, the average cost of nonnuclear power will increase sharply due to logistics; whereas the cost of isotopic power should be nearly independent of this factor. Obviously a 60-watt generator is of insufficient size to provide all power to an offshore drilling platform while actual drilling is in progress, however, it is not inconceivable that if the economic cost objectives of the SNAP-23A can be met, larger power sources would be even more efficient.

2. A continuing problem in offshore drilling is the marking of completed underwater well heads. Successful exploratory drilling may have been accomplished in an oil lease region; however, significant periods of time may elapse before the field is developed. It is difficult and costly to locate the capped-off well heads without some type of acoustical signal. These signals are currently powered by battery powered energy sources which are replaced at 3 - 6 month intervals. In the Gulf of Mexico, an average cost of about $2,000 is incurred per servicing. A milliwatt isotopic generator could economically power these transponders for longer periods of time thus reducing the servicing charge. Again, remoteness from an established logistical base of operations would further enhance the attractiveness of the isotopic power sources. A cost analysis would, of course, be required to determine economic feasibility for each application.

3. The 1968 Marine Science Affairs[1] report contains the results of an analysis of the ranges of applicability of underwater power sources. This analysis, partially based on economics, and partially based on physical size limitations is displayed as figure (10). Note that beyond about 80 days mission duration at the one kilowatt level, an isotopic power generator seems to be the only competitive energy source that can be considered.

I have cited but three of the potential usages and possible economic or logistical advantages of isotopic fueled generators --others could include an analysis of the merits of these devices for microwave repeater stations, underwater cable boosters, unattended polar weather stations or midocean buoys used for gathering weather information, navigational beacons, lighthouses, aircraft navigational aids, sonar beacons, deep-sea transponders, seismic stations, tidal wave (tsunami) gauges, oceanographic instrument packages, passive sonar listening devices, and blowout preventers for offshore drilling rigs. These are all potentially "immediate" applications that could be employed with a minimum of additional developmental work. Perhaps the second generation SNAPs-21 and -23 will provide the economic competitiveness necessary to make some of these applications practical.

Although the economic characteristics of isotopic fueled generators for yet other applications appear to be attainable, they are significantly beyond current technology and will require extensive R&D effort.

E. Future Prospects

There appears to be little doubt that both the short-term and the long-term development and usage of moderate power level isotopic power sources appear bright. If even a fraction of the above potential application is realized, the needs could exceed the currently forecast availability of Sr-90 and Pu-238 fuels.

While we have covered briefly the future of terrestrial and oceanographic applications of relatively small power producers, we should recognize that these quantities of power are insufficient for many applications. As oceanographic studies send us deeper and deeper into the sea, we will require considerably higher energy

1. Marine Science Affairs - A Year of Plans and Progress. The Second Report of the President to the Congress on Marine Resources and Engineering Development, March 1963. U. S. Gov't. Printing Office, p. 152.

levels if we are to ever staff underwater testing stations, military installations, and laboratories. To date, the development of large isotope and small reactor systems in the ocean environment has not received adequate emphasis.

The kilowatt isotopic power source development plan, however, appears to have been recently given significant support and sense of urgency by the Energy Source Panel of the National Research Council's Committee on Underseas Warefare. Their recommendations indicated that isotope power sources, utilizing either static or dynamic conversion systems, should be developed by the Navy-Atomic Energy Commission team on a priority basis to meet future energy requirements of the Navy involving extended mission duration (1-3 years or more) and at power levels up to 10 or 15 kw. It was further recommended that the isotope power systems be developed on a modularized design basis and that they be developed and qualified for use in a maximum depth environment. The Panel further concluded that design and development of the specific isotope power systems chosen should be conducted by the AEC in accordance with detailed engineering criteria established by the Navy.

It would therefore appear that increased emphasis and funding support will be placed on the development at this power level, and that other potential economic applications for this type device will follow in due course.

F. Problem Areas

Technological advancements in isotopic fueled power sources have progressed in an orderly and disciplined manner in the past twelve years. There have been no unexpected technical breakthroughs. The developmental programs to date have been successful, however, there still remains considerable work to be accomplished. Efficiencies are low--in some applications unacceptably so. Lifetimes are increasing, but we have hardly begun to realize anywhere near the potential of these devices. Reliability has been good, but there is room for considerable improvement. Basic material properties at elevated temperatures are not clearly understood; long term effects of creep, material compatibility, and radiation environment exposure are extrapolated projections of short term tests. Safety considerations are reasonably well delineated; however, we are still concerned about public and official acceptance of these devices. This last item may be of considerable consequence if, for example, isolated radioisotope fueled navigational buoys are deployed on a vast scale. Mr. I. C. Clingan of Trinity House when addressing himself to this subject recently noted[1],

1. I. C. Clingan (Isotopic Generators in Marine Navigational Aids), Isotope Generator Information Center, Newsletter No. 6, May 1968, p. 79.

"The sea is a big place and anything jettisoned into it, or which breaks adrift may find its way almost anywhere. The stringent precautions and safety factors embodied in the design and construction of these units are known, but even so, this problem will exist. Experience . . . has already given some idea of the extent of the administrative difficulties that may have to be faced. Some of the problems are undoubtedly psychological and will disappear with time, but there will still be some awkward situations to be negotiated, and at some stage international agreement and regulation will undoubtedly be necessary."

In recognition of these types of problems, safety considerations have been accorded an emphasis that rivals all other factors in design importance. Public safety criteria from all credible accident conditions have been carefully established--including all of the ramifications of radioactive materials entering into any portion of the various food cycle chains. This general subject of safety will be covered in considerable detail by the following speaker; I shall thus not usurp his material. Suffice it to say, that safety considerations are significant factors that relate to all design and developmental conditions and in fact, may be the determining criteria which controls basic device design. You will note from a quick glance at the topics to be covered by the following speakers concerning compatibility, fuel containment, and encapsulation techniques that safety is not a subject lightly considered. As Mr. Clingan points out, however, problems will still occur, and some type of international regulation regarding the deployment of radioisotope power sources will probably be necessary in the future.

The final problem area I wish to mention is a problem of reliability--not of the device itself, nor of its power conversion system. If we are successful in our endeavors to design and build prototype isotope fueled units which can produce power for up to ten years of unattended life, are there now, or will there be available, suitable electronics and electrical equipment to match the lifetimes of these isotopic powered energy sources? This is a situation to ponder, and a question that should be asked of our colleagues in the electrical disciplines.

Thank you.

FIGURES AND ILLUSTRATIONS

SNAP-7 ISOTOPIC POWER SYSTEMS

Designation	Power	Use	Date of Installation	Status
SNAP-7A	10 watts	U.S. Coast Guard Buoy Curtis Bay, Md.	Jan. 1964	Removed from buoy in FY 1967 for disassembly and examination
SNAP-7B	60 watts	Offshore Oil Platform Gulf of Mexico	Aug. 1966	Performance stable in Chesapeake Bay lighthouse for 2 years. Relocated to Gulf oil platform
SNAP-7C	10 watts	U.S. Navy Weather Station, Antarctica	Feb. 1962	Established record for unattended Antarctica weather station operation. Operation satisfactory.
SNAP-7D	60 watts	U.S. Navy NOMAD Weather Station located in center of Gulf of Mexico	Jan. 1964	System successfully withstood major hurricanes. Performance stable.
SNAP-7E	7.5 watts	U.S. Navy Acoustic Beacon Atlantic Ocean, 750 miles east of Jacksonville, Fla.	July 1964	System operation satisfactory
SNAP-7F	60 watts	Disassembled	--	Operated for 6 months on offshore Gulf oil rig; subsequent power loss. Disassembled and being examined.

FIGURE 1

TERRESTRIAL ISOTOPIC POWER -- CURRENT R&D DEVELOPMENTAL PLAN

1. PROTOTYPE DEVELOPMENT OF IMPROVED DEVICES IN THOSE AREAS WHERE SUFFICIENT TECHNOLOGY EXISTED TO INSURE SUCCESS AND IMPROVEMENT OF EXISTING DEVICES.

   A. 100 - 1000 MICROWATTS (PACEMAKER -- 162 μ WATTS)
   B. 10 - 100 WATT RANGE
      (1) OCEANOGRAPHIC APPLICATIONS (SNAP-21 -- 10, 20 WATTS)
      (2) TERRESTRIAL APPLICATIONS (SNAP-23A -- 25 to 100 WATTS)

2. CONCEPTUAL DESIGN, PARAMETRIC, APPLICATION AND TRADE-OFF STUDIES OF THOSE POWER LEVELS NOT PREVIOUSLY EXPLORED OR WHERE IMMEDIATE DEVELOPMENT NOT CONSIDERED WARRANTED.

   A. 10 - 100 MILLIWATTS
   B. 1 - 10 KILOWATTS

3. SUPPORTING TECHNOLOGY

   A. INSULATION SYSTEMS AND CONCEPTS
   B. IMPROVED THERMOELECTRIC MATERIALS
   C. LARGE FUEL BLOCK TECHNOLOGY
   D. LONG TERM MATERIALS TESTING
   E. HEAT TRANSFER STUDIES
   F. Sr-90 SAFETY

FIGURE 2

FIGURE 3 - RADIOISOTOPE CARDIAC PACEMAKER

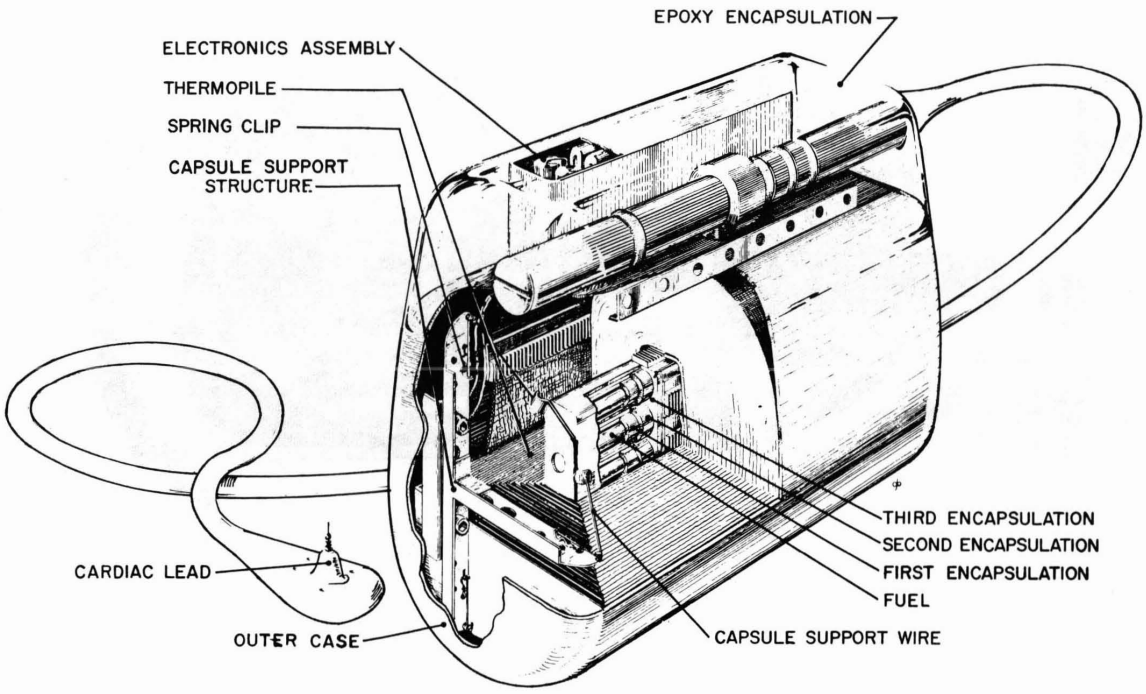

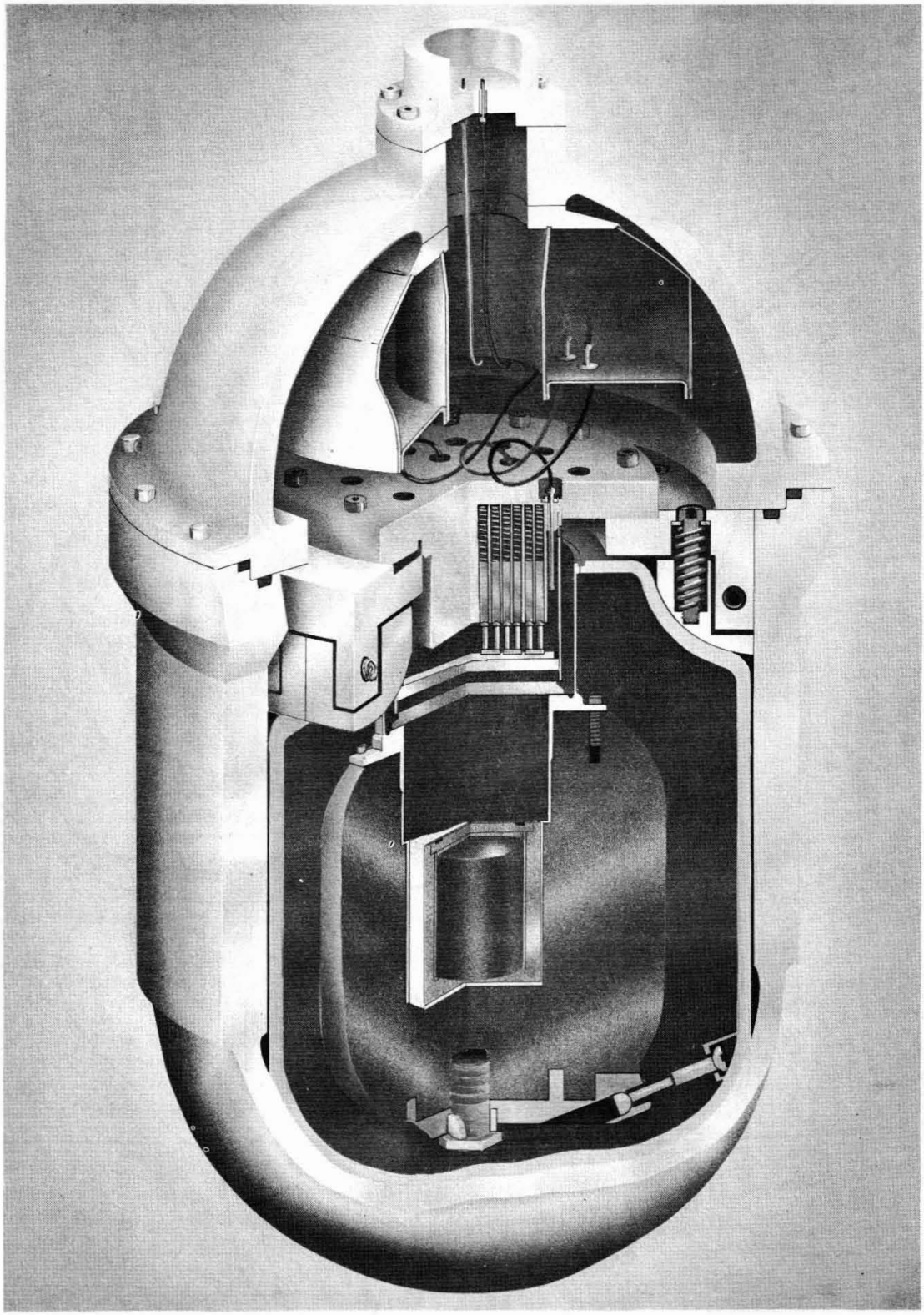

Figure 4. SNAP-21

TERRESTRIAL ISOTOPIC POWER

DEEPSEA GENERATORS (SNAP-21)

POWER	FUEL	LIFE	WEIGHT	SCHEDULE
10 WATTS	Sr-90	5 YEARS	650 LBS.	FABRICATION INITIATED FY 1966 ENVIRONMENTAL TESTING FY 1969
20 WATTS	Sr-90	5 YEARS	900 LBS	FABRICATION FY 1969 -70 ENVIRONMENTAL TESTING FY 1960 - 71

DESIGN PRESSURE: 10,000 PSI

PROJECTED APPLICATIONS: NAVIGATIONAL AIDS, SEISMOLOGICAL STATIONS
OCEANOGRAPHIC RESEARCH, HYDROPHONE AMPLIFIERS

FIGURE 5

SNAP-23A-60 WATT(e) UNIT

FIGURE 6

TERRESTRIAL ISOTOPIC POWER

SURFACE GENERATORS (SNAP-23)

POWER	FUEL	LIFE	WEIGHT	EFFICIENCY	STATUS
25 WATTS	Sr-90	10 YRS. MIN.	700 LBS.	6.0-6.5%	FABRICATION FY 1970-71 ENVIRONMENTAL TESTING FY 1972-73
60 WATTS	Sr-90	10 YRS. MIN.	1000 LBS.	6.5-7.0%	FABRICATION FY 1969-70 ENVIRONMENTAL TESTING FY 1970-71
100 WATTS	Sr-90	10 YRS. MIN.	1600 LBS.	6.5-7.0%	FABRICATION FY 1970-71 ENVIRONMENTAL TESTING FY 1972-73

PROJECTED USE: OFFSHORE NAVIGATIONAL AIDS; UNMANNED SEISMOLOGICAL STATIONS; MICROWAVE REPEATER STATIONS; AIRCRAFT LANDING SYSTEMS; REMOTE COMMUNICATIONS.

* END-OF-LIFE

FIGURE 7

ISOTOPE KILOWATT DESIGN CRITERIA

POWER LEVEL:	1 - 10 KILOWATTS (e)
OPERATING LIFETIME:	3 MONTHS - 5 YEARS
ISOTOPE FUEL:	COBALT - 60 METAL STRONTIUM - 90 TITINATE/OXIDE CERIUM - 144 OXIDE
POWER CONVERSION:	STATIC: THERMOELECTRIC THERMIONIC DYNAMIC: BRAYTON CYCLE ORGANIC RANKINE CYCLE LIQUID METAL RANKINE CYCLE STIRLING ENGINE
ENVIRONMENTAL:	MARINE (INCLUDING DEEPSEA) AND REMOTE TERRESTRIAL

FIGURE 8

TERRESTRIAL ISOTOPIC POWER - PROGRAM ELEMENTS

Power Level	Microwatts	100 - 1000 Milliwatts	10 - 100 Watts	1 - 10 Kilowatts
Isotope Selection	Pu-238	Pu-238/Sr-90 Pm-147	Sr-90	Co-60/Sr-90 Ce-144
Energy Conversion	Metallic Thermoelectric	Semiconductor or Metallic Thermoelectric	Segmented Semiconductor Thermoelectrics	Thermoelectric Thermionic Diode Organic Rankine Brayton Cycle Stirling Engine
Areas of Application	Cardiac Pacemaker Biomedical Stimulation	Oceanographic Instrumentation Cable Boosters Underwater Weapons	Weather Stations Buoys, Microwave Repeater Stations Oceanographic Seismographs & Instrumentation Navigation Aids	Antarctic Support Stations Deep Sea Mining & Exploration Military Communications Offshore Oil
Application Criteria	Extended Life Reliability Safety Size & Weight	Costs Ease of Handling Reliability Safety	Costs Extended Life Reliability Safety	Costs Reliability Safety

FIGURE 9

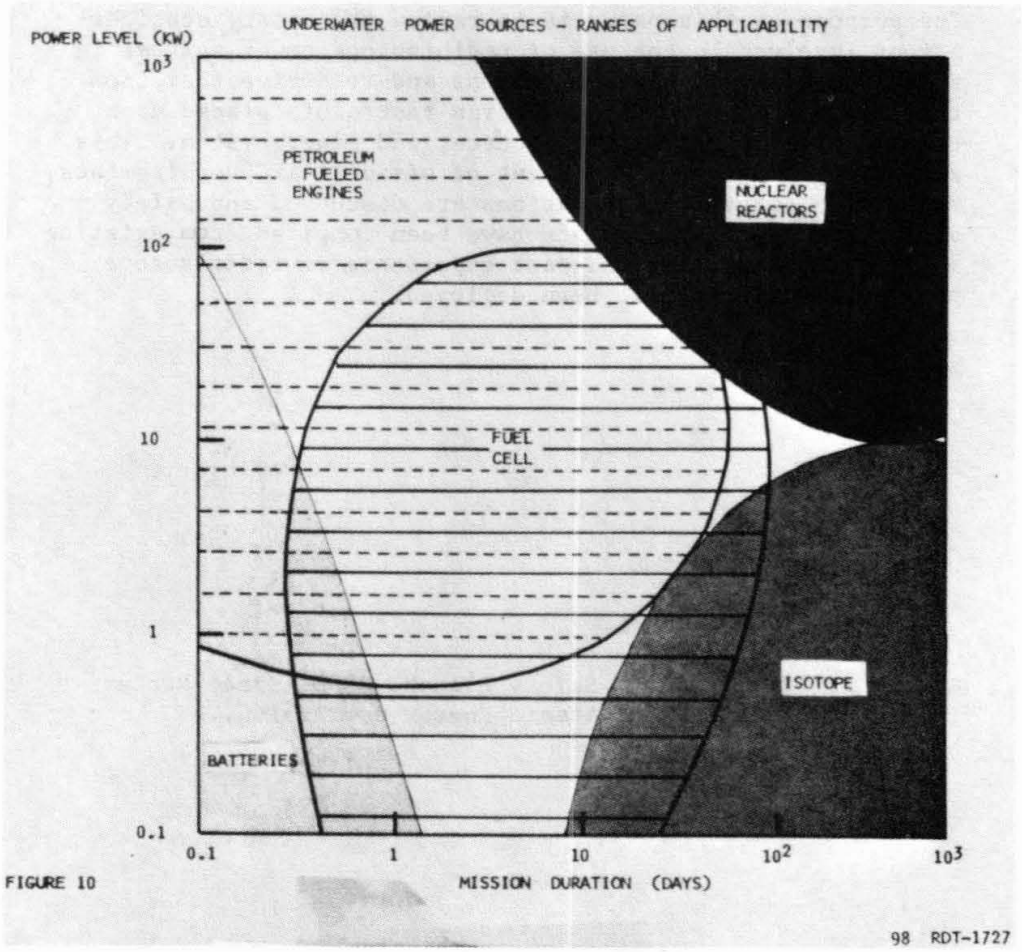

FIGURE 10

Safety Considerations for Radioisotope Power Systems

George P. Dix

Abstract

The purpose of this paper is to review the safety considerations involved in the use of radioisotope power systems in space and terrestrial applications and to derive therefrom the safety requirements and design restraints placed upon the radioisotope fuel, heat source, and power system. This survey paper is not a statement of official AEC requirements, rather the safety considerations are discussed and safety design and test requirements have been compiled from existing applicable guidelines and past experience on radioisotope power systems that have been deployed.

George P. Dix is Chief, Safety Branch, SEPO, Space Nuclear Systems Division, U. S. Atomic Energy Commission, Washington, D. C. 20545

INTRODUCTION

The purpose of this paper is to review the safety considerations involved in the use of radioisotope power systems in space and terrestrial applications and to derive therefrom the safety requirements and design constraints placed upon the radioisotope fuel, heat source, and power system.

Although the radiological safety criteria are identical for both space and terrestrial systems and there is often commonality in safety design requirements, the approaches to achieving system safety vary appreciably because of the differences in the potential accident environments between terrestrial and space systems.

The "sedentary" nature of most terrestrial applications is recognized. Including transportation to and from the site of deployment, the potential safety problems associated with terrestrial systems are: (1) unauthorized access; (2) accidents resulting in thermal transients or impulsive mechanical loads; and (3) loss of radiological control and eventual loss of shielding and/or containment. In general, the above considerations are quite similar to those associated with the packaging, handling, storage, and transport of any large quantity of radioactive material and are inherent in existing requirements set forth by the AEC, DOT, and IAEA.

The dynamic nature of the normal and potentially adverse environments of space nuclear systems poses many unconventional safety considerations and unique design constraints. The potential accident environments traverse a wide spectrum of adverse thermal, mechanical, and chemical conditions and the accident occurrences are quite variable in space and time. The major potential safety problems are: (1) launch pad aborts yielding propellant fires, explosions, incident fragments, followed by system impact; and (2) system reentry and impact at random uncontrolled locations. The latter is similar to the unauthorized access and potential loss of containment problem associated with terrestrial systems. Safety criteria are being published by the AEC for space nuclear systems and precedents for criteria, requirements, and constraints are being established on a system-by-system basis as each prototype system goes forward for flight approval.

SAFETY CONSIDERATIONS FOR TERRESTRIAL SYSTEMS

TERRESTRIAL APPLICATIONS

Terrestrial applications include power sources for remote weather stations in the Arctic (1) and Antarctic, weather platforms at sea coupled to weather satellites, marine navigation aids such as buoys, ocean bottom oceanographic stations, and sources of emergency power for remote land and sea installations (2). As a rule the terrestrial systems are fueled with fractions of a megacurie of a long-lived radioisotope,

are designed to produce continuous power for several years, and are deployed in areas of low or no population density.

TERRESTRIAL SYSTEMS

A typical device is fueled with several hundred thousand curies of Strontium-90 titanate pellets and produces on the order of 60 to 100 watts for two to five years. In a typical system the heat source consists of three to six successive sealed containment barriers. The heat source is placed in a biological shield which in turn is surrounded by a heat accumulator block which transfers heat to a thermoelectric converter, all of which are contained in a generator casing having a finned radiator. Figure 1 shows a typical terrestrial generator (SNAP 7). These various components when viewed collectively constitute up to a dozen or so fuel containment barriers. On occasion, a shipping container is also used for additional protection during transport to add one or more additional barriers.

The power source and/or installation are designed to provide the necessary shielding to maintain external radiation doses within working limits. The heat source is designed to withstand transportation collisions, fires, and explosions and in some cases potential impulsive loads at the site of deployment (e.g. ship collisions with nuclear powered buoys). In addition, in marine applications power sources are designed to contain the fuel for ten or so half-lives under static pressures characteristic of water depths of up to 20,000 feet. Finally, the design of the system and installation, the site parameters, and operational procedures are such as to minimize human contact, unauthorized access, and certain undefined events associated with the term "vandalism".

SAFETY CONSIDERATIONS FOR TERRESTRIAL SYSTEMS

The above discussion leads one to the conclusion that the system when deployed has an overabundance of safeguards and that it is quite resistant to any accident or event that one could postulate. Two thoughts are worth mentioning at this point. First, the terrestrial systems generally possess the luxury of weight, but in the event streamlining is desired, designers should consider the bifunctionality of components for containment and shielding such as shields, heat accumulator blocks, generator casings, and the installation for the generator. This philosophy leads the author to avoid using specific terms such as fuel capsule and encapsulation in preference to the term containment. Second, although a system may appear overdesigned for its operating lifetime, additional consideration should be given to possible loss of radiological control over some types of units and the long term degradation of their containment.

Figure 2 summarizes the safety considerations associated with terrestrial systems. It is important that the fuel possesses thermal, mechanical, and chemical stability in order to immobilize the radionuclide in the event of a short or long term breach of containment or

a loss of radiological control. In time, this primary attack on the hard core of safety problems will simplify systems and reduce their cost. Redundant and bifunctional containment-shield components are desired. Configuration control and material selections to minimize the effects of adverse environments (such as static and impulsive loads, thermal transients, and corrosion by common reagents) are implicit in any design. Shields are designed to minimize radiation doses during transport, installation, maintenance, and repair, but most important the shield must maintain its integrity in the event of an accident. Shielding and containment designs will serve to safeguard against unauthorized access, vandalism, and a possible loss of radiological control. However, ingenuity in siting, power system installation, lack of access and lack of portability by typical intruders, operational procedures, and even "burglar" aids are additional considerations for some of the ill-defined human factor situations. The system should be physically secured in a practical manner, and clearly and permanently marked as to its radiation.

The designer should be encouraged to design safety into the system at the onset. A subtle way of accomplishing this is to have him perform a safety analysis and evaluation before he fabricates his hardware. Although the system safety engineering approach is only organized common sense, experience has demonstrated that unanticipated safety problems are the damaging ones and that most problems are the result of human factors, which often prevail in the case of unattended terrestrial systems.

SAFETY REQUIREMENTS FOR TERRESTRIAL SYSTEMS

In translating the safety considerations for terrestrial systems into safety design requirements it is also necessary to specify analyses and tests that demonstrate conformance of the design to the requirements.

As a general requirement the designers should perform a safety analysis and evaluation of the system, site environment, and intended application. In particular, the potential accidents should be identified and the limits of various adverse environments should be quantified. The test environments are so defined and the ability of the device to withstand them should be determined. When proof tests are not practical, theoretical analyses and/or overtests should be substituted. This should be documented for the record and used for approval purposes and constitutes a Safety Analysis Report.

During transport the system and/or shipping container should meet the requirements established by the AEC, DOT, and IAEA.

Figure 3 summarizes the safety design requirements for terrestrial radioisotope power systems.

SAFETY DESIGN REQUIREMENTS

Fuel

The fuel should exhibit thermal, mechanical, and chemical stability when subjected to normal and adverse environments for a time commensurate with the half-life, containment capability, and application. In particular, the fuel form should have a high melting point, a high resistance to mechanical degradation into respirable aerosols (<10 microns in size), and its overall behavior should be predictable and, preferably, reproducible.

Containment

The system should provide redundant barriers for containment of the fuel. The containment should maintain its integrity against mechanical (overpressure, impact), thermal (fires, loss of thermal control), and chemical (corrosion by common reagents) attack as a result of potential transport and on-site accidents. Barriers in contact with the fuel should be compatible with the fuel under normal and accidental thermal conditions and containment structures should compensate for internal pressures from gases evolved from the fuel. The containment should maintain its integrity against long term adverse environments (i.e. corrosion, external pressure) for a period of time commensurate with the fuel half-life, site, and intended application.

Shielding

The design of the system and installation should maintain radiation doses to workers and the general public within limits specified by the AEC in Manual Chapter 0524. The shield should maintain its integrity in the event of accidents.

System

The system, comprised of the heat source, shield, heat accumulator, and generator casing should be configured and materials of construction employed to minimize the effects of vibration, impact, overpressure, incident fragments, fires, loss of thermal control, and corrosion by common reagents. The system should be equipped with aids to assist in its location and recovery in the event of a loss of radiological control.

Installation

The installation accepting the power system should provide for a positive method of securing the power system and/or preventing direct access to it by conventional methods.* If accessible, the system should not be detachable or portable by conventional methods, and the system

---

*One cannot hope to safeguard a system against a well-organized and equipped conspiracy to steal or destroy it. On the other hand, reasonable safeguards against an ad hoc attack by a curious, demented or vandalistic individual should be employed.

and installation should be clearly and permanently marked to notify the general public of any external radiation hazard involved in tampering with the system. Provisions should be made to recover the system after its operational lifetime.

Site

Selection of a remote site with natural restrictions to public access should be considered. The site environment should minimize the possibility of natural and man-made accidents and the loss of radiological control.

Operational Procedures

Operational procedures should be prepared which include provisions for clear responsibility and authority for the system, emergency plans and procedures, and procedures for installation, maintenance, and post-mission disposition.

SAFETY ANALYSIS AND TEST REQUIREMENTS

Figure 4 summarizes safety analysis and test requirements for terrestrial systems. Test requirements generally follow those set forth for the transport of radioactive materials (3-4). In some cases additional analyses and/or tests are required for unique applications (e.g. deep sea hydrostatic pressures), and fuel tests appear to be a logical future criterion.

Fuel

Although there are no formal fuel test requirements, fuel tests are generally performed in the course of fuel and heat source development programs. These include determinations of its thermal stability, purity, dosimetry, mechanical response, gas evolution rate, and solubility. Long term tests on aging fuel to determine the effects of time and daughter growth are performed. Radiobiological experiments often accompany the above tests. The possible requirement of setting aside control fuel specimens is noteworthy.

Containment

A number of tests are performed on the heat source and system to determine containment integrity. These include the following:

Impact. Free fall drop tests are conducted with impact on a flat surface at the critical angle. Vehicular impact analyses are performed.

Puncture. Heat source puncture tests are conducted by impacting the heat source with a non-yielding steel bar.

Fire. Systems are exposed to a transportation fire for 30 minutes at 1475°F.

Thermal Shock. The heat source is subjected to thermal shock by being raised to operating temperature and immersed in water.

Pressures and Static Loads. The heat source is subjected to static loads, hydrostatic pressures, shock overpressures, and cyclic vibration loads.

Leak Tests. Leak tests are performed before and after many of the above tests to see if the fuel remained contained.

Corrosion. Corrosion tests are performed on the heat source materials and closures.

Shielding

The radiation dose of the system is measured after assembly to assure conformance with transport and handling requirements (5-6). Shield integrity determinations are implicit in system tests described above.

SAFETY CONSIDERATIONS FOR SPACE SYSTEMS

SPACE APPLICATIONS

Space applications include power sources for navigation and weather satellites in high altitude orbits, power sources for lunar or interplanetary missions, and large radioisotope units for low altitude orbits in manned or unmanned spacecraft. A typical power system would contain tens of kilocuries of ^{238}Pu and would be designed to produce continuous power for one to five years.

SPACE SYSTEMS

Figure 5 shows the SNAP 19 system for the Nimbus B weather satellite. In a typical system the fuel is placed in one or more metal containers which are either sealed or vented to relieve the internal helium pressure. The heat source is placed in a graphite ablator which provides reentry protection. In the case of SNAP 27, which will be used on the lunar surface, the heat source/ablator assembly is not integrated with the converter and generator housing at launch, rather the heat source is launched in the ablator and is mated with the generator on the lunar surface by the Apollo astronauts, and the ablator is discarded there. In systems used in earth orbit (i.e. SNAP 19) the heat source/ablator assembly and generator are integrated at launch. The space systems are characterized by light weight, minimal shielding (low dose), reentry protection and often include vented heat sources. Shipping containers are employed for ground transportation.

SAFETY CONSIDERATIONS FOR SPACE SYSTEMS

Figure 6 summarizes the safety considerations associated with space systems. Aside from potential transportation accidents, which are common to both terrestrial and space systems, the potential accidents associated with space systems are of two general types (7).

The first type of potential accident is the launch abort in which the booster vehicle fails on the launch pad or downrange on ascent. A demonstrative example of this type of accident was the SNAP 19 abort where the booster went off course and had to be destructed at 100,000 feet altitude at a velocity of 3000 feet per second after two minutes of flight. In this case the generators impacted intact downrange at sea. The most severe potential launch accident is a pad abort in which the booster propellants explode due to intentional destruct or fallback of the launch vehicle. This environment can yield fireball temperatures of 5000°F for seconds, shock overpressures, incident fragments, followed by free fall impact of the system and/or its immersion in a propellant fire at 1800°F for 30 minutes. The system design takes this into account by hardening the fuel form and containment against impulsive loads and thermal transients. It is noteworthy that the location of this type of accident is controlled to a government site or to unpopulated ocean regions downrange by conventional range safety practice. Passive and active location and recovery aids are considered to assist in returning the heat source to radiological control.

The second type of potential accident is failure to achieve orbit on ascent or uncontrolled random orbital decay from a short-lived orbit. This event is characterized by a severe reentry heating pulse (stagnation temperatures up to 5000°F for five minutes) and impact of the heat source on the earth's surface at velocities of 100 to 500 feet per second. Although more than 80% of these types of events will occur over oceans and/or unpopulated polar regions, the random reentry and land impact event predominates in the system design. The intact reentry and intact impact design philosophy is currently employed for systems under development. This dictates reentry protection with an ablator surrounding a heat source which is designed to survive impact at terminal velocity on a rigid target.

In space nuclear systems the fuel form is the first safeguard against potential accidents. In the event of a breach of containment due to ablator failure on reentry or containment loss at earth impact, it is necessary to minimize the amount of respirable particles (<10 microns) formed immediately and later by long term degradation and to interdict the entry of the radionuclide into man's environment and food web. In the past year the AEC has been intensifying its efforts on fuel form stability by: (1) analyzing fuel configuration control to minimize reentry heating pulses and impact loads, and (2) developing fuel forms resistant to adverse environments, such as reentry heating, impact, and long term exposure. The purpose of this effort is to improve the fuel form to relax the containment weight and complexity for system optimization and product improvement.

Another major consideration in space nuclear systems is their early return to radiological control in the event of an accident or the positive confirmation that they are in a safe location (i.e. deep ocean) out of the active biosphere. The AEC, DoD, and NASA have embarked on joint programs to evolve location and recovery aids for ascent aborts resulting in land or shallow water impact. In addition, studies are being conducted on how to track errant nuclear spacecraft in orbit and through reentry to identify the region of impact. Radiometric, infrared, and electronic methods have shown promise in early experiments, and it is clear that many location and detection aids already in use for other applications can be applied to finding lost space nuclear systems. Studies are also being performed on controlled deorbit systems and post-mission recovery of large space nuclear systems used in low earth orbits. However, we currently possess the technology to assure system safety in the event of random impact of heat sources.

SAFETY REQUIREMENTS FOR SPACE SYSTEMS

The safety requirements for space systems are approached on the basis of individual systems and missions at the present time by establishing precedent. The scope and intent of these requirements includes the protection of people including launch operations personnel, other on-site personnel, off-site civilians, and the worldwide population at large. Also treated are safeguards against incidents which could constitute potential international relations problems that may or may not involve real safety problems (8). Risk versus benefit is also a non-quantitative consideration to designers. The following safety requirements should be viewed as evolutionary, are by no means rigidly applicable to all space nuclear systems, and are an early attempt at standardization.

As in terrestrial systems, a general requirement is that the designer should perform a safety analysis and evaluation of the system, the mission, and launch vehicle and spacecraft. A dialogue between the designers of two different systems used in different missions, would soon reveal that the systems (even fuel) and accident environments of each will be different. However, each designer would readily identify similarities in safety design requirements such as containment during reentry and impact. Both designers would discuss the probabilistics of accidents,* breach of containment, and loss of radiological control. Probabilistics is inherent in the safety evaluation of space nuclear systems because they are always dependent upon the reliability (1 minus reliability equals failure probability) of the booster and spacecraft. Unfortunately, we are not yet ready to specify sweeping probabilistic safety design requirements for space nuclear systems. However, probabilistics can identify the operational phase and location where the accident is most likely to occur, as was so lucidly demonstrated by recent SNAP 19 abort.

*It is noteworthy that human error accounts for about one-third of all missile failures and appears to have been responsible for the two aborts of nuclear powered spacecraft.

Figure 7 summarizes the safety design requirements for a typical space nuclear system used in a high altitude orbit application.

SAFETY DESIGN REQUIREMENTS

Transportation and Ground Handling

The system and/or shipping container should be designed and handled to satisfy the containment and radiation exposure requirements specified by the AEC and DOT prior to launch.

Fuel

The fuel should exhibit inherent thermal, chemical, and mechanical stability when exposed to normal and accident environments (high melting point, high mechanical resistance to aerosol formation, insolubility) on a short and long term basis. Every attempt should be made to prevent the production, release, and dissemination of aerosols before, during, and after impact.

Containment

The heat source should be designed to contain the fuel when unprotected by the spacecraft and/or generator structure. It should be designed to contain the fuel during and after launch pad aborts, ascent aborts, in-orbit, reentry, and impact.* Provisions should be made to accommodate internal pressures due to helium and other entrained gases.

Heat Source

The heat source should be configured and materials of construction employed to minimize the effects of vibration, propellant fires, shock overpressures, incident fragments, reentry heating, loss of thermal control, impact, and corrosion. The heat source should be designed so that the fuel can be recovered intact from the earth's surface or shallow water.

System

Location and recovery aids should be incorporated into the generator system or spacecraft to facilitate location and return to radiological control after near off-shore aborts.

Spacecraft

Care should be given to the location of the system in the spacecraft and spacecraft materials to minimize thermochemical reactions affecting containment integrity in launch aborts and reentry.

---

*The time of containment after earth impact should be maximized. However, consider requiring a contractor to guarantee containment for 10 half-lives when one half-life is 90 years.

Operational Procedures

Operational procedures should be prepared which include provisions for clear responsibility and authority for the system during manufacture, transport, ground handling, launch, and in the event of an accident.

SAFETY ANALYSIS AND TEST REQUIREMENTS

Figure 8 summarizes safety analysis and test requirements for space radioisotope power systems. Since the dynamic accident environments associated with space systems are more severe than those specified for transportation accidents, the following requirements will satisfy transportation safety requirements. The hypothetical safety analysis and test requirements for a typical system used in a high altitude orbit application are given.

Fuel

The response of the fuel to the various accident environments should be evaluated by test and analysis. This includes both short and long term effects, thermal stability in propellant fires and reentry, mechanical stability during vibration, impact, and post-impact, and chemical stability in hard vacuum and seawater conditions. In these evaluations particular emphasis should be made in measuring aerosol production in adverse environments and in maintaining control or historical specimens of fuel. Fuel tests are followed by post-mortem analyses to determine the post-test characteristics of the fuel. Radiobiological experiments should be performed to evaluate the effects of inhalation, ingestion, and epidermal exposure from fuel.

Containment

Impact. Impact tests to determine the containment integrity of the heat source at terminal velocity and critical angle conditions are conducted on rigid media. Precursor tests are conducted to determine the stability and velocity of the heat source at impact. Analyses are performed on the post-impact burial depth of heat sources in various media.

Fire. The heat source is subjected to simulated propellant fireball and after fire environments using radiant heating and/or simulated propellant fires.

Reentry. Analyses and tests are performed to determine the ability of the heat source/ablator to withstand reentry. Aerodynamic stability and mass removal rates are analyzed. Postmortem tests are conducted to determine the degree of fuel containment integrity.

Internal Pressure. Tests are conducted to determine the ability of the heat source to retain or relieve internal gas pressures without particulate fuel release. Heat source leak tests and vent tests are conducted.

Dosimetry. Dosimetric measurements are made of the fuel, heat source, and system.

Corrosion. Tests of the ability of heat source materials and closures to resist corrosion by typical reagents (oxygen, seawater, propellants, etc.) are conducted.

Shock, Vibration, Time at Temperature. The assembled heat source/ablator is tested, bare and installed in the system, to excessive flight level shock and vibration at temperature.

COMPARISON BETWEEN SAFETY REQUIREMENTS OF TERRESTRIAL AND SPACE SYSTEMS

The safety design requirements of terrestrial and space systems have much in common. The fundamental point of commonality is the fuel form, which is the first line of defense to any potential accident. Although the adverse environments characteristic of space systems are much more severe in magnitude than those of terrestrial systems, the thermal, mechanical, and chemical stability of the fuel is the primary safety consideration. A favorable fuel form should physically and chemically immobilize the radionuclide and resist degradation into respirable aerosols and larger particulates which can become airborne and interact with man via direct and indirect routes. Particulates of any fuel having sufficient specific activity to produce useful power can cause damage to tissue. Fuel tests, as described above, are an important input to the system designer, and a stable fuel will make his life easier and reduce the system cost and complexity.

Up to a dozen containment redundancies are found in some terrestrial systems which are not weight-limited. This constitutes an effective method of fuel immobilization. Weight-limited space systems cannot afford this luxury and must rely upon thermal and mechanical hardening by design ingenuity. Currently, one approach is configuration control to minimize the effects of thermal and mechanical transients. Although the requirements are similar, there is a basic dissimilarity between space and terrestrial systems in how containment is achieved.

The human factor is a problem shared by both terrestrial and space systems. Although the siting of some terrestrial systems can often minimize this problem, the unpredictable nature of human action after system deployment causes the user to employ cumbersome design and operational safeguards and procedures. The human factor causes about 33% of all missiles to fail and is the major cause of past accidents involving nuclear powered spacecraft. The unpredictability of human behavior combined with fuel cost prompts space system designers to investigate means to facilitate recovering heat sources after accidents or determine that they are beyond human access.

CONCLUSION

In conclusion, an attempt has been made in this paper to review the safety considerations and derive the safety design and test requirements for terrestrial and space radioisotope power systems. It is emphasized that these are general requirements and that they will vary somewhat depending upon the specific fuel, system, and application.

REFERENCES

1. Dix, G. P., Riggs, C.O., Hazards Summary Report 5-Watt Radiostrontium Generator for an Unattended Meteorological Station, February 1960.

2. Atomic Energy Research Establishment, Colloquium on Isotopic Thermoelectric Generators and Their Applications, January 30, 1968.

3. Code of Federal Regulations, Title 10, Part 71, Packaging of Radioactive Materials for Transport, July 27, 1966.

4. International Atomic Energy Agency, Regulations for the Safe Transport of Radioactive Materials, No. 6, 1967.

5. Code of Federal Regulations, Title 10, Part 20, Standards for Protection Against Radiation, April 5, 1966.

6. International Atomic Energy Agency, Basic Safety Standards for Radiation Protection, Safety Series No. 9, 1967.

7. Hagis W., Dobry T., Dix G., Nuclear Safety Analysis of SNAP III for Space Missions, American Rocket Society Journal, Vol. 31, No. 12, December 1961.

8. Dix, G. P., Future Considerations in Space Nuclear Safety, Twelfth Annual Meeting of the American Nuclear Society, June 21, 1966.

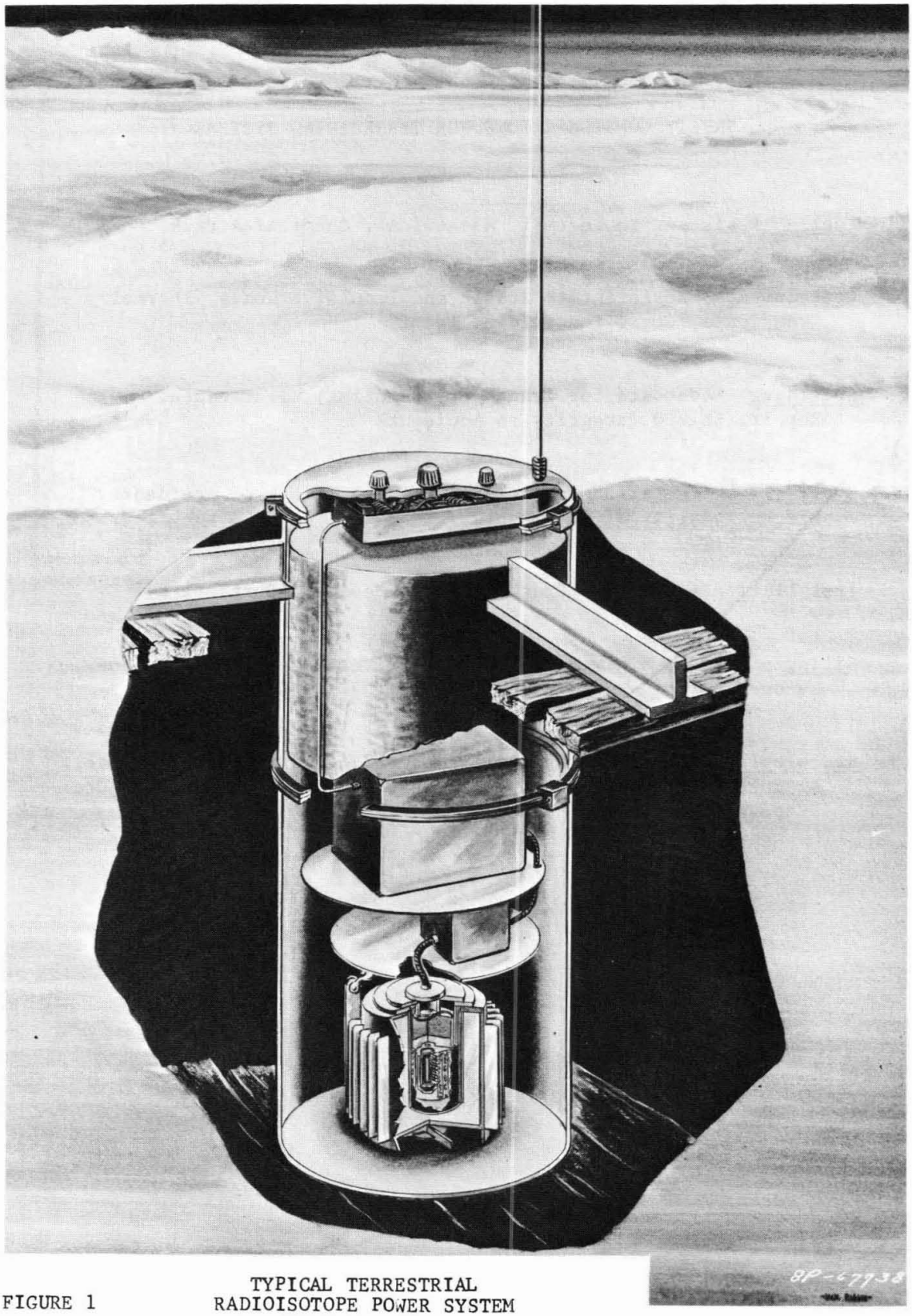

FIGURE 1 TYPICAL TERRESTRIAL RADIOISOTOPE POWER SYSTEM

FIGURE 2

SAFETY CONSIDERATIONS FOR TERRESTRIAL SYSTEMS

Fuel - Resistant to Thermal, Mechanical, Chemical Attack

Containment - Resistant to Static and Impulsive Loads, Thermal Transients, Corrosion, "Idiot Proof"

Shielding - Adequate for Transport, Handling, Maintenance, Repair, Shield Integrity in Accidents

System - Configuration Control to Minimize Effect of Accidents, Bifunctionality of Components

Installation - Preclude Unauthorized Access and Portability

Siting - Remote, Minimize Direct or Indirect Human Interactions, Recoverability

Radiological Control - Physically Secured, Clearly Marked, Protect Against Long Term Events, Ingenuity, Assure Effective Post-Use Disposal, Operational Procedures

FIGURE 3

SAFETY DESIGN REQUIREMENTS FOR TERRESTRIAL SYSTEMS

Fuel - High melting point; High strength; Minimal aerosols; Predictable; Reproducible

Containment - Redundant barriers; Resistant to overpressures, impact, fire, loss of thermal control, corrosion; Materials compatible with fuel; Compensates for internal pressures; Long term integrity

Shield - Maintains external doses to AEC limits; Integrity in accident

System - Design and materials minimize accident effects; Location and recovery aids; Component bifunctionality

Installation - Positive means of securing system; Prevention of direct access; Non-portable; Radiation markings

Site - Remote; Natural restrictions to public access; Selection to minimize accident probability

Operational Procedures - Procedures include clear responsibility, emergency plans, plans for installation, maintenance, disposal

FIGURE 4

SAFETY ANALYSIS AND TEST REQUIREMENTS FOR TERRESTRIAL SYSTEMS

Fuel -	Thermal Stability
	Dosimetry
	Mechanical Response
	Gas Evolution
	Solubility
	Aging
	Radiobiological Experiments
Containment -	Impact
	Puncture
	Fire
	Thermal Shock
	Pressures and Loads
	Leak Tests
	Corrosion
Shielding -	Dosimetry
	Shield Integrity

FIGURE 5
TYPICAL SPACE NUCLEAR POWER SYSTEM

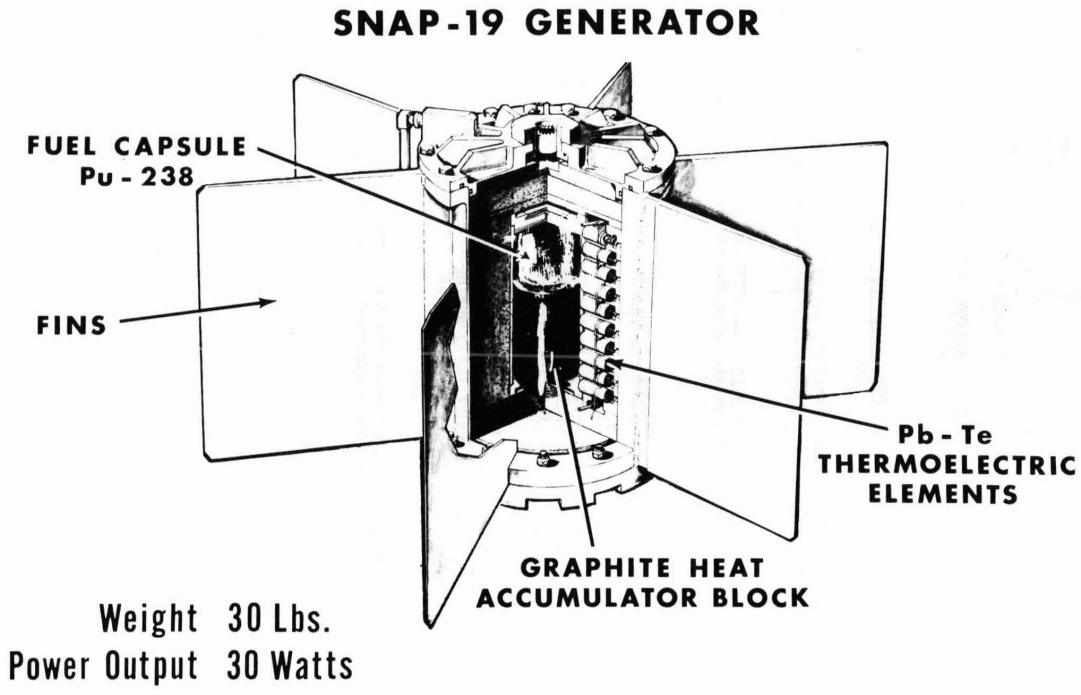

FIGURE 6

SAFETY CONSIDERATIONS FOR SPACE SYSTEMS

POTENTIAL ACCIDENTS

Launch Abort - Propellant fire and explosion; Impact on land or in ocean; Impact location controlled by range safety

Uncontrolled Random Reentry - Reentry heating, random impact on land (20%), or in sea and unpopulated polar regions (80%).

SAFETY CONSIDERATIONS

Fuel - Resistant to reentry heating, propellant fires, and impulsive loads; Minimize aerosols; Insoluble, not readily assimilated into man's environment over long term

Containment/System - Control configuration to minimize heating, impact effects; Containment during reentry and impact; Post-impact containment time maximized.

Radiological Control - Recovery and location aids; Controlled deorbit; Post-mission recovery or disposal beyond active biosphere.

FIGURE 7

SAFETY DESIGN REQUIREMENTS FOR SPACE SYSTEMS

Transport and Ground Handling - System and/or shipping container to AEC, DOT requirements

Fuel - Thermal, mechanical, chemical stability short and long term; High melting point, minimizes aerosols at and after impact; Insoluble; Predictable; Reproducible.

Containment - Containment during launch aborts, in orbit, reentry, earth impact; Accommodates internal pressure

Heat Source - Design and materials minimize effects of vibration, fire, shock, fragments, reentry, impact, corrosion

System - Location and recovery aids to facilitate return to radiological control

Spacecraft - Materials minimize thermochemical reactions on containment

Operational Procedures - Specify responsibility, authority and procedures for transport, ground handling, and emergencies

FIGURE 8

SAFETY ANALYSIS AND TEST REQUIREMENTS FOR SPACE SYSTEMS

Fuel -
- Thermal stability (fire, reentry)
- Mechanical stability (vibration, impact)
- Chemical stability (propellants, vacuum, air, seawater)
- Tested at temperatures
- Long and short term
- Dosimetry
- Radiobiological experiments
- Tests at temperature

Heat Source -
- Impact (terminal velocity, critical angle, various media)
- Propellant fire (fireball, afterfire)
- Reentry (stability, heating rate, ablation)
- Internal pressure or vent tests
- Dosimetry
- Corrosion
- Shock, vibration
- Leak tests
- Tests at temperature

RADIOISOTOPE REQUIREMENTS AND AVAILABILITIES FOR POWER APPLICATIONS

An Overview

George Y. Jordy
Wilton J. Lindsey
James A. Powers

Abstract

Firm and probable needs for radioisotopic power are given along with near and far-term availabilities. The following isotopes are considered: plutonium-238, curium-244, polonium-210, thulium-170, cobalt-60, promethium-147 and strontium-90. Plutonium-238 and curium-244 have limited near-term availability due to current shortage of feedstock; however, production could be increased in the early 1970's by irradiating feedstocks (neptunium-237 and americium-243) recovered from power reactor spent fuels. In contrast to the transplutonium isotopes, suitable feedstocks are readily available for polonium-210, cobalt-60 and thulium-170. Substantial production acceleration of cobalt-60 and thulium-170 could be achieved in about one year. The near-term availabilities of polonium-210, strontium-90 and promethium-147 are limited by the capability of AEC developmental facilities to perform separation, conversion and encapsulation operations.

George Y. Jordy is Assistant Director for Planning and Evaluation in the Division of Isotopes Development, Wilton J. Lindsey is Chief of the Production Reactors Branch in the Division of Production, and James A. Powers is Chief of the Space Isotopic Fuels and Materials Branch in the Division of Space Nuclear Systems of the U.S. Atomic Energy Commission, Washington, D. C.

INTRODUCTION

The primary sources of radioisotopes for power applications are the AEC production reactors and the commercial power reactors. The major radioisotopes are produced either through deliberate irradiation of target materials in these reactors or are recovered as by-products of the burnup of reactor fuels. One important isotope, plutonium-238, is to some extent, a combination product since its precursor, neptunium-237, is derived from burnup of uranium-235 fuel and is then deliberately irradiated as a target to make plutonium-238.

Predicting the availability of isotopes involves predicting the future operation of reactors. This is difficult, so availability forecasts are always hedged with qualifications and are generally shown as a range of possibilities. With the production reactors, there are two uncertainties: the number of reactors in operation and the fraction of their capacity that can be made available for isotopes after priority production demands are met. However, isotope production technology is well established and capability per reactor is known quite accurately. In the case of power reactors, production technology is still in a state of flux and the number and types of reactors that will be operating in the next two decades is quite uncertain. A further uncertainty is the extent to which fission products and neptunium-237 will be recovered during processing of power reactor spent fuels.

This paper includes a fairly detailed discussion of isotopes production and the most recent estimates of requirements. No attempt is made to compare the supply and demand for each isotope, because in most cases the potential supply is quite flexible and substitution of one isotope for another to meet a particular requirement is often feasible.

RADIOISOTOPE REQUIREMENTS

Requirements are defined as falling into three categories -- firm, probable and possible. Firm requirements are those which are associated with a scheduled event, e.g., delivery of a fueled system or carrying out a developmental test, and formalized by the AEC and the user agency in a letter agreement of some type. Probable requirements are those which are on a tentative schedule. In many instances there is a letter of interest from the user but generally the requirement is in the planning stages and beyond the current budget cycle. Possible applications are those which are quite speculative possibly because the mission itself is very tentative or in early planning, because another power system has been assigned to the mission, or because another isotope has been assigned to the program.

The isotope requirements have been defined after considering the needs of various agencies for electrical power in space, terrestrial and marine applications. In the case of space missions, the following classes of applications are attractive for isotope power systems:

NASA Missions

Manned	5-20 kwe
Communications	1-20 kwe
Lunar Surface	0.5-20 kwe
Planetary and Interplanetary Probes	0.1-2 kwe
NIMBUS	0.05-0.1 kwe

DOD

Manned	3-10 kwe
Communications	1-20 kwe
Navigational	0.03-0.10 kwe

For marine and terrestrial applications, radioisotope thermoelectric generators are being developed in the following power ranges:

Marine and Terrestrial Applications

Biomedical, Marine	1 watt electric
Navigational Aids, Relay Stations	10-100 watts electric

There are multihundred watt and kilowatt size requirements for terrestrial and marine applications also. The larger units will utilize dynamic conversion systems.

Strontium-90 and plutonium-238 are the primary candidates for terrestrial and space power requirements, respectively. Because of special characteristics, cobalt-60, thulium-170, polonium-210 and curium-244 are also under development for isotope power applications.

The possible terrestrial cumulative requirements for isotope power are shown in Table 1. These quantities are translated into kilograms of cobalt-60 and strontium-90 since these isotopes are being developed primarily for terrestrial use. However, it should be stated that because of cost and availability both isotopes are being considered for space applications. Cobalt is attractive for power applications in concentrations in the range of 200 to 400 curies per gram. At 300 curies per gram the specific power of cobalt-60 is 4.6 watts per gram and the power density is 40 watts per cubic centimeter.

Table 2 illustrates the firm and probable requirements for polonium-210. There are possible applications, depending on the outcome of DOD and NASA studies, which could add another 3 kilograms per year beginning in 1973. The firm requirement for polonium at this time is a SNAP-29 ground demonstration unit scheduled for December 1969. This test will utilize approximately 125 grams of polonium as a fueled heat source. The heat source will be used to power a 400 electrical watt unit for about 100 days. In the 1970-1971 time period, the quantities listed will be in support of developmental and possibly flight test units. It might be necessary to support scheduled flight missions beginning in 1972. The polonium-210 heat source program is based upon receiving irradiated bismuth which contains 50 to 100 curies of

polonium-210 per pound of bismuth. The availability, projected cost, radiation (weight) and power density are all advantages of polonium-210. However, the chemical activity of the polonium fuel form is such that concurrent development work is being performed on another isotope, i.e., thulium-170. While a need for both thulium-170 and polonium-210 is not foreseen at this time, if thulium-170 is selected instead of polonium, then requirements for thulium would be approximately 25 kilograms per year, in place of 2 kilograms per year of polonium-210, in the 1972-1976 time period.

Plutonium-238 requirements are shown in Table 3. Requirements for this isotope have been discussed in previous papers. The SNAP-27 heat source program will be finished in FY 1969. A large radioisotope heat source development unit will be delivered to NASA in 1971. This Table assumes the space use of kilogram units in the post 1975 time period.

Curium-244 is considered as an alternate, replacement, or possibly a supplement for plutonium-238. Requirements for other than developmental quantities for this material do not exist at present. Additional curium-244 technology development will be carried out over the next several years. Preliminary data indicates this isotope will be acceptable for isotopic power applications in the temperature range spanning thermoelectrics (1000°F) to thermionics (3000°F) applications.

PRESENT AND FUTURE AVAILABILITIES

Details of this subject are covered in subsequent paragraphs under the headings, Review of Production Methods, Production Problems, Production Plans and Future Availability. A brief summary of the current outlook is as follows:

Isotope	Production Potential
Cobalt-60	large in relation to expected demand
Thulium-170	large in relation to expected demand up to restriction imposed by supply of natural thulium
Polonium-210	potentially large in relation to expected demand but currently limited to existing facilities for chemical processing
Plutonium-238	current supply about equal to demand; production cannot be expanded until neptunium-237 feedstock becomes available from power reactors
Curium-244	only experimental amounts available at present; additional supply could become available in about four years; much larger amounts would depend on recovery of feedstock (americium-243) from power reactors

REVIEW OF PRODUCTION METHODS

Cobalt-60

This isotope is made by addition of a neutron to readily-available monoisotopic cobalt, cobalt-59. The AEC has a capability for producing hundreds of megacuries of cobalt-60. In May 1961, the AEC withdrew from the production and distribution of cobalt-60 of greater than 30 curies-per-gram specific activity (modified in 1965 to greater than 45 curies per gram) in view of industry capability to serve routine commercial applications such as teletherapy and radiography. The Commission recently withdrew from the production and distribution of cobalt-60 sources of 45 curies-per-gram specific activity and less, in light of private capability to produce such material.

High specific activity cobalt-60 (approximately 200 ci/g) could be produced in reactors having neutron fluxes as low as 6×10^{13} n/cm^2/sec, but 6 years would be required; to obtain 200 ci/g product in 3 years or less, a flux of 1×10^{14} or higher would be needed.

Thulium-170

This isotope is made by addition of a neutron to thulium-169, a rare earth. Thulium-170 could be supplied from AEC production reactors in up to megawatt quantities per year. The availability of thulium-170 depends upon the availability of thulium-169 target material, flux levels to produce the desired specific activity fuel form, and facilities to convert the irradiated targets into a usable isotopic source. Multi-kilowatt quantities of thulium-170 could be produced in existing commercial facilities on relatively short notice.

Polonium-210

This isotope is made by addition of a neutron to readily-available monoisotopic bismuth, bismuth-209. Because of the very low cross section for the reaction (0.019 barn), many tons of bismuth must be irradiated and processed to produce polonium-210 in large quantities. Furthermore, since its recovery cost is related to the amount of bismuth which must be processed, it is preferable to irradiate the bismuth at high flux levels to obtain as high as possible a concentration of polonium-210 in the bismuth target discharged from the reactor.

At present, there is no commercial capability to process polonium-210 or manufacture polonium-210 heat sources. Such capability exists only at Mound Laboratory and its encapsulation capability is currently limited. By 1969, however, the process facilities at Mound Laboratory will have been improved and a new facility for encapsulating polonium-210 will have been completed. Mound Laboratory will then have the capability to supply kilowatt quantities for developmental purposes. During the early 1970's, this capability will be expanded in order to support scheduled mission requirements.

Plutonium-238

Plutonium-238 is made by the addition of a neutron to neptunium-237. Neptunium-237 is a by-product formed in a reactor fuel element by (a) addition of a neutron to uranium-236 which may be formed in about 20% of the neutron captures by uranium-235 and (b) (n, 2n) reaction with uranium-238.

Since neptunium-237 is primarily a by-product of nuclear power generation, any increase in planned nuclear power generating facilities would increase the amount potentially available from that source. If the neptunium-237 expected to be available from the commercial reprocessing of power reactor fuels is recovered and accumulated and then irradiated in government or private reactors to produce plutonium-238, the total annual supply of plutonium-238 in the late 1970's could increase rapidly. Thus, recovery of neptunium-237 from irradiated power reactor fuel could make a major contribution to the future availability of plutonium-238 for isotopic applications.

Curium-244

This isotope is made by addition of a neutron to americium-243. Americium-243 is produced by a series of neutron additions, starting with plutonium-239. These reactions can be carried out deliberately in a production reactor, preferably at high flux to shorten the time required, or advantage could be taken of the fact that they will take place automatically in power reactors when fuel is taken to high burnup projected for the future. The power reactor source has potential for greatly increasing the supply and reducing the cost of americium-243, but two problems have to be dealt with: (a) facilities will have to be added to the commercial plants which reprocess power reactor fuel in order to recover americium-243, and (b) as recovered, americium-243 will be mixed with americium-241 from which it cannot be separated economically. Irradiation of the mixture will result in a mixture of curium-242 and curium-244 that also is inseparable as a practical matter. One solution would be to store the 242/244 mixture until the short-lived curium-242 (half-life, 163 days) largely decays away to plutonium-238, leaving a mixture of long-lived curium-244 (half-life, 18 years) and the still longer-lived plutonium-238 (half-life, 89 years) which could be separated, if desired.

At present, there are no large-scale facilities for fabricating americium-243 into targets or for separating the targets after irradiation. The current separation of curium-244 at Savannah River, which will recover about 5 kgs, is being carried out in pilot scale equipment. No expansion of the Savannah River facility is contemplated unless firm requirements for curium-244 develop.

PRODUCTION PROBLEMS

Production problems for the reactor-produced isotopes range from minor to major, depending on the isotope:

Cobalt-60

For cobalt-60, there are essentially no problems; target material is readily available, permanent encapsulation can be done in a cold condition prior to irradiation and the cobalt-60 can be ready to use when it leaves the reactor. Irradiation is practical in power reactors for specific activities up to about 100 curies per gram, and in production reactors up to about 400 curies per gram.

Thulium-170

For thulium-170, the only apparent problem is the preparation of oxide targets of sufficient strength that they can be handled without breaking during post-irradiation encapsulation. Specific activity in the 1 to 2 watts/gram range are feasible, depending on the flux level available. Prompt handling is essential because of short half-life (125 days).

Polonium-210

Production of large quantities of polonium-210 is, as a practical matter, restricted to the AEC reactors at Savannah River and Richland where substantial in-reactor space can be made available. The nuclear cross section of bismuth is so low that large amounts of target material must be accommodated. This large bulk is also a problem after irradiation when untransmuted bismuth must be separated from the polonium-210 products by chemical processing. Short half-life (138 days), very high specific power (141 watts per gram), and intense alpha activity also complicate the separation process. The current limitation on polonium-210 production is the capacity of the planned separation facilities at Mound Laboratory which will be able to handle about 3 to 6 kgs per year in the early 1970's.

Plutonium-238

Neptunium feedstock for plutonium-238 production is obtained primarily as a by-product, being recovered during chemical processing of spent fuel from AEC production and test reactors. Short of deliberate burnup of additional uranium-235, very little can be done to enhance the neptunium supply, and AEC efforts to increase production have been adversely affected by the shutdown of seven out of 14 production reactors during recent years. Beginning about 1971, recovery of neptunium from power reactor fuel will be possible and there is potential for a rapidly increasing supply in future years, as discussed in a later section. However, because conversion of neptunium is a cyclic process, in which only about 20% of available inventory can be transmuted to plutonium-238 each year, it will be about 1975 before power reactors could significantly add to the plutonium-238 supply. After that, production could increase very rapidly.

Curium-244

Curium-244 has not yet been produced on a large scale, but the current experimental production campaign at the Savannah River Plant is providing useful experience as well as sufficient curium for experimental use. The apparent production problems are: (a) preparation of feedstock (americium-243) is slow and expensive under current circumstances, and (b) substantial investment will be required for construction of target preparation and chemical separation facilities. Americium-243 is potentially recoverable from spent power reactor fuel and if this is economically attractive, a rapidly increasing production of curium-244 is possible.

PRODUCTION PLANS

AEC production plans will continue to be responsive to four principal factors: (a) ability and willingness of private producers to meet some or all of the requirements at reasonable prices, (b) availability of funds for production operations and construction of facilities, (c) availability of space in the production reactors, and (d) requirements for the isotopes.

In the case of cobalt-60, AEC has recently withdrawn from production in favor of private industry and, in the future, would be a supplier only under special circumstances, primarily if private production were inadequate. AEC has no plans for large-scale production of thulium-170 but the capability exists if such demands should develop. Polonium-210 will be produced in existing facilities at rates in the 1-3 kg per year range. Plutonium-238 will continue to be produced with feedstock available from AEC reactors. Purchase of neptunium from power reactors is being considered. AEC has no current plans to produce curium-244 and future arrangements will depend to a considerable extent on the outcome of research and development work with curium-244 from the experimental production run. The AEC's present nominal capacities to provide strontium-90 and promethium-147 are about 14 kilograms (2 million curies) and 1.1 kilograms (3.0 million curies) per year, respectively, as encapsulated source. The potential supplies of crude strontium-90 and promethium-147, separated from other fission products originating at the Hanford site in the chemical processing of reactor fuels, are not limited to these amounts; the limiting capacity is that concerned with processing these feed to usable forms, such as strontium titanate and promethium oxide, and encapsulating these materials as heat sources. These latter functions are performed at the Oak Ridge National Laboratory's Fission Product Development Laboratory for strontium-90 and at the Pacific Northwest Laboratory for promethium-147. Requirements for these fission products are presently being satisfied from accumulated inventories.

FUTURE AVAILABILITY

A continuing study of the future quantities of various isotopes potentially recoverable from spent fuels discharged from U.S. nuclear power reactors is carried out for the AEC's Division of Isotopes

Development by the Systems Engineering Department of the Pacific Northwest Laboratory. Such projections involve consideration of the following: (a) the number and types of reactors that will be operating, (b) the method and schedule of their operation, and (c) the detailed composition of spent fuels for both startup and equilibrium fuel cycles.

The projection of isotope production and availability from power reactors is, of course, more dependent on the assumed nuclear power growth than any other parameter. The current AEC projection (1) is for 120 to 170 thousand net electrical megawatts of installed nuclear capacity by 1980 with the best estimate at 150 thousand net electrical megawatts. This is taken as the basis for the projection used in this study, which increases to 500,000 electrical megawatts installed at the end of 1990.

The annual and cumulative installation of nuclear capacity used in this study are given in Table 4. It is recognized that the annual figures contained in Table 4 differ somewhat from those of the referenced forecast. This is primarily due to two factors: (a) subsequent slippages in the dates at which various nuclear plants under construction or definitely planned are expected to become operational and (b) smoothing of the growth curve. The differences, however, are considered to be within the range of uncertainty of the referenced projection and do not constitute a basis for a "new" forecast.

Certain other pertinent assumptions and ground rules are summarized: (a) installed nuclear capacity and isotope production and availability are stated as of the end of the year, (b) yearly nuclear capacity additions start up at midyear, (c) nuclear power plant life is thirty years, (d) nuclear power plant capacity factor of 85% during the first fifteen years of plant life, declining linearly to 50% at the end of plant life, (e) one year elapses between reactor discharge and isotope recovery, (f) chemical processing recovery efficiency of 98% for plutonium and uranium, (g) by-product recovery efficiency of 90%, (h) promethium-147 and curium-244 final purification delayed three years after fuel discharge to allow for promethium-148 and curium-242 decay, respectively, and (i) plutonium-238 formed by curium-242 decay, except for that formed during the first year (following fuel discharge and prior to fuel processing), is recovered at the time of curium-244 final purification.

The installed civilian nuclear capacity is assumed to be wholly composed of 1000 eMW light water reactors. The fuel discharge histories used for installations prior to 1980 are typical of the Brown's Ferry boiling water reactor (BWR) and the Diablo Canyon pressurized water reactor (PWR). A more advanced design for both the BWR and PWR in which the specific power is increased approximately 15% is assumed for the post seventy period.

Two cases are presented: one in which the plutonium recovered from spent fuel is not recycled; in the other in which the recovered plutonium is blended with natural uranium and recycled in 1000 eMW light water reactors operating exclusively on this type of fuel cycle

throughout their 30-year lives. Plutonium recycle reactors are installed at a rate consistent with minimizing x-reactor plutonium inventory. It is assumed that one year after spent fuel discharge, plutonium is recovered and available for reactor charging as fabricated plutonium enriched fuel. Plutonium recycle is of particular interest in considering radioisotope production since it is plutonium that is the source of the americium and curium isotopes.

In a period of rapid growth, such as is predicted for the next two decades, reactor startup cycle effects are quite significant. The projected new capacity additions for each year range from over 100% to no less than 10% of the previously existing capacity through the year 1990. Hence, there is always a significant fraction of capacity in the startup phase during this period. The calculation of isotope production and availability from power reactors should therefore reflect the effects of low fuel exposure conditions during startup cycles.

The annual availabilities (a year after spent fuel discharge) of incidentally produced neptunium-237 and the americium (Am-241 and Am-243) are given in Tables 5 and 6 for the years 1970, 1975, 1980, 1985 and 1990. Plutonium recycle reduces the uranium-236 formation since it displaces the in-reactor inventory of uranium-235 and increases that of plutonium. This has the effect of reducing neptunium formation from neutron capture by uranium-236 while increasing that of americium. Concomitantly, the recycled plutonium contains a greater fraction of higher isotopes, thereby increasing the in situ plutonium-242 inventory and markedly enhancing the formation of americium-243 relative to americium-241 as shown in Table 6.

The plutonium-238 potentially available from three sources: (a) neptunium-237 target irradiation, (b) decay of curium-242 in the curium recovered from spent fuels, and (c) decay of curium-242 produced in americium target irradiation is given in Table 7. The principal source of plutonium-238 is from neptunium-237 target irradiation. Neptunium-237 availability is converted to plutonium-238 availability on the assumption that prior to 1981 neptunium targets are irradiated in AEC facilities and in power reactors thereafter. Only a relatively small amount of plutonium-238 is obtained from the 163 days half-life curium-242 decay during the two-year aging of curium recovered from spent fuels. This quantity could be increased, possibly doubled, since a rather conservative assumption was adopted that the first year's decay of curium-242 would not be recoverable (lost to other plutonium isotopes).

The irradiation of americium targets results in two products: curium and plutonium-238. Plutonium-238 is formed when the curium-242 (produced from americium-241 neutron capture) decays during the assumed one-year target irradiation and the two-year aging period between target irradiation recovery of the product. This aging period is required to reduce the activity of the curium for processing and to stabilize the activity in the curium-244 product. The production of high purity plutonium-238 is difficult because of the partial decay of americium-242 to plutonium-242.

The curium-244 potentially available from two sources: (a) directly from spent fuel, and (b) americium target irradiation is given in Table 8.

Annual availability summaries for promethium-147 and strontium-90 recovered from spent power reactor fuels are given in Tables 9 and 10.

COST AND ECONOMIC CONSIDERATIONS

The cost of producing isotopes for power sources depends on so many factors that it is necessary that we define our assumptions before proceeding with further discussion. First, it is assumed that production will be carried out in government-owned facilities, primarily the existing production reactors at Savannah River and Richland, along with related facilities for fuel fabrication and separation. To the extent that suitable facilities for target preparation and separation do not exist at these or other AEC sites, it is assumed they will be built. Second, it is assumed that the scale of production will be large or, alternatively, if the production rate is not sufficient to require the exclusive use of a whole reactor, other products will be made in the remaining space and will pay a proportionate share of operating costs. Third, it is assumed that the isotopes are being produced for transfer to another Federal agency at costs computed in accordance with current accounting practices.

Even with these limitations, it is difficult to project manufacturing costs for radioisotopes without defining amounts and specifications and also assuming that favorable circumstances will exist in the AEC production complex at the time in question. For example, unfavorable circumstances would be additional shutdowns of AEC production reactors or need for all reactor capacity for programs other than production of radioisotopes. Another possible problem would be inability to obtain funds for construction of target handling facilities which are quite limited in some cases. However, to meet the need for cost information that can be used for comparing one isotope with another and with competitive sources of heat energy, all of the necessary favorable assumptions have been made and manufacturing cost goals for the major radioisotopes have been developed which reflect what might be achievable over production campaigns of reasonable size and length.

The following cost goal ranges have been estimated for large quantities produced over campaigns of appreciable length for use by Federal agencies. These intergovernment charges do not include final encapsulation or several factors such as depreciation and profit which must be included in commercial prices.

Isotope	Manufacturing Cost Goal Range $/Thermal Watt
Cobalt-60	7 - 25
Thulium-170	10 - 25
Polonium-210	10 - 25
Plutonium-238	500 - 700
Curium-244	100 - 500

These estimates assume that the isotopes are produced, processed (if necessary), converted to a fuel form (if necessary) and sealed in a primary containment capsule. In some cases, such as cobalt-60 and thulium-170, the initial encapsulation applied before irradiation may be all that is necessary.

REFERENCE

"Forecast of Growth of Nuclear Power," WASH-1084, December 1967.

Table 1

Cumulative Terrestrial Power Requirements

Year	1970	1972	1974	1976	1978	1980
Requirements (kw)	10	30	50	75	100	125
Requirements (kg)						
Strontium-90	10	31	52	78	104	130
Cobalt-60	0.57	1.7	2.9	4.3	5.7	7.2

Table 2

Estimated Firm and Probable Space Requirements for Polonium-210 through 1976
(kilograms)

	1969	1970	1971	1972	1973	1974	1976	1978	1980
Annual Requirements	0.3	0.7	1	2	2	2	2	2	2
Cumulative Requirements	-	1.0	2	4	6	8	12	16	20

Table 3

Estimated Firm and Probable Requirements for Plutonium-238 through 1980
(kilograms)

	1969	1970	1971	1972	1973	1974	1976	1978	1980
Annual Space Requirements	5	20	33	22	26	30	115	120	120
Annual Other Requirements	4	4	6	10	10	10	10	10	10
Total Annual Requirements	9	24	39	32	36	40	125	130	130
Cumulative Requirements	-	33	72	104	140	180	400	660	920

Table 4

Estimate of Cumulative Capacity of Domestic Civilian Nuclear Power Plants

Year Ending	10^3eMW	Year Ending	10^3eMW
1960	0.3	1975	70
1961	0.5	1976	83
1962	0.5	1977	97
1963	0.6	1978	112
1964	0.6	1979	130
1965	0.6	1980	150
1966	1.0	1981	174
1967	1.0	1982	200
1968	3.0	1983	230
1969	5.7	1984	261
1970	12	1985	296
1971	23	1986	332
1972	34	1987	371
1973	45	1988	411
1974	57	1989	454
		1990	500

Table 5

Neptunium-237 Annual Availability from Spent Power Reactor Fuels
(kilograms/yr.)

	Without Pu Recycle	With Pu Recycle
1970	15	15
1975	375	375
1980	1220	1130
1985	2580	2290
1990	4520	3860

Table 6

Americium Annual Availability from Spent Power Reactor Fuels
(kilograms/yr.)

	Without Pu Recycle		With Pu Recycle	
	Kgs.	% Am-243	Kgs.	% Am-243
1970	3	57	3	57
1975	88	57	88	57
1980	290	57	620	63
1985	550	57	2170	65
1990	840	55	5330	69

Table 7

Plutonium-238 Annual Availability from Power Reactor By-Products (kilograms/yr.)

	Neptunium Target Irradiation	Curium Aging	Americium Target Irradiation	Total
Without Pu Recycle				
1970	6	0	0	6
1975	75	1	2	78
1980	481	5	29	515
1985	583	11	81	675
1990	1192	16	157	1365
With Pu Recycle				
1970	6	0	0	6
1975	75	1	2	78
1980	467	7	36	510
1985	534	25	186	745
1990	1050	59	536	1645

Table 8

Curium-244 Annual Availability from Power Reactor Spent Fuels and By-Products (kilograms/yr.)

	Recovered From Fuel	Americium Target Irradiation	Total
Without Pu Recycle			
1970	0	0	1
1975	3	1	4
1980	25	20	45
1985	55	65	120
1990	65	135	200
With Pu Recycle			
1970	0	0	1
1975	3	1	4
1980	53	27	80
1985	280	175	455
1990	720	600	1320

Table 9

Aged Promethium-147 Annual Availability from Power Reactor Fuels
(kilograms/yr.)

1970	2
1975	36
1980	190
1985	490
1990	1000

Table 10

Strontium-90 Annual Availability from Power Reactor Fuels
(kilograms/yr.)

	Without Pu Recycle	With Pu Recycle
1970	19	19
1975	522	522
1980	1450	1360
1985	3180	2910
1990	5890	5210

RADIOISOTOPES FOR POWER APPLICATION

J. S. Griffo

Abstract

The decay energy of selected radioisotopes provides a unique source of heat which can be coupled with static and dynamic power conversion units to provide useful quantities of electrical energy. Based on selection criteria the fission and neutron produced isotopes ^{238}Pu, ^{210}Po, ^{244}Cm, ^{170}Tm, ^{90}Sr, and ^{147}Pm are primary contenders for potential use in heat sources for space applications. Currently, major effort in the Space Nuclear Systems Division is directed toward the development of fuel forms of ^{238}Pu, ^{210}Po, and ^{244}Cm. This paper provides a brief evaluation of the potential of these isotopes and how this potential is determined from their properties.

J. S. Griffo is an isotopic fuels specialist with the United States Atomic Energy Commission, Washington, D.C.

The United States Atomic Energy Commission supports a number of projects directed toward exploiting the unique source of energy provided by the decay of radioisotopes for space, terrestrial and marine power applications. The first space electric power generators were fueled with plutonium 238 and were used for navigational aid purposes. The first terrestrial power systems used strontium 90 heat sources and were placed in several marine and remote terrestrial sites for use in navigational beacons, weather buoys and polar region unattended weather stations. These early devices have been invaluable in demonstrating the reliability of isotopic power. The method whereby thermoelectric power is obtained from isotopic heat energy is illustrated on Fig. 1. The fundamental design of this generator is relatively simple, consisting of a centrally located isotopically fueled heat source; thermoelectric elements for conversion of heat to electrical energy; and electrical taps to which the thermoelectrics are connected in series to provide for integration of the unit into a desired electronic system.

Basically, similar criteria apply in the selection of isotopic fuels for terrestrial or space applications. Isotopic availability, cost, half-life, radiation characteristics, and the potential for conversion to stable compounds are principal factors in defining specific fuels for given mission requirements. However, in considering total mission requirements conditioned by environmental requirements, obvious differences between space and terrestrial applications demand more rigorous specifications to be imposed upon space fuels and power systems. As, for example, a weight factor acceptable for terrestrial sources may be prohibitive for space applications which may be best served using a fuel of greater specific power and requiring less shielding. By the same token, a radiation factor that can be hazardous with respect to manned space missions as well as disastrous to sensitive scientific equipment placed onto space vehicles for long-term operation may be perfectly acceptable in many terrestrial applications. In general, the operating environments reflecting requirements for intact space power sources are presented in Fig. 2. It is apparent that under these conditions a power capsule must be a self-contained, integrated system in itself. Ideally, both the clad and capsule contents, consisting of a stable fuel form, should be capable of surviving extreme conditions portrayed in this Figure. In the event of capsule rupture or loss of containment, the developed fuel form should provide the thermal, mechanical and chemical stability required to maintain the release of radioactive materials to within rigorously specified limitations. Briefly stated then the fueled capsule designed to operate at a specified temperature (500° - 2500°F) for a given mission period which may range in time from a few months to several years must also be capable of surviving a launch pad fireball, reentry thermal pulse followed by earth impact, or exposure to aqueous environment. Under these conditions, in the event that recovery is not a requirement, the mode of disposition should present no hazard due to controlled release of radioactive material.

With appropriate emphasis then placed on each of the described selection criteria, Table 1 lists candidate space fuels currently considered for advanced development for power applications. As mentioned previously, ^{90}Sr has been primarily applied and is being further developed in the form of the titanate for terrestrial power requirements. However, since this isotope continues to be attractive because of its low cost and availability, it is retained as a potential space fuel candidate. The major disadvantage for space applications stems from the high energy radiation associated with the isotope. Strontium 90 has a decay daughter, ^{90}Y, in secular equilibrium which emits a very high energy beta particle (2.27 Mev). The intense, high energy beta activity of ^{90}Y, as well as softer beta of ^{90}Sr (approximately 0.5 Mev), results in high energy bremmstrahlung. This would, therefore, require thick shielding or result in a certain amount of inconvenience in remote handling equipment and procedures that would be required on the launch pad. A highly reliable capability for intact reentry would also appear to be required if ^{90}Sr is to be used in space missions. The power density of the typical strontium fuel form, the titanate, is approximately 1.0 W_t/cc based on the density value currently obtained (approximately 4.5 g/cc) by hot pressing techniques.

Promethium 147 may be considered as a pure beta emitter since it has only one step in its decay scheme to stable ($t_{\frac{1}{2}}$ = 10" yr) ^{147}Sm. The energy of the beta emission is relatively low (maximum value approximately 0.23 Mev), therefore, the bremsstrahlung will have low energy. However, in the irradiation process, energetic gamma emitting 42 day ^{148}Pm is formed by neutron capture of ^{147}Pm. Additionally, gamma radiation can be expected from trace amounts of ^{146}Pm which is also present. Promethium 146 has a short half-life of about 1.9 years which approximates that of ^{147}Pm. For ^{148}Pm, with its half-life of 42 days, aging for about one ^{147}Pm half-life is sufficient to reduce the total shielding requirements to about that which would be expected for shielding bremsstrahlung and gammas from ^{147}Pm and ^{146}Pm. The disadvantage of this process, however, is that the quantity of ^{147}Pm is also reduced by approximately fifty percent which additionally mitigates against cost and availability. Currently, ^{147}Pm has been used to fuel a fifty thermal watt microthruster for space applications and a sixty-five thermal watt Air Force inertial guidance heater. In subsequent fiscal years through 1970 one thermal kilowatt per year is programmed for use in R&D programs. The Air Force is forecasting a potential heater requirement utilizing 13 thermal kilowatts per year, beginning in 1969. The power density of the sesquioxide fuel form as currently produced containing 82 w/o ^{147}Pm is 1.8 watts/gram.

In contrast to ^{90}Sr and ^{147}Pm, which are obtained as fission products, ^{170}Tm with a half-life of 0.35 years is a neutron product produced by irradiation of natural ^{169}Tm. Gamma emission from ^{170}Tm also includes bremsstrahlung from beta particles emitted with energies of 0.969 and 0.885 Mev. Bremsstrahlung for ^{170}Tm emitted in the energy range of 0.2-0.77 Mev is equivalent to the low energy bremsstrahlung from ^{90}Sr (0.5-0.8 Mev); however, the shielding required for ^{170}Tm is less than for ^{90}Sr due to additional higher energy radiation (1-2 Mev) associated with ^{90}Sr. The common fuel form of ^{170}Tm is the sesquioxide having a practical specific power of approximately 2.4 watts/gram.

Preliminary synthesis and characterization studies of thulium fuel forms funded by the AEC's Division of Isotopes Development are directed toward establishing the feasibility of thulium oxide as a space fuel for operation at temperatures up to 1500°C, for periods of 180 days. Considering the power density and radiation characteristics of ^{170}Tm, as compared with ^{210}Po, it is not impossible that this fuel may serve as an alternative to ^{210}Po for short-term space applications.

However, since currently alpha emitters are preferred over beta emitters for use in space heat sources because of their higher specific power and more favorable radiation characteristics, major emphasis is presently placed on the development of fuel forms of ^{210}Po, ^{238}Pu, and ^{244}Cm.

The radiation characteristics of ^{238}Pu are especially attractive. These characteristics have made plutonium a prime candidate for biomedical applications. The gamma radiation associated with ^{238}Pu is quite minimal, the abundance of primary gamma being 10^{-4} times that of the alpha radiation. Additionally, the most abundant gamma radiation has practical energies in the order of 150 kev and should be readily shielded by the isotope containment material. Penetrating gamma radiation is essentially nonexistent from the ^{238}Pu isotope. However, ^{236}Pu, which is present as an impurity in parts per million concentration, does have a hard, gamma-emitting daughter product, ^{208}Tl. This radiation must be taken into account in designing large ^{238}Pu heat sources if radiation sensitive instruments are to be located in close proximity to the source. Neutron radiation is also present as a result of a 10^{10} year spontaneous fission half-life and (alpha, n) reactions with oxygen in the PuO_2. Although nothing can be done to alter the emission rate of the spontaneous fission neutrons, oxygen exchange reactions have been investigated to produce plutonium dioxide which is depleted in the ^{17}O and ^{18}O isotopes. Experiments have shown that a tenfold reduction in the abundance of the ^{17}O and ^{18}O as compared to their natural abundance will reduce the neutron radiation by a factor of 4 or 5, or essentially to that of the spontaneous fission background.

Because of its half-life, cost and availability, ^{238}Pu is being considered for space missions of extended duration (two years and beyond) or for those applications where fuel recovery is possible. Power levels for these various missions range from a few hundred thermal watts to thermal kilowatts.

To quote an example, the AEC has agreed to provide 50 kilograms of ^{238}Pu to NASA in an effort to ground test an isotope-powered Brayton engine. This test is to begin in 1972 and should play a very important role in the future application of kilowatt size heat sources. This quantity of fuel represents a considerable financial investment on the part of the Government and, therefore, as shown in Table 2, the recovery and reuse of plutonium at the end of each mission is extremely desirable. The use of plutonium under these conditions would amount to less than one dollar per thermal kilowatt hour. However on including the cost and efficiency of the conversion unit, and additional costs of recovery and fuel reprocessing following recovery, the cost of ^{238}Pu isotopic power could range anywhere from $5 to $20 per electrical kilowatt hour.

Now considering fuel forms of ^{210}Po and ^{244}Cm, both isotopes have favorable properties, based on the previously described selection factors, that are being further developed to realize their full potential for space applications. Polonium 210, with a half-life of 138 days, a specific power of 144 watts per gram, and with relatively soft gamma radiation having maximum energy in the range of approximately 0.8 Mev, is desirable for short-term missions of a few weeks to several months in duration. This isotope is a neutron product readily prepared in reactors by irradiation of ^{209}Bi to ^{210}Bi which decays by a beta emission with a half-life of 5.4 days to ^{210}Po. Although currently the production of relatively small amounts in the order of a few hundred grams per year is sufficient to support the development work being conducted on polonium fuels, no major problems are anticipated in scaling up to kilogram quantities in the early 1970 time period. It is further tentatively estimated that by the mid-seventies time period, capability should exist to enable fabrication of heat sources at a cost of approximately $\$20/W_t$ for the encapsulated isotope.

The rare earth polonides with melting points of up to $2200^{\circ}C$ represent the most stable compounds of ^{210}Po and currently gadolinium, along with several other rare earth polonides are being actively investigated for the development of composite and microsphere fuel forms. With respect to thermal stability and resistance to oxidation, the hollow microsphere composite fuel form shown in Fig. 3 appears to offer greatest potential for high temperature applications. Briefly described, this concept entails the application of a rare earth polonide onto hollow microballoon substrate by vacuum vapor deposition. Subsequently, a thin protective layer is applied onto the fueled surface prior to application of a strength member, and an oxidative coating followed by compaction. This fuel form is still in the developmental phase. However, when it is completed it should provide for the three major features including fuel containment, helium retention in the central voids of each microsphere and high temperature stability including resistance toward oxidation.

Curium 244, with a half-life of 18 years, has five times the power density of ^{238}Pu and has more attractive thermal characteristics for isotopic power applications. Being an alpha emitter with a power density of approximately 2.6 watts per gram renders the isotope sufficiently suitable for both thermoelectric and thermionic power applications. For this reason, ^{244}Cm has greater performance potential for space applications as compared to ^{238}Pu. Over a period of the next few years, several kilograms of ^{244}Cm are planned to be used to better evaluate the applicability of this isotope for various heat source applications. The fuel form development activities with ^{244}Cm closely resemble those presently in progress with ^{238}Pu. A sol-gel process is being considered for production of microspheres as well as the development of composite fuel forms that may further immobilize the radioisotope under operating conditions. More radioactive than ^{238}Pu by a factor of 5 with respect to alpha radiation and by several orders of magnitude from the standpoint of neutron dose rates, it is expected that curium will be more difficult to process and will require considerably more radiation shielding.

As with ^{238}Pu, program plans for ^{244}Cm are synchronous with the planned availability from power reactor operations. A recent Pacific Northwest Laboratory study indicates that the availability of ^{244}Cm will be quite limited until the middle to late 1970's and this schedule should give us adequate time to accomplish the very difficult task of fuel form development and chemical process development necessary to arrive at economical and efficient production methods.

Curium could conceivably be used in many space missions for which ^{238}Pu is currently assigned. For missions whereby radiation is not of concern, ^{244}Cm heat sources would certainly be lighter than plutonium sources. Estimated future costs of curium range from $100 to $500 per thermal watt. Obviously, the cost is of great significance. Without fuel recovery, and if the $500 per watt cost estimates are accurate, ^{244}Cm would have initial cost advantages over ^{238}Pu. With fuel recovery, however, and considering the differences in half-life, curium costs are comparable to those of ^{238}Pu.

Table 3 shows some of the SNAP units for which heat sources have been supplied fueled with plutonium and curium isotopes. Polonium 210 is not shown on this list but currently the isotope is planned for use with the SNAP 29 unit which is presently being developed. Therefore, to summarize in general, although the main emphasis on isotope selection and fuel form development is currently placed on the alpha emitters ^{238}Pu, ^{210}Po and ^{244}Cm, the alternate isotopes ^{90}Sr, ^{147}Pm and ^{170}Tm are still considered primary contenders for space applications. Strontium fuel forms have provided service in terrestrial isotopic power generators, promethium has been used to fuel and test a micro-thruster for space applications and, recently, further efforts have been directed toward investigating fuel forms of ^{170}Tm.

Current efforts are directed toward establishing new fuel forms of predictable and reproducible properties and to make these products available for higher temperature space applications required to enhance systems safety and power requirements. Fundamentally, this work entails fabrication, extensive characterization, and safety testing in the development stages prior to scale-up and production of space qualified fuel forms, and it is some of the results and details of these studies that will be described in the following papers to be presented during this session.

References

1. J. A. Powers, "Considerations in the Use of Actinides as Power Sources," ACS presentation, April 5, 1968.

2. P. K. Smith, J. R. Keski, C. L. Angerman, "Properties of Thulium Metal and Oxide," Savannah River Laboratory, Report DP-1114, June 1967.

3. S. J. Rimshaw, E. E. Ketchen, "Curium Data Sheets," Oak Ridge National Laboratory, Report ORNL-4187, December 1967.

4. H. T. Fullam, H. H. VanTuyl, "Promethium Isotopic Power Data Sheets," Pacific Northwest Laboratory, Report BNWL-363, February 1967.

5. "Plutonium 238 and Polonium 210 Data Sheets," Mound Laboratory, Report MLM-1441, November 9, 1967.

6. S. J. Rimshaw, E. E. Ketchen, "Strontium 90 Data Sheets," Oak Ridge National Laboratory, Report ORNL-4188, December 1967.

7. E. D. Arnold, "Handbook of Shielding Requirements and Radiation Characteristics of Isotopic Power Sources for Terrestrial, Marine, and Space Applications," ORNL-3576, April 1964.

8. "Radioisotopes Production and Development of Large Scale Uses," U.S. Atomic Energy Commission, WASH No. 1095, May 1968.

Table 1

Candidate Space Fuels

Isotope	Half-Life (Years)	Chemical Form	Melting Point (°C)	Practical Power Density (Watts/cc)	Significant External Radiation	Shielding Requirement	Cost Range $/Thermal Watt	Possible Availability Kwt/Year 1975-1980	Production Method
Sr^{90}	28	$SrTiO_3$	1910	1	Gamma	Heavy	25-30	700	Fission Product
Pm^{147}	2.6	Pm_2O_3	2130	1.8	Gamma	Minor	200-600	25	Fission Product
Tm^{170}	0.35	Tm_2O_3	2377	9.6	Gamma	Moderate	10-25	> 1000	Neutron Product
Pu^{238}	87.5	PuO_2	2240	2.6	- -	Minor	400-700	150	Neutron Product
Po^{210}	0.38	RePo	14-2200	45	- -	Minor	10-25	> 1000	Neutron Product
Cm^{244}	18	Cm_2O_3	20-2200	13	Neutrons	Moderate	100-500	> 10	Neutron Product

September 4, 1968

Table 2. Plutonium 238 Isotopic Power Costs

With Fuel Recovery

Efficiency of Conversion Unit (%)	Average Cost ($/$kw_e$ hr.)
5	9.2
10	4.6
20	2.3

Without Fuel Recovery

Mission Length (Years)	Efficiency of Conversion Unit (%)	Average Cost ($/$kw_e$ hr.)
2	5	580
	20	145
5	5	320
	20	80

Table 3. SNAP Uses of Actinides

Unit	Isotope	Thermal Power (W_t)	Electric Power (W_e)
3	Pu-238	55	3
9	Pu-238	535	20
11	Cm-242	900	20
13	Cm-242	300	20
19	Pu-238	570	25
27	Pu-238	1500	60

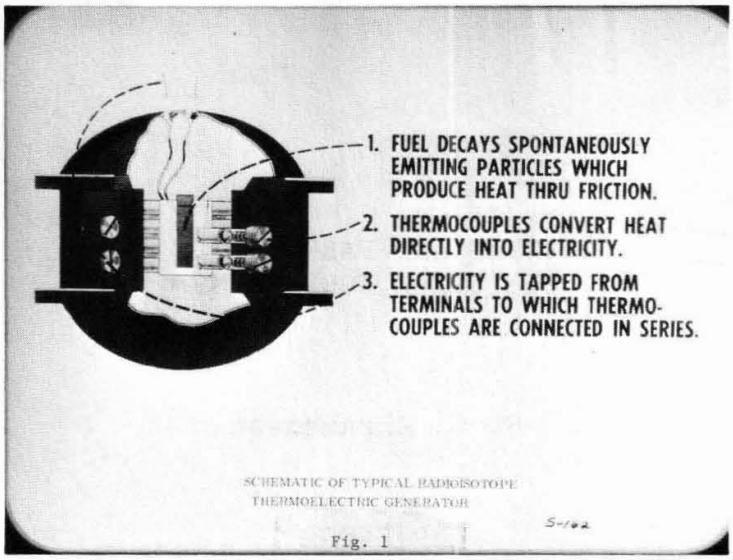

Fig. 1

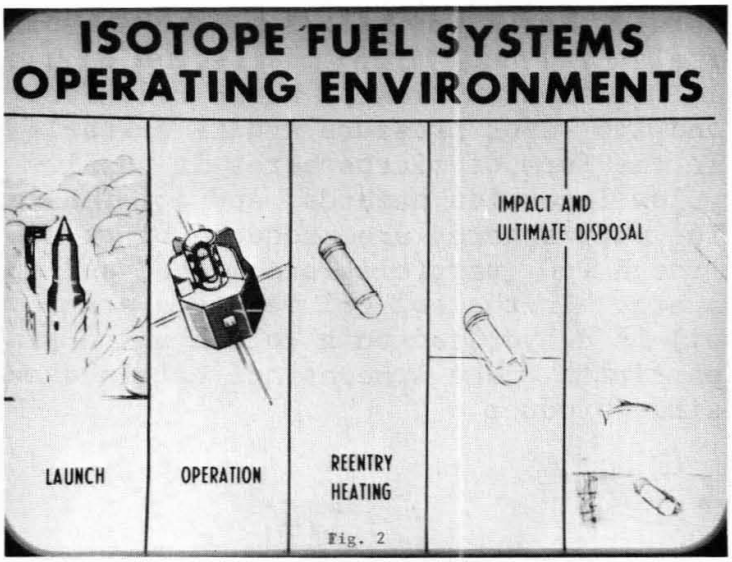

Fig. 2

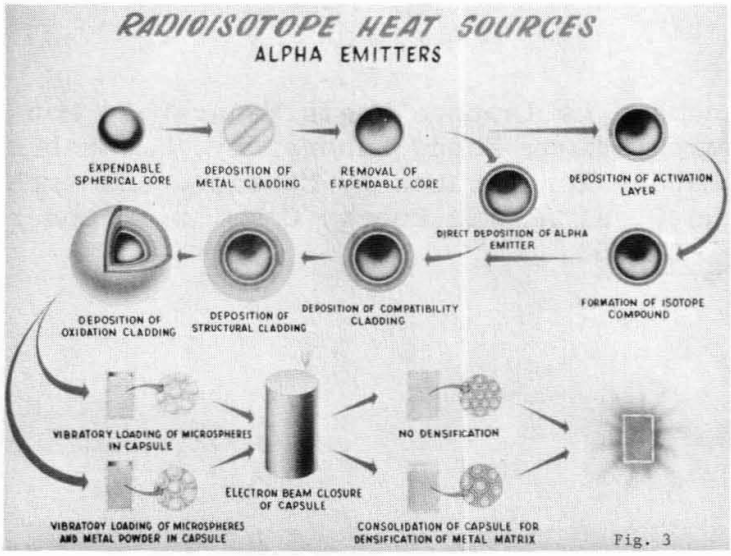

Fig. 3

PROPERTIES AND FABRICATION OF PLUTONIUM FUEL FORMS

S. G. Abrahamson

Abstract

Plutonium metal, plutonium-zirconium alloys, solid solutions, composite fuels, and PuO_2 microspheres can be used as heat source fuels. Plutonium dioxide has a relatively high melting point and low vapor pressure and is suitable for large sources. In the form of microspheres it has low aqueous solubility, low ingestion hazards, and low inhalation hazards. The microspheres are produced by two methods. In one method rough PuO_2 particles are melted and spheroidized in a plasma arc. In the sol-gel method a stable plutonium colloid (sol) is dehydrated on a column which produces spherical particles. The spheres are calcined and sintered for the desired product.

S. G. Abrahamson is Isotope Fuels Manager at Monsanto Research Corporation, Mound Laboratory, Miamisburg, Ohio. Mound Laboratory is operated by Monsanto Research Corporation for the U. S. Atomic Energy Commission under Contract No. AT-33-1-GEN-53.

Introduction

There are five major ^{238}Pu fuel forms which can be used for heat source applications. These are the metal, plutonium-zirconium alloys, solid solutions, composite fuels and plutonium dioxide microspheres. Physical, chemical and radiation characteristics and fabrication techniques govern the suitability of these fuel forms for various applications. Some of these characteristics are briefly reviewed in this paper. [Since some characteristics have not been determined with ^{238}Pu, analogous characteristics for ^{239}Pu will be given whenever it can be assumed that this characteristic is not altered with isotope (1).]

Radiation Properties

Plutonium-238 decays by alpha emission with a half-life of 87.4 yr. The thermal energy dissipated with this decay has been used as a convenient analytical tool to determine the half-life of this isotope and to determine quantitatively the amount of isotope. However, in recent years this heat dissipation has been used in heat source applications. The alpha decay modes of ^{238}Pu in addition to other radiation properties are illustrated in Table 1. These radiation properties are independent of fuel form; any changes in radiation are due to nuclear reactions with elements added in compound formation or with impurities. For example, it is of importance to compare the total neutron emission of the metal, which undergoes spontaneous fission,with the oxide in which ^{18}O and ^{17}O undergo (α,n) reactions. The neutron and gamma emissions greatly increase the radiation hazard of handling the material and require that additional radiation protection be utilized.

Metallic ^{238}Pu

Some basic properties of ^{238}Pu metal,which can be prepared with relative ease by conventional techniques of reduction from the oxide, are given in Table 2. Of the various ^{238}Pu fuel forms, the metal has the highest power density. This characteristic must be given prime consideration when a small heat source is designed with maximum power output.

The relatively high thermal conductivity is characteristic of metals. However, the low melting point of ^{238}Pu, ~640°C, poses a serious limitation to its application in heat

sources. Molten plutonium is corrosive to all metallic materials, and prolonged exposure threatens the integrity of a container of even the most corrosion resistant materials. Consequently the use of ^{238}Pu metal as a heat source is limited to low-temperature applications for limited periods of time.

Plutonium-Zirconium Alloys

A solution to this limitation is to increase the melting temperature of the fuel by alloying. The solidus temperature of the alloy must be considered as the limiting temperature because a destructive reaction with the container can occur when only a trace of liquid is present. Zirconium is one of the most attractive alloying elements for increasing the melting temperature of plutonium. As shown in the plutonium-zirconium binary phase diagram, Fig. 1, ε-Pu and β-Zr form a continuous solid solution series (2). Both the solidus and liquidus temperatures of this solid solution rise rapidly with increasing zirconium content because of the high melting point of zirconium. Even a small concentration of zirconium is significant protection against melting in a plutonium-rich alloy. The solidus temperature is 715°C for the Pu-10 at. % Zr alloy and 810°C for the Pu-20 at. % Zr alloy; the liquidus temperatures are 820 and 940°C, respectively.

Some of the basic properties of Pu-10 at. % Zr alloy are listed in Table 3. These results show the power density is slightly decreased. However, the increase in melting point (solidus temperature) and thermal conductivity should increase the desirability of this fuel form for heat source applications.

Iron is an impurity which commonly occurs in ^{238}Pu metal. A eutectic reaction at a composition of Pu-9 at. % Fe produces liquid at 413°C; this reaction can be detected in plutonium containing only a trace of iron (<500 ppm). The addition of zirconium eliminates the eutectic reaction when iron is not present in high concentration. The final solidification products at the solidus temperature are epsilon phase (a solid solution of zirconium and iron in plutonium) and $(Pu,Zr)Fe_2$ solid solution. The addition of 2 at. % Fe to the Pu-20 at. % Zr alloy does not result in eutectic liquid at 413°C, and the bulk of the alloy is solid above 800°C with only a trace of liquid which solidifies over the temperature range.

The use of composite fuels and solid solutions as a fuel form for heat source application is still in a development stage. The fuel in the proposed composites is PuO_2 microspheres. The microspheres are contained within a metal or ceramic matrix. Since these fuel forms are still in a development stage, no further elaboration will be made at this time.

$^{238}PuO_2$

The ^{238}Pu fuel form that has the best characteristics for most heat source applications is the binary plutonium compound PuO_2. It has rather high stability; the free energy of formation (ΔG°) varies from -240 kcal $mole^{-1}$ at 298°K to -144 kcal $mole^{-1}$ at 2675°K. These high free energy values indicate that plutonium dioxide is certainly a stable fuel form. It has a rather low vapor pressure ($\sim 10^{-7}$ atm at 1500°C for $PuO_{1.98}$) and will form substoichiometric oxides at high temperatures. Some additional properties of plutonium oxides are given in Table 4.

Preparation of $^{238}PuO_2$ Microspheres

Plutonium dioxide can be utilized as a powder or as pressed parts. However, due to low solubility, low ingestion hazards and negligible amounts of inhalation particles, the form of dioxide usually chosen is microspheres. These microspheres can be prepared by one of two main methods. The first method is fusion by plasma torch. The method of preparation of fuel material is listed in Table 5.

The coarse particles of PuO_2 fall through the plasma arc and form spheres due to the surface tension of the melt. This is illustrated schematically in Fig. 2. A photograph which shows the feed material transiting the plasma is given as Fig. 3.

The product which is obtained by this method is shown in Fig. 4. This figure illustrates that the product which is obtained has a glazed surface. The microspheres are nearly isoluble in water and have good mechanical properties.

The second method of preparing microspheres is a sol-gel technique. Sol-gel techniques have been studied extensively at Oak Ridge National Laboratory (3). Mound Laboratory also has been examining this technique for application in the preparation of $^{238}PuO_2$ microspheres (4). Although some of

the parameters must be altered to suit a specific compound or isotope under study, the general method, outlined in Table 6, is the same.

In the sol-gel process a solution of plutonium nitrate is adjusted to the +4 oxidation state; then NH_4OH is added to precipitate a Pu(IV) polymer. After the polymer is washed and digested, a nitric acid solution is added, and the resulting polymer is peptized. The peptized sol is then adjusted to a constant volume to yield a black sol. The black sol is baked until a particular nitrate:plutonium ratio is obtained. This sol can be resuspended in an aqueous solution. The sol solution is then put on a drying and spheroidizing column. The spheroidizing column is illustrated in Fig. 5.

As the sol is dehydrated, spheres are formed. When they reach a desired density, they drop into the sphere-collecting device and are calcined and sintered at the desired temperature. The particles which are obtained by this method are shown in Fig. 6. The surface characteristics illustrate the similarity between plasma-fired microspheres and sol-gel microspheres.

Properties of $^{238}PuO_2$ Microspheres

Some of the basic properties of $^{238}PuO_2$ microspheres are listed in Table 7.

Note that since microspheres are utilized the power density by necessity is decreased to approximately 2.7 W cm^{-3}. This is understandable when one considers that the closest packing which one can theoretically obtain with spheres contains 26% void space.

Properties of a typical sample of production-grade microspheres are given in Table 8. A small amount of ^{236}Pu is found in the sample. It is of importance to determine this isotope quantitatively since it ultimately decays to ^{208}Tl, which has a 2.61 Mev gamma ray. Special note should be given to the solubility. The dissolution rate in distilled water and sea water of 1.26×10^{-3} μg $day^{-1} mm^{-2}$ indicates that the solubility is indeed small. The dissolution of plutonium dioxide in acid solutions is also small, and one has to use a catalyst, such as fluoride, in dissolving microspheres or use some fused salt method. Although additional work needs to be done on the biological

hazards of these fuel forms, experiments conducted by Battelle Northwest Laboratory have shown that there is negligible ingestion hazard from this material.

It should also be noted that the neutron flux is 1.9×10^4 n $sec^{-1} g^{-1}$. However, it has already been shown that the spontaneous fission of ^{238}Pu itself is approximately 2.5×10^3 n $sec^{-1} g^{-1}$. The additional neutron flux is due to (α,n) reactions which occur with ^{17}O and ^{18}O. Thus, it is apparent that the use of normal oxygen, which contains approximately 0.07% ^{17}O and 0.204% ^{18}O, in the preparation of PuO_2 will result in this additional neutron emission. In order to reduce the amount of ^{17}O and ^{18}O one must replace the ^{17}O and ^{18}O with ^{16}O. A high-temperature exchange technique has been developed for this purpose (5). Although plasma-fired PuO_2 will not exchange at ordinary temperatures, experiments have shown that PuO_2 in a powdered form or uncalcined sol-gel produced PuO_2 microspheres will exchange at elevated temperatures. The rate of exchange of oxygen with powdered PuO_2 is illustrated in Fig. 7.

Similar results have been obtained with uncalcined sol-gel microspheres (6). When ^{16}O is added to PuO_2 with a normal oxygen ratio, an exchange will occur within a very short period, i.e., approximately 15-20 min. An exchange reaction at 700°C coupled with sintering at 1200°C for several hours reduces the neutron emission of microspheres to a predicted value of 5.0×10^3 n $sec^{-1} g^{-1}$. The neutrons above the 2.5×10^3 n $sec^{-1} g^{-1}$ for normal fission of ^{238}Pu occur since ^{16}O cannot be obtained that does not contain a small amount of ^{18}O and ^{17}O. The preparation of PuO_2 enriched in ^{16}O is of great importance for use in heat source applications where people are near the source for extended periods.

Conclusions

The selection of any of the five ^{238}Pu fuel forms for future heat source application should be based on the characterization of the fuel form of interest. The main consideration in selection of a ^{238}Pu fuel form is the temperature range of interest; however, it should be noted that the use of large heat sources and, consequently, the use of higher temperature ranges do suggest that PuO_2 in the form of a microsphere, composite fuel, or solid solution will have the greatest applications for heat source programs. The ease of fabrication indicates that microspheres should be of primary concern.

References

1. Plutonium-238 and Polonium-210 Data Sheets, MLM-1441, Mound Laboratory, Miamisburg, Ohio, 1967, 91 pp.
2. J. A. C. Marples, The Plutonium-Zirconium Phase Diagram, J. Less-Common Metals, 2, 1960, p. 333.
3. P. A. Hass et al., Sol-Gel Process Development and Microsphere Preparation, ORNL-P-2159, Oak Ridge National Laboratory, Oak Ridge, Tenn., 1966, 42 pp.
4. D. L. Plymale and W. H. Smith, The Preparation of Plutonium-238 Microspheres by the Sol-Gel Process, MLM-1450, Mound Laboratory, Miamisburg, Ohio, 1968, 7 pp.
5. D. L. Plymale, The Exchange of Isotopically Enriched Oxygen with $^{238}PuO_2$, J. Inorg. Nucl. Chem., 30, 1968, pp. 886-890.
6. D. L. Plymale, The Exchange of Isotopically Enriched Oxygen with $^{238}PuO_2$ Microspheres, MLM-1462, Mound Laboratory, Miamisburg, Ohio, 1968, 8 pp.

Table 1. Basic Radiation Properties of ^{238}Pu Metal

Type		Energy, Mev	Emission (calculated), particles W^{-1} sec^{-1}
Alpha	1	5.491	$\sim 8 \times 10^{11}$
	2	5.448	$\sim 3 \times 10^{11}$
	3	5.350	1.45×10^{9}
	4	5.200	5.59×10^{7}
	5	5.000	7.87×10^{4}
Beta		Stable	--
Gamma	1	0.776	$\sim 5. \times 10^{6}$
	2	0.203	4.47×10^{4}
	3	0.1531	1.12×10^{7}
	4	0.0998	1.01×10^{8}
	5	0.0435	4.25×10^{8}
	6	0.017	--
Bremsstrahlung		Negligible	

Neutron (Spontaneous Fissions) $\sim 2.5 \times 10^{3}$ n sec^{-1} g^{-1}

Table 2. Basic Properties of ^{238}Pu Metal

Composition:	Pu
Melting Point:	~640°C
Specific Power:	~0.45 W g^{-1} 13.7 Ci g^{-1}
Power Density:	6.8 - 7.3 W cm^{-3}
Density:	15-16 g cm^{-3}
Viscosity:	3.5 centipoise at 1000°C
Surface Tension:	550 dyne cm^{-1} at 640°C
Thermal Conductivity:	$30. \times 10^{-3}$ cal cm^{-1} $°C^{-1}$ sec^{-1} at 100°C
Solubility:	Soluble in most acids; insoluble in glacial acetic acid and nitric acid -- due to protective oxidation coat.

Table 3. Basic Properties Pu-10 at. % Zr

Composition	wt %
^{238}Pu	76.7
^{239}Pu	15.8
^{240}Pu	2.4
^{241}Pu	0.8
Zr	4.1

Solidus Temperature:	715°C
Specific Power:	~0.44 W g^{-1}
	13.1 Ci g^{-1}
Power Density:	6.5 W cm^{-3} (calculated)
Density:	14.8 g cm^{-3} (calculated)
Viscosity:	~10 centipoise
Surface Tension:	~700 dyne cm^{-1}
Thermal Conductivity:	40 x 10^{-3} cal cm^{-1} $°C^{-1}$ sec^{-1} (estimated)

Table 4. Basic Properties of PuO_2

Composition:	PuO_2
Melting Point:	~2230°C
Specific Power:	0.40 W g^{-1}
	12.13 Ci g^{-1}
Power Density:	4.58 W cm^{-3}
Density:	11.46 g cm^{-3}
Linear Expansion:	~10 x 10^{-6} cm cm^{-1} $°C^{-1}$
Viscosity:	32 centipoise
Surface Tension:	523 dyne cm^{-1}
Thermal Conductivity:	14.3 x 10^{-3} cal cm^{-1} $°C^{-1}$ sec^{-1} at 300°C
	5.6 x 10^{-3} cal cm^{-1} $°C^{-1}$ sec^{-1} at 1200°C
Thermal Diffusivity:	19 x 10^{-3} at 300°C to 6.6 x 10^{-3} cm^2 sec^{-1} at 1200°C
Solubility:	With difficulty in HNO_3-HF solutions

Table 5. Plasma Torch Technique

I.	Precipitate Pu^{4+} by OH^- or $C_2O_4^{--}$
II.	Calcine to PuO_2
III.	Press and sieve to coarse particles
IV.	Spheroidize in plasma torch

Table 6. Sol-Gel Technique

I.	Precipitate Pu^{4+} with NH_4OH
II.	Wash, digest, and peptize polymer
III.	Concentrate and bake
IV.	Resuspend in solution
V.	Spheroidize on drying column

Table 7. Basic Properties of PuO_2 Microspheres

Density:	9.8-10.4 g cm^{-3} (production-grade)
Bulk Density:	6.7 g cm^{-3}
Power Density:	2.7 W cm^{-3}
Hardness:	1163 kg mm^{-2}
Solubility:	Dissolving is difficult in HNO_3-HF solution

Table 8. Characteristics of Microspheres

Impurities:	0.58%
Actinide Impurities:	0.10%
^{236}Pu:	1.0 ppm
Crush Strength:	259 g
Melting Point:	2165°C
Stoichiometry:	2.00
Isotopic Ratio:	80.9% ^{238}Pu
Solubility in H_2O:	1.26 x 10^{-3} μg day^{-1} mm^{-2}

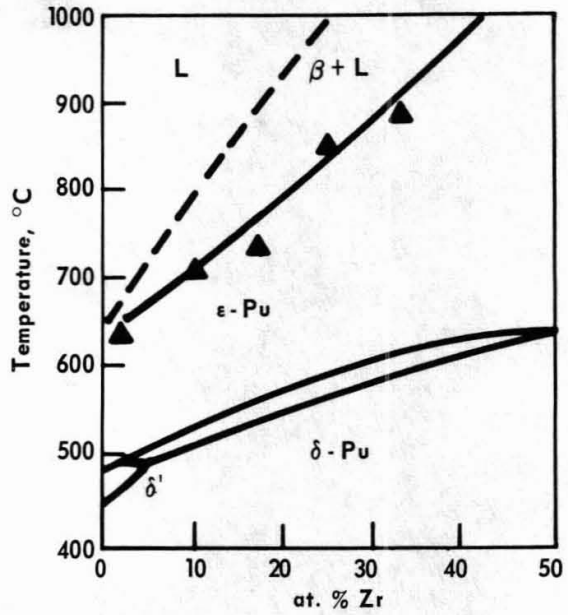

Fig. 1. Plutonium-zirconium phase diagram

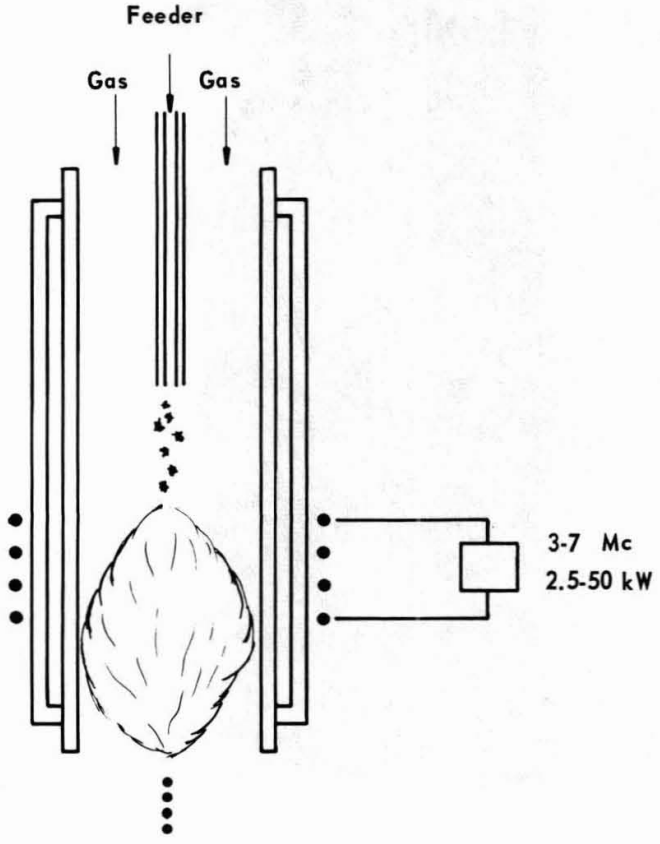

Fig. 2. Schematic of plasma torch

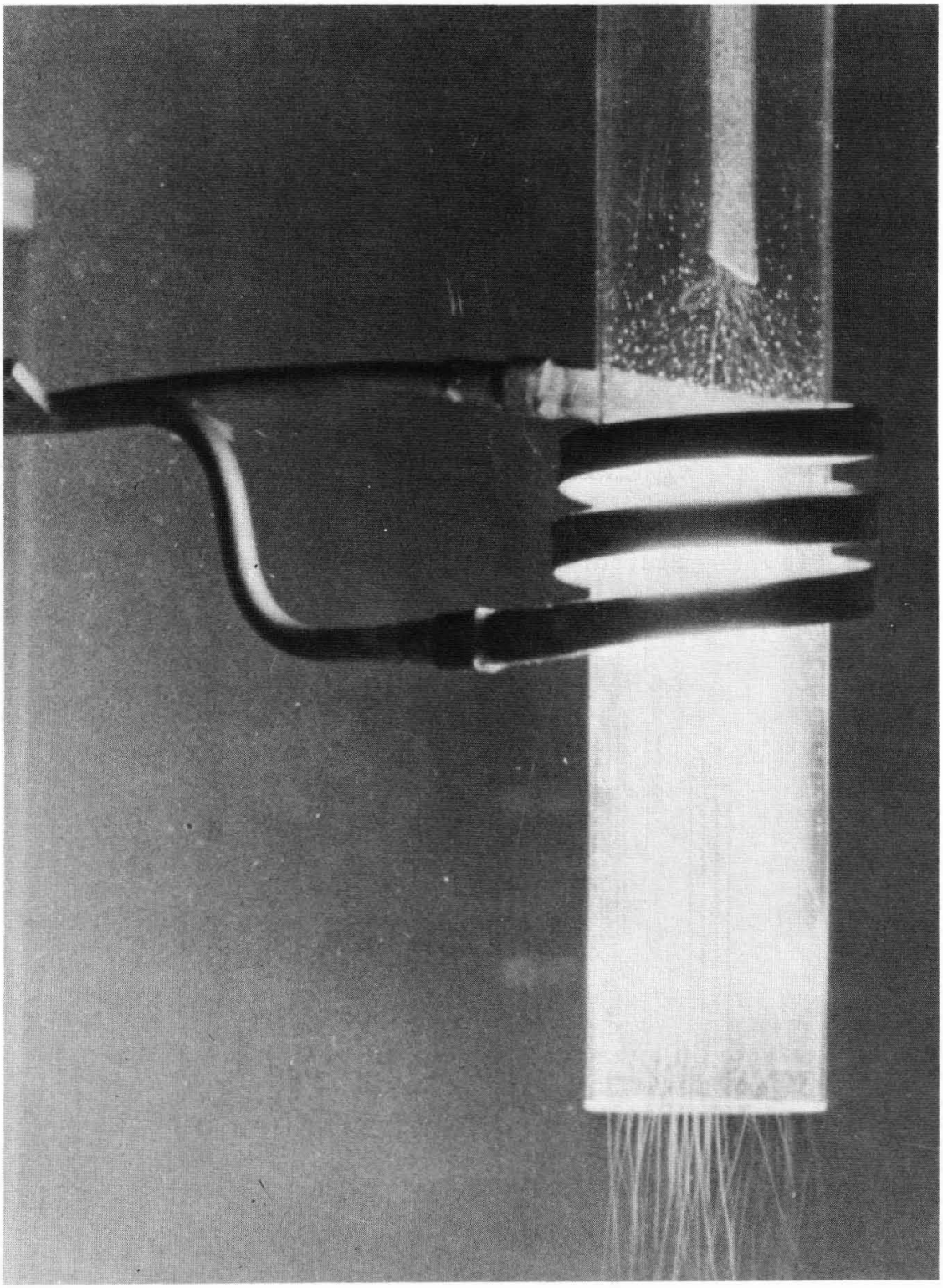

Fig. 3. Feed material transiting the induction-coupled plasma torch

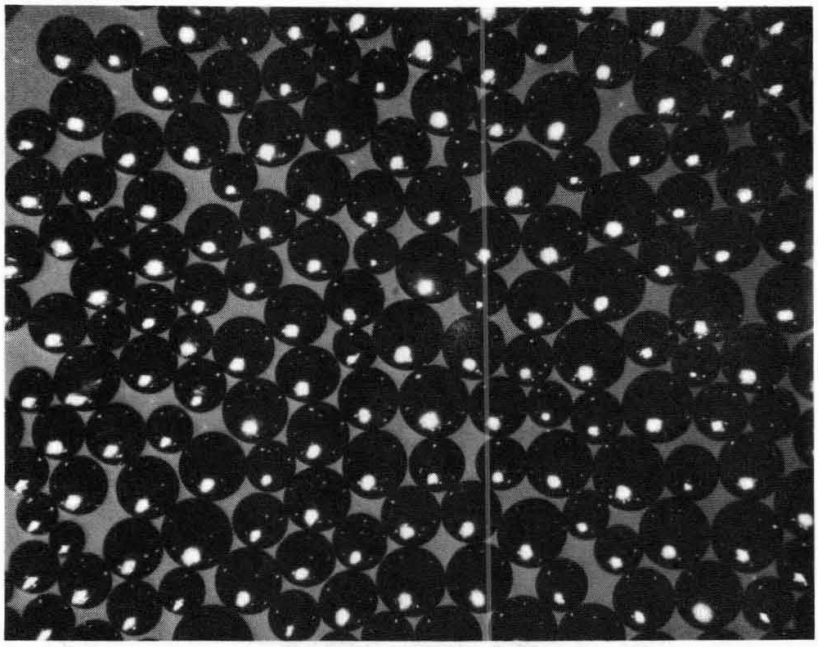

Fig. 4. Plasma-fired microspheres(50X)

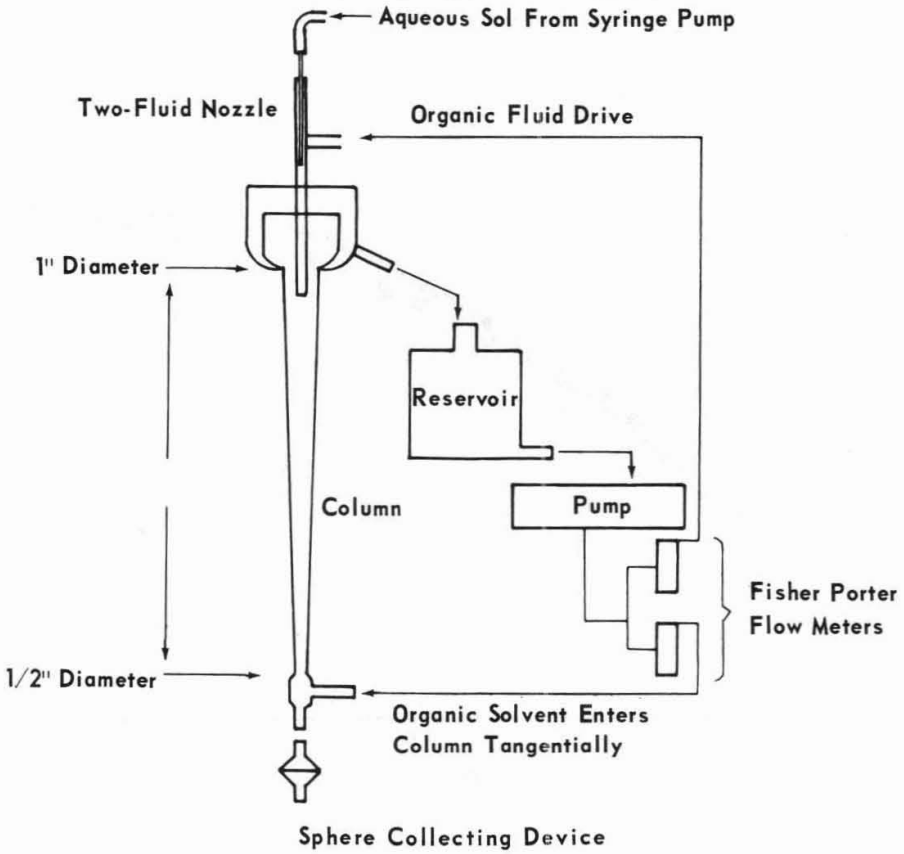

Fig. 5. Sol-gel column

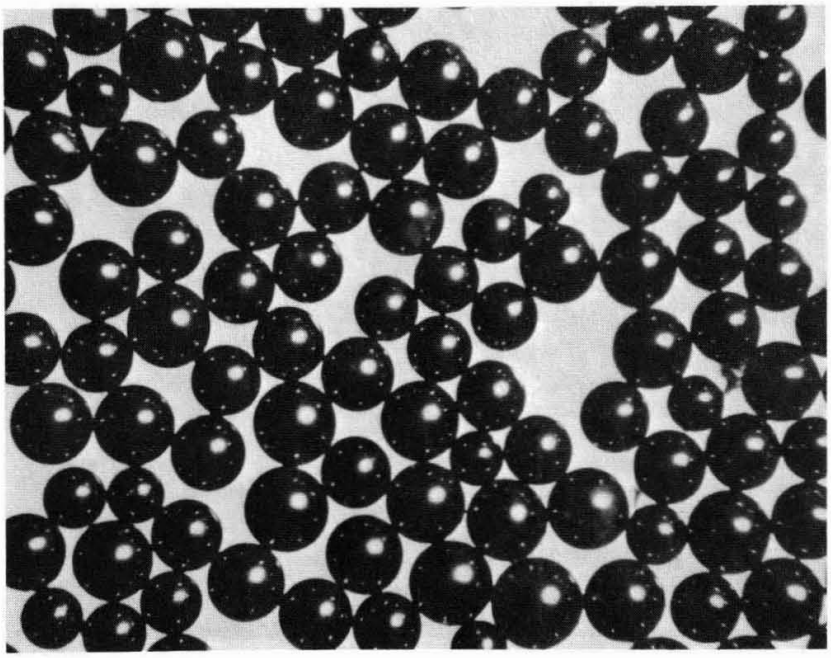

Fig. 6. Sol-gel microspheres(50X)

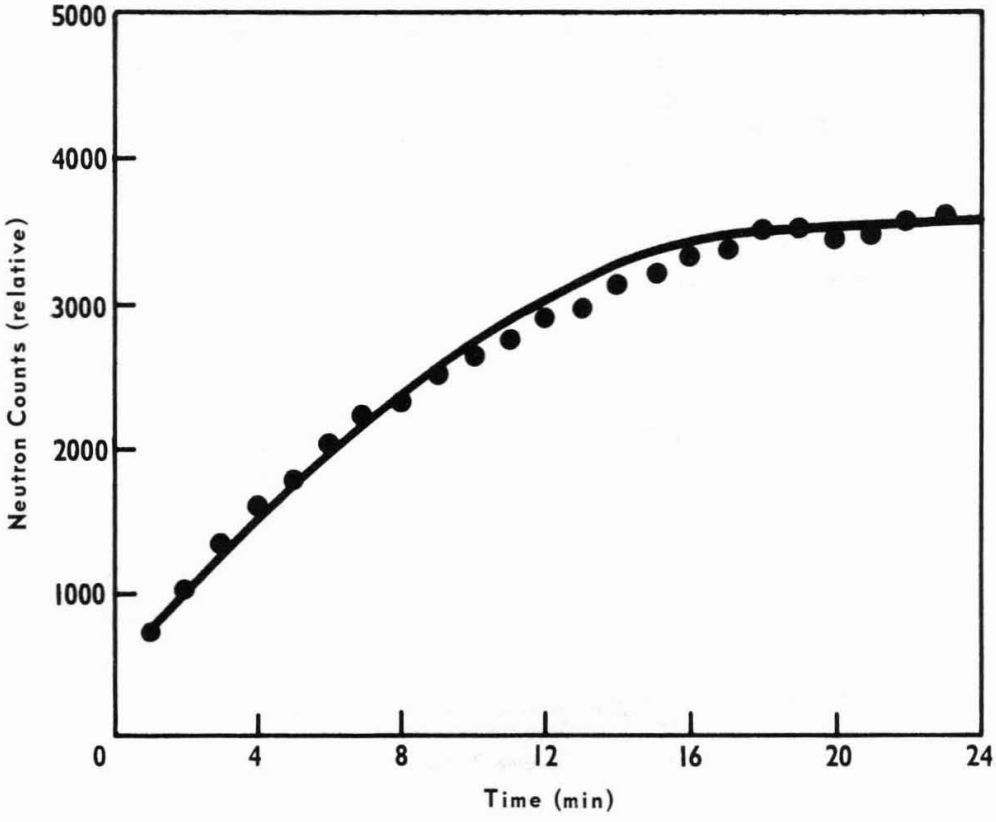

Fig. 7. Neutron counts as a function of ^{18}O exchange reaction time

PROPERTIES AND FABRICATION OF ^{210}Po FUEL FORMS

C. J. Kershner

Abstract

The available literature data on ^{210}Po are reviewed in this paper, especially information of significance in the use of ^{210}Po as an isotopic fuel. However, the major portion of this paper deals with the data from research and development for isotopic fuel applications. The methods are described for producing a fuel form which best utilizes the attributes of a high specific power, short half-life, alpha emitter; namely, ^{210}Po. Fabrication techniques and properties of other fuel forms, such as matrices, are also covered. Applications, such as the POODLE space thruster, demonstrate fuel form concepts in actual development. Investigations are described which have the goal of improving present polonium fuel forms, especially their high-temperature chemical stability.

C. J. Kershner is a Senior Research Specialist with Monsanto Research Corporation, Mound Laboratory, Miamisburg, Ohio.
Mound Laboratory is operated by Monsanto Research Corporation for the U. S. Atomic Energy Commission under Contract No. AT-33-1-GEN-53.

Introduction

Polonium-210 (RaF) has attracted considerable scientific attention since the time of its discovery by the Curies in 1898. This interest has been whetted by the fact that the element polonium has no known stable isotope, and ^{210}Po is one of the rarest of naturally occurring isotopes. The early polonium chemistry was carried out on trace quantities with most of the work devoted to its extraction and isolation from uranium ores. However, with the advent of nuclear reactors, the prospect of artificially produced gram quantities of ^{210}Po changed the entire outlook for this isotope. Not only are milligram quantities made available for scientific investigation, but the technologist now has sufficient material available for applications that he could only hypothesize before.

In ^{210}Po the technologist has found an almost unique alpha-emitting isotope in that:

1. It decays almost entirely by the emission of a 5.3-Mev alpha particle with only minor contributions from an 0.8-Mev gamma ray and from soft x-rays;
2. The decay product is stable lead-206;
3. The 138.4-day half-life affords a high specific activity, but is long enough for practical applications;
4. It can be readily produced by neutron irradiation of natural ^{209}Bi;
5. Its chemistry is such that it can be readily separated from the target material and isolated in a highly purified form; and
6. The alpha decay has sufficient energy to make coated alpha sources feasible and to make possible high flux neutron sources with most light elements.

It was these properties which led to the use of ^{210}Po in (α,n) neutron sources and finally in heat sources.

The application of ^{210}Po as an isotopic fuel requires a unique approach due to the nature of the element; thus, although the metallic form is the most basic fuel and affords a specific power of 144 W g^{-1}, its low melting and boiling points limit its use to applications below 500°C. Therefore, to fully utilize the potential of ^{210}Po a series of chemical and physical alterations must be performed upon the basic metallic form to achieve a fuel possessing a major portion of the following characteristics:

1. The fuel must be physically stable above 1000°C;
2. It must exhibit chemical stability above 1000°C toward both containment materials and operating environment;

3. Radiation damage must not result in a compromise of the above properties;
4. The chemical and physical stability must not be affected by helium evolution;
5. The chemical and physical stability must be relatively insensitive to radioactive daughter ingrowth;
6. Minimal power density reduction should be maintained for the final fuel forms;
7. The fabrication process should not be complex or time-consuming.

The steps involved in preparing such fuel forms of ^{210}Po and the characteristics of those fuel forms will be traced starting with the preparation of the metal and ending with a form suitable for encapsulation and use at temperatures of 1000°C or above.

^{210}Po Metal

Preparation

Quantities of ^{210}Po suitable for isotopic power applications are produced artificially by neutron irradiation of natural bismuth metal according to the following reaction:

$$^{209}_{83}Bi + ^{1}_{0}n \longrightarrow ^{210}_{83}Bi \xrightarrow[5.4\ days]{\beta} ^{210}_{84}Po.$$

After neutron irradiation, the bismuth slugs, in aluminum jackets, are removed from the reactors and shipped to Mound Laboratory for processing. The processing of ^{210}Po metal is carried out in three phases: 1) decanning, 2) concentration, and 3) purification.

The first step involves melting the bismuth and allowing the melt to flow from small holes in the bottom of the aluminum can into a quenching water bath. In the second phase, the pelletized bismuth is dissolved in a mixture of nitric and hydrochloric acids. An approximately hundredfold concentration is accomplished by denitrating the above solution with formic acid and passing the bismuth chloride-polonium chloride solution through a bismuth powder bed. The bismuth powder with the ^{210}Po deposit is dissolved and the entire sequence repeated only using an order of magnitude smaller bismuth reduction bed to collect the same quantity of ^{210}Po. At this point the ^{210}Po has been concentrated approximately 1,000 times.

Separation and purification are accomplished by a selec-

tive reduction with stannous chloride, an ammonium hydroxide precipitation, and an electrodeposition. The ^{210}Po metal is obtained as a plate on platinum gauzes with >95% purity. The chemical composition of ^{210}Po metal produced in this manner is given in Table 1.

Properties

The starting material for any ^{210}Po fuel form is the metal. Some of its radiation properties are illustrated in Table 2 (1,2). These radiation properties, other than the neutron emission, are intrinsic with the isotope and, thus, independent of fuel form. Changes in the neutron emission can occur due to (α,n) reactions with elements added in compound formation or with impurities. Due to these radiations, handling and use of ^{210}Po requires complete confinement and moderate radiation protection. The biological tolerances and established concentration guides for ^{210}Po are shown in Tables 3 and 4 (3,4).

The physical properties of the metal approximate those of bismuth and lead whereas much of its chemistry resembles that of the other group VI-A elements, especially tellurium. The silver-gray metal exists in two allotropic forms: a low-temperature alpha phase with a simple cubic habit, and a high-temperature form with a simple rhombohedral structure. The phase change appears to occur at about 36°C with a region of coexistence between 18 and 54°C. The metal melts at 254°C, has a boiling point of 962°C, and is volatile at elevated temperatures below its boiling point; it preferentially condenses on some metals, such as platinum and palladium.

Polonium-210 metal dissolves in dilute hydrochloric and concentrated nitric and sulfuric acids. The metal slowly oxidizes in air at room temperature to form the basic dioxide, which sublimes in air at 885°C and decomposes under vacuum at 500°C. In its cationic role ^{210}Po forms oxides, sulfides halides, nitrates, sulfates, phosphates and other salts of mineral and organic acids. However, it is in the intermetallic or polonide type compounds where the most thermally stable ^{210}Po-containing materials are found. Most of the alkali, alkaline earth, rare earth and some of the transition metal polonides have been prepared. The most stable compounds in this class were found to be the rare earth polonides. The basic physical, chemical and nuclear properties of ^{210}Po metal are summarized in Table 5 (1,5).

Metallic ^{210}Po was used as the fuel in the first demonstration of the thermoelectric conversion of radioactive decay energy into electrical energy. Chromel-constantan

thermocouples were employed as energy converters in this experiment, which was carried out by J. H. Birden and K. C. Jordan at Mound Laboratory in the early 1950's. The metal was also used in the first demonstration of a dynamic conversion device, also carried out at Mound in 1954. The SNAP-3 generator, fabricated by Martin Company and demonstrated for President Eisenhower in 1959, was also fueled with ^{210}Po metal.

In the typical fueling procedure the metal is vacuum vaporized from the platinum gauzes into the source container. This is carried out in a "gun" assembly, which delivers the gaseous polonium into the source containment vessel where it is condensed by cooling with water or liquid nitrogen. Although the metallic fuel form has been used as described above, it is limited to low-temperature applications (approximately 500°C or less) due to the low melting and boiling points and to the reactivity of gaseous ^{210}Po with most containment metals at elevated temperatures.

^{210}Po Fuel Compounds

The high-melting-temperature compounds of ^{210}Po afford a solution to the temperature limitation of the metallic fuel form. Of the known compounds and alloys of ^{210}Po, those of the intermetallic type with the rare earth class of metals exhibit the highest thermal stability. These compounds possess many of the characteristics desired in an isotopic fuel material, with the exception of air environmental stability. Thus, their integrity must be assured by some form of complete containment.

Preparation

All of the rare earth monopolonide compounds are readily formed when the rare earth metals are heated with gaseous ^{210}Po in a sealed vessel at less than 1000°C. As with the analogous selenide and telluride systems, the rare earth polonide compounds most easily produced by this process, and the most stable, are of the 1:1 stoichiometry(6). The reaction can conveniently be monitored by employing segmented reaction vessels, initially separating the reactants and then tracing the ^{210}Po uptake in the rare earth chamber with a collimated gamma probe. Differentially wound furnaces are used to selectively control the vapor pressure and position of the gaseous ^{210}Po within the reaction vessel. A typical experimental reaction apparatus is shown in Fig. 1(7).

Properties

In order to ascertain the suitability of any ^{210}Po compound for heat source applications a number of physical, chemical, radiation, and preparation characteristics must be examined. Those data presently available on the rare earth polonides, and those for analogous selenides and tellurides which can be safely used as first approximations for predicting polonide characteristics, will be reviewed.

Some of the basic properties of a rare earth polonide type compound are given in Table 6(7,8). The gadolinium polonide compound is used in Table 6 and will be used throughout the remainder of this paper as exemplifying the series of possible polonides formed with the rare earth metals (elements of atomic number 57 through 71).

All the rare earth monopolonides possess the B1 sodium chloride type structure with densities of approximately 10 g cm^{-3} with the exception of the Group II types, which have slightly lower densities. Thus, none of the compounds result in more than a 50% lowering of the power density; e.g., the GdPo compound retains a formidable power density of 806 W cm^{-3}.

All the rare earth polonides melt well above 1000°C with the general trend toward higher melting points for those of higher atomic numbered rare earths. Gadolinium polonide, with a melting point of 1675°C, falls approximately midway in the range for the series. The size and electronegativity relationships are such that the melting points of the rare earth polonides are not greatly affected until approximately 35% of the ^{210}Po has decayed to lead. A partial phase diagram for the $GdPb_xPo_{1-x}$ alloy system is presented in Fig. 2. The salient feature of this system is the single phase region which exists for compositions ranging from $x = 0$ to $x \approx 0.3$-0.6.

At the present time the vaporization characteristics of only a limited number of the polonides have been investigated. These all were found to vaporize incongruently under vacuum Knudsen cell type conditions.

Thus, chemical stabilization via the polonide compounds has increased the temperature range of applicability for ^{210}Po fuels by at least 1000°C over the metal form. This has been accomplished without a significant sacrifice in power density and radiation characteristics. Also, the polonide compounds are largely unaffected by the ingrowth of the daughter product ^{206}Pb.

Matrix Fuel Form

After the polonide compound stabilization, properties must still be built into the fuel form that will provide for sufficient mechanical stability, optimum thermal conduction geometry, helium evolution and environmental stability. One successful approach for accomplishing this has been the development of a matrix fuel form. Basically, this concept involves the distribution of a finely divided form of the fuel compound in a porous matrix formed by powder compaction techniques. These matrices can be formed into a geometry specific to the particular application. The porosity of the matrix satisfies both the helium evolution and the ease of fabrication criteria. The latter will be evident when the preparation procedure is described in the following section.

Porous, annular, tantalum metal matrices with gadolinium polonide fuel compound were successfully employed in the POODLE demonstration thruster.

Preparation

The matrix fuel form is fabricated in four steps: 1) matrix and rare earth powder preparation; 2) matrix compaction; 3) dehydrogenation; and 4) activation. Although the first three require inert atmosphere or vacuum handling facilities, only the last step required a radioactive control area. The matrix fabrication flow diagram and quality control steps are presented in Fig. 3.

Since the reproducibility of compaction characteristics is important, the matrix metal powders require rigid control of particle size, shape and surface area. This is accomplished by selection on the basis of mesh size [Fisher-Sub-Sieve size (ASTM-B330-65) and Scott Density (ASTM B329-61)]. Impurity limits are also maintained at low levels especially for light elements which can produce (α,n) reactions. The metal powder is degassed at 750°C for 8 hr at 10^{-5} torr before use.

The degassed matrix metal and the rare earth powders are weighed and mixed in the desired ratio and transferred to an automatic hydraulic press. A metered quantity of powder is delivered to the die by means of a vacuum filling tube. A solenoid switching device allows alternating loading of the filler and discharging of the powder into the die cavity. A gas driven press applies 50,000 to 60,000 psi on the powder; the matrices are pressed to a predetermined density, are ejected from the die and are dimensionally checked. The die set and the automatic press used to prepare matrix fuels for

research and development studies are shown in Figs. 4 and 5.

Prior to reaction with polonium, the matrices are degassed by heating at 1000°C under vacuum. The matrix is activated with polonium in a sealed reaction bomb. The reaction bomb (Fig 6) is designed so that it serves as the polonium metal storage can prior to fueling to reduce the amount of handling of the active material. Reactions are carried out using 0.5 to 1.0 g of ^{210}Po metal and can involve a number of matrices, depending upon size and power requirements. The reactions are complete within 1 hr at 700-800°C. The sealed reaction vessels are then opened; the fuel content in the matrix is analyzed by gamma counting and the degree of oxygen contamination measured by neutron counting. If the results of these measurements are within the predetermined limits, the matrices are encapsulated. A typical matrix is shown in Fig. 7.

Properties

Since the properties of the matrix fuel form can be varied greatly by the choice of matrix metal, density, geometry and fuel loading, a typical annular gadolinium polonide fueled tantalum matrix will be used to exemplify this fuel form type. Some basic properties of such a typical fuel matrix are given in Table 7.

The optimum density for a tantalum matrix compacted from -80+140 mesh powder has been found to be approximately 75% of the theoretical value. This density provides sufficient mechanical strength to withstand impact and vibration and yet allows for sufficient porosity to obtain better than 90% yields in the activation reaction.

Thus, rare earth polonide dispersed in a refractory metal possesses all the desired fuel form characteristics for high-temperature heat source use, with the exception of air environmental stability. The containment must still be relied upon for this protection. Compatibility of polonium fuel forms with suitable containment materials will be discussed in another paper and will not be dealt with here. However, it must be understood that fuel forms and containment are inseparable in their roles in accomplishing a workable heat source.

Conclusion

Since ^{210}Po has a relatively short half-life, its greatest applicability as an isotopic fuel lies in the high-temperature uses. Because of this, the present effort is concentrated on gathering more basic thermophysical data on

^{210}Po compounds and on developing means of stabilizing the fuel, especially with respect to environmental reactivity. The first effort involves vapor pressure, phase equilibria, oxidation rate and compatibility measurements on rare earth polonides in an effort to select the most stable polonium compound. The second effort consists of developing techniques for air environmental stabilization of fuel forms. Such techniques as microencapsulation and protective matrices are being pursued in this area.

References

1. H. V. Moyer (ed.), Polonium,TID-5221, Atomic Energy Commission, 1956, 392 pp.

2. A. G. Khabakhpashev, The Neutron Spectrum of a Po-α-O Source, Kernenergie, 3:4, 1960, pp. 392-394.

3. K. Z. Morgan (ed.), Report of the ICRP Committee II on Permissible Dose for Internal Radiation, Health Physics, 3, 1960, p. 219.

4. USAEC Manual Chapter 0524, Standards for Radiation Protection.

5. M. Haissinsky, Polonium, MLM-1165(tr), Mound Laboratory, Miamisburg, Ohio, 1964, 65 pp.

6. J. F. Miller and R. C. Himes, Rare Earth Intermetallic Compounds with Elements of Group V and VI, Rare Earth Research, E. V. Kleber (ed.), MacMillan, New York, 1961, pp. 232-240.

7. C. J. Kershner et al., Rare Earth Polonides, J. Inorg. Nucl. Chem., 28, 1966, pp. 1581-1588.

8. V. P. Zhuze et al., Electrical Properties of Rare-Earth Monochalcogenides (Cerium Group), Soviet Phys - Solid State (English Transl.), 6, 1964, pp. 205-212.

Table 1. Composition of ^{210}Po Metal

Isotope/Element	Concentration, wt %
^{210}Po	95-98
Tellurium	~1
Selenium	~0.1
Oxygen	2-4
Lead	Varies with age of material

Table 2. Radiation Properties of ^{210}Po Metal

Type	Energy, MeV	Emission (calculated), Particles $W^{-1}sec^{-1}$
Alpha 1	5.298 ± 0.002	1.155×10^{12}
2	4.5	1.410×10^{7}
Gamma	0.804 ± 0.005	1.41×10^{7}
X-ray 1	0.077 ± 0.002	1.7×10^{6}
2	0.01 to 0.015	3.4×10^{8}
Neutron	1.0 to 2.5	2.1×10^{3}

Table 3. Biological Tolerances for ^{210}Po

Solubility	Critical Organ	Permissible Body Burden, μCi	Biological Half-Life, days
Soluble	Spleen	0.03	60
	Kidney	0.04	70
Insoluble	Lung	--	--

Table 4. Radioactivity Concentration Guides for ^{210}Po

	Controlled Area		Uncontrolled Area	
Solubility	Air, μCi/cc	Water, μCi/cc	Air, μCi/cc	Water, μCi/cc
Soluble	5×10^{-10}	2×10^{-5}	2×10^{-11}	7×10^{-7}
Insoluble	2×10^{-10}	8×10^{-4}	7×10^{-12}	3×10^{-5}

Table 5. Basic Properties of ^{210}Po Metal

Melting Point:	254°C
Boiling Point:	962°C
Specific Power:	144 W g^{-1} 4,500 Ci g^{-1}
Power Density:	1324 W cm^{-3} (α phase) 1353 W cm^{-3} (β phase)
Vapor Pressure:	$\text{Log } P_{torr} = \frac{-5377.8 \pm 6.7}{T, °K} + 7.23 \pm 0.0068$
Solubility:	Soluble in most mineral acids and strong bases.
Density:	9.196 g cm^{-3} (α phase) 9.398 g cm^{-3} (β phase)

Table 6. Basic Properties of GdPo

Composition:	
^{210}Po	57.2 wt %
Gadolinium	42.8 wt %
Melting Temperature:	1675 $\pm$ 50°C
Lattice Constant:	6.295 $\pm$ 0.003 Å (NaCl Type)
Density:	9.78 g cm^{-3}
Specific Power:	82.4 W g^{-1} 2,573 Ci g^{-1}
Power Density:	805.8 W cm^{-3}
Thermal Conductivity:	1.9×10^{-3} cal (sec $cm^2)^{-1}$(°C $cm^{-1})^{-1}$
Solubility:	0.5 to 3.0 μCi ml^{-1} in distilled water at 25°C

Table 7. Basic Properties of a Matrix Fuel Form

Composition (typical):	
GdPo	9 wt %
Tantalum	91 wt %
Density:	10.3 g cm^{-3} (64% theoretical)
Specific Power:	7.5 W g^{-1} 233.9 Ci g^{-1}
Power Density:	77.2 W cm^{-3}
Thermal Conductivity:	7.2×10^{-2} cal (sec $cm^2)^{-1}$(°C $cm^{-1})^{-1}$ at 298°K

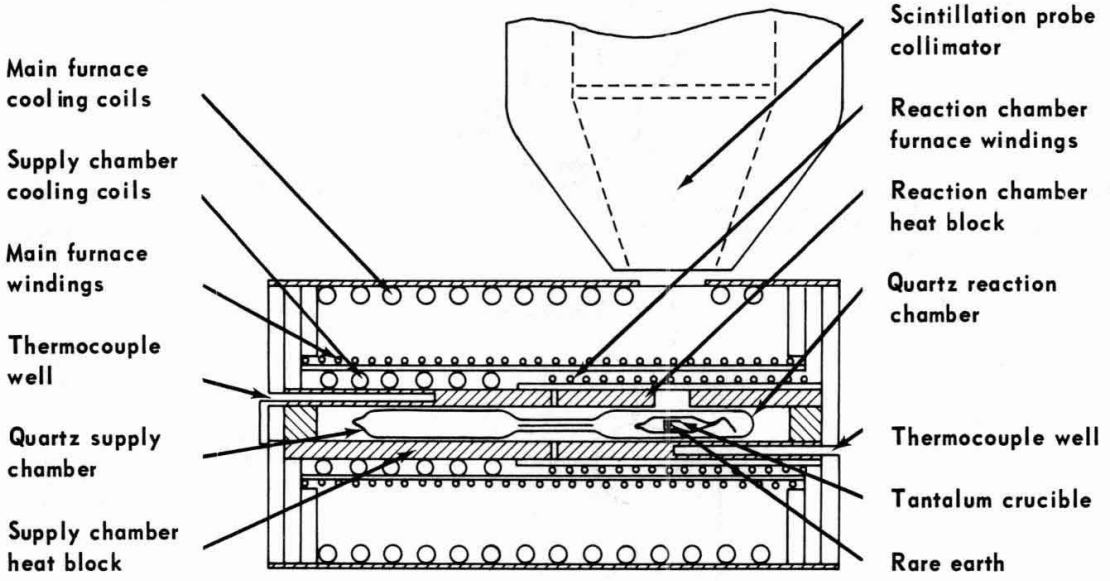

Fig. 1. Polonide reaction furnace

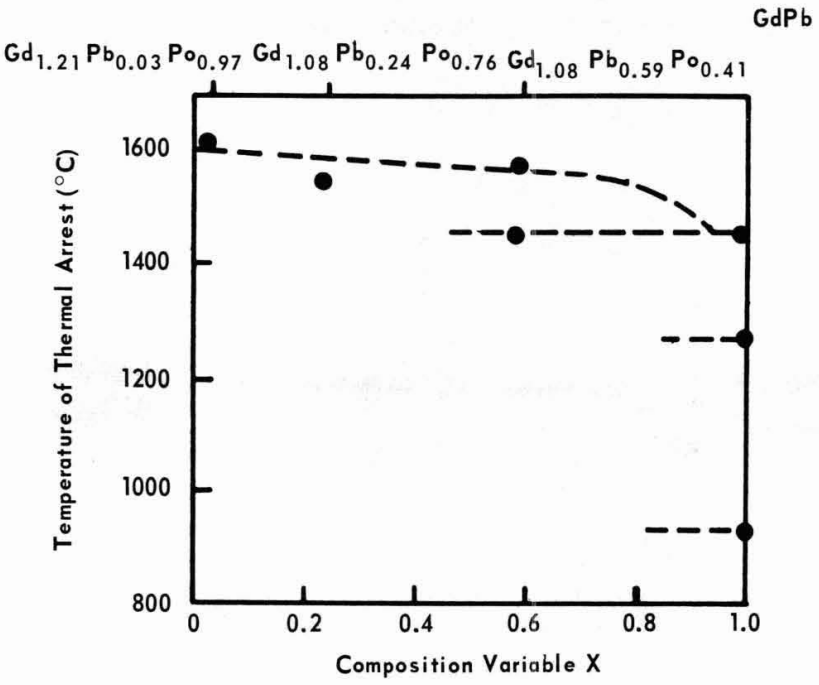

Fig. 2. Partial phase diagram for the $GdPb_xPo_{1-x}$ system

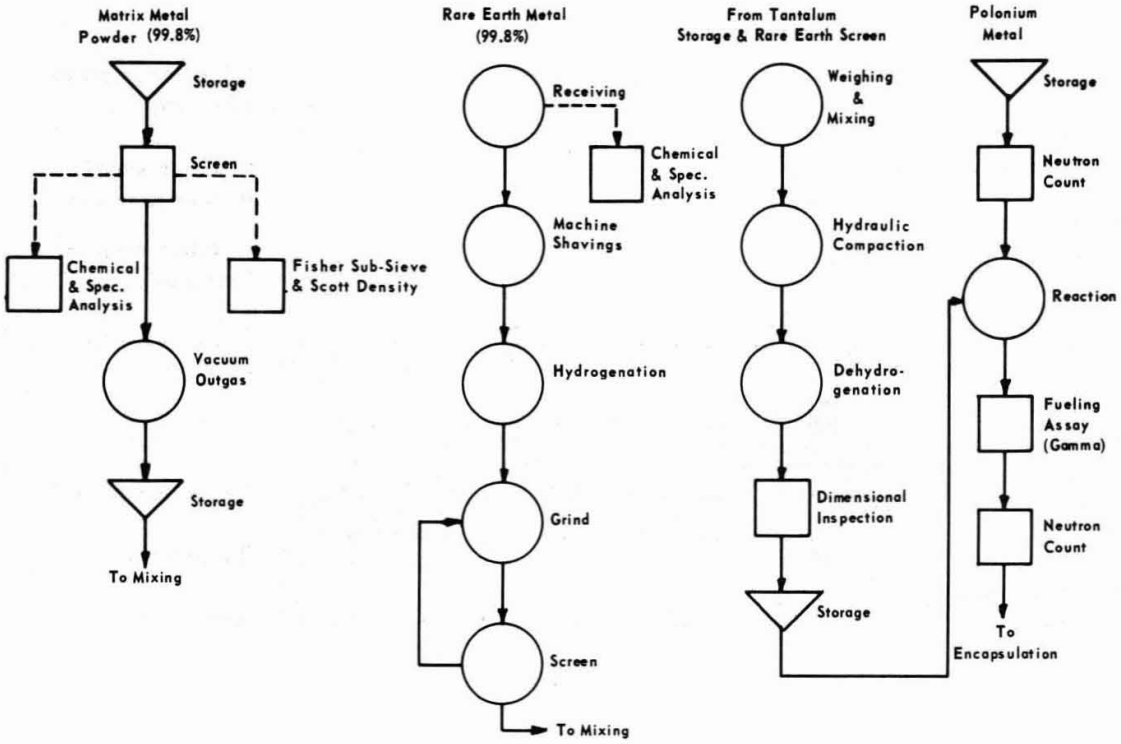

Fig. 3. Polonium-210 matrix fuel process flow diagram. The squares represent inspections; the triangles represent storage; and the circles represent operations in the process. Process flow is indicated by the solid lines connecting the activities; sample flow is indicated by broken lines.

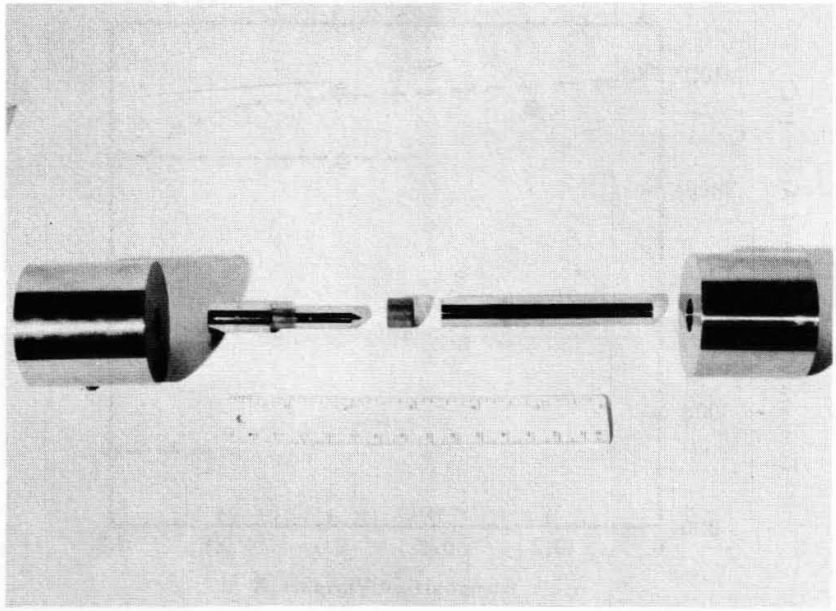

Fig. 4. Typical matrix die set

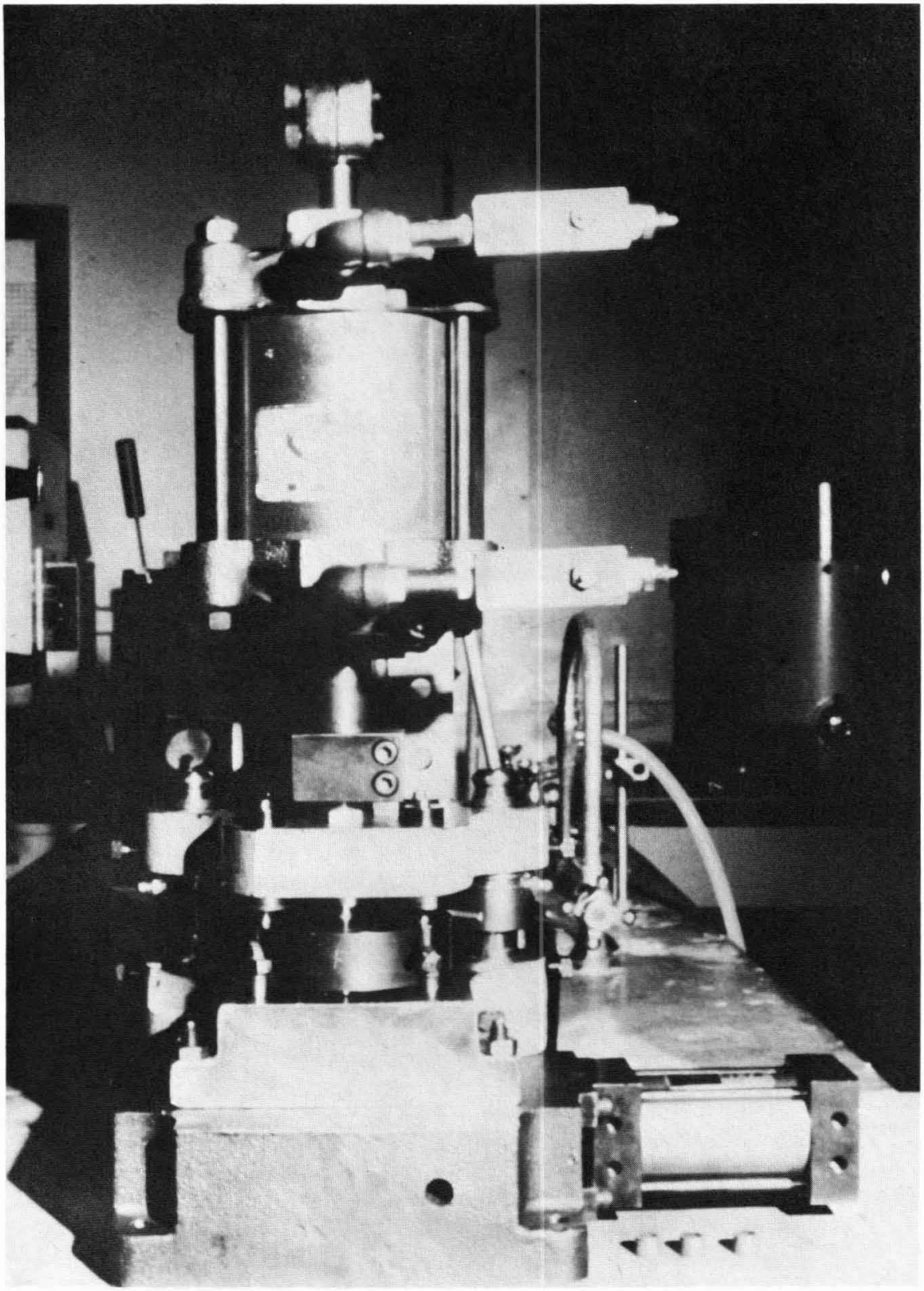

Fig. 5. Automatic matrix press

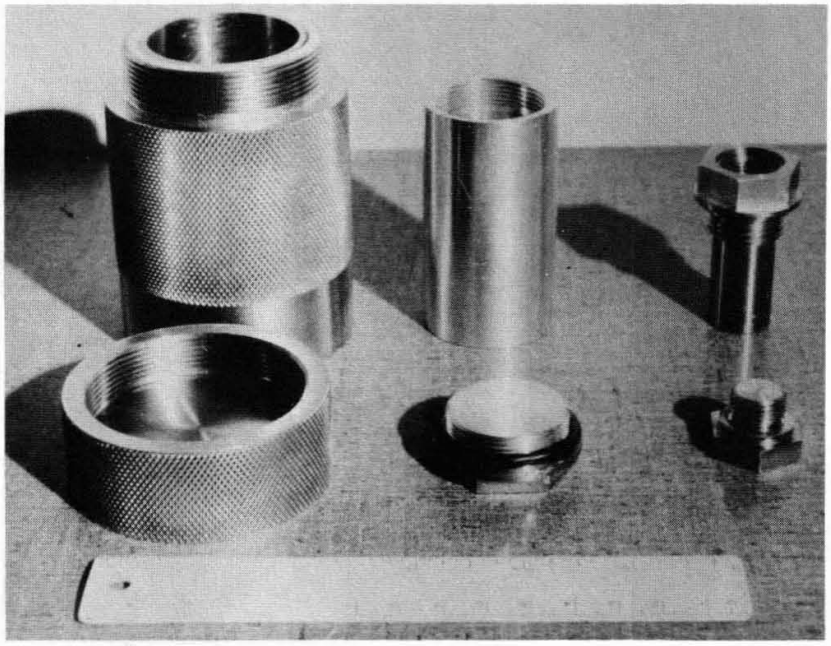

Fig. 6. Matrix reaction assembly

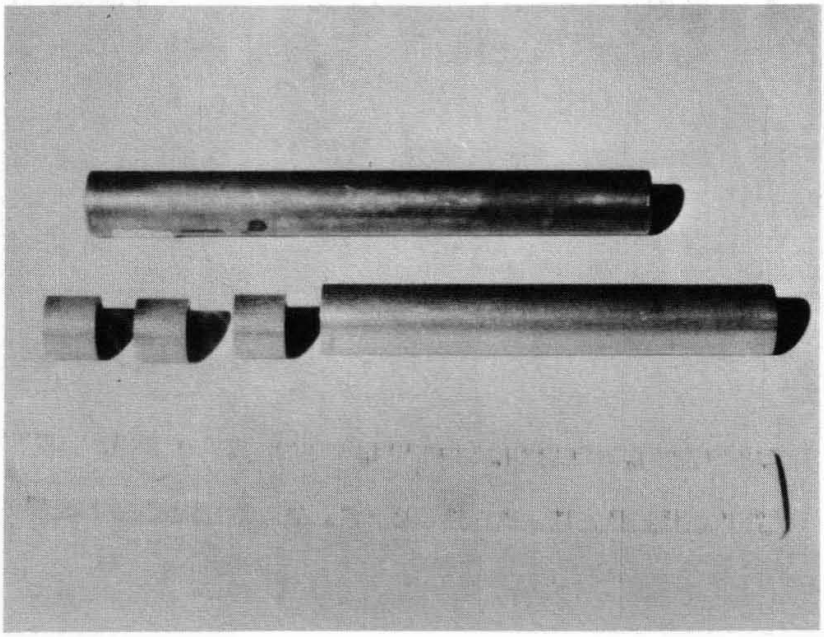

Fig. 7. Typical fuel matrix

PROPERTIES AND FABRICATION OF CURIUM-244 AND STRONTIUM-90 FUEL FORMS*

R. E. McHenry

Abstract

The compounds $^{244}Cm_2O_3$, SrO, $SrTiO_3$, and Sr_2TiO_4 are being developed for use as isotope fuel forms for generation of high temperature heat fluxes which can be converted to electric power. The efficient and safe use of these isotope fuels requires that a suitable compound be prepared and fabricated into a suitable form with fully characterized physical and chemical properties. The task elements for accomplishing this program consist of 1. compound preparation, 2. compound fabrication, 3. compound characterization, 4. source design, and 5. prototype testing. Techniques developed for accomplishing these tasks and the results achieved to date are reviewed.

*Research sponsored by the U. S. Atomic Energy Commission under contract with the Union Carbide Corporation.

R. E. McHenry is a research chemist with the Oak Ridge National Laboratory, Oak Ridge, Tennessee.

Introduction

The safe and efficient use of radioisotopes as heat sources in the varied applications (extant, proposed, or envisioned) requires a choice of compounds of suitable isotopes (1) with known physical and chemical properties and demonstrated fabrication technology. The properties and the fabrication of ^{90}Sr oxide and titanates and ^{244}Cm oxide are reviewed in this paper. Other compounds of both ^{90}Sr and ^{244}Cm have been considered as candidate source compounds, including the silicides of strontium and curium (2); the oxide, carbide, nitride, sulfide, oxysulfide, phosphide, and phosphosulfide of curium (2); the borides of strontium and curium (3); and strontium metal and alloys (4).

In addition to the more extensive characterization of SrO, $SrTiO_3$, Sr_2TiO_4, and Cm_2O_3 reported here, other compounds have been prepared and characterized to a lesser extent. The solubility, thermal conductivity, and density of SrF_2 were investigated at Martin Company (5). Strontium fluoride was prepared on a pilot-plant scale at ORNL by a dry method and by a homogeneous precipitation procedure (6,7). Dense compacts of SrF_2, strontium metal, and SrSi and CeB_6, Ce_2S_3, Ce_2O_2S, and CeF_3 compounds (using cerium as a stand-in for curium) were prepared at ORNL and compatibility studies (7,8) were carried out. The compounds Ce_2O_2S and Ce_2S_3 have been prepared on a pound scale by a procedure (9) which should be applicable to curium compounds.

The properties of a radioisotopic power fuel which must be known to predict the behavior of the fuel can be divided into two categories (Table 1): those which relate primarily to terrestrial safety and operational aspects, and the additional properties primarily for aerospace safety.

Several methods for the fabrication of materials (especially polycrystalline ceramics) into dense compacts are described in the literature. In general these methods consist of the application of heat and/or pressure over a period of time, which can be applied simultaneously or in sequence. Forming methods can be divided into three groups: 1. Cold forming (10-13), which usually consists of applying pressure to the material. Types of cold forming include slip casting, extrusion, injection molding, die pressing, isostatic pressing, and vibratory compaction. Compacts produced by cold forming can be subsequently heated to yield higher densities. 2. Hot forming (14-27), which consists of the simultaneous application of heat and pressure. The pressure can be applied uniaxially (hot pressing or hot swagging), biaxially, or multiaxially (isostatic hot pressing with gas or liquid medium or with semifluid sand). 3. Melt casting, which consists of the application of heat without pressure.

The pressure in any hot- or cold-forming method can be applied by a high energy rate procedure (28-33) such as pneumatic impaction, explosion, or electrical discharge.

All of the cold-forming, hot-forming, and melt-casting methods were evaluated for use with strontium and curium fuels. Some methods were tested experimentally: die press (heat treat), isostatic press (heat treat), uniaxial hot press, biaxial hot press, and melt cast. Isostatic hot pressing and pneumatic impaction at high temperature were evaluated by consultation and literature survey.

Although cold-forming methods (with the exception of isostatic pressing and firing) are simple and inexpensive for use in a hot cell,

the densities achieved are low and very poor dimensional control in the finished product is obtained after firing. These factors are difficult to control even with powders prepared by highly reproducible procedures. The control of particle size (a critical parameter in cold-forming methods) of strontium and curium fuels is unfeasible. In the case of isostatic pressing, high green (unfired) densities may be obtained if the pressure exceeds the strength of the particles. The small additional shrinkage on firing allows good control of dimensions. The high cost and complicated equipment are disadvantages of isostatic pressing.

The hot-forming method (except isostatic hot pressing) has two distinct advantages over the other methods: the dimensional accuracy of the compact formed and the adaptability of the method to a wide variety of materials. The hot-forming method also has the advantage that two materials can be allowed to react to produce the desired compound as the compact is being formed (reactive hot pressing). Isostatic hot pressing gives poor dimensional control unless the powder is prepressed to densities >85% of theoretical, which is difficult to achieve because of the uncontrolled particle sizes obtained in radioactive fuels. In addition, isostatic hot pressing is difficult and expensive for use in hot cell operation. Uniaxial or biaxial hot pressing can be accomplished readily in a hot cell with moderate equipment cost.

Melt-cast methods are most applicable to materials which melt at <1200°C. With strontium and curium fuels having high melting points ($SrTiO_3$, ~1950°C, Sr_2TiO_4, ~1850°C; SrO, ~2400°C, and Cm_2O_3, ~2260°C), the melt-cast method is not considered competitive with hot pressing. In general the densities obtained by casting are low due to high void volumes and casting pipes.

The fabrication of ^{90}Sr and ^{244}Cm fuels and the properties of these fuels are reviewed in this paper including brief discussions of the methods of property measurements and the results.

Strontium-90 and Curium-244 Compounds

Curium Fuel

The production of ^{244}Cm on a kilogram scale has been described by Groh et al. (34) who also describe the radiochemical purity of production quality $^{244}CmO_2$. The following chemical purity (35) is anticipated:

Elemental impurities	Maximum wt % of curium
Li + Na + K (total)	0.1
Si + Zn (total)	0.1
Fe, Cr, Ni (each)	0.2
Any other single impurity (except Am and Zr)	0.2
Total of all impurities (except Am and Zr)	1.0
Total of all impurities (including Am and Zr)	3.0

The isotopic composition (36) is anticipated to be:

Nuclide	Mass abundance, wt %	Nuclide	Mass abundance, wt %
^{242}Cm	0.02	^{247}Cm	0.07
^{243}Cm	0.002	^{248}Cm	0.05
^{244}Cm	95.3	^{243}Am	0.5
^{245}Cm	0.9	^{252}Cf	$<4 \times 10^{-5}$
^{246}Cm	2.7		

Curium, like the actinides plutonium and americium and the lanthanides cerium and praseodymium, can exist as an oxide in more than one oxidation state. Asprey et al. (37) prepared a black oxide by ignition at ~400°C and cooled it in air. A white or faint tan oxide was prepared by thermal decomposition of the black oxide at 600°C and 10^{-4} torr. These oxides were deduced to be CmO_2 (black) and Cm_2O_3 (tan) by X-ray analysis. Posey et al. (38) investigated the composition of curium oxide as a function of temperature and oxygen partial pressure. By using thermal gravimetric analysis CmO_2, Cm_2O_3, and two intermediate phases of composition, $CmO_{1.71}$ and $CmO_{1.83}$ (Fig. 1), were identified. Stable Cm_2O_3 was readily formed by thermal decomposition of a higher oxide in vacuum or nonoxidizing atmospheres. Mosley (39) confirmed the work of Posey et al. (38). Chikalla and Eyring (40) confirmed the earlier work and extended the investigation of the curium-oxygen system. They report the partial molar free energies of oxygen.

Wallman (41) studied the effect of self-radiation on curium sesquioxide (bcc, a = 11.00 ± 0.01 Å) which he prepared by heating $^{244}CmO_2$ at 600°C in vacuum. He identified an A-type Cm_2O_3 (hexagonal, a = 3.80 ± 0.02 Å, c = 6.00 ± 0.03 Å) produced by self-radiation. Haug (42) succeeded in preparing B-type Cm_2O_3 (monoclinic, a = 14.282 ± 0.008 Å, b = 3.65 ± 0.003 Å, c = 8.900 ± 0.005 Å, β = 100.31 ± 0.05°) by heating C-type Cm_2O_3 above 850°C. The A-type Cm_2O_3 was prepared by Mosley (39) by heating B-type Cm_2O_3 above 1600°C, where a reversible transformation occurs. He reported the monoclinic form of Cm_2O_3 to be resistant to alpha radiation. Mosley reevaluated the lattice constants of all the forms of Cm_2O_3 (Table 2) and compared the transformation to those that occur in lanthanide oxides (Fig. 2). He concluded that B-type Cm_2O_3 is structurally best suited for a source form. Phase diagrams for the curium-oxygen system have been tentatively proposed by Smith (43) and Chikalla (40) (Figs. 3 and 4, respectively). Smith's construction of a phase diagram is from the data of Mosley (39) and Posey (38) and is for the condition in air at atmospheric pressure. Chikalla's construction is from his thermal analysis data and covers the composition range of Cm_2O_3 to CmO_2.

Strontium Fuel

The processing of fission products for the separation and purification of ^{90}Sr has been described in the literature (44). The production of ^{90}Sr fuel compounds began in early 1961 with the fueling of the weather station generator (45). More recently ^{90}SrO and Sr_2TiO_4 have been prepared at ORNL. A compendium of the development of ^{90}Sr fuels including the current practice is in preparation (46).

Fission-produced (46) ^{90}Sr consists of 55% ^{90}Sr, 43.9% ^{88}Sr, and 1.1% ^{86}Sr. In addition to the stable isotopes of strontium, lesser amounts of stable Ca, Ba, and Mg, which are not separated during processing, are present. Typical compositions (47) for the strontium fuel compounds, SrO, Sr_2TiO_4, and $SrTiO_3$, are given in Table 3.

The system SrO-TiO_2 has been studied by Dryś and Trzebiatowski (48) who prepared a phase diagram (Fig. 5). They indicate that the system SrO-TiO_2 forms three compounds, $SrTiO_3$, Sr_2TiO_4, and $Sr_3Ti_2O_7$; the latter compound is stable only at temperatures below 1640°C.

The dioxide of titanium is known to reduce to TiO_{2-x}, where x varies between 0 and 0.5 depending on the temperature and oxygen pressure (49). Strontium titanates likewise are reducible under severe conditions. From the data of Moser et al. (49) $SrTiO_3$ at 1300°C and an oxygen pressure of 1 μ Hg would be reduced to $SrTiO_{2.999}$. The reduced strontium titanate is jet black but otherwise indistinguishable from material of stoichiometric composition.

Fabrication of Strontium-90 and Curium-244 Fuel Forms

Strontium-90 and ^{244}Cm fuel forms are fabricated by hot pressing except under unusual circumstances. Both isotopes have been prepared by pressing and sintering, but this method is not discussed in this paper.

The densification of powdered materials by hot pressing can be described by assuming a plastic flow model (10,11) which is a function of time, temperature, and pressure. The plastic flow model has been successfully applied (12,13,19) to experimental data.

If pressure is applied to a material at a given temperature, the density of the material increases as a reciprocal log function of time and asymptotically approaches a relative value of density. This value is usually referred to as the end point density for that particular pressure and temperature. An increase in pressure increases the relative value of the end point density. A function of the density (18), f(D), is directly porportional to pressure:

$$f(D) = kp, \qquad (1)$$

where

p = pressure
$k = 1/2\tau_c$
$f(D) = 1 - (1 - D)^{2/3} \ln 1/(1 - D)$
τ_c = yield point of material.

An increase in temperature increases the end point density. A complex function for the effect of temperature on the end point density has been given by McClelland and Smith (18) (Figs. 6 and 7) for BeO and Al_2O_3. They conclude that at sufficiently high temperatures, where the yield point of the material is small as compared with the pressure applied, the end point density rapidly approaches the theoretical density. Experience with strontium and curium fuel compounds has indicated that in all cases tested 4000 psi and 1400°C are sufficient to assure that τ_c is small compared with the pressure applied.

Several hot presses for the fabrication of ^{90}Sr and ^{244}Cm fuels have been designed and successfully tested (Table 4). The first two presses in Table 4 have been described by Quinby et al. (50). The four presses currently in use are illustrated in Figs. 8-11.

Prototype Production of SrO by Hot Pressing

Hot Pressing with a Liner. Three 202-w ^{90}Sr heat sources (Table 5) were prepared by hot pressing ^{90}SrO in platinum sheaths and then encapsulating the fuel in welded Hastelloy-X inner containers and welded Hastelloy-C outer containers.

The pellets were prepared at the Fission Products Development Laboratory from four batches of ~35,000 Ci each of $^{90}SrCO_3$. The dried $^{90}SrCO_3$ powder was calcined in air at 1200°C for a minimum of 24 hr. The resulting products were assayed for ^{90}Sr by weighing increments of the powder and determining the heat output. Small samples of powder were dissolved in nitric acid and analyzed spectrographically for inert contaminants (Table 6); these solutions were also analyzed for radioisotopic contamination. The mass analysis for ^{90}Sr indicated 53.3 ± 0.5%. The average density attained for SrO was 4.27 g/cm^3.

The fuel pellets were prepared by pressing (Fig. 8) the SrO in a platinum-lined graphite die. The platinum liner remained with the SrO pellet to protect it from the atmosphere. The temperature of the hot press was increased from ambient to 1200°C. At this temperature, the pressure was raised to 3700 psi at a rate of 800 psi/min and maintained at 3700 psi for 1 hr. The pellets were of excellent appearance with no change in appearance or dimensions after 10 days.

Hot Pressing Without a Liner. Since most of the densification occurs at <800°C, tests were made by applying full pressure (4000 psi) to the die punch from ambient temperature to 1200°C. If the temperature is increased at a rate of 100°C/hr from 750 to 850°C, complete densification is attained at 850°C. However, if the temperature is increased above 1200°C before pressure is applied, the density does not exceed 94% of theoretical density even if the temperature is increased to 1600°C. These experiments were done in a vacuum hot press (Fig. 10) of capacity up to 1-in.-dia pellets. The results of the above experiments suggest that either a large change occurs in the surface energy of the powder at 850°C or a sintering aid which exists as an impurity in the SrO powder is destroyed at that temperature. The latter is more likely. Small amounts of either $Sr(OH)_2$ or $SrCO_3$ could be present and could account for the low temperature sintering. Pellets are heated to 1200°C after densification to destroy any $Sr(OH)_2$ or $SrCO_3$ which may be present.

At temperatures of <1500°C, SrO will not react with carbon to produce SrC. This conclusion is based on thermodynamic calculation. Since the final procedure does not require a temperature in excess of 1200°C, SrO was hot pressed directly in graphite dies. No SrC was found in the SrO pellets. The SrO did not stick to the graphite die and punch material. The platinum liner is used only to provide protection for moisture when pellets are fabricated in ambient air hot cells.

Hot Pressing of $SrTiO_3$ and Sr_2TiO_4

Although a hot-pressing procedure is relatively insensitive to the history of the powder, it has been observed that higher densities (for given pressing conditions) can be obtained with freshly prepared powder. The next highest densities are obtained with aged titanate powder and the lowest, with highly sintered or previously hot-pressed and crushed material.

In general at higher pressing temperatures, higher densities (up to 100% dense) are obtained; also less time and lower pressure are required to obtain a given density. The temperature should never exceed 1450°C

because the pellet rapidly decreases in density with extensive fragmentation, probably due to a solid-solid phase transition at this temperature. At 1350°C densification of all powders tested was sufficiently rapid, and pressing times of <1 hr were required.

The pressure which can be applied to a die is limited by the die geometry and the strength of the graphite. A pressure of 4000 lb is adequate for a pressing time of <1 hr. Die designs for 4000 psi on 4-in.-dia compacts are considered practicable. Pressures in excess of 4000 psi (where strength considerations permit) reduce the pressing time required. Sintering of $SrTiO_3$ powder occurs at an appreciable rate at 900-1000°C. For this reason, the pressure should be applied at 900°C.

Strontium-90 Titanate Fabrication. Strontium titanate pellets of 2 in. dia were hot pressed to essentially theoretical density by using 1000 psi at 1000°C, then increasing to 4000 psi at 1200°C for 1 hr. The theoretical density of pure $SrTiO_3$ is 5.11 g/cm^3. The calculated density of fission-product $^{90}SrTiO_3$ containing Mg, Ca, and Ba impurities (Table 3) is 5.03 g/cm^3 (Table 7).

Strontium Orthotitanate (Sr_2TiO_4) Fabrication. Hot-pressing conditions for Sr_2TiO_4 are very similar to those for $SrTiO_3$ except that slightly higher temperatures are used. The calculated density of fission-product $^{90}Sr_2TiO_4$ is 4.93 g/cm^3 (Table 7). Pellets of Sr_2TiO_4 were hot pressed by using 1000 psi at 800°C, then increasing to 4000 psi at 1400°C for 30 min. The average density of 24 pellets pressed under the above conditions was 4.94 g/cm^3.

Pellet Dimensional Integrity

Future applications of $SrTiO_3$ may require sources with diameters up to 5 in. Strontium titanate which is treated at high temperatures (1200-1400°C for hot pressing) in a neutral or reducing atmosphere undergoes a reduction in the oxygen stoichiometry. Under hot pressing conditions, $SrTiO_3$ has the composition (49) $SrTiO_{2.994}$. Pellets of reduced $SrTiO_3$ are jet black. If the pellets are of high density and reduced, they are severely strained and subject to cracking. Annealing cannot be accomplished at <2000°C. Pellets of both active and inactive $SrTiO_3$ of 3 in. dia have been hot pressed. All of the radioactive pellets exhibited extensive cracking due to thermal gradients. Pellets of nonradioactive $SrTiO_3$ are highly sensitive to thermal shock and also frequently crack. To help maintain the integrity of the pellets, several factors were studied to determine their influence on cracking. The only significant result is that low density pellets (<4.0 g/cm^3) are much less likely to crack.

Two methods to prevent cracking were tested successfully on 1-in.-dia pellets. One method consists of incorporating randomly oriented 5-mil wire, 1/4 in. long, in the pellet; in the other method, the pellet is sheathed with nickel or platinum wire gauze which is mechanically bonded to the surface of the pellet. Further work is required to demonstrate either technique on 4-in.-dia pellets.

Vacuum Hot Pressing

When compacts are formed by hot pressing in an inert atmosphere (argon) small bubbles of argon at a pressure equal to that used in forming the compact can be occluded. The gas may subsequently diffuse into the void volume and cause an increase in the pressure inside a capsule.

With vacuum hot pressing, this possibility is precluded and also in general the pellets have less porosity (and higher density).

Fabrication of Curium-244 Sesquioxide

The fabrication of Cm_2O_3 has been limited to experiments with small pellets of ~1/4 in. dia. Only within the past few months has sufficient material been available for large-scale fabrication tests. Equipment is currently being assembled at ORNL to fabricate 1-in.-dia $^{244}Cm_2O_3$ pellets by vacuum hot pressing (Fig. 11).

The conditions chosen for the fabrication of small test pellets of $^{244}Cm_2O_3$ were vacuum hot pressing at 4000 psi and 1380°C for 30 min. (The hot press is shown in Fig. 9.) These conditions were chosen from extensive tests made on Ce_2O_3, Pr_2O_3, Nd_2O_3, Gd_2O_3, Tm_2O_3, and ThO_2. In all cases, essentially 100% dense pellets were obtained under the above conditions. However, the densities of Cm_2O_3 obtained varied widely (from 50 to 96.5% of theoretical). The erratic results were probably due to variations in die friction (an important and difficult factor to control in the hot pressing of very small pellets). At least, the results indicate that hot pressing of $^{244}Cm_2O_3$ to high density can be accomplished at moderate pressures and temperatures below 1400°C.

The use of $^{244}Cm_2O_3$ microspheres formed by a sol-gel process is under study at ORNL as a means of fabricating curium sources.

Fabrication of Special Source Designs

Specially designed sources will be required in some applications, especially with large thermionic sources where helium release, heat flux control, mass transport, and/or large thermal gradients may be controlling factors. Posey and McHenry (53) and Posey (54,55) have studied the effect of these factors on source designs. Some elements of source design, such as high thermal gradients and heat flux, can be controlled (51-53) by the use of oriented or randomly distributed metal in the source fuel. These sources would require fabrication methods not yet fully demonstrated. The retention of helium in curium fuel is under investigation at ORNL. One approach to the helium problem is to fabricate pellets with a high percentage of interconnecting voids. Cottrell et al. (56) state that in the release of fission gases from UO_2, the release rate is independent of sample size for all samples of <95% of theoretical density.

Fuel Properties

The properties of a radioisotope heat source inevitably change with time. The source is, at best, a pure compound only at the instant it is formed; thereafter, due to radioactive decay, it is a system of changing composition. In addition to the changes resulting from the accumulation of decay products, the effect of self-radiation must also be considered. The changes in the properties produced by self-radiation are primarily those which occur as a result of changes in the structure of the solid. Properties most likely to be affected include density, thermal conductivity, helium release, mechanical strength, and leach rate. Other properties such as vapor pressure, melting point, heat capacity, boiling point, heat of vaporization, and heat of fusion are essentially unaltered by radiation damage. As the temperature of a heat source increases, annealing of defects produced by radiation damage increases, so that at

a given temperature steady state is established between the effects of annealing and those of radiation damage. At the temperatures at which heat sources will be used, steady state is established in a short time compared with the mission life of the source.

Property measurements made on nonradioactive samples (strontium fuels) or properties inferred from measurements made on analogous nonradioactive materials (actinide and rare-earth stand-ins for curium fuels) are valid only if the property being determined is unaffected by radiation damage. Property measurements of nonradioactive samples can be assumed to represent the values at time zero when radiation damage is nil. To completely describe the physical properties of a heat source, the effects of radiation damage-thermal anneal at steady state must be determined, and the transient effects of radiation damage and composition changes with time must be established. In this section of the paper the property measurements made in the continuing effort to characterize ^{90}Sr and ^{244}Cm heat source fuels are reviewed. Estimated values for properties of ^{90}Sr and ^{244}Cm which have not been measured are reported by Rimshaw and Ketchen (47,57).

Strontium Fuel Properties

Density. The theoretical densities of strontium fuels are given in Table 7. The table includes the theoretical densities of the pure compounds and typical strontium fuel products. Measured densities of strontium fuel products are also given. The density of strontium fuel varies slightly with the composition of the fuel. The densities of the fuel form (i.e., the fuel, matrix, but excluding the capsule) depend on the source design (see page 7).

Thermal Coefficient of Expansion. The mean linear coefficient of expansion of SrO has been determined to be $13.92 \times 10^{-6}/°C$ from 20 to 1200°C by Beals and Cook (58) using X-ray measurements of the lattice parameters. The coefficient of expansion (59) of $SrTiO_3$ is reported to be $11.2 \times 10^{-6}/°C$ over the range of 100-700°C.

The coefficient of expansion (60) of two nonradioactive strontium fuels, SrO and $SrTiO_3$, has been determined to 1400°C with a Brinkman Model 5440 dilatometer (Table 8). To simulate a typical radioactive strontium fuel, samples were prepared with a composition of 92.3 wt % Sr, 3.7 wt % Ca, 3.7 wt % Ba, and 0.3 wt % Mg. The $SrTiO_3$ sample was 1 in. in length and contained 5% excess TiO_2 over the stoichiometric ratio of $SrO \cdot TiO_2$. The SrO sample was 1/2 in. in length. (Both samples were prepared by hot pressing.)

The measured values given are the mean coefficient of expansion for the temperature intervals shown. The mean coefficient of expansion, A_m, is defined as

$$A_m(t_o,t) = \Delta L/L\Delta t, \qquad (2)$$

where

$A_m(t_o,t)$ = mean coefficient of expansion from t_o to t°C,
ΔL = change in sample length over Δt,
L = sample length at temperature t_o°C, and
Δt = temperature interval from t_o°C to t°C.

The data for $SrTiO_3$ are in good agreement with values previously reported to 700°C by Bloom. Above 1400°C, the $SrTiO_3$ sample became semiplastic and distorted under the light load imposed by the dilatometer.

This is probably due to a small amount of liquid phase of composition $SrTiO_3$ plus TiO_2 (due to 5% excess TiO_2) which melts at 1440°C (see phase diagram for the system SrO-TiO_2, Fig. 5).

Specific Power and Power Density. The specific power of elemental 100% ^{90}Sr as calculated from the maximum beta energies (max E ^{90}Sr, 0.545 Mev; av E ^{90}Sr, 0.20 Mev; max E ^{90}Y, 2.27 Mev; av E ^{90}Y, 0.944 Mev) and half-life (28.0 yr) is 0.954 w/g. Theoretical and typical values for strontium fuels are given in Table 9.

Leach Rate. Dissolution rate studies (61) were performed using three SrO pellets prepared by hot pressing at 1300°C and 4000 psi for 1 hr. In the test, a specimen weighing 43.962 g with a density of 4.54 g/cm^3 was suspended from an analytical balance beam in a container through which a constant linear flow rate of 4.4 cm/min of distilled water was maintained. Periodic weighings of the specimen were recorded for 7 days.

The dissolution rates for SrO calculated from the data in the above experiment are given in Table 10. The values were calculated on the basis of the initial surface area of the pellet. The surface area of the pellet was not measured after the start of the experiment. The values after the first day are low as expected but are consistent with the assumption that the rate is linear with time and is equal to the value reported in Table 10 for the time interval 0-1 day.

The leach rates of several ^{90}Sr titanate fuels (62) of various compositions (see Table 11) were determined in distilled water. The fuels include SNAP-7A samples (recovered from SNAP-7A fuel capsules after 7 years of operation) prepared by sintering and samples of aged and freshly prepared ^{90}Sr titanate prepared by hot pressing. The tests using 0.5-in.-dia by ~3/8-in.-high samples have been in progress for 45 days and are continuing.

The apparatus for the leach-rate experiments can contain 12 samples. A sample is placed in a perforated 3-cm-dia glass cylinder, which is immersed in a 1.5-liter glass flask containing the test solvent (distilled water). The solvent is agitated by pulsing 100 ml of the solvent in and out of the flask and into a surge pot-sampler every 30 sec. Sampling is accomplished by valving off solvent in the surge pot-sampler and by draining the sample into a sample container. All samples are filtered immediately through a Millipore filter prior to dilution and assay.

The results of the leach rate experiments up to 45 days are shown in Fig. 12. (Samples 11 and 12 disintegrated within a few hours, and no quantitative measurements of leach rate could be made.) Data from the samples have been correlated under the assumption that the leach rate follows the parabolic law. Data shown in Fig. 12 are in agreement with data obtained during the first few days of similar experiments (63) using freshly prepared $SrTiO_3$ (sintered) containing ^{85}Sr tracer and freshly prepared $^{90}SrTiO_3$ (sintered). In the previous work, a large deviation from the parabolic law occurred after 10 days due to disintegration of the samples. This effect has not yet been seen in the aged sintered or freshly hot-pressed samples.

Radiation and Shielding. Shielding requirements on ^{90}Sr fuels are necessary due to the high energy bremsstrahlung produced by the interaction of beta particles with matter. Arnold (64) has calculated shielding thicknesses of various sizes and shielding materials for ^{90}Sr fuels.

Thermal Conductivity. The thermal conductivities of nonradioactive SrO, Sr_2TiO_4, and $SrTiO_3$ have been determined up to 900°C by Ketchen and

McHenry (65) by using a comparator-type apparatus on typical samples of fission-product ^{90}Sr fuels. The correlated data, the confidence limit on the curves, and the equations for each fuel are shown in Fig. 13. The thermal conductivities of several samples of $^{90}SrTiO_3$ (Table 12) have been measured using an absolute method in which the self-heat of the radioactive sample provides the heat flux (66). Data on the thermal conductivity of samples A, B, and C did not show any statistically significant differences among samples even though they differ in composition, in age, and slightly in density. Data were combined and fitted by least mean squares to an equation:

$$1/k = 19.754 + 0.026\ T(°K). \qquad (3)$$

The thermal conductivity of the SNAP-7A fuel (sample D) differs significantly from the other three samples in Table 12. The derived equation for the SNAP-7A sample is

$$1/k = 37.69 + 0.0562\ T(°K). \qquad (4)$$

The difference in the thermal conductivity of the SNAP-7A fuel and the other samples is attributed to the differences in density and age (accumulated radiation damage and ZrO_2 content).

Melting Points. The melting point (67) of SrO is reported to be 2457°C. The melting points of Sr_2TiO_4 and $SrTiO_3$ are shown in the phase diagram of Fig. 5.

Curium Fuel Properties

Density. The density of B-type (monoclinic) Cm_2O_3 as reported by Mosley (39) is 11.7 g/cm^3 at room temperature. This value was calculated from x-ray data assuming six molecules per unit cell. The densities of A- and C-type Cm_2O_3 are given in Table 2.

Thermal Coefficient of Expansion. The thermal coefficient of expansion (39) of monoclinic Cm_2O_3 is shown in Fig. 14 for temperatures up to 1420°C. The density of monoclinic Cm_2O_3 at 1600°C (obtained by extrapolation) is 10.9 g/cm^3. The density of A-type Cm_2O_3 at 1650°C (see Table 2) is 11.4 g/cm^3. Mosley suggests that the change in density from B-type to A-type structure at ~1600°C may affect the integrity of fabricated Cm_2O_3.

Specific Power and Power Density. The specific power of elemental 100% ^{244}Cm as calculated from decay energies and half-life (18.1 yr) is 2.78 w/g. The specific power of production quality $^{244}Cm_2O_3$ will approach 2.43 w/g depending on the level of ionic impurities. The theoretical power density of production quality $^{244}Cm_2O_3$ is 28.4 w/cm^3 at room temperature. If the pellets are assumed to have 95% of theoretical density, the density after fabrication is 27 w/cm^3.

Radiation and Shielding. The radiation characteristics of $^{244}Cm_2O_3$ product are given in reference 36. Arnold (64) has made calculations on the shielding requirement for curium isotope power fuels.

Helium Release. Data from the helium release experiments (68) using $^{244}Cm_2O_3$ microspheres and pellets have been correlated to obtain the "apparent diffusion coefficients" for microspheres in the range of 390 to 1200°C and for pellets in the range of 1100 to 1400°C. Data were obtained by allowing the 100-μ-dia microspheres to reach steady-state helium release at the desired temperature, a condition which was attained

in a few hours at 390°C and in a few minutes at 1200°C. The samples were then degassed at 1750°C to obtain the steady-state helium inventory.

The apparent diffusion coefficients (Table 13) were calculated from the average helium concentration (derived from Fick's Law):

$$C_{av} = R^2P/15D_a \qquad (5)$$

where

C_{av} = average helium concentration in microsphere,
P = helium production rate,
D_a = apparent diffusion coefficient, and
R = radius of microsphere.

The curium oxide pellets (cylindrical geometry) were prepared in a molybdenum crucible by melting a sample and then cooling rapidly (in ~2 min) to the required temperature. The difference in the coefficients of expansion between curium oxide and molybdenum provided clearance around the 0.254-cm-radius by 0.55-cm-high pellet. Values for helium release rates were observed as a function of time at the transient state beginning at t = 0 and approaching the equilibrium value. The apparent helium diffusion coefficients (Table 14) were calculated by computer program by using the relationship

$$dv/dt = f(t, D_a) \qquad (6)$$

where

dv/dt = helium release rate, cm^3/g of Cm_2O_3, and assuming $dv/dt = 0$ at $t = 0$.

As can be seen by comparison of the apparent diffusion coefficients in Tables 13 and 14, the values for pellets and microspheres differ by three orders of magnitude. If it is assumed that the diffusion rate, dv/dt, is independent of sample geometry (as for UO_2 of <95% density, see page 7), a correlation of D_a/R^2 is constant. The calculated equivalent superficial radius of the pellets used in these experiments was 0.22 cm. The superficial dimensions of the right cylinder were 0.25-cm radius by 0.55-cm height, indicating good correlation. This correlation of D_a/R^2 indicates that the pellets and perhaps the microspheres have extensive open porosity. Whether the open porosity was due to fabrication or was possibly caused by radiation or helium accumulation damage is not known. Neither is the cause of a decrease in the apparent diffusion coefficient at high temperatures known. However, it could possibly result from closing of the porosity by a sintering process. The data in Table 13 probably represent minimum values for the true diffusion coefficient.

Thermal Conductivity. The thermal conductivity (69) of curium sesquioxide was estimated for temperatures up to 1450°C from thermal diffusivity data determined by Pacific Northwest Laboratory (70) on samples prepared at ORNL and from molar heat capacity data for plutonium sesquioxide (71). (It is assumed that the molar heat capacity of Cm_2O_3 is the same as that of Pu_2O_3.)

The thermal diffusivity (70) was determined on a 4.40-mm-dia by 1.17-mm-high pellet with a density of 11.24 g/cm^3, which was prepared on November 1, 1967, by hot pressing at 1380°C for 30 min at an atmospheric pressure of 50 μ. The material was spectrographically analyzed on March 17, 1967. The material contained the following impurities (ppm of curium oxide): Zr, <150; B, <10; Si, 50; Mn, 10; Pb, 10; Fe, 1000;

Sn, 150; Cr, <25; Co, <50; Ni, 100; Bi, <10; Al, 100; Mo, <10; Cu, 100; Cd, <50; Zn, <500; Li, <50; Na, 100; Ca, 400; Ag, <10; and Mg, 50. The sample also contained ~4% plutonium from decay of curium.

The calculated thermal conductivity values are given in Fig. 15 and Table 15. The thermal conductivity is the product of thermal diffusivity and volume heat capacity, where the volume heat capacity is the product of molar heat capacity and density divided by molecular weight. Smoothed values of the thermal diffusivity were used. The density was assumed to remain constant at 11.24 g/cm^3.

The data indicate that accumulated radiation damage and/or retained helium have no significant effect above 400°C. The lower thermal diffusivity values initially obtained at <400°C were not observed on heating above 400°C or subsequently below 400°C.

The estimated thermal conductivity is lower than expected. The thermal conductivity (72) of ZrO_2, which is among the lowest of the oxide-type ceramics, is given in Fig. 15 for comparison. There is a general tendency for the thermal conductivities of oxides to decrease with increasing atomic weight. The relatively small change in thermal conductivity of $^{244}Cm_2O_3$ with temperature is typical of impure materials (the $^{244}Cm_2O_3$ contained 4% PuO_2).

Measurements on the thermal conductivity of $^{244}Cm_2O_3$ are in progress at ORNL using an absolute method (66).

Melting Point. The melting point of a sample $^{244}Cm_2O_3$ of unknown purity was reported by McHenry (73) to be 1950°C. Subsequently, measurements made on highly purified Cm_2O_3 (low plutonium content) gave higher melting points. Smith (74) reports 2255-2277°C for his most purified material and 2173-2186°C for material of composition similar to production quality $^{244}Cm_2O_3$. Chikalla (75) made similar measurements of purified Cm_2O_3 and obtained melting temperatures of 2220-2240°C.

Critical Mass. The critical mass of $^{244}Cm_2O_3$ has been calculated (76) at ORNL from cross-section data. The results (Table 16) indicate an underestimation of the critical mass, compared with replacement measurements made at Los Alamos (76).

Vapor Pressure and Heats of Vaporization and Formation. The vaporization rates of $^{244}Cm_2O_3$ have been measured by Smith (43) using a conventional Knudsen effusion technique. From Knudsen effusion data, the vapor pressures and heats of vaporization can be determined if the vapor species are known. Since the vapor species are not known (however, they are inferred by Smith from thermodynamic considerations to be Cm plus O), he arbitrarily expresses his vapor pressure data (Fig. 16) in terms of one mole of solid Cm_2O_3 vaporizing to one mole of gaseous (hypothetical) Cm_2O_3. He gives the heats of vaporization for the hypothetical condition of one mole of solid Cm_2O_3 vaporizing to 5 moles of gaseous atoms. When the vaporization reaction is determined, his vaporization rate data can readily be adjusted for the vaporization reaction to obtain true vapor pressures and heats of vaporization. The equation for the vapor pressure is

$$\text{Log } P_E \text{ (atm)} = 7.32\ (\pm\ 0.26) - \frac{29050\ (\pm\ 590)}{T(^\circ K)}. \qquad (7)$$

The equation was fitted to the data by least mean squares. Errors are standard deviation.

The heat of vaporization of one mole of Cm_2O_3 to 5 moles of gaseous atoms over the temperature range of 1800-2600°K was calculated to be 665 ± 13.5 kcal per mole of Cm_2O_3. The heats of vaporization were calculated to be 678.5 ± 8.0 and 670 ± 10 kcal per mole of Cm_2O_3 at 0°K as derived from the Third Law and Second Law of thermodynamics, respectively.

The heat of formation at 0°K was estimated by Smith (43) to be -429 ± 14 kcal per mole.

REFERENCES

1. C. A. Rohrmann, Radioisotopic Heat Sources, USAEC Rpt. HW-76323, Rev. 1, Hanford Atomic Products Operation, October 15, 1963.

2. E. E. Ketchen, Oak Ridge National Laboratory, November 14, 1963 (unpublished work).

3. S. J. Rimshaw, ORNL-3741 (classified), Oak Ridge National Laboratory, December 1964.

4. W. D. Box, Oak Ridge National Laboratory, August 13, 1965 (unpublished work).

5. J. J. Keenan, Strontium-90 Power, Final Summary Report, Rpt. MND-SR-1676, Martin Nuclear, 1960.

6. E. Lamb, Oak Ridge National Laboratory, personal communication, September 1965.

7. E. Lamb, Oak Ridge National Laboratory, personal communication, March 1965.

8. W. D. Box and R. S. Crouse, Compatibility Tests for Selection of Radioisotope Heat Source Compounds, USAEC Rpt. ORNL-4298, Oak Ridge National Laboratory (to be published).

9. E. E. Ketchen, Preparation and Forming of High-Purity Cerium Oxysulfide, USAEC Rpt. ORNL-TM-2117, Oak Ridge National Laboratory, March 1968.

10. P. W. Clark and J. White, Transactions of the British Ceramic Society, 49, 1950, pp. 305-39.

11. J. K. Mackenzie and R. Shuttleworth, Proceedings of the Physical Society (London), 62, 1949, pp. 833-52.

12. P. W. Clark, J. H. Cannon, and J. White, Transactions of the British Ceramic Society Incorporating British Ceramic Abstracts, 52, 1953, pp. 1-49.

13. E. B. Allison and P. Murray, A Fundamental Investigation of Sintering Phenomena, AERE Rpt. M/R 1099, Harwell, England, January 1953.

14. J. D. McClelland and E. H. Zehms, Semi-Continuous Hot Pressing, Rpt. NAA-SR-6453, Atomics International, November 15, 1961.

15. R. M. Spriggs et al., The American Ceramic Society Bulletin, 42, 1963, pp. 477-9.

16. J. S. Jackson, Powder Metallurgy, 8, 1961, pp. 73-100.

17. J. D. McClelland, Kinetics of Hot Pressing, Rpt. NAA-SR-5591, Atomics International, January 1, 1961.

18. J. D. McClelland and W. M. Smith, Research Hot Pressing, Rpt. NAA-SR-6441, Atomics International, October 30, 1961.

19. P. Murray, E. P. Rodgers, and A. E. Williams, Practical and Theoretical Aspects of the Hot Pressing of Refractory Oxides, AERE Rpt. M/R 893, Harwell, England, 1952.

20. R. P. Levey, Jr. and R. L. Huddleston, Tooling Development for Very High-Pressure Pressing, USAEC Rpt. Y-DA-470, Union Carbide Corporation, September 1963.

21. L. R. McCreight, The American Ceramic Society Bulletin, 30, 1951, pp. 127-9.

22. P. B. Archibald, Industrial and Engineering Chemistry, 53, 1961, pp. 737-8.

23. R. P. Levey, Jr., Isostatic Hot Pressing, USAEC Rpt. Y-1487, Union Carbide Corporation, June 1965.

24. S. J. Paprocki, E. S. Hodge, and P. J. Gripshover, Gas-Pressure Bonding, Rpt. DMIC-159, Battelle Memorial Institute, September 25, 1961.

25. G. W. Cunningham and J. W. Spretnak, The Mechanism of Pressure Bonding, Rpt. BMI-1512, Battelle Memorial Institute, April 6, 1961.

26. S. J. Paprocki (ed.), Progress on the Use of Gas-Pressure Bonding for Fabricating Low-Cost Ceramic, Cermet, and Dispersion Fuels, Phase II Report on AEC Fuel-Cycle Program, Rpt. BMI-1475, Battelle Memorial Institute, November 7, 1960.

27. S. D. Beck and M. A. Gedwill, Jr., The Role of Creep in the Gas-Pressure-Bonding Proeess, Rpt. BMI-1351, Battelle Memorial Institute, June 23, 1959.

28. E. W. Feddersen, Journal of Metals, 12, 1960, pp. 682-6.

29. P. M. McKenna, J. C. Redmond, and E. N. Smith, Process for the Explosive Pressing of Powdered Compositions, U. S. Patent 2,648,125, August 11, 1953.

30. A. Cross, Iron Age, 184, 1959, pp. 48-50.

31. H. P. Furth and R. W. Waniak, Society of Automotive Engineers Journal, 70, 1962, pp. 38-40.

32. D. F. Brower, Society of Automotive Engineers Journal, 70, 1962, pp. 38-40.

33. K. Naruki, Journal of Nuclear Science and Technology, 1, 1964, pp. 58-67.

34. H. J. Groh et al., Nuclear Applications 1, 1965, pp. 327-36.

35. R. L. Folger, Savannah River Laboratory, to E. Lamb, Oak Ridge National Laboratory, personal communication, December 20, 1967.

36. D. H. Stoddard (comp.), Radiation Properties of ^{244}Cm Produced for Isotopic Power Generators, USAEC Rpt. DP-939, Savannah River Laboratory, November 1964.

37. L. B. Asprey et al., Journal of the American Chemical Society, 77, 1955, p. 1707.

38. J. C. Posey, P. R. Kuehn, and R. E. McHenry, The Influence of Temperature and Oxygen Pressure on the Composition of Curium Oxide, 150th Meeting, American Chemical Society, Atlantic City, New Jersey, September 12-17, 1965.

39. W. C. Mosley, B-Type $^{244}Cm_2O_3$ - A Candidate Isotopic Power Fuel, Abstracts of Papers, American Chemical Society, San Francisco, March 31-April 5, 1968.

40. T. D. Chikalla and L. Eyring, The Curium-Oxygen System, USAEC Rpt. BNWL-CC-1569, Pacific Northwest Laboratory, February 13, 1968.

41. J. C. Wallman, Journal of Inorganic and Nuclear Chemistry, 26, 1964, p. 2053.

42. H. O. Haug, Journal of Inorganic and Nuclear Chemistry, 29, 1967, p. 2753.

43. P. K. Smith and D. E. Peterson, High Temperature Evaporation and Thermodynamic Properties of Cm_2O_3, Abstracts of Papers, American Chemical Society, San Francisco, March 31-April 5, 1968.

44. W. W. Schulz, J. E. Mendel, and G. L. Richardson, IEC Process Design and Development, 2, 1963, p. 134.

45. W. R. Corliss and D. G. Harvey, Radioisotopic Power Generation, Prentice-Hall, Inc., Englewood Cliffs, New Jersey, 1964.

46. Roberta W. Shor and R. H. Lafferty, Jr. (eds.), Strontium-90 Heat Sources (to be published).

47. S. J. Rimshaw and E. E. Ketchen, Strontium-90 Data Sheets, USAEC Rpt. ORNL-4188, Oak Ridge National Laboratory, December 1967.

48. M. Dryś and W. Trzebiatowski, Roczniki Chemii, 31, 1957, p. 492, reported in E. M. Levin, C. R. Robbins, and H. F. McMurdie, Phase Diagrams for Ceramists, The American Ceramic Society, Inc., Columbus, Ohio, 1964, p. 119.

49. J. B. Moser, R. N. Blumenthal, and D. H. Whitmore, The Journal of the American Ceramic Society, 48, 1965, p. 384.

50. T. C. Quinby, E. E. Pierce, and R. E. McHenry, Hot Presses for Glove Box and Manipulator Cell Use, USAEC Rpt. ORNL-TM-1900, Oak Ridge National Laboratory, August 1967.

51. W. D. Copeland and R. A. Swalin, Journal of Physics and Chemistry of Solids, 29, 1968, pp. 313-25.

52. J. F. Lynch, C. G. Ruderer, and W. H. Duckworth (comps. and eds.), Engineering Properties of Selected Ceramic Materials, The American Ceramic Society, Inc., Columbus, Ohio, 1966, pp. 5.4.4-1, 5.4.3-1.

53. J. C. Posey and R. E. McHenry, Heat Transfer in the Design of Large Radioisotopic Heat Sources, in Proceedings of the American Nuclear Society National Topical Meeting, March 1966, Augusta, Georgia, Large Scale Production and Applications of Radioisotopes, Vol. II, USAEC Rpt. DP-1066, Savannah River Laboratory, May 1966, pp. 111-31.

54. J. C. Posey, Limiting Physical Factors in the Design of Radioisotope Heat Sources, Fall Meeting of the Nuclear Division of the American Ceramic Society, Portland, Oregon, October 1966 (unpublished).

55. J. C. Posey, Consequences of Internal Heat Flow in Radioisotope Heat Sources, in Proc. of the Second International Symposium on Nucleonics in Aerospace, P. Polishuk (ed.), Plenum Press, New York, 1968, p. 267.

56. W. B. Cottrell et al., Fission-Product Release from UO_2, USAEC Rpt. ORNL-2935, Oak Ridge National Laboratory, September 1960.

57. S. J. Rimshaw and E. E. Ketchen, Curium Data Sheets, USAEC Rpt. ORNL-4187, Oak Ridge National Laboratory, December 1967.

58. R. J. Beals and R. L. Cook, The Journal of the American Ceramic Society, 40, 1957, p. 284.

59. Justin L. Bloom, Characteristics of Fuel Compounds and Encapsulation Materials in Radioisotope Heat Sources, USAEC Rpt. MND-P-2975, Nuclear Division, Martin Co., April 17, 1963.

60. E. Lamb, ORNL Isotopic Power Fuels Quarterly Report for Period Ending September 30, 1966 (classified), USAEC Rpt. ORNL-4045, Oak Ridge National Laboratory, 1966.

61. T. C. Quinby, Oak Ridge National Laboratory, May 1967 (unpublished).

62. W. D. Box, Oak Ridge National Laboratory, May 1968 (unpublished).

63. R. E. McHenry, Leach Rate of $^{90}SrTiO_3$ Radioisotopic Power Fuel, Transactions ANS 1965 Annual Meeting, Gatlinburg, Tennessee, June 1965.

64. E. D. Arnold, Handbook of Shielding Requirements and Radiation Characteristics of Isotopic Power Sources for Terrestrial, Marine, and Space Applications, USAEC Rpt. ORNL-3576, Oak Ridge National Laboratory, April 1964.

65. E. E. Ketchen and R. E. McHenry, Thermal Conductivities of ^{90}Sr Heat Source Materials, USAEC Rpt. ORNL-TM-1905, Oak Ridge National Laboratory, September 1967.

66. E. E. Ketchen, Oak Ridge National Laboratory, May 1968 (unpublished).

67. L. Brewer, Chemical Reviews, 52, 1953, pp. 1-75.

68. P. Angelini and R. E. McHenry, Diffusion of Helium in Curium-244 Fuel Forms, Abstracts of Papers, American Chemical Society, San Francisco, March 31-April 5, 1968.

69. J. C. Posey, Oak Ridge National Laboratory, May 1968 (unpublished).

70. T. D. Chikalla, Pacific Northwest Laboratory, April 1968 (unpublished).

71. F. L. Oetting, Chemical Reviews, 67, 1967, pp. 261-97.

72. W. D. Kingery et al., The Journal of the American Ceramic Society, 37, 1954, p. 108.

73. R. E. McHenry, Transactions of the American Nuclear Society, 8, 1965, p. 75.

74. P. K. Smith, Melting Point of Cm_2O_3, USAEC Rpt. DP-MS-68-37, Savannah River Laboratory, April 1968.

75. T. D. Chikalla, Pacific Northwest Laboratory, June 1968 (unpublished).

76. R. A. Robinson, Brayton-Cycle Radioisotope Heat Source Design Study, Phase I (Conceptual Design) Report, USAEC Rpt. ORNL-TM-1691-del., Oak Ridge National Laboratory, August 1967, pp. 107-13.

Table 1. Isotopic Power Fuels Properties

Operation and Terrestrial Safety Analysis	Aerospace Safety Analysis[a]
Density	Heat capacity
Coefficient of expansion	Emissivity
Specific power	Boiling point
Power density	Heat of vaporization
Radiation and shielding	Heat of fusion
Helium release	Viscosity
Leach rate	Surface tension
Mechanical strength	
Thermal conductivity	
Melting point	
Critical mass	
Vapor pressure	
Compatibility[b]	

[a] In addition to properties for operational analysis.
[b] Compatibility is discussed in a separate paper at this symposium.

Table 2. Structure of Cm_2O_3[a]

Composition: $CmO_{1.50 \pm 0.01}$

C-type, body-centered cubic structure:	a = 10.997 ± 0.003 Å
Density: 10.7 g/cm^3	
C-B transformation: 800-1300°C (depends on crystallinity of C-type Cm_2O_3)	
B-type, monoclinic structure:	a = 14.276 ± 0.008 Å
Density: 11.7 g/cm^3	b = 3.656 ± 0.001 Å
Six Cm_2O_3 molecules per unit cell	c = 8.913 ± 0.004 Å
Space group C_{2h}^3 (C2/m)	β = 100.39 ± 0.03°
Coefficient of linear thermal expansion	
9.6 x 10^{-6}/°C (25-1000°C)	
12.0 x 10^{-6}/°C (25-1400°C), slightly anisotropic	
B-A transformation: 1600°C (reversible)	
A-type, hexagonal structure (1650°C):	a = 3.845 ± 0.005 Å
Density: 11.4 g/cm^3 (1650°C)	c = 6.092 ± 0.005 Å

[a] See reference 39.

Table 3. Composition of Strontium Fuels

Fuel Compound	Constituent	Weight, %
SrO	SrO	94.3
	CaO	4.1
	BaO	0.9
	MgO	0.7
Sr_2TiO_4	Sr_2TiO_4	93.2
	Ca_2TiO_4	5.0
	Ba_2TiO_4	0.8
	Mg_2TiO_4	1.0
$SrTiO_3$	$SrTiO_3$	92.5
	$CaTiO_3$	5.6
	$BaTiO_3$	0.8
	$MgTiO_3$	1.1

Table 4. Description of Hot Presses

Max Pellet Size, in. Dia	Height	Pressure Application	Press atm	Maximum Temp, °C	Use
3	2	Uniaxial	Argon	1800	^{90}Sr fuels
1/2	1/2	Uniaxial	Vacuum	1800	^{244}Cm fuels & research[a]
1	1	Biaxial	Vacuum	2000	Research
1	1	Uniaxial	Vacuum	1500	^{90}Sr & ^{244}Cm fuels[b]
4	2	Uniaxial	Argon	1400	^{90}Sr fuels

[a]Used in glove box facilities.
[b]Used in water-shielded cells.

Table 5. Composition and Dimensions of Hot-Pressed ^{90}SrO Pellets

Pellet No.	Diameter, cm	Height, cm	Weight, g			Volume, cm^3			Density, g/cm^3		Power Density, w/cm^3
			SrO	Pt	Total	SrO	Pt	Total	SrO	Pellet	
1	5.56	5.46	527	105	632	127	5	132	4.2	4.8	1.52
2	5.56	5.41	531	87	618	127	4	131	4.2	4.7	1.53
3	5.56	5.11	525	100	625	120	5	125	4.4	5.0	1.61

Table 6. Analysis of Strontium Oxide

Component	Amount, wt %
SrO	85.4
CaO	12.65
BaO	0.92
MgO	0.29
FeO	0.21
SiO_2	0.18
Al_2O_3	0.31

Table 7. Densities of Strontium Fuels (25°C)

Fuel	Theoretical Density, g/cm^3		Actual Density,[a] g/cm^3
	Pure Compounds	Typical Product	Typical Product
SrO	4.98[b]	4.87[c]	4.3 – 4.7
Sr_2TiO_4	4.99	4.93	4.5 – 4.9
$SrTiO_3$	5.11	5.03	4.5 – 4.9

[a]Densities attainable depend on source design.
[b]Density calculated from lattice constants of Copeland and Swalin (51).
[c]Density calculated using densities of CaO, MgO, and BaO from Lynch et al. (52).

Table 8. Coefficient of Expansion of SrO and $SrTiO_3$

Temp Interval, °C	Mean Linear Coefficient of Expansion	
	$SrTiO_3$	SrO
0-100	10.8×10^{-6}/°C	11.0×10^{-6}/°C
0-200	10.7×10^{-6}/°C	11.0×10^{-6}/°C
0-300	10.7×10^{-6}/°C	11.1×10^{-6}/°C
0-400	10.8×10^{-6}/°C	11.1×10^{-6}/°C
0-500	10.9×10^{-6}/°C	11.1×10^{-6}/°C
0-600	11.0×10^{-6}/°C	11.1×10^{-6}/°C
0-700	11.1×10^{-6}/°C	11.1×10^{-6}/°C
0-800	11.2×10^{-6}/°C	11.2×10^{-6}/°C
0-900	11.3×10^{-6}/°C	11.2×10^{-6}/°C
0-1000	11.4×10^{-6}/°C	11.2×10^{-6}/°C
0-1100	11.6×10^{-6}/°C	11.2×10^{-6}/°C
0-1200	11.7×10^{-6}/°C	11.3×10^{-6}/°C
0-1300	12.0×10^{-6}/°C	11.3×10^{-6}/°C
0-1400	12.1×10^{-6}/°C	11.3×10^{-6}/°C

Table 9. Specific Power and Power Densities of Strontium Fuels

Fuel	Specific Power, w/g		Power Density, w/cm^3	
	Max Theoretical	Typical Fuel[a]	Max Theoretical	Typical Fuel
SrO	0.809	0.419	4.03	1.8 -2.0
Sr_2TiO_4	0.586	0.300	2.92	1.35-1.47
$SrTiO_3$	0.460	0.232	2.35	1.05-1.15

[a]Based on compositions given in Table 3 and isotopic composition on page 4.

Table 10. Dissolution Rates for SrO in Distilled Water

Time Interval, days	Rate, g/cm^2.day
0-1	1.485
1-2	1.22
2-3	1.22
3-4	1.24
4-5	0.96
5-6	1.12
6-7	0.76

Table 11. Description of ^{90}Sr Titanate Leach Rate Samples

Sample	Density, g/cm^3	SrO/TiO_2 Mole Ratio
SNAP-7A fuel	3.13	1.04
SNAP-7A fuel	3.26	0.915
Freshly prepared $SrTiO_3$	4.63	1.0
Aged $SrTiO_3$	4.47	1.0
Freshly prepared Sr_2TiO_4	4.51	2.0

Table 12. Description of $^{90}SrTiO_3$ Thermal Conductivity Samples

Item	A	B	C	D[a]
Age of $SrTiO_3$, yr	0.5	3.5	4.25	~7
Age of fabricated sample, days	23	17	42	~7 yr
TiO_2/alkaline earth oxide mole ratio	0.86	0.95	1.25	0.94
Density, g/cm^3	4.61	4.84	4.57	3.15
Power, w	5.885	5.167	5.244	4.165
Composition, wt %				
SrO	53.70	46.13	43.98	44.50
CaO	5.06	4.18	2.27	4.02
TiO_2	41.23	43.64	49.47	42.93
ZrO_2	Trace	2.67	2.27	8.43
BaO	Trace	3.44	1.79	0.22
MgO	--	--	0.22	--

[a]Fuel from dismantled SNAP-7A.

Table 13. Apparent Helium Diffusion Coefficients for $^{244}Cm_2O_3$ Microspheres

Temp, °C	D_a, cm^2/sec
390	4.1×10^{-10}
600	1.74×10^{-9}
800	2.7×10^{-9}
1000	4.1×10^{-9}
1100	2.58×10^{-9}
1200	2.77×10^{-9}
	3.45×10^{-9}

Table 14. Apparent Helium Diffusion Coefficients for $^{244}Cm_2O_3$ Cylindrical Pellets

Temp, °C	D_a, cm^2/sec
1100	5×10^{-6}
1200	5.8×10^{-6}
1300	7×10^{-6}
1400	5×10^{-5}

Table 15. Estimated Thermal Conductivity of Curium Sesquioxide

Temp, °C	Thermal Diffusivity, cm^2/sec	Molar Heat Capacity, cal/°C.mole	Volume Heat Capacity, $cal/cm^3.°C$	Thermal Conductivity	
				cal/cm.sec.°C	w/cm.°C
27	0.0053	31.50	0.654	0.00347	0.0145
127	0.0052	35.00	0.726	0.00378	0.0158
327	0.0049	38.32	0.794	0.00389	0.0162
527	0.0047	40.26	0.835	0.00392	0.0164
727	0.0046	41.80	0.866	0.00399	0.0167
927	0.0044	43.06	0.894	0.00393	0.0164
1127	0.0043	44.02	0.913	0.00393	0.0164
1327	0.0042	44.80	0.929	0.00388	0.0162
1427	0.0041	45.14	0.936	0.00384	0.0160

Table 16. Results of Critical Mass Calculations

Core		Reflector		Critical Mass, kg	Critical Radius, cm
Mixture[a]	Density, g/cm^3	Mixture	Thickness, cm		
Cm_2O_3	10.60	Bare		21.1	7.8031
Cm_2O_3	9.01	Bare		29.2	9.1803
Cm_2O_3	10.60	Au-H_2O	4.0-15.0	11.9	6.4540
Cm_2O_3	10.60	Au-H_2O	2.0- 7.5	13.5	6.7188
Cm_2O_3	10.60	Au-H_2O	0.5- 2.0	16.5	7.1966

[a] 98.07 wt % ^{244}Cm; 1.93 wt % ^{241}Pu.

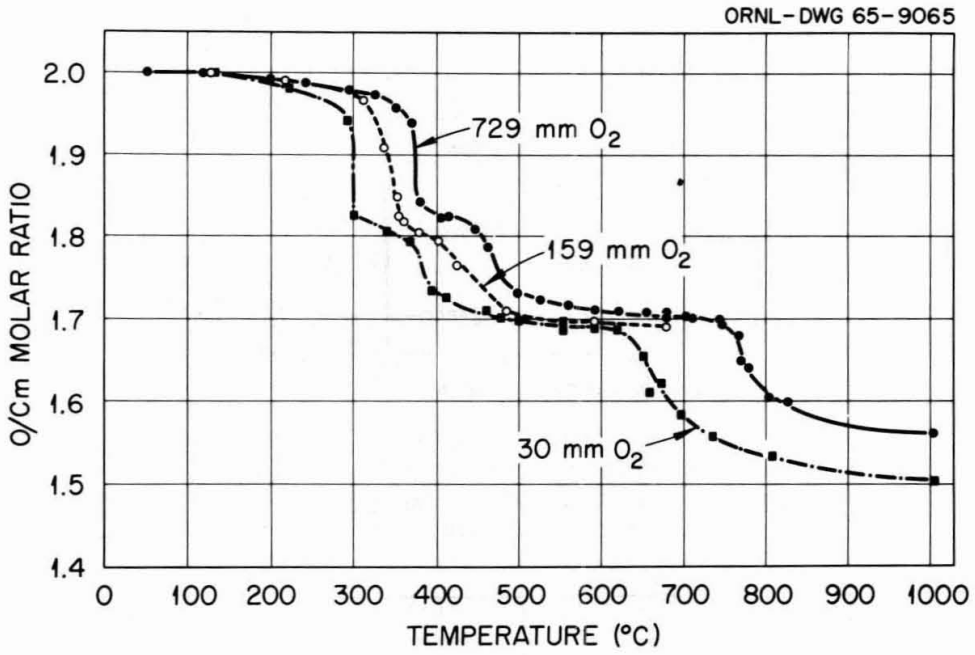

Fig. 1. Composition of curium oxide

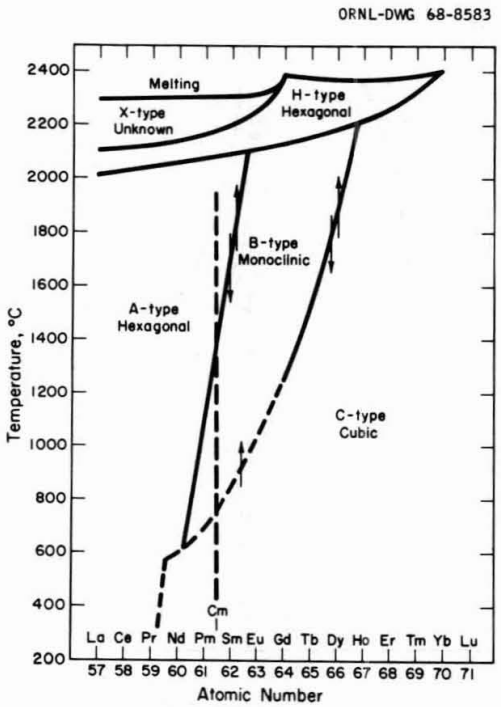

Fig. 2. Stabilities of rare-earth sesquioxides (W. C. Mosley, B-Type $^{244}Cm_2O_3$ - A Candidate Isotopic Power Fuel, Abstracts of Papers, Am. Chem. Soc., San Francisco, March 31-April 5, 1968)

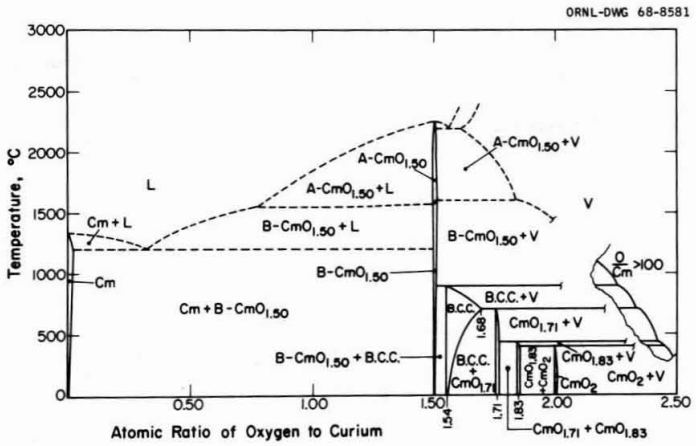

Fig. 3. Curium-oxygen system (P. K. Smith and D. E. Peterson, High Temperature Evaporation and Thermodynamic Properties of Cm_2O_3, Abstracts of Papers, Am. Chem. Soc., San Francisco, March 31-April 5, 1968)

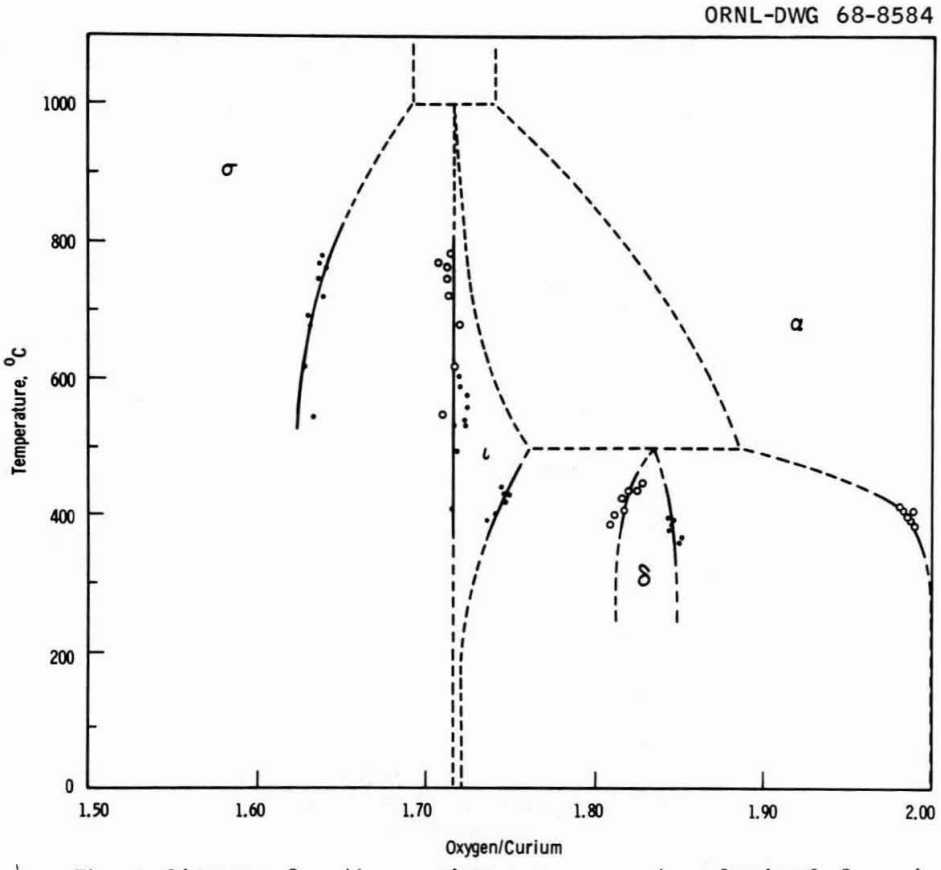

Fig. 4. Phase diagram for the curium-oxygen system derived from isobaric temperature--composition data. o and ● represent phase transitions on heating and cooling, respectively. Dashed lines and peritectoid reaction temperatures are uncertain and included for completeness [T. D. Chikalla an L. Eyring, The Curium-Oxygen System, USAEC Rpt. BNWL-CC-1569, Pacific Northwest Laboratory (February 13, 1968)]

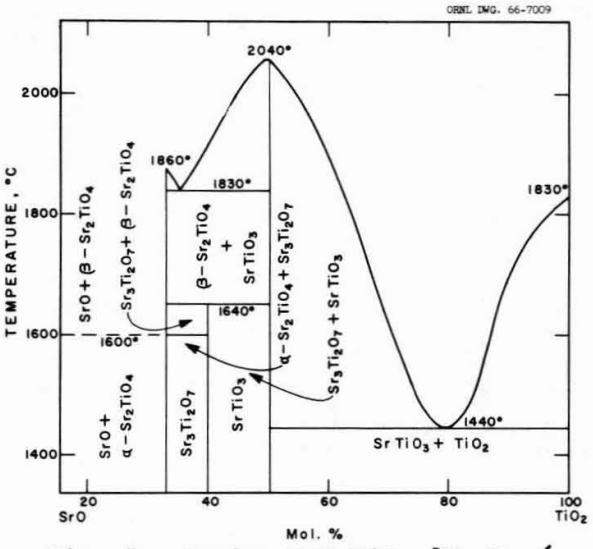

Fig. 5. System SrO-TiO_2 [M. Drys and W. Trzebiatowski, Roczniki Chem., 31, 492, (1957); reported in E. M. Levin, C. R. Robbins, and H. F. McMurdie, Phase Diagrams for Ceramists, The American Ceramic Society, Inc., Columbus, Ohio, 1964, p 119)]

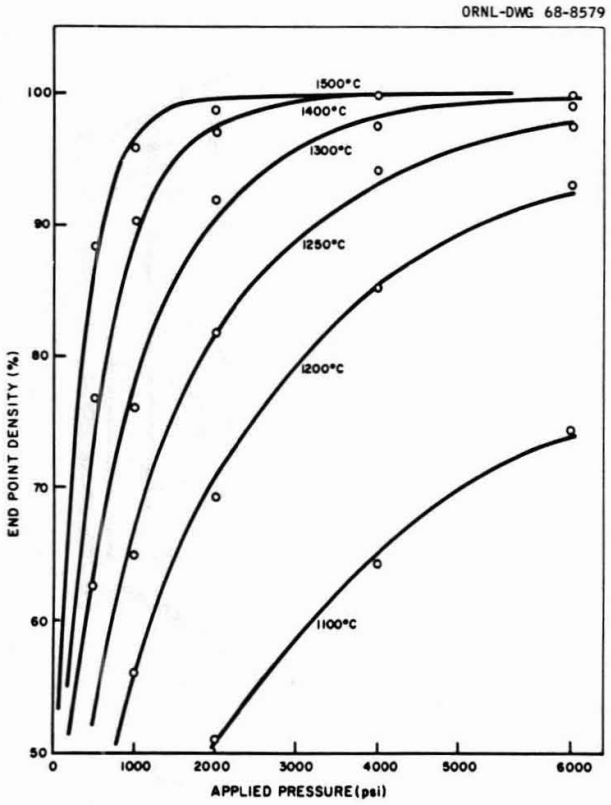

Fig. 6. Effect of pressure on the end-point density of alumina. o experimental data; - calculated data [J. D. McClelland and W. M. Smith, Research Hot Pressing, Rpt. NAA-SR-6441, Atomics International (October 30, 1961)]

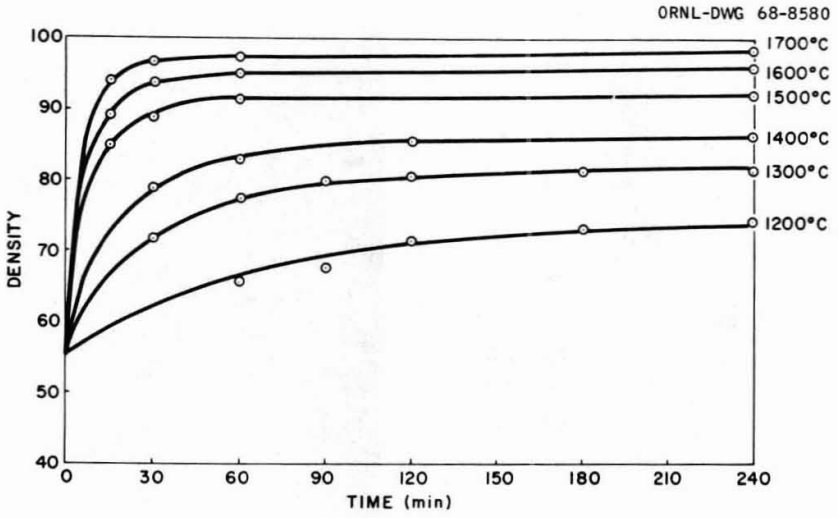

Fig. 7. Time-temperature dependence of density of beryllium oxide [J. D. McClelland and W. M. Smith, Research Hot Pressing, Rpt. NAA-SR-6441, Atomics International (October 30, 1961)]

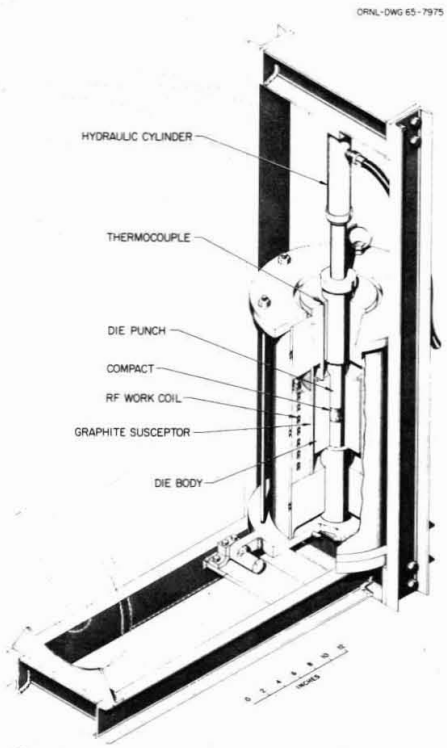

Fig. 8. Hot press for remote operation

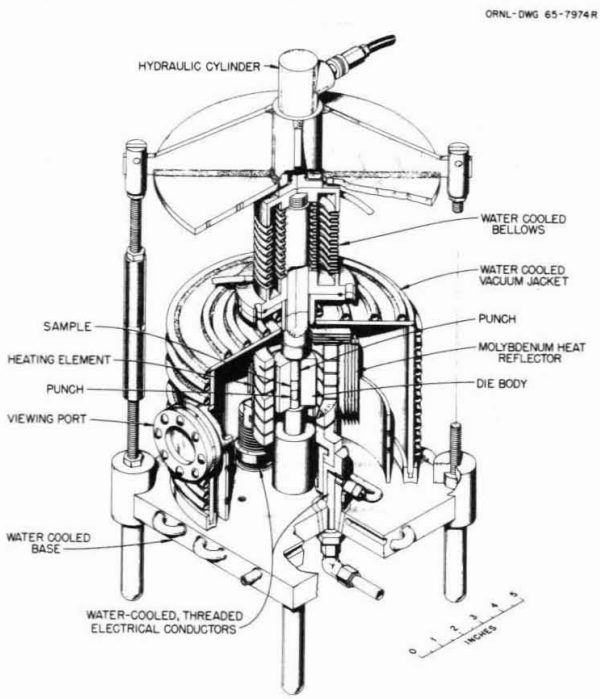

Fig. 9. Miniature hot press

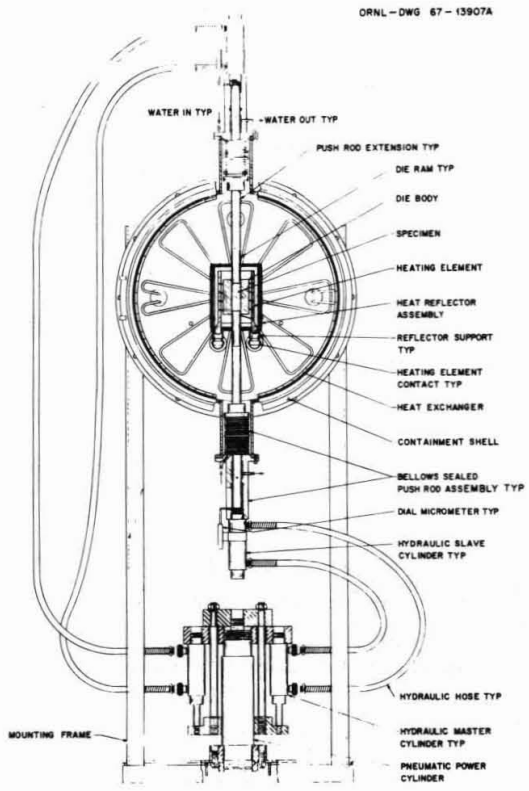

Fig. 10. Vacuum hot press assembly

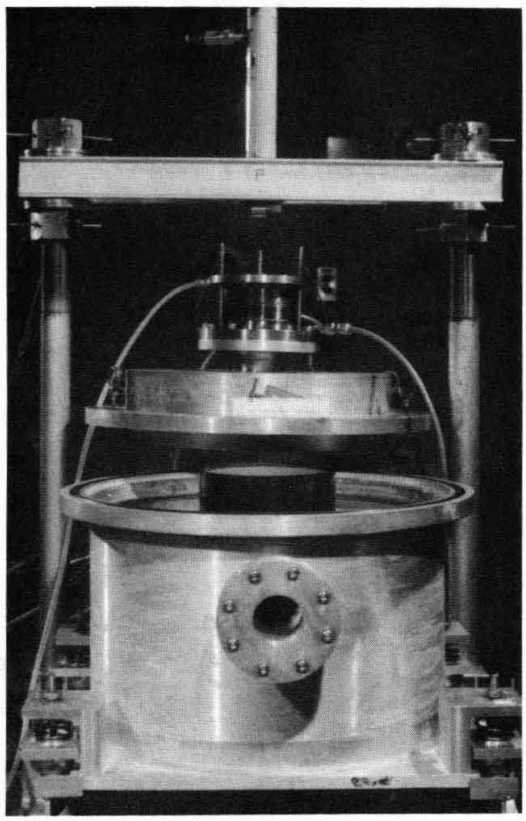

Fig. 11. Vacuum hot press

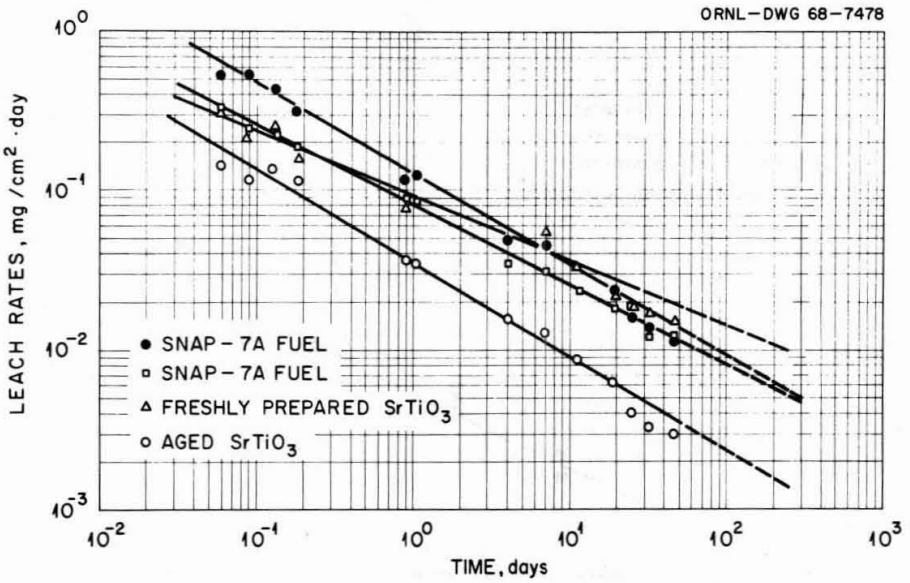

Fig. 12. Leach rates of strontium-90 titanate fuels

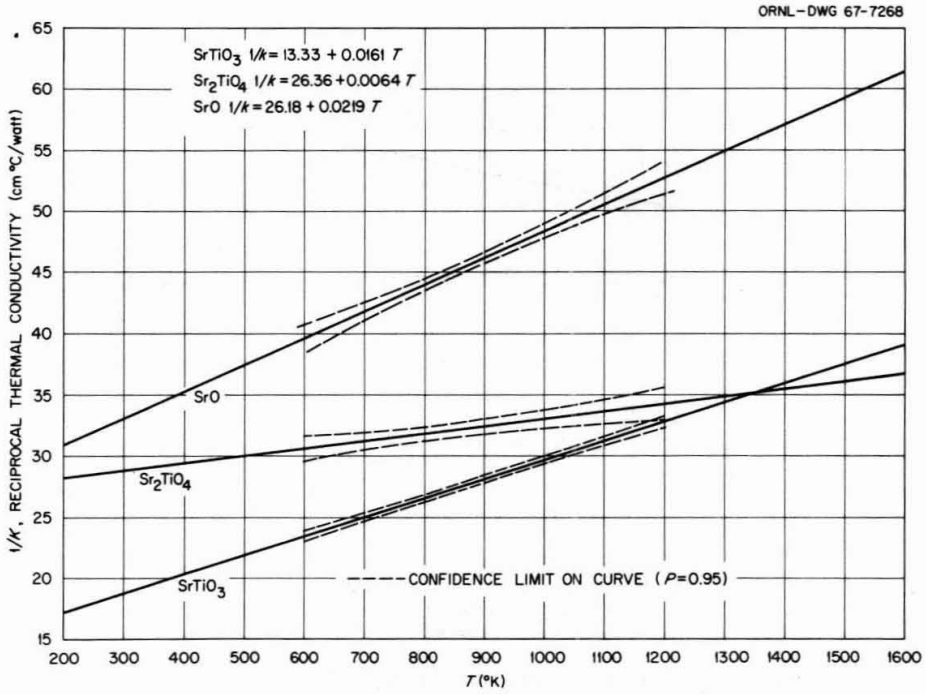

Fig. 13. Correlation of thermal conductivity data for SrO, Sr_2TiO_4, and $SrTiO_3$

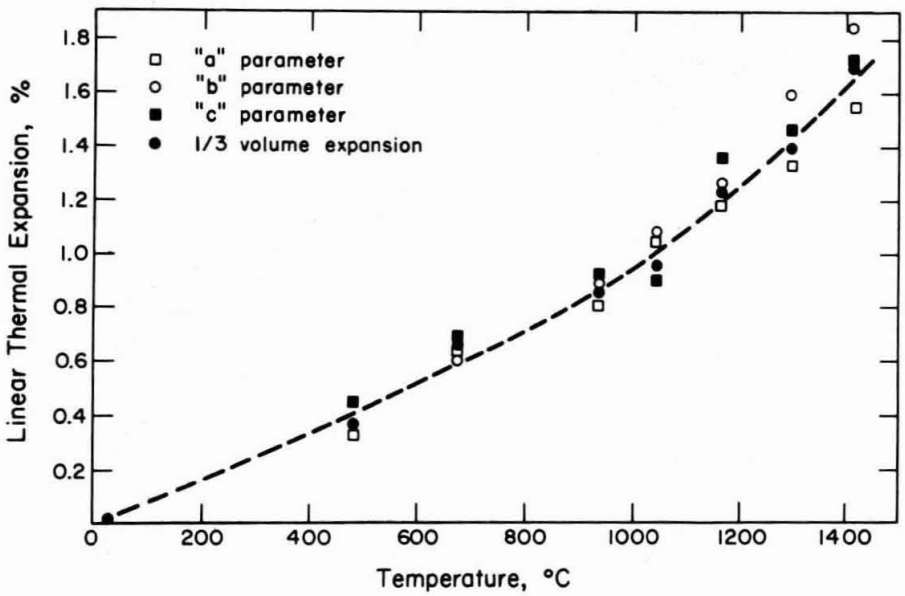

Fig. 14. Thermal expansion of B-type curium sesquioxide (W. C. Mosley, B-Type $^{244}Cm_2O_3$ - A Candidate Isotopic Power Fuel, Abstracts of Papers, Am. Chem. Soc., San Francisco, March 31-April 5, 1968)

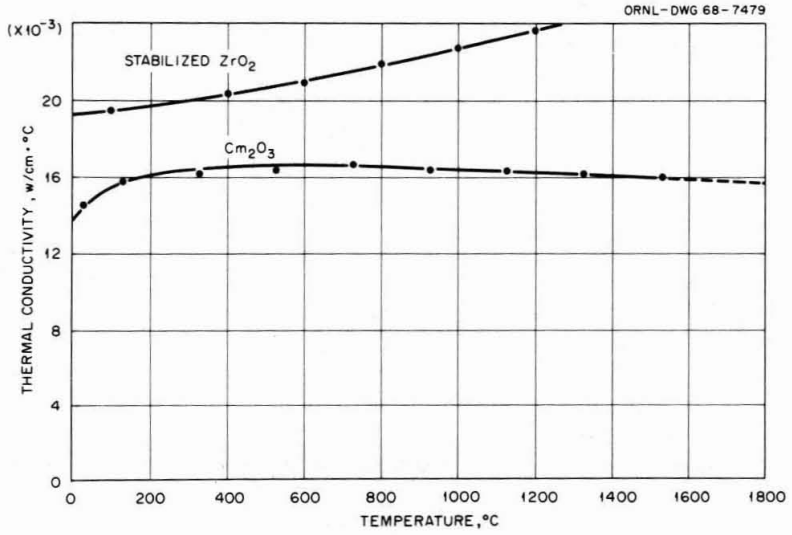

Fig. 15. Thermal conductivity of curium sesquioxide

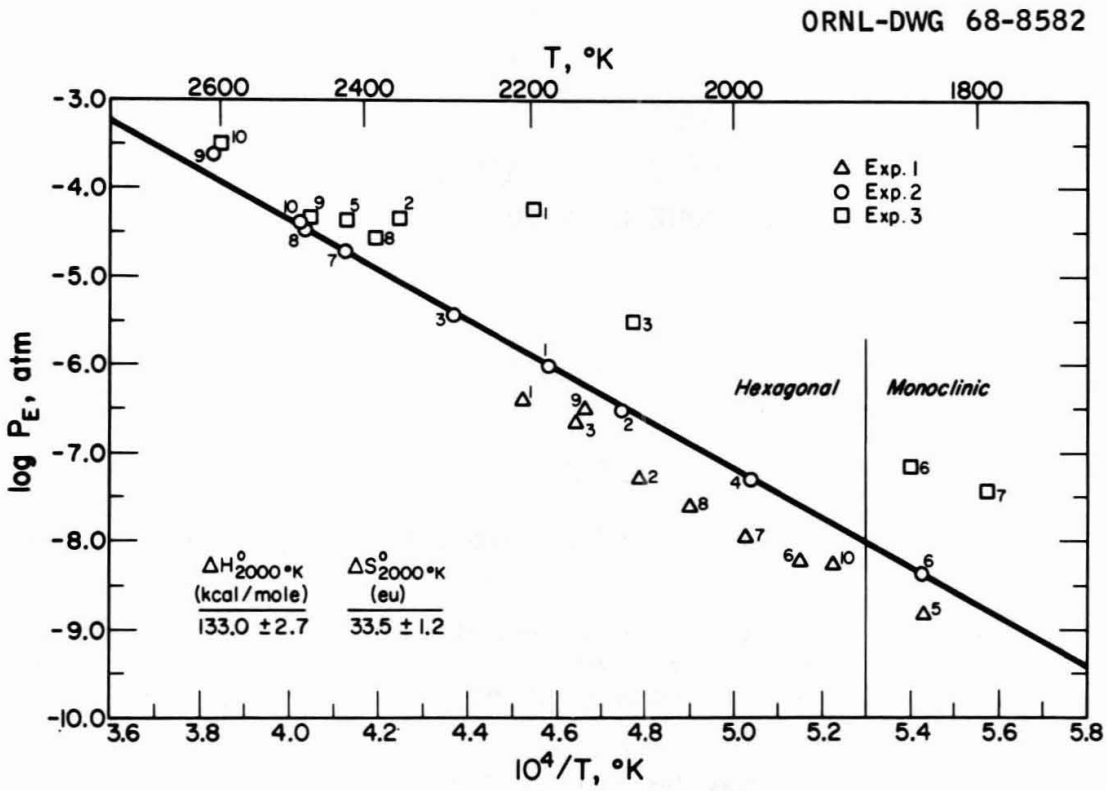

Fig. 16. Log P_E versus 1/T for vaporization of curium sesquioxide (P. K. Smith and D. E. Peterson, High Temperature Evaporation and Thermodynamic Properties of Cm_2O_3, Abstracts of Papers, Am. Chem. Soc., San Francisco, March 31-April 5, 1968)

PROPERTIES AND FABRICATION OF PROMETHIUM FUEL FORMS

K. Drumheller

Abstract

Most experience in processing promethium has been with the Pm_2O_3 fuel form.

Promethium oxide at 90% of theoretical density has a specific power of 0.27 watt/gm. The half life is 2.62 years. Promethium is a soft beta emitter and is fairly easily shielded.

Promethium oxide has been densified by conventional pressing and sintering, hot pressing, and pneumatic impaction. Other processing methods are being investigated.

Cold pressing, followed by sintering in air, is a suitable process for fabrication of simple configurations in pellet sizes up to approximately one inch diameter by 1/2 inch thick. With larger pellets, pressing and sintering may be suitable but self-heating may introduce thermal stress problems.

K. Drumheller is Associate Manager, Chemistry and Metallurgy Division, Pacific Northwest Laboratory, Battelle Memorial Institute, Richland, Washington.

This paper is partially based on work performed under United States Atomic Energy Commission Contract AT(45-1)-1830; other work is referenced.

Pneumatic impaction has been utilized for densification of encapsulated promethium oxide. This process produces a very high density fuel form.

Encapsulation materials have included a shielding material such as tantalum and a supplemental clad to provide compatibility with the environment. Closures have been made by TIG and electron beam welding.

Most fabrication has been done in lead shielded glove boxes. The fuel material is handled with tongs and local shielding is used where possible.

Heat sources have been fabricated for several experimental programs.

INTRODUCTION

One of the most desirable characteristics of promethium-147 is the relative ease with which its radiation can be shielded. While it has a very high specific activity, the radiation is primarily soft beta and can be shielded to make promethium useful in a variety of applications.

Promethium has been fabricated in oxide form and cermet form. It is expected that at some time in the not too distant future, metal will be available for fabrication development.

In the oxide form, promethium has the desirable characteristics of being relatively easy to fabricate, having a high degree of stability in a variety of environments, and being capable of fairly high temperature operation.

In cermet form the additional desirable characteristics of higher thermal conductivity and improved stability under some environmental conditions are achieved.

Experimental sources have been fabricated for the radioisojet program[1] and an aircraft inertial guidance heater program.[2] Operation of the sources has been very satisfactory.

In addition to fabrication for specific applications, there has been process development work on four basically different processes. These are: pneumatic impaction, cold pressing and sintering, hot isostatic pressing, and cermet processing.[3] Cermet processing includes plasma fusion, coating, and consolidation.

Work has been carried out using stand-in materials to demonstrate the feasibility of other processes. Work with stand-in materials includes slip casting,[4] cold isostatic pressing and sintering, and thin film deposition.[6]

PROPERTIES

General

Promethium-147 has a half life of 2.62 years. In the oxide form the theoretical density is 7.43 gm/cm^3. The specific power of the oxide in a 90% TD form is 0.27 watt/gm.

Work is in progress to determine the physical properties of promethium metal and promethium oxide. Properties under study include thermal conductivity, thermal expansion,

electrical conductivity, phase relationships, and chemical properties.[7]

Typical properties of promethium oxide are shown in Table I.

Thermal Conductivity

The thermal conductivity of Pm_2O_3 is 0.02 watt/cm.-°C and is nearly independent of temperature. This value was calculated from the thermal diffusivity data obtained by a laser pulse technique using an estimated heat capacity.

Thermal Expansion

The thermal expansion of Pm_2O_3-Sm_2O_3 mixtures has been measured from 20°C to 1700°C in vacuum using a tungsten pushrod dilatometer. The average linear expansion coefficient increases with Sm_2O_3 in-growth. A typical value found for Pm_2O_3 - 12% Sm_2O_3 is 9.8×10^{-6} in./in.-°C.

Electrical Resistivity

The electrical resistivity of Pm_2O_3 has been measured and found to vary from 3×10^8 ohm-cm at room temperature to 100 ohm-cm at 1000°K. The results indicate that promethium oxide is a semiconductor in the temperature interval studied with a calculated intrinsic band gap width of 2.0 ev.

Melting Point

Melting point data were obtained on nearly pure Pm_2O_3 using a resistance heat filament technique. The melting point obtained was 2320°C on a rhenium filament.

FABRICATION DEVELOPMENT

General

Combinations of open faced hoods, lead shielded glove boxes and shielded remote fabrication facilities have been used for promethium fuel fabrication.

Most fabrication operations are carried out in lead shielded glove boxes using leaded gloves (Fig. 1). Tongs are used where possible to maintain as much distance between the operator's hands and the source as practical. No direct hand contact is allowed with multi-curie sources of ^{147}Pm. Local shielding within the glove box is used as much as practical.

Severe ozone rotting has occurred with regular rubber gloves. A life of only one to two weeks may be experienced. This problem has been controlled by the use of polyester coated rubber gloves which have a life of several months.

Precautions are necessary during transfer operations to prevent overheating of the source or components which it contacts. Transfers are usually made in a chill block with an area large enough to maintain suitable temperatures.

Special care is necessary in bagging operations. The heat from the source can very well melt plastic bags and release contamination.

Care may also be necessary in testing operations which may involve placing the source in cold water. The temperature is usually lowered gradually to minimize thermal shock.

The soft beta characteristics of promethium provide unique requirements for radiation protection. A conventional beta-gamma survey meter will not detect small amounts of promethium. It is necessary to use a thin window type detector, and the detector must be within a few inches of the source to detect small amounts of contamination.

The actual radiation measurements from a 60 watt promethium oxide source encapsulated in 0.060 inch thick tantalum and 0.200 inch thick cobalt alloy are shown in Fig. 2. The radiation from this source at 18 inches is only 35 mR/hr.

Pressing and Sintering

Conventional cold pressing and sintering has been used most extensively and at the present time is felt to be a practical process for most applications. This process can be used to produce pellets with good mechanical strength and good dimensional control. Pellet densities of 93% of theoretical are readily achieved.

The pressing and sintering process is illustrated by the fabrication of two sources mentioned above; the radioisojet source,[1] and the inertial guidance heater source.[2] These sources represent two different size ranges.

Size is a peculiarly important feature in the fabrication of promethium oxide sources because self-heat from the source material introduces thermal stresses, the magnitude of which will vary with the source size.

Radioisojet pellets were pressed with a split die system which was developed to minimize cracking of the cold pressed pellets. This was necessary partly because, in general, the

pellets are pressed without binder.

The die consists of a thin walled tool steel cylinder having a slit running lengthwise over its entire length and a matching restraining die into which the slit cylinder is inserted. Both parts are tapered and have sufficient interference so that the slit in the cylinder is closed up as the cylinder is pressed into the restraining die. After a pellet is pressed, The slit cylinder is ejected from the restraining die and springs back to its original diameters, thus causing the pellet to fall free.

Nominal 1/4 inch thick by 1 inch diameter pellets were pressed at 63 tsi. The density was 73% of theoretical. These pellets were sintered 45 hours at 1355°C. The final density was approximately 90% of theoretical.

A simple grinding process for final sizing of pellets is illustrated in Fig. 3. This process utilizes a simple belt sander with a special holding tool which allows the pellet to rotate while it is being sanded. Pellets were readily reduced in diameter by 20mils.

The guidance system pellet was a pellet containing 227 grams of promethium oxide with a power output of 60 watts.

This pellet was pressed from pre-pressed powders. The powder was pressed at approximately 25 tsi then crumbled through a 12 mesh screen into relatively high density particles. This produces a bulk density of approximately 30%. This operation results in higher initial densities in cold pressed pellets and reduces handling problems with the powder.

The die used for this pellet had dome shaped plugs to produce a radius on the pellet ends. Difficulty was encountered in obtaining a one-piece pellet.

The best pellet was obtained by pouring the powder into the die and allowing it to reside in a pre-pressed condition before pressing. This presumably allowed the pellet to reach nearly the thermal gradients it would encounter in the pressed condition and hence reduce thermal stresses.

The pellet was sintered at 1450°C for 30 hours.

Pneumatic Impaction

Pneumatic impaction has been used to produce promethium oxide sources which are near theoretical density. In general, in pneumatic impaction the source is consolidated and encapsulated simultaneously or densified after encapsulation.

The encapsulated core material is placed in a mold. This mold is sealed, heated, and dropped into a cylindrical die in a pneumatic mechanical high energy-rate forging machine. The machine is fired and a cylindrical punch strikes the assembly. Pressures up to 400,000 psi are achieved.

While this process produces a very high density source, at the present time it does not have the dimensional control capability of the other processes.

Hot Pressing

Densities of 95-96% of theoretical density have been achieved by hot pressing under the conditions of 5100 psi at 1590°C for 30 minutes.[5]

The advantages of hot pressing are the desirable characteristics of higher density and perhaps better dimensional control. A possible slight disadvantage for some applications is that the equipment is generally a little more complex.

Cermet Fabrication

Cermets have been made by fusing high density spherical particles utilizing a plasma torch.[3] These particles were coated with tungsten by vapor deposition then consolidated into an encapsulated cermet by pneumatic impaction.

Processing with Stand-in Materials

Processing with stand-in materials has included cold isostatic pressing and sintering, slip casting,[4] and thin film deposition.[6]

Isostatic pressing experiments have been carried out using a silastic mold and a conventional hydraulic press. The mold is placed in a cylindrical die, filled with powder, and pressed with a cylindrical punch. Because this is not a completely isostatic system, diameter variations have resulted in most cases. To date basic experiments have been carried out using samarium oxide as a stand-in material. The samarium oxide is heated to simulate the self-heating with promethium oxide by inserting a heater into the material.

Green slip cast chapes of samarium oxide were formed and fired at 1500°C.[4] Densities of 93% of theoretical density were achieved. This process does not appear to have dimensional control capability equal to that of the cold pressing and sintering process.

Several methods have been used to produce thin films of samarium oxide on metal substrates.[6] Thin films of

promethium oxide may have application to systems for the direct conversion of beta decay to electrical energy.

Very uniform films of approximately 0.002 inch thickness of samarium oxide were obtained by vacuum vapor deposition.

Encapsulation

Encapsulation of source materials is accomplished by conventional techniques.

One unique problem encountered is that the very high specific activity of promethium makes decontamination of the weld zone difficult. However, decontamination has been readily accomplished and techniques have been developed which make it possible to decontaminate prior to welding in a matter of a few minutes.

Closures are generally produced by TIG welding or electron beam welding. The complete process for a typical source is shown in Fig. 4. The source for which this process is used is shown in Figure 5.

Discussion

While process feasibility has been demonstrated for several different processes, conventional pressing and sintering has been most utilized at present.

The desirable characteristics of pressing and sintering are low equipment cost, relative ease of fabrication, good mechanical strength and good dimensional control. The process does not yield the highest density.

The desirable features of hot pressing are higher density, possibly better dimensional control, and ultimately perhaps more mechanical strength. The process requires slightly more complex equipment and is not as readily adaptable to a variety of sizes and high production rates.

Pneumatic impaction produces a very high density material; dimensional control is not as good.

Isostatic pressing, followed by sintering, may produce better mechanical strength by reducing potential for laminations in large pellets. Dimensional control is not likely to be as good.

Cermets with the fuel dispersed in a continuous metal matrix can be readily produced.

Significant improvements can be made in all of the processes discussed above through detailed investigation of individual variables.

REFERENCES

1. Goddard Space Flight Center, Radioisojet Program Summary Report, No. X-734-67-475, Goddard Space Flight Center, Greenbelt, Maryland, September, 1967, p. 17-24.

2. R. L. Moore, Division of Isotope Development Programs Quarterly Report, July - September 1967, No. BNWL-681, Battelle-Northwest, Richland, Washington, January 1968, p. 1-20.

3. R. S. Cooper and R. L. Andelin, Development of High Temperature Isotope Heat Sources, ^{147}Pm, D. W. Douglas Laboratories, ANS Transactions, Vol. 10, No. 2, November 1967, 1967 Winter Meeting, Chicago, Illinois, November 5-9, 1967.

4. H. T. Fullam, Slip Casting of Rare Earth Oxides, No. BNWL-437, Battelle-Northwest, Richland, Washington, June 1967.

5. H. T. Fullam and C. J. Mitchell, Hot Pressing of Rare Earth Oxides, No. BNWL-448, Battelle-Northwest, Richland Washington, June 1967.

6. W. R. Mikelsen, Basic Design Considerations for Radioisotope Electrogenerators, The Dane Company, Ft. Collins, Colorado. Paper presented at 3rd Intersociety Energy Conversion Engineering Conference, Boulder, Colorado, August 13-16, 1968.

7. Personal Communication, T. D. Chikalla, H.T. Fullam, and C. E. McNeilly.

8. H. T. Fullam and H. H. Van Tuyl, Promethium Isotopic Power Data Sheets, No. BNWL-363, Battelle Northwest, Richland, Washington, February, 1967.

Table I

PROMETHIUM OXIDE PROPERTIES[7,8]

^{147}Pm

Half Life	2.62 yr.
Specific Power, Pm_2O_3	0.27 watt/gm
Density	7.43 gms/cm^3
Coefficient of Linear Thermal Expansion (With 12% Sm, average over the range 70°C-1000°C)	9.8×10^{-6} in./in.-°C
Melting Point	2320°C
Thermal Conductivity	
Oxide	0.02 watt/cm-°C
Electrical Resistivity	3×10^8 ohm-cm, 300°K 100 ohm-cm, 1000°K
Type of Radiation, Major	0.23 MeV β
Biological Hazard	2×10^{-8} MPC, Ci/cm^3

Fig. 1. Lead Shielded Glove Box for Promethium Work

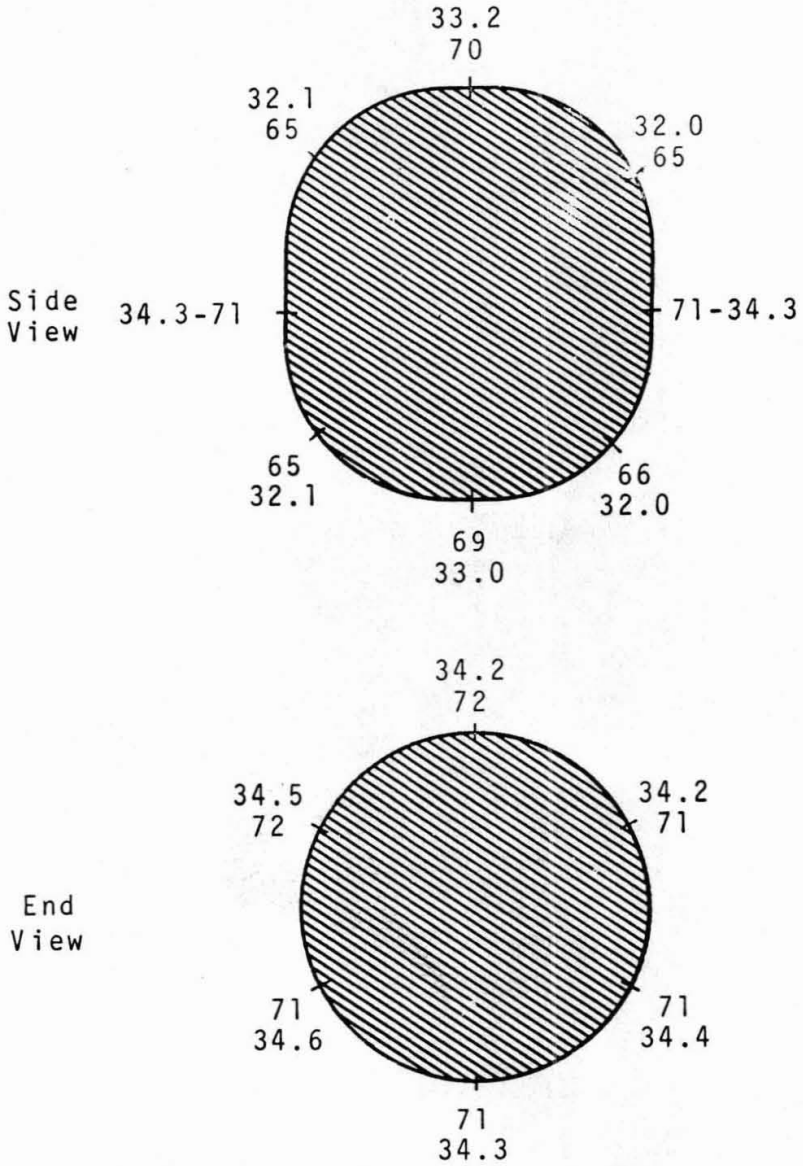

Inner Numbers are 12" from Center of Capsule, in mr/hr
Outer Numbers are 18" from Center of Capsule

Fig. 2. Radiation Measurements for a 60-watt Promethium Oxide Source Encapsulated in 0.060 inch Thick Tantalum and 0.200 inch thick cobalt alloy.

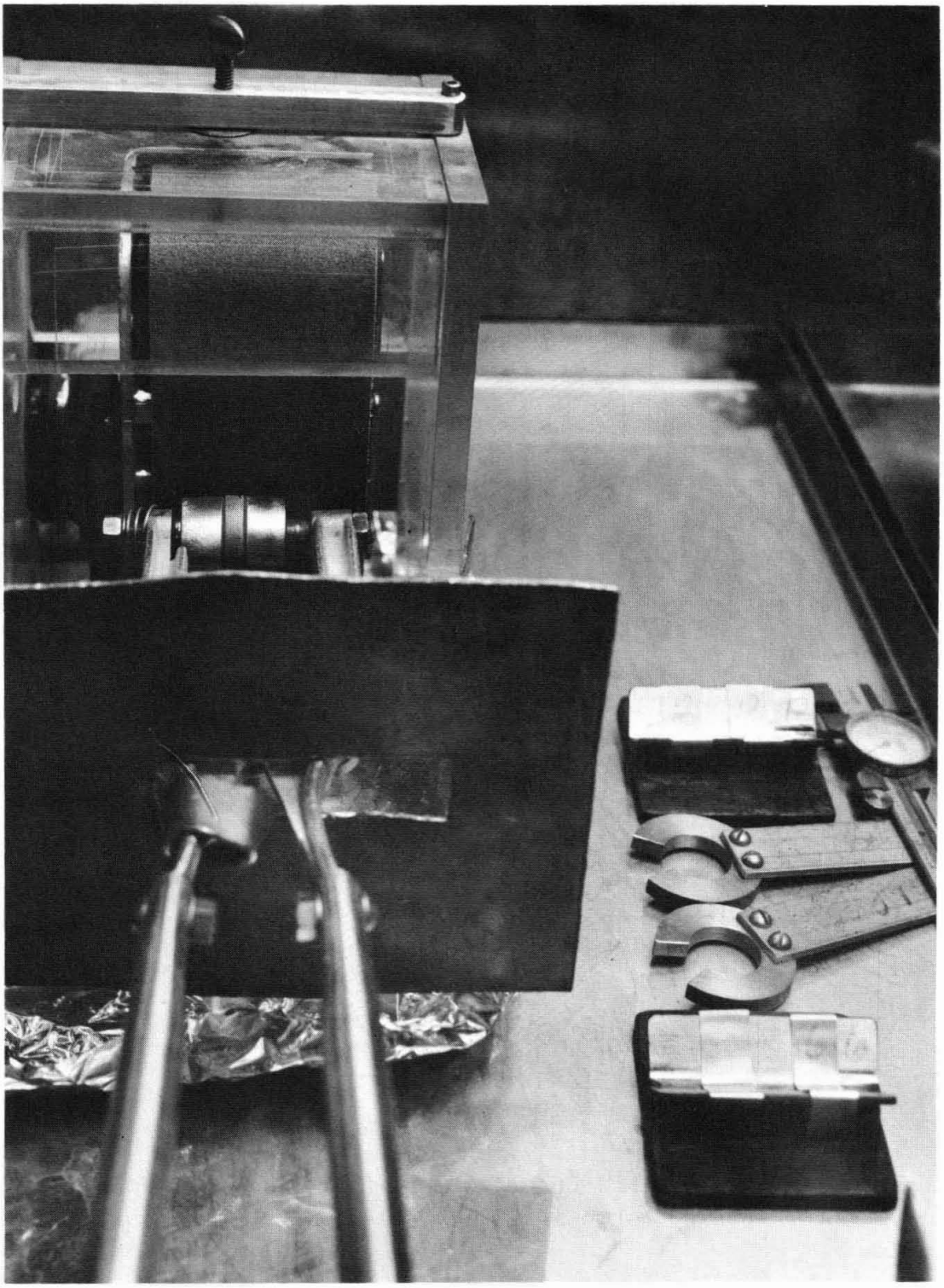

Figure 3. Belt Grinder for Final Sizing of Promethium Oxide Pellets.

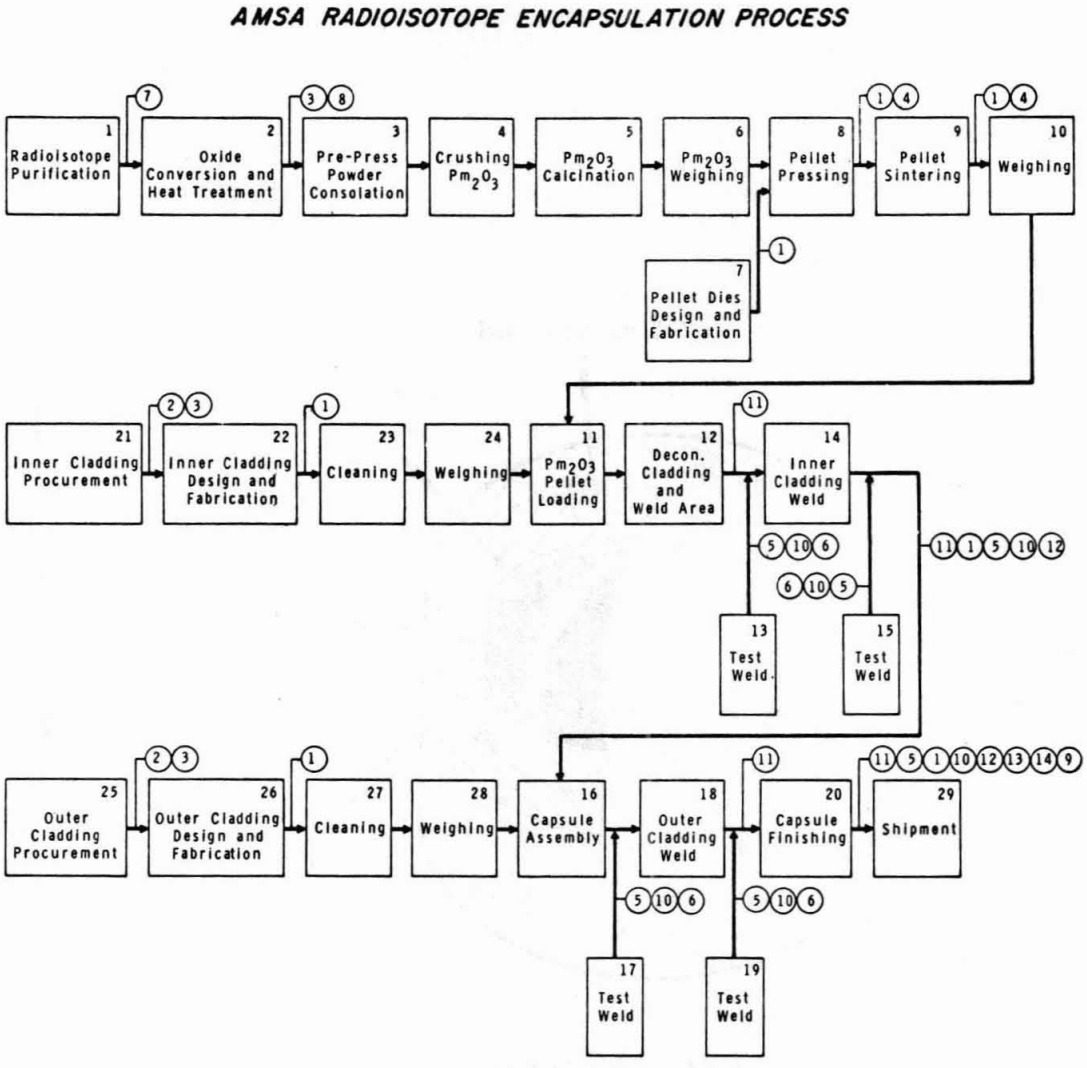

Fig. 4. Process Flow Sheet for Typical Promethium Oxide Heat Source.

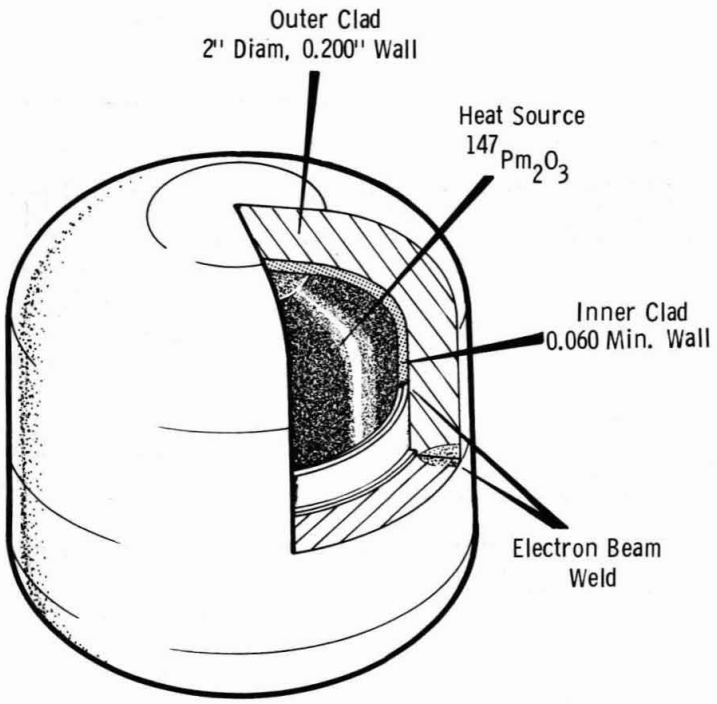

AMSA THERMAL POWER CAPSULE

Fig. 5. Section of Promethium Oxide Heat Source

PROPERTIES AND FABRICATION OF THULIUM-170 OXIDE TARGETS

J. R. Keski and P. K. Smith

Abstract

Natural thulium sesquioxide is a candidate target material to produce ^{170}Tm fuel forms for direct application in short-lived radioisotopic heat sources. Physical and chemical properties of Tm_2O_3 are reviewed. Fabrication of oxide wafers to 97% of theoretical density and characteristics of wafers irradiated to an activity of about 2 w/gm are described.

J. R. Keski, a ceramist, and P. K. Smith, a physical chemist, are at the Savannah River Laboratory, E. I. du Pont de Nemours & Co., Aiken, S. C. 29801.

Introduction

Thulium-170, a beta-emitting radioisotope with a 128-day half-life, may be a useful heat source in short-term applications where its penetrating radiation can be tolerated. As part of a program to develop technology for large-scale production of a number of radioisotopes including ^{170}Tm (1), natural thulium metal and sesquioxide targets have been irradiated in Savannah River production reactors to power densities over 2 w/gm.

The properties of thulium metal and sesquioxide were evaluated by Smith, Keski, and Angerman (2) and by Smith (3). Thulium sesquioxide is especially well suited as a fuel compound for use in high-temperature heat sources. Because of its very high stability, it has a good potential for meeting nuclear safety criteria governing both accident situations and normal operating conditions.

One advantage of ^{170}Tm is that postirradiation processing may be eliminated by irradiating a fabricated oxide fuel form of natural thulium to produce a ^{170}Tm product that can be used directly in heat sources. Until recently, little technology has been reported on fabrication techniques for thulium sesquioxide (Tm_2O_3). A fabrication procedure was developed and the properties of fabricated wafers were described by Keski and Smith (4). A similar effort was performed by Eastly and Matson, but their results are available only in abstract form (5).

This paper reviews the properties and fabrication of Tm_2O_3 and describes its irradiation behavior. Some applications and the development status of ^{170}Tm heat sources are discussed.

Properties of Thulium Oxide

Many factors must be considered in the selection of an isotope for use in a heat source system. Some of the more important factors are: half-life, type of activity, shielding requirements, power density, cost, availability, safety, and stability of the fuel form.

Half-Life

Use of ^{170}Tm as a heat source is limited to short-term applications because of its 128-day half-life (6). The principal decay mechanism is beta emission to form stable ^{170}Yb as shown in Fig. 1. This decay occurs by emission of 0.967 Mev (approximately 76%) and 0.882 Mev (24%) beta particles.

Radiation and Shielding

Bremmsstrahlung associated with the beta emission is the primary contributor to radiation doses (7). Arnold has calculated the gamma and Bremmstrahlung dose rates that would be expected from an unshielded 1-kw ^{170}Tm power source (8). A dose rate of about 1500 rads per hr was calculated at 100 cm from the center of the unshielded 1-kw source. A 1-cm lead shield would reduce the dose rate to about 25 rads per hr, while a 1-cm uranium shield would reduce the rate to approximately 3 rads per hr.

Sanders, Kerrigan, and Albenesius (9) have experimentally verified shielding calculations for ^{170}Tm power sources. Thermoluminescent dosimeters were used to measure radiation from a source containing 3 kCi of ^{170}Tm (6.80 w) and 1.7 kCi of ^{171}Tm (0.06 w). Using tantalum shields of varying thicknesses, they found the ratio of calculated to measured dose rates to be about 1.2/1. With, for example, a shield thickness of 1.549 cm, the calculated and measured rates were 54.1 and 45.0 rem per hr, respectively. Thus the method of calculating shielding requirements was substantiated. In general, some weight penalty may be incurred in manned space applications because of shielding requirements.

Power Density

The specific power of pure ^{170}Tm is 13.5 ± 0.6 w per gm of metal, corresponding to an activity of 6,020 Ci per gm, which was calculated using the measured half-life of 128 days (6) and a measured value of 445 ± 20 Ci/w (2). For Tm_2O_3 (the best fuel compound) the corresponding specific power is 11.8 ± 0.5 w per gm of Tm_2O_3. By irradiating Tm_2O_3 in the Savannah River reactors at a fairly high flux, power densities of 2 to 3 w per gm of Tm_2O_3 (17 to 26 w per cc of Tm_2O_3) can be obtained. Hence, the available power density is sufficient for applications in thermionic converters.

Cost

Thulium oxide is presently produced as a by-product of the production of yttrium and other rare earth oxides primarily for the television industry. Several thousand pounds per year are available and more could be made available if required by the market. The cost of encapsulated ^{170}Tm is related in part to the price of thulium oxide, which can vary depending on whether thulium is a by-product or principal product of mining operations. A recently estimated future price is $10 per thermal watt (10).

Safety

One of the most vital factors in the use of radioisotopic power supplies is the assurance of radiological safety. To meet this criterion, the fuel form selected for a particular application should have a high melting point, be fully oxidized, have a low vapor pressure, and have no deleterious phase transitions or decomposition products under any hazard condition. Thulium sesquioxide, Tm_2O_3, has a high potential for meeting these demands, even at the high temperatures required for thermionic converters. Some of the properties of Tm_2O_3 are given in Table 1.

Stability and Physical Properties

Thulium sesquioxide is the only known solid oxide of thulium. It is an essentially stoichiometric compound, exhibiting only a very small range of solid solution at high temperatures. Keski and Smith (4) found evidence for oxygen loss to a composition of $Tm_2O_{2.90}$ after heating the sesquioxide in helium in a tantalum container for 24 hr at 1925°C. Thulia maintains a cubic structure to temperatures in excess of those for projected thermionic applications. Föex and Traverse (11) have reported a transition from cubic to hexagonal symmetry (A-type rare earth oxide) at 2280°C.

The melting point of Tm_2O_3 has been measured to be 2375°C using a V-filament furnace (4). With a heat of formation of -451.4 kcal per mole at 298°K (14), thulia is one of the most stable oxides. Because of this high stability, thulia cannot readily be reduced or oxidized to form other oxide phases. Similarly, interaction with containment metals is unlikely.

An analysis of the thermal stability of thulium oxide has been made by Smith (3). He established the vaporization process and vapor pressure by thermodynamic arguments based on limited data on Tm_2O_3 and extensive data on related rare earth oxides. Congruent vaporization in vacuum occurs to form predominantly gaseous atoms of thulium and oxygen (Reaction 1 in Fig. 2). Competing with this process is vaporization to form TmO(g) and oxygen (Reaction 2 in Fig. 2). Uncertainty in the dissociation energy of TmO(g) precludes establishment of the relative importance of TmO(g) compared to Tm(g). Panish (15) has shown, however, by mass spectrometry that Tm(g) is a factor of 10 more important than TmO(g) in equilibrium with Tm_2O_3(s).

Below its melting point, the total pressure of thulia is given by the expression: $\log_{10}P_T(atm) = 7.37 - 31{,}500/T$ (°K). At 2000°K the calculated vapor pressure is 4.2×10^{-9} atm. Tm_2O_3 has about the same vapor pressure as ThO_2. Extrapolation of the vapor pressure to 1 atmosphere

establishes the boiling point as 4150°C. Calculated curves for Log P_T versus 1/T for both vaporization processes are shown in Fig. 2. Although the vapor pressure is low, the oxide will be significantly redistributed in thermionic capsules if even small temperature gradients exist. The mass transport rates at various temperatures and in several temperature gradients have been calculated by Smith, Mosley, and Keski (16).

The tabulated values for linear thermal expansion given in Table I are taken from a curve of lattice expansion determined by high-temperature X-ray techniques (2,17). The behavior is typical of that exhibited by other rare earth sesquioxides.

Eastly and Matson (5) report the thermal conductivity of Tm_2O_3 to be 0.125 (cal-cm) per (sec-cm^2-°C) at 500°C, a value comparable to that of BeO. However, this appears high by a factor of 10 when compared to Y_2O_3 and most other oxides. A value of 0.006 to 0.019 (cal-cm) per (sec-cm^2-°C) at 1000°C was estimated (2) based upon the conductivity shown by other oxides. McElroy substantiated this estimate by recent measurements of the conductivity of two wafers of Tm_2O_3 that were fabricated at the Savannah River Laboratory to approximately 95.5% of theoretical density. A thermal conductivity of about 0.01 (cal-cm) per (sec-cm^2-°C) was obtained from 35° to 190°C. Ketchen (13) obtained values of about 0.012 decreasing to 0.008 (cal-cm) per (sec-cm^2-°C) for Tm_2O_3 at 200° and 800°C, respectively, on material fabricated at Oak Ridge National Laboratory. The low thermal conductivity suggests cermets might be required to prevent high center temperatures in fuel forms for thermionic applications.

The decay product of ^{170}Tm is ^{170}Yb, another rare earth whose chemistry is quite similar to that of thulium. Ytterbium forms in solid solution with Tm_2O_3 and should not change the fuel properties appreciably even for large percentages of ytterbium. In fact, no dimensional changes, lattice parameter changes, or microstructural degradation of fabricated pieces were observed after irradiation and decay to form up to 15 wt % of ytterbium in the Tm_2O_3 (4).

Fabrication of Thulium Oxide

A distinct advantage of thulia is the potential to be fabricated into the final fuel form prior to neutron irradiation. In view of the short half-life, valuable time is saved if chemical separation and fuel fabrication are not required after irradiation.

As part of a demonstration of production feasibility, procedures for fabricating high-density thulium oxide wafers

were developed and described by Keski and Smith (4). Densities up to 97% of theoretical were obtained by reprocessing commercial thulium oxide powders to obtain a high-surface-area powder for sintering. Densities of only about 75% of theoretical were achieved when as-received oxide powders were cold-pressed and sintered.

A conventional cold pressing and sintering technique, outlined in Fig. 3, produced high-density material. Thulium sesquioxide of 99.9% purity was reprocessed by dissolving the powder in 5M nitric acid at 75° to 80°C. After a one-hour digestion period, the nitrate solution was cooled to room temperature, and thulium hydroxide was subsequently precipitated by addition of 5M sodium hydroxide. The hydroxide, calcined in air at 750°C, decomposed to an oxide powder of high surface area. The surface area was 22.5 m^2 per gm.

Wafers suitable for direct use as heat source fuel after irradiation were made by cold-pressing reprocessed powder at 10,000 psi, using an organic binder as a pressing aid, and then sintering the compact in air at 1700°C. The wafers may then be ground to the required dimensions for a particular application. The microstructure of sintered wafers is shown in Fig. 4. Preliminary hot-pressing experiments with graphite die and rams indicate that densities of about 99% of theoretical may be obtained at 3000 psi and 1500°C.

The fabrication must be closely controlled to avoid introduction of deleterious impurities. These impurities may arise from a variety of sources, such as reprocessing equipment or furnace refractories. In general, thulia wafers may be fabricated by the above procedure to purities of approximately 99.5%.

A silicon impurity of 2 wt % in thulia (introduced into thulia during reprocessing in glass* labware) reacted with tantalum after heating for 24 hr at 1925°C in a sealed tantalum capsule containing helium, and formed a layer of Ta_5Si. Although the Tm_2O_3 per se did not interact with the tantalum in the sealed capsule, the thulia and a tantalum substrate did interact in flowing helium. A reaction product identified as $TmTaO_4$ formed after one hour at 1900°C, apparently because Tm(g) or TmO(g) was swept from the system, allowing the reaction to proceed. Wafers reacted with Al_2O_3 "setters" during sintering at 1750°C in air to form a perovskite compound. Introduction of aluminum impurities was prevented by using coarse thulia powder beneath the wafers.

* Silicon was subsequently held at 0.1 wt % by using polyethylene labware in the processing operations.

Irradiation of Thulium Oxide

Thulium sesquioxide wafers, 0.7 in. in diameter by 0.1 in. thick, fabricated in the above manner, were irradiated in aluminum containers in Savannah River reactors to demonstrate production capability for $^{170}Tm_2O_3$. About 0.6 kw of $^{170}Tm_2O_3$ was produced with a power level of about 2 w per gm of Tm_2O_3 at discharge. An activity level of 2.5 w per gm of Tm_2O_3 was obtained in experimental irradiations during an earlier high flux demonstration at Savannah River (1), and a level of 3 w per gm is believed attainable in a specially designed experiment.

Effects of reactor irradiation on thulia were assessed by examining wafers before and after exposure. This examination indicated that no dimensional changes occurred during irradiation. Some minor changes in weight were noted, but these were attributed to chipping or to pickup of surface contamination from the aluminum holders. No evidence of microstructural changes was noted (Fig. 4).

The possibility of interaction between Tm_2O_3 and aluminum containers used during irradiation was evaluated by differential thermal analysis of mixed thulia and aluminum powders (4). An exothermic reaction began at 585°C. Since the Al-Tm_2O_3 interface is considerably below this temperature during irradiation, no interaction was expected or observed on postirradiation examination.

Diametral compression tests on three irradiated wafers showed a tensile strength of approximately 5000 psi, about equal to that of unirradiated wafers. No evidence of microcracking was found in irradiated wafers.

About two-thirds of the irradiated wafers were found broken into two or more pieces when removed from the aluminum containers. This breakage is believed due to mechanical damage during target assembly and disassembly operations or to thermal stresses during irradiation. In a more recent irradiation, these procedures were altered to minimize breakage during handling of the brittle materials. Only one wafer of twenty seven examined was broken as a result of the handling techniques used. With reasonable care, breakage does not constitute a serious problem.

Status and Applications of Thulium Sesquioxide

Thulium sesquioxide has been shown to be a material with excellent potential for meeting operational and safety requirements for high-temperature power sources. A process has been developed to fabricate high-density oxide wafers suitable for irradiation and use in a heat source capsule,

and background technology exists for the manufacture of other fuel forms (such as microspheres or cermets) that might be required for specific applications. Irradiation procedures to produce ^{170}Tm with high power densities in Tm_2O_3 or thulium metal targets have been developed. The major development areas remaining are long term compatibility testing, alternative fuel form fabrication, life test demonstrations of heat source capsules, and safety evaluation.

There is no mission designated to use a ^{170}Tm power source at present. However, Sanders Nuclear Corporation has demonstrated a low temperature, 300-mw generator prototype as part of an in-house project (18,19). Sanders Nuclear is also investigating the use of $^{170}Tm_2O_3$ as a fuel for other isotopic power devices under contract to the USAEC; in this program, they will be concerned primarily with fuel material properties and fuel capsule compatibility (19).

Thulium-170 is a possible substitute for ^{210}Po, an alpha emitter with a half-life of 138 days, in short-term heat source missions. Thulium-170 is especially well suited for fueling high temperature sources, where it possesses a number of unique advantages:

- Tm_2O_3 is a truly refractory, full-oxidized fuel material, which greatly enchances its probability of meeting nuclear safety requirements.
- Because ^{170}Tm is a beta emitter, no problems arise due to helium formation.
- No large and expensive inventory of target material is required to produce ^{170}Tm.
- Following irradiation, thulium sesquioxide may be used directly as a heat source fuel.

The major disadvantage in the use of ^{170}Tm is the heavy shielding required because of the Bremmsstrahlung associated with the beta decay.

Acknowledgment

The information contained in this article was developed during the course of work under Contract AT(07-2)-1 with the United States Atomic Energy Commission.

REFERENCES

1. J. L. Crandall (compiler), The Savannah River High Flux Demonstration, USAEC Report DP-999, Savannah River Laboratory (1965).

2. P. K. Smith, J. R. Keski, and C. L. Angerman, Properties of Thulium Metal and Oxide, USAEC Report DP-1114, Savannah River Laboratory (1967).

3. P. K. Smith, High Temperature Stability of Thulium Oxide, USAEC Report DP-1116, Savannah River Laboratory (1967).

4. J. R. Keski and P. K. Smith, Thulium Sesquioxide for Isotopic Heat Sources, presented at the 12th Pacific Coast Regional Meeting of the American Ceramic Society, San Francisco, Calif., November 1-4, 1967.

5. M. R. Eastly and M. W. Matson, Engineering Properties of Tm_2O_3, Amer. Ceram. Soc. Bull., 44, 1965, p. 389.

6. W. J. Kerrigan, Calorimetrically Measured Half-Life of Thulium-170, J. Inorg. Nucl. Chem., 29, 1967, pp. 2657-2658.

7. Nuclear Data Sheets, 1959-1965, Academic Press, Inc., New York, 1966, pp. 1867-68, 1887.

8. E. D. Arnold, Handbook of Shielding Requirements and Radiation Characteristics of Isotopic Power Sources for Terrestrial, Marine, and Space Applications, USAEC Report ORNL-3576, Oak Ridge National Laboratory (1964).

9. S. M. Sanders, W. J. Kerrigan, and E. L. Albenesius, Radiation Shielding for Small Power Sources of ^{170}Tm, ^{171}Tm, USAEC Report, Savannah River Laboratory (to be issued).

10. Characteristics of Radioisotopic Heat Sources, Battelle Northwest, Jan. 22, 1968. (From C. A. Rohrmann, Radioisotopic Heat Sources, USAEC Report HW-76323, Pacific Northwest Laboratory, Battelle Memorial Institute, Rev. 1, Table VI, p. 52, Oct. 5, 1963. Reissues are made about twice a year to include the most current data).

11. M. Föex and J. P. Traverse, Investigations About Crystalline Transformation in Rare Earths Sesquioxides at High Temperatures, Rev. Int. Hautes Temp. Refract., 3, 1966, pp. 429-453.

12. D. L. McElroy, Oak Ridge National Laboratory, Private communication, April 1968.

13. E. E. Ketchen, Oak Ridge National Laboratory, Private communication, May 1968.

14. E. J. Huber, Jr., E. L. Head, and C. E. Holley, Jr., The Heat of Combustion of Thulium, J. Phys. Chem., 64, 1960, pp. 379-380.

15. M. B. Panish, Vaporization of the Rare Earth Oxides, J. Chem. Phys., 34, 1961, pp. 2197-2198.

16. P. K. Smith, W. C. Mosley, and J. R. Keski, High Temperature Stability of ^{244}Cm and ^{170}Tm Oxide, Proceedings of Thermionic Conversion Specialists Conference, Palo Alto, Calif., October. 30-Nov. 1, 1967.

17. S. Stecura and W. J. Campbell, Thermal Expansion and Phase Inversion of Rare-Earth Oxides, USAEC Report BM-RI-5847, Bureau of Mines, College Park Metallurgy Research Center, Md. (1960).

18. Nucleonics Week, 9(8), September 7, 1968, p. 6.

19. Nucleonics Week, 8(36), February 22, 1968, p. 4.

Table 1. Properties of Thulium Sesquioxide

Power Density, w/gm	2 - 3
Structure,	
To 2280°C: Body-centered cubic,	a = 10.482 Å
2280°C to melting: Hexagonal,	a = 3.78 Å (estimated from c/a = 1.60[11])
	c = 6.04 Å
Density, gm/cc	8.884
Melting Point, °C	2375 ± 25
Heat of Formation, kcal/mole, 298°K	-451.4
Vapor Pressure, atm at 2000°K (estimated)	4.2×10^{-9}
$\log_{10} P_T = 7.37 - 31500/T(°K)$	
Linear Thermal Expansion, %	
At 500°C	0.4
1000°C	0.8
1500°C	1.3
Thermal Conductivity, w/(cm)(deg)	
Savannah River Tm_2O_3 (12):	
At 34°C	0.0420
66°C	0.0424
110°C	0.0422
140°C	0.0413
190°C	0.0383
ORNL Tm_2O_3 (13):	
At 200°C	0.0518
400°C	0.0433
600°C	0.0372
800°C	0.0326

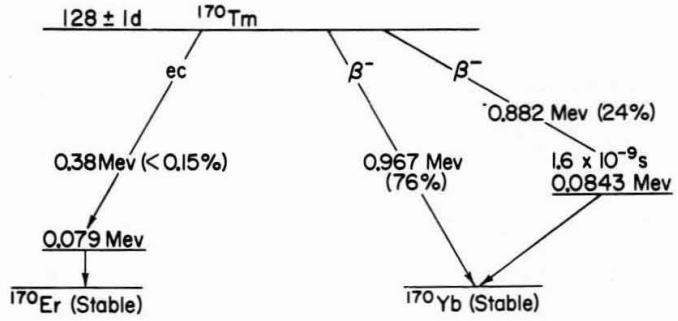

FIG. 1 DECAY SCHEME FOR ^{170}Tm

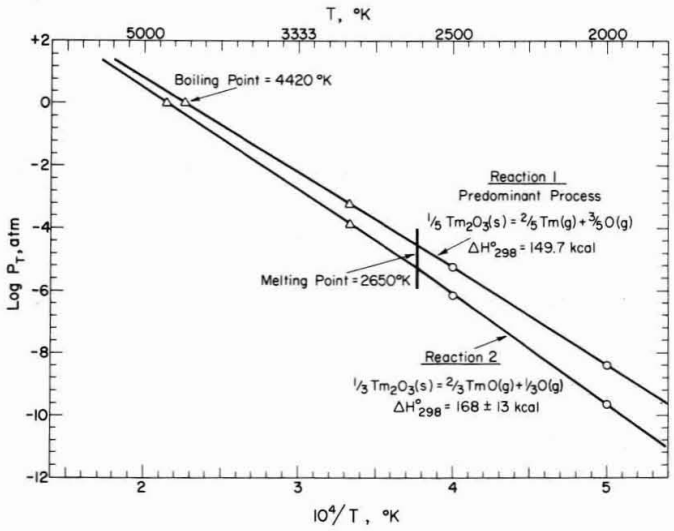

FIG. 2 TOTAL PRESSURE FOR CONGRUENT VAPORIZATION OF THULIUM SESQUIOXIDE

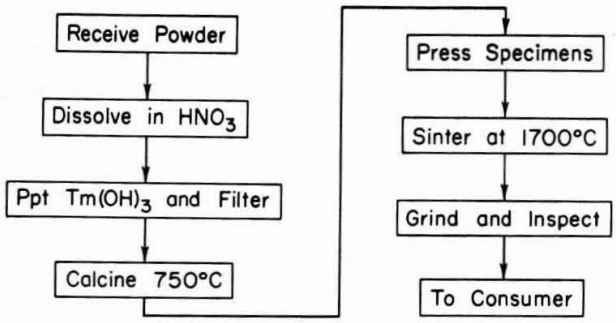

FIG. 3 FLOW CHART FOR THULIUM OXIDE WAFER FABRICATION

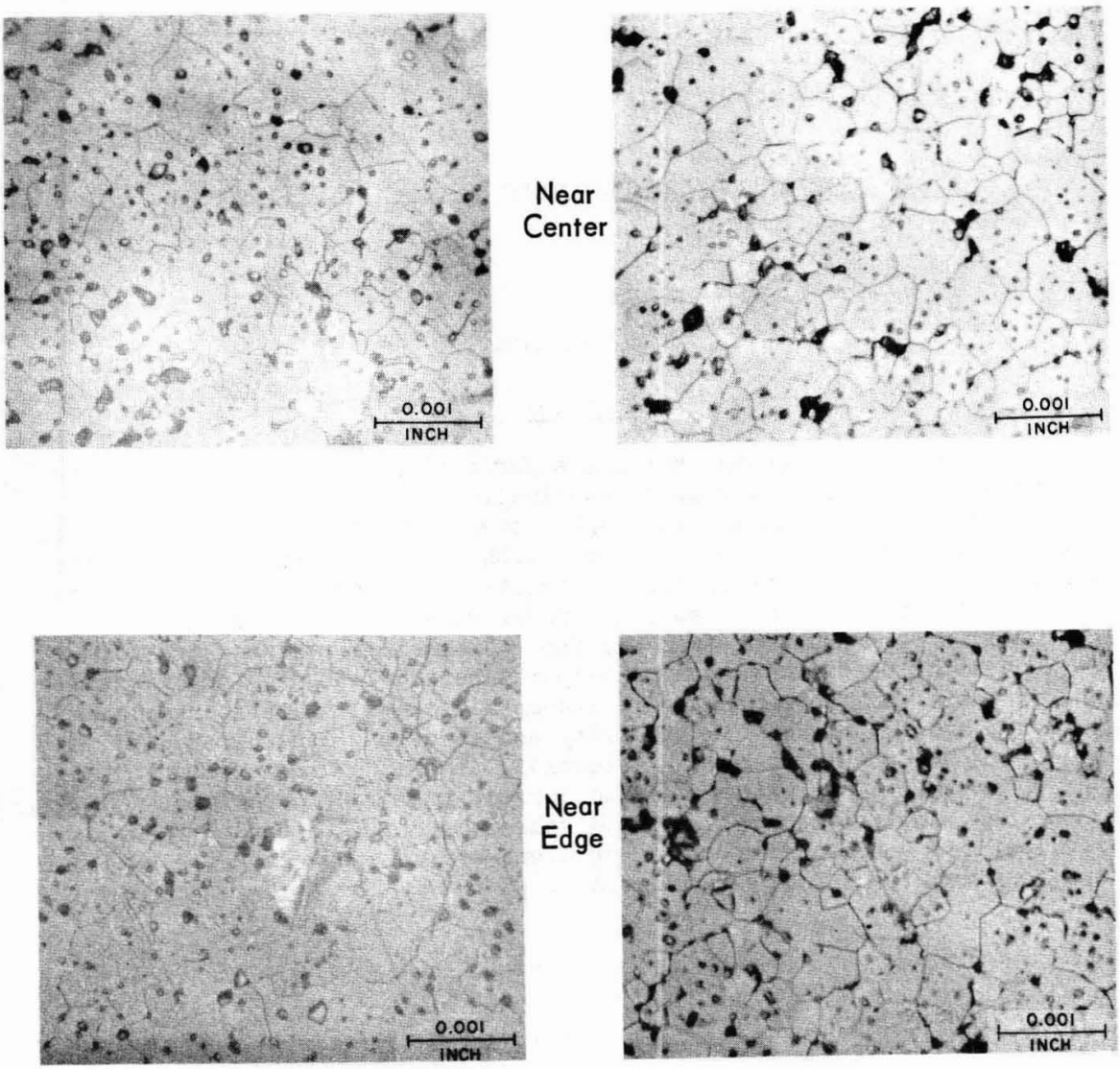

FIG. 4 MICROSTRUCTURE OF Tm_2O_3 SAMPLE

REQUIREMENTS OF RADIOISOTOPE CAPSULE MATERIALS

J. R. Holland

Abstract

The requirements of capsule materials for radioisotope heat sources are demanding particularly for space applications where the requirements often exceed current materials capabilities and knowledge. The capsules are generally multilayered structures with each layer having a definite function relative to the operating conditions and probable environments. One may classify the radioisotope capsule material requirements as follows: those resulting from (a) the radioisotope fuel and its form, (b) operating conditions such as temperature and life, (c) anticipated and potential environments, e.g., launch accidents, space vacuum, and reentry, and (d) mutual compatibility and stability considerations, arising from capsule materials selection. These requirements are discussed in this paper with regard to current practice, materials knowledge, and future needs. The discussion is biased toward space applications since the materials problems encountered seem more exacting and less facile in those applications.

J. R. Holland is supervisor of the Space Power Research Division, Sandia Laboratories, Albuquerque, New Mexico.

Introduction

Snap 3B was a signal achievement as it initiated the use of radioisotope electrical power generators in space. Since the June 29, 1961, launch of SNAP 3B7, which is still producing power, the design concepts of the generators are basically unchanged. However, the materials used for the capsule, the energy converter, and throughout the generator have changed and are still changing in rather dramatic but not surprising ways. The potential use of thermionic conversion units presages even greater changes in the materials technology and requirements. What has already started in capsule technology is that increasing temperature and life requirements have started a trend away from nickel or cobalt based superalloys to refractory metals and noble metal alloys. In time dispersion-strengthened alloys, fiber eutectic alloys, composite alloys, and ceramics may prove advantageous for capsule structures. In many ways, the increasing sophistication of the materials used in capsules is analogous to jet engine turbine bucket development over the past twenty years.

The capsule and the radioisotope fuel it contains is the heart of the system since it is the source of energy. The function of the capsule is to contain the radioisotope in a usable form during operation and to minimize safety hazards associated with the radioisotope fuel. The latter capsule function, and the design ramifications thereof, are critically dependent on the mission safety philosophy, i.e., fuel dispersal, intact reentry, intact through impact, or post impact integrity. The current and potential future requirements for capsule materials for space applications are reviewed here. The need to extend present materials capabilities for the relatively long service life and high reliability required for space uses is stressed as vital.

Materials Requirements

The requirements for capsule materials are dependent to a large extent on the intended use of the radioisotope power generator. This applies for terrestrial and biomedical applications as well as the space applications considered here. The capsule materials requirements may be arbitrarily categorized into four areas. First there are requirements that are a direct result of the radioisotope fuel and its chemical form. For example, with a gamma emitting radioisotope such as ^{60}Co, shielding may be a prime consideration; however, for an alpha emitting radioisotope such as ^{238}Pu shielding is a very minor consideration except in multi-kilowatt man rated systems. Helium gas containment or venting may be the dominant criteria. A second category of requirements is a consequence of the operating conditions, in particular temperature and service life. Thirdly, there are the requirements imposed by the operating environments and potential accident environments. These environments are of such paramount importance that they are discussed in a separate session in this volume. In the accident environments, the prime concern is to insure safety and all other considerations such as reliable power generation are distinctly secondary. Fourthly, there are requirements that are dependent on the

materials selected to meet previous criteria; these include fabricability, mutual compatibility, and thermodynamic stability. In general the requirements for terrestrial use differ from those for space in that the normal and accident environments are much less severe for the terrestrial application from a materials standpoint. In addition, since weight is not a prime consideration for terrestrial applications, much larger safety factors may be used.

Because of the difficulties encountered in meeting the varied materials requirements, presently designed radioisotope capsules are generally multi-layered structures. The material for each layer is selected because it possesses one or more of the required attributes. Hence, a capsule may require five or six consecutive layers of materials across which good thermal conductivity is required. In Fig. 1 is a schematic drawing of a hypothetical capsule which illustrates the principles involved and does not represent the capsule for any SNAP generator. The essential layers represented are: 1) capsule liner, 2) structural shell, 3) diffusion barrier, 4) oxidation resistant cladding, and 5) emittance and/or ablation coating. Chemical compatibility with the fuel is the principal selection criterion for a liner. The material selection for the structural shell is directed primarily by the operating conditions and secondarily by the environments. The selection also depends, in the case of alpha emitting fuels, on whether the capsule is vented. The diffusion barrier is selected to limit the interdiffusion between shells and hence is selected to improve the mutual compatibility and interface stability. An oxidation resistant cladding is often required because of the earth operating environment and the oxidation characteristics of the structural shell, particularly if the shell is a refractory metal or alloy. An outer emittance and/or ablation layer may frequently be desired for self-evident reasons.

The situation described here is a rather exacting materials problem. It also calls for ingenuity and extension of current materials capabilities. In recent capsule designs the use of alloys such as T-111 (Ta-8%W-2%Hf) and TZM (Mo-0.5%Ti-0.08%Zr) represents the first use, to the author's knowledge, of refractory alloys for long service life (~10,000 hours) under stress at reasonably high temperatures (>800° C). Other innovative uses of materials will no doubt follow as operating conditions require higher service temperatures or longer service lives, or both. As we focus attention on the various categories of materials requirements, the need to extend current materials technology becomes more apparent.

Requirements Associated with Fuel Form

First, one considers the requirements associated with the radioisotope fuel and its form. The alpha emitting fuels have been favored for space applications. However, cheaper fuels such as ^{90}Sr have been used for terrestrial applications. The release of helium from fuels such as PuO_2 and the resulting increase in internal gas pressure impose the need for creep strength on structural materials used in unvented capsules. This requirement will continue to exist until it is demonstrated that helium can be reliably vented. Until such time, capsules for alpha fuels probably will continue to be pressure vessels. An exception might occur if the helium could be retained in the fuel itself.

Most of the alloys with high temperature capability were designed for service lives of from 1000 to 5000 hours or less. Accordingly, very little creep data exists beyond these anticipated service lifetimes. Capsule materials for an alpha emitting isotope such as ^{238}Pu (half-life, 87.5 yr.) usually must operate for greater than 10,000 and possibly for longer than 100,000 hours. In a recent capsule designed as a test vehicle for the Large Radioisotope Heat Source Capsule Program (1,2), Fig. 2, the requirement on the structural shell was that it should exhibit a creep strain of less than 1 percent in seven years. This capsule was designed for an operating life of five years and an operating capsule surface temperature of approximately 1100°C. The rationale for the creep strain limitation of 1 percent in seven years was that capsule integrity could be assured with some confidence over that strain and time interval. It was also assumed that the capsule would be launched within a year after encapsulation of the PuO_2 fuel. The candidate materials for this capsule structural shell were alloys of columbium and molybdenum, T-111, and Ta-10% W. In this case T-111 was picked because of its superior creep strength and excellent impact resistance. This particular test capsule was intended for use in generating materials data applicable to the NASA Brayton Cycle demonstration. It should be noted, however, that capsules for a new generation of thermoelectrics, i.e., Si-Ge and cascaded thermoelectrics, will require similar operating times and temperatures.

With beta and gamma emitting radioisotopes, the need for creep strength in the structural material diminishes. Instead, the question of providing gamma shielding and impact strength in the capsule arises. Tungsten and its alloys are candidate materials that meet these criteria and also have high temperature utility.

The chemical activity of radioisotope fuel forms requires that chemical compatibility between the radioisotopic fuel and the capsule be provided. This problem can be particularly severe as the fuels often chemically attack potential capsule materials in localized areas such as grain boundaries and weld zones. In general, compatibility can only be established by isothermal experiments performed at the temperatures of interest. For example, limited results are now available from compatibility tests of PuO_2, Po, GdPo, Cm_2O_3, $SrTiO_2$, Pm_2O_3, Tm_2O_3, and Co; this work is still in progress at Mound Laboratory, Oak Ridge National Laboratory, Battelle Northwest Laboratory, and Savannah River Laboratory. Materials such as platinum, Pt-Rh alloys, tantalum, and Ta-10%W are current candidates for liner materials for use with PuO_2. Changes in the fuel form and its characteristics, such as purity, will modify the chemical interaction with the container or liner materials. Since the fuels are often incompatible with the structural material, capsules are designed with a liner whose function is to provide primary containment of the fuel. The liner material is selected from compatibility considerations and is not required to contribute significantly to the overall strength of the capsule.

Requirements Associated with Normal Operating Conditions

The requirements arising from the operating conditions are straightforward. The primary considerations are the operating temperature and

desired lifetime. These requirements basically modify those for adequate creep strength and fuel-capsule compatibility discussed above. As temperature and lifetime increase, the demands on capsule materials become more exacting. Hence, as thermoelectric technology moves from PbTe to higher temperature thermoelectric materials, such as Si-Ge alloys, then the applicability of nickel and cobalt based superalloys becomes marginal.

Requirements Associated with Abnormal Environments

The environmental requirements are less well defined. This simply reflects a lack of knowledge of the severity of many accident situations and of the behavior of materials in abnormal or extraterrestrial environments. Even the anticipated environments are difficult to define. The predictable requirements from anticipated environments for space use include pre-launch atmospheric effects (e.g., oxidation), launch abort, space vacuum, reentry and aerodynamic heating, capsule impact, and oxidation and corrosion in post impact environments. More detailed accounts of these environments are presented in another section of this volume. In this paper, only the ramifications of these environments on capsule materials requirements are indicated.

The prelaunch atmospheric effects are negligible when the capsule structure has inherent oxidation resistance. One reason for this is that capsule surface temperatures when in air are roughly one-half to two-thirds of the equilibrium surface temperature in space vacuum. Thus, for service temperatures within the capability of Haynes-25 or Hastelloy-N, prelaunch oxidation effects are insignificant. Capsule structural shells fabricated from refractory metals require protection prior to launch. In many cases it is preferable to provide this protection by cladding the capsule with a noble metal alloy. This cladding also provides oxidation protection for reentry and post reentry conditions and selection is usually based primarily on these conditions.

The environments related to launch abort, such as pad fires (fireballs) and explosions, and premature reentry, essentially demand an extension of the normal environment requirements. For example, in launch pad fires and fireballs the capsule should not release fuel by melting or structurally degrade to a significant degree. In an explosion, the capsule should be capable of withstanding the explosive force without rupture. In addition, it should be resistant to shrapnel penetration. The aerodynamic heating in a premature reentry has a different profile than normal reentry but the materials requirements are very similar in that the capsule should be highly resistant to thermal degradation and melting.

Vaporization losses and changes in surface condition in space vacuum are causes of concern. Therefore, capsule materials that are exposed to space vacuum should have very low vapor pressures (less than the vacuum pressure of space) at the operating temperatures. In general, it is difficult to offset this requirement by providing a positive pressure of inert gas within the generator because of potential leaks and micrometeoroid penetration. Vaporization losses of constituents and the breakdown of normal surface oxides in space could potentially have deleterious effects on the creep resistance. While there is no direct evidence related to this, it is known that surface active agents can

drastically alter the deformation and creep characteristics of many materials by alteration and removal of the surface oxides (3-6).

The requirements for capsule materials varies depending on the reentry conditions, such as ballistic coefficient and reentry angle, and upon the safety philosophy involved, i.e., intact reentry, intact impact, or dispersal. In a dispersal capsule the objective is to breach the capsule at very high altitude and effect a wide dispersal of the fuel. The capsule breach may be designed to occur from capsule melting at a localized hot spot. For either intact reentry or intact impact, the objective is to minimize capsule structural damage due to reentry heating. Therefore, the capsule structural material must have a melting point sufficiently high to preclude weakening both by general melting and melting of any of the alloy phases. Secondary recrystallization and exaggerated grain growth effects may be important but they have not been a major concern.

Capsule impact requirements seem to be becoming increasingly important. The reason for this is related to recent efforts to insure that capsules retain their integrity through and after impact. The rationale is that if the fuel is contained through impact, it is relatively safe. Release well after impact is likely to occur at relatively slow rates and there is a reasonably high probability against any gross fuel release. Also, the probability of atmospheric resuspension of the fuel is greatly reduced. This discussion is germain to alpha emitting fuels that are stable in air and probably does not apply to such fuels as ^{210}Po, ^{90}Sr, or ^{60}Co. For these latter isotopes <u>total</u> containment on earth is highly desirable; therefore, capsule integrity well after impact is a necessity unless the capsule can be effectively buried in acceptable locations such as ocean depths.

Impact resistance is of great importance, but this characteristic cannot be reliably predicted. Typical impact velocities are in the range of 100 to 600 feet per second. It is generally considered that the most severe condtion is impact on granite; hence most capsules are impact tested against granite. The capsule temperature at the time of impact and the effects of the thermal and stress history of the capsule complicate the situation. The capsule should absorb the energy of impact by deforming without fracturing. The capsule structural material should exhibit good impact resistance in an aged condition, a situation that is illustrated in Figs. 3, 4, and 5. Lack of notch sensitivity and good ductility seem to contribute to this characteristic.

Protecting the capsule in post impact environments is difficult at best. Cladding and coating layers tend to abrade or strip away during impact. This has been experimentally observed for Pt-Rh claddings up to 0.040 in. thick (7). Greater strength and hardness in the cladding is needed, but it is difficult to provide. A capsule lying on the ground or totally immersed in water (either fresh or sea) will maintain a temperature much reduced from the steady state operating temperature in space because of improved thermal transfer. Therefore, in this situation a refractory metal capsule structural shell might have appreciable life. The tantalum alloys containing hafnium may be useful in this regard since they have a limited degree of oxidation self protection if sufficient hafnium is present.

Stress corrosion in sea and fresh water are also of concern. Paucity of data regarding these effects makes it difficult to assess the material requirements. Capsule burial with resulting soil corrosion is another area in which it remains difficult to determine the materials needs. (See, for example, Fig. 6.) The capsule temperatures vary depending on soil type. A buried capsule that reacts with the soil to form a molten slaglike mass may represent a method of safe containment of radioisotopes.

One must also consider individual material stability, interaction of materials in various layers, and the possibility of significantly modifying the materials by interdiffusion across interfaces. The severity will depend on the materials selected, but, to the extent feasible, instabilities should be avoided. This is vital where the structural shell is concerned. Formation of Laves phases in cobalt base superalloys, pick-up of interstitial contaminants by refractory metals, and formation of new phases, particularly embrittling intermetallic compounds, can all have dire consequences during service, reentry, and impact. An example of potential problems from diffusion is platinum diffusing into a tantalum base alloy. Formation of any of the several known Ta-Pt intermetallics could potentially degrade a tantalum alloy structural shell. For problems such as these, an indicated solution is to provide diffusion barriers to minimize problems across materials interfaces. Stable oxides such as Al_2O_3 and ThO_2 are being considered for this purpose.

Fabricability

Finally, the problem of fabricability has to be taken into account. Formability and weldability are vital practical requirements. Capsules are relatively complicated to fabricate and this is further complicated by the presence of the radioisotopic fuel during assembly and weld closure. Thus, formability and weldability assume greater importance than usual.

Summary

In summary, the materials requirements are manifold. High temperature strength, creep resistance, high strain rate ductility, oxidation resistance, chemical stability, resistance to environmental effects, high melting point, phase stability at high temperature, and impact energy absorption are vital characteristics of materials selected for the structural shell of radioisotope capsules for space use. Since it is unusual to find these characteristics to an acceptable degree in a single material, capsules are generally multilayered. Each layer provides for one or more of these materials needs. Terrestrial capsules have less stringent requirements than space capsules because the environmental effects are less varied and are more predictable and greater safety factors may be employed.

Acknowledgements

This review was supported under the auspices of the United States Atomic Energy Commission.

REFERENCES

1. Large Radioisotope Heat Source Capsule, First Quarterly Progress Report, Atomics International Report NAA-SR-12578, September 1967.

2. Large Radioisotope Heat Source Capsule, Second Quarterly Progress Report, Atomics International Report AI-AEC-12642, December 1967.

3. I. R. Kramer and L. J. Demer, Progress in Materials Science, Vol. 9, Pergamon Press, Oxford, 1961, p. 131.

4. I. R. Kramer and L. J. Demer, Trans. Met. Soc. AIME, 221, 780-786, 1961.

5. I. R. Kramer, Trans. Met. Soc. AIME, 221, 989-993, 1961.

6. I. R. Kramer, Trans. Met. Soc. AIME, 227, 1003-1010, 1963.

7. Radioisotope Heated Propellant Control Systems, Second Quarterly Report, Technical Report AFRPL-TR-66-275, prepared by TRW Systems, October 1966.

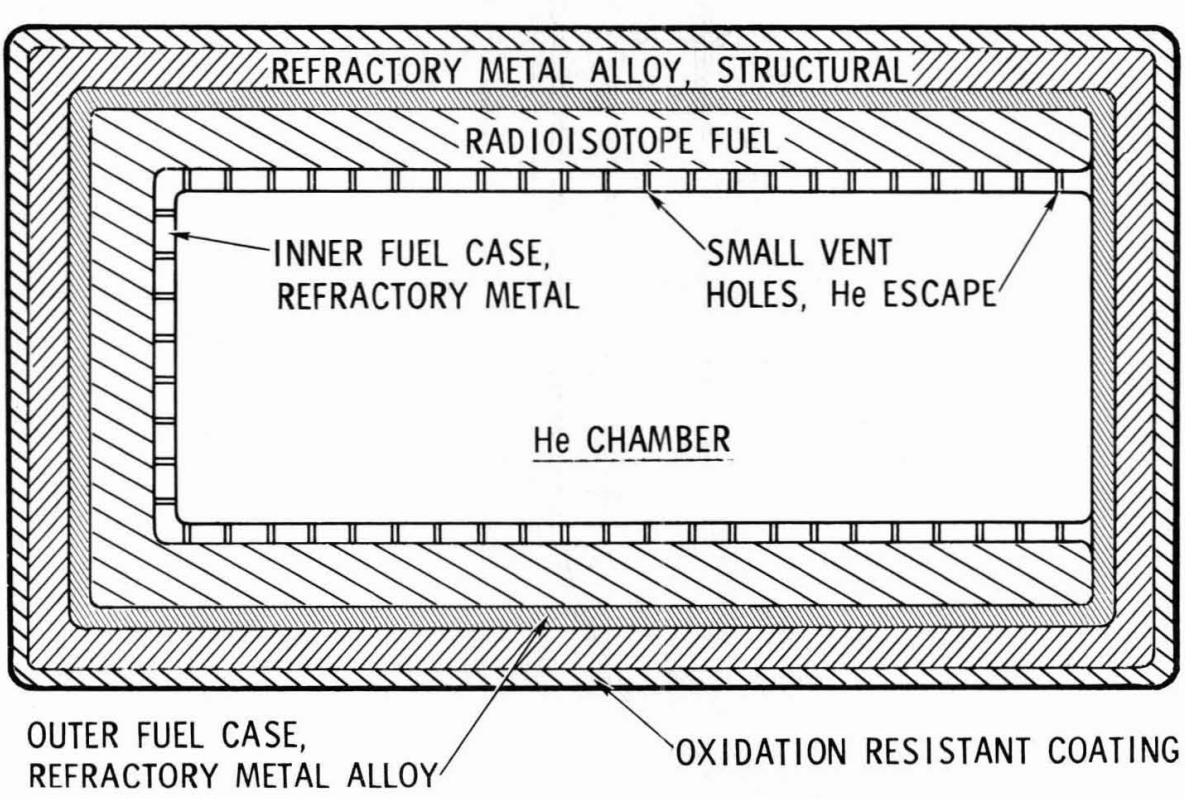

Fig. 1 Schematic of hypothetical radioisotope fuel capsule for space applications. The capsule is for alpha emitting radioisotopes and illustrates a multilayered approach to capsule design and materials selection.

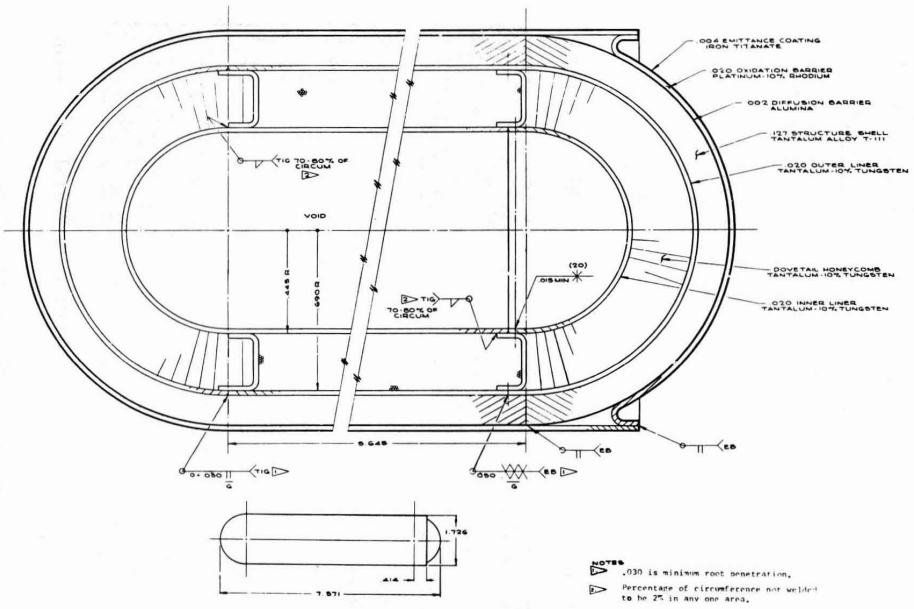

Fig. 2 The Large Radioisotope Heat Source Capsule. The cross section gives the materials layers and dimensions. The inner liner is 0.020 in. Ta-10% W, the outer liner is 0.020 in. Ta-10% W; the structural shell is 0.127 in. tantalum alloy T-111; the diffusion barrier is 0.002 in. alumina; the oxidation cladding is Pt-10%Rh; the emittance coating is 0.004 in. iron titanate. The shock mitigating structure is a honeycomb structure of Ta-10% W.

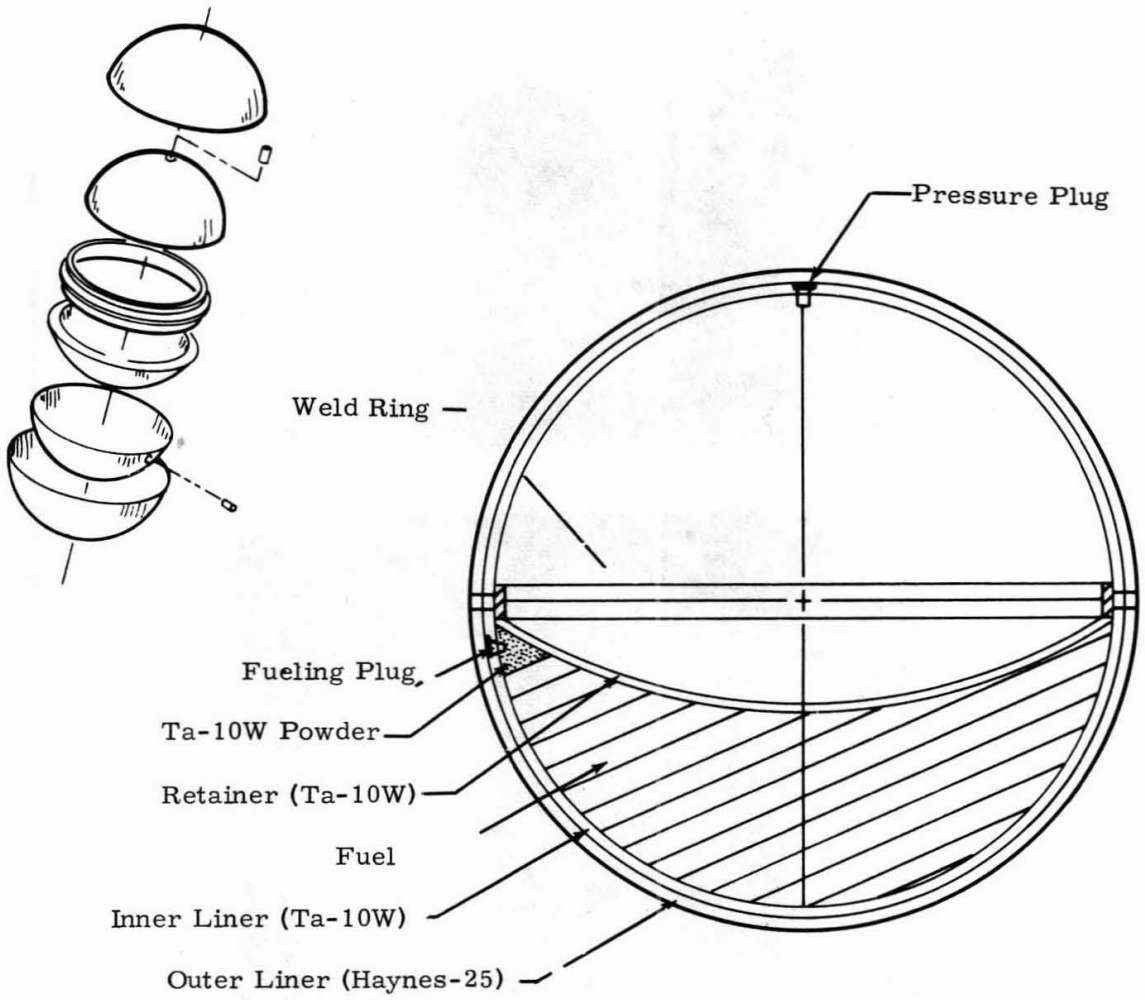

Fig. 3 Cross section of a spherical capsule designed by Hittman Associates. The structural shell is Haynes-25. The liner material is Ta-10% W. Capsule assembly is also indicated. This capsule design has been extensively impact tested.

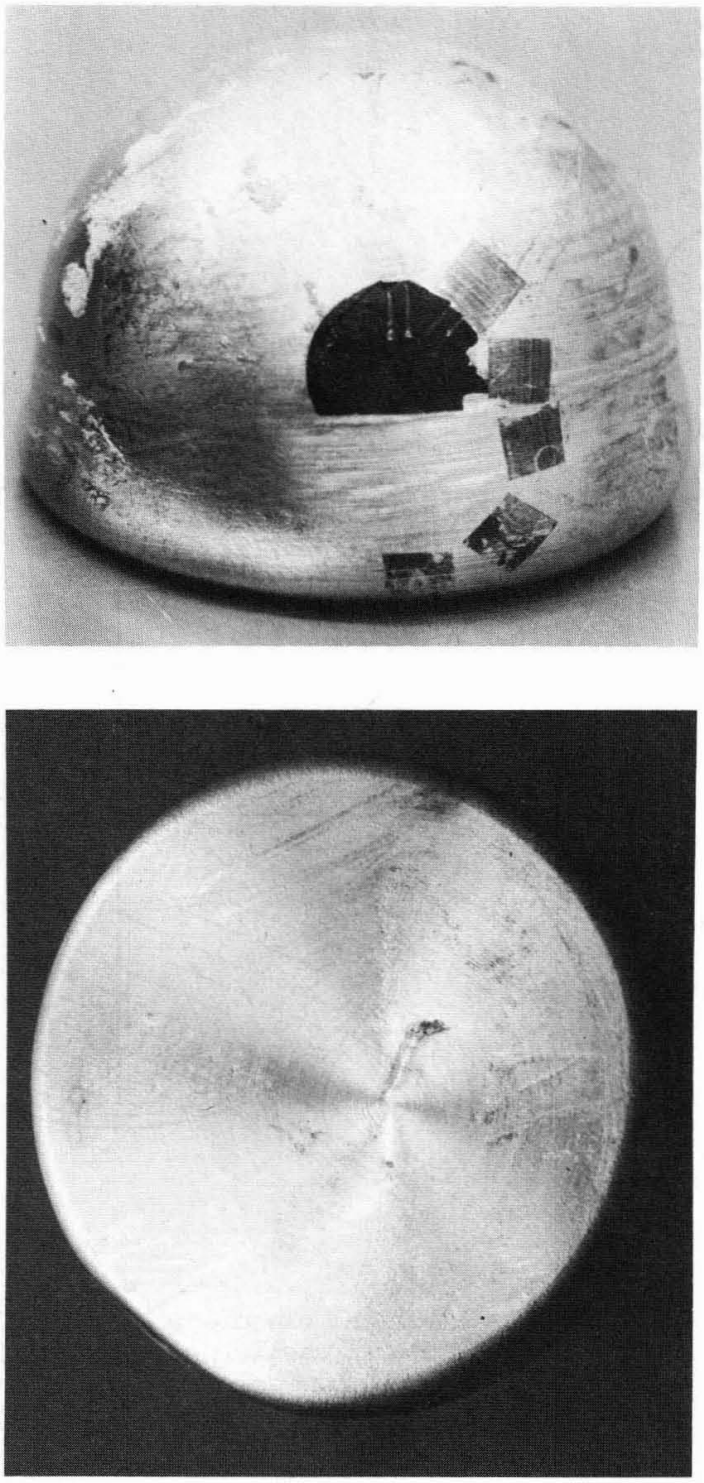

Fig. 4 Spherical capsule shown in Fig. 3 (a) side view; (b) bottom view, after impact onto granite. The capsule was in an unaged condition, the nominal capsule temperature at impact was 260° C, and the impact velocity was 452 feet per second. The apparent capsule integrity was confirmed by subsequent post impact examination.

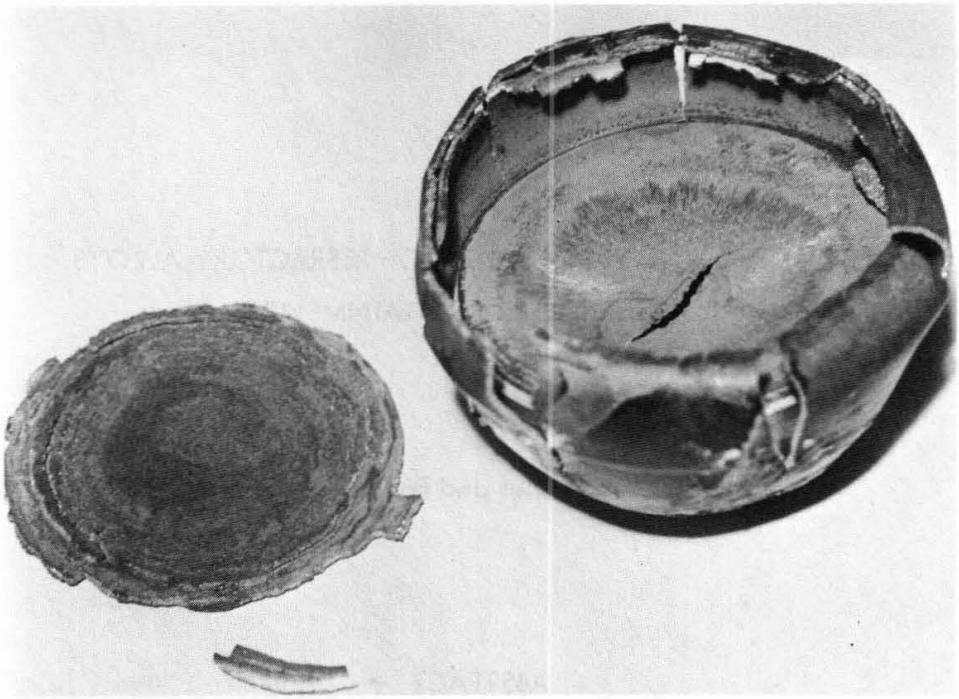

Fig. 5 Spherical capsule shown in Fig. 3 after impact onto granite. The capsule had been aged 1000 hours at 816°C; the nominal capsule temperature at impact was 260°C; the impact velocity was 374 feet per second.

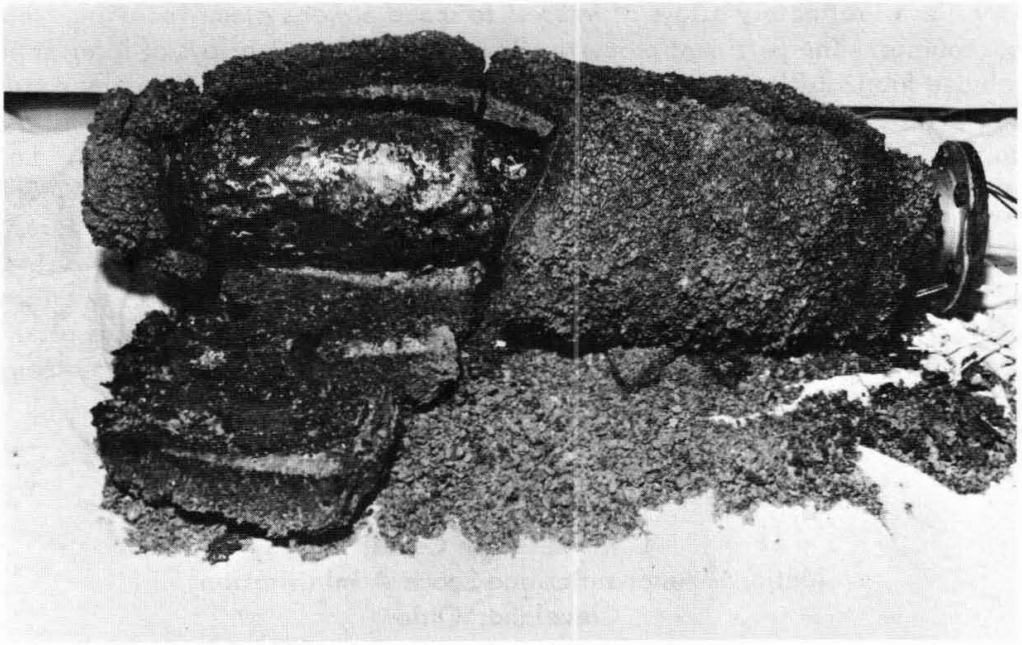

Fig. 6 Burial test of the SNAP 27 capsule. The capsule temperature exceeded 1374°C, the total burial time was 48 hours, and the soil was bentonite.

PROPERTIES AND FABRICATION OF REFRACTORY ALLOYS FOR ISOTOPE CONTAINMENT

By Robert Lee Davies and Paul E. Moorhead

ABSTRACT

Use of isotopic fuels in a high-temperature heat source requires the use of refractarymetal alloys for containment and also for structure in order to hold fuel capsules in a given geometry. Programs have been conducted to determine properties of refractory alloys of interest to space power systems including isotope heat sources. The pertinent properties investigated for the alloys of interest have included fabricability, elevated temperature stability and long-time creep strength. Data will be presented on the bend ductility of various refractory alloys in the wrought, electron-beam welded and tungsten inert gas welded conditions. Long-time data will be presented on the structural stability of the T-111 (Ta-8W-2Hf) alloy. Also presented will be creep strength data for various alloys of interest for application to isotope heat sources. In addition, stronger alloys are of interest because they would allow a reduction in structural material thickness or an increase in safety without a weight penalty. The study of advanced alloys has resulted in a fabricable, weldable tantalum alloy having a useful design strength at temperatures up to 2600°F.

Lewis Research Center
National Aeronautics and Space Administration
Cleveland, Ohio

INTRODUCTION

Space power systems using isotope heat sources are of interest for future long-duration space missions. One such system is the isotope-Brayton system under investigation at the NASA Lewis Research Center (Ref. 1). As a part of this investigation, studies have been conducted by the AEC and NASA to define an isotope-containment capsule compatible with the design requirements of the isotope-Brayton system. These studies have indicated the necessity for the development of a refractory-metal-alloy capsule for operation at 2000° F, utilizing plutonium-238 as the fuel. At present, Atomics International under contract to the AEC is conducting a program to develop the technology of a refractory alloy isotope fuel capsule capable of operating in a space environment at a surface temperature of about 2000° F for five years or more (Ref. 2).

The use of refractory alloys will require the determination of alloy properties at the anticipated operating conditions. In this paper, the properties discussed for refractory alloys of interest were generated under NASA contract. These properties include long-time creep strength, and elevated temperature stability and its effect on ductility and fabricability. The alloys would be applicable to the isotope-Brayton, as well as to other isotope-using concepts requiring refractory alloys.

MATERIALS REQUIREMENTS

The refractory metals used for isotope encapsulation, whenever total containment is required, must possess high strength at elevated temperatures and for long times, compatibility with isotope fuel, and sufficient ductility and weldability to permit capsule fabrication. At the present time, tantalum-base alloys offer the greatest potential for the containment material. A liner is provided to separate the fuel from the tantalum-alloy strength member. An oxidation-protection layer is also required. Shown in Fig. 1 is a typical capsule config-

uration generated to satisfy the aforementioned requirements (Ref. 2). The capsule consists of a liner, a primary-containment strength member of tantalum alloy, and a platinum alloy for oxidation protection. A diffusion-barrier layer is provided between the tantalum and platinum to prevent interaction and embrittlement of the capsule materials. The outside is coated with a high-emissivity coating since the design heat-transfer mode is radiation.

The strength requirement imposed on the containment alloy is a result of the decay of the fuel. An alpha-emitting isotope, such as plutonium, releases helium during decay causing helium pressure in an unvented capsule. Based on the assumption of 100 percent helium release from the fuel matrix, Fig. 2 shows this characteristic pressure buildup with time and the characteristic temperature decrease. Initially, the gas pressure in the capsule is low and the temperature is a maximum; however, as the fuel decays, pressure builds up while the temperature decreases. At about 2 half-lives, the temperature decrease more than offsets the additional gas generated. and the pressure begins to decrease. The temperature of the capsule has fallen to 700° F when the maximum gas pressure of about 15 000 psi is reached at 2 half-lives. Subsequently, the gas pressure decreases to a value of approximately 10 000 psi and remains essentially constant.

CREEP STRENGTH

The creep strengths of various alloys have been investigated in tests conducted in ultrahigh vacuums. Shown in Fig. 3 are several of the ion-pumped creep-test rigs being utilized for these tests. The vacuum chambers are capable of continuous operation at 10^{-9} torr, and the accuracy of specimen-extension measurements is ± 50 μinches. The high vacuum is required to prevent contamination of the materials, which would otherwise lead to incorrectly predicted strengths for the refractory alloys. The creep properties of the alloys to be discussed have been generated by TRW Inc. under NASA contract (Ref. 3).

In Fig. 4, the stress to produce 1 percent creep in various alloys

is related to the Larson-Miller parameter P where

$$P = T\,(15 + \log t)$$

T = temperature, ^{o}R

t = time, hr

For 1 percent creep in 10 000 hours with a stress of 2000 psi, the following would be the maximum allowable operating temperatures.

Alloy	Temperature ^{o}F
T-111	2300
ASTAR-811C	2650
W	2750
W-25Re	2800

The design of an isotope-capsule strength member predicted upon any single combination of stress and temperature would be erroneous and could lead to an unsafe design or to one that is too conservative, thus suffering a weight penalty. Therefore, a procedure is necessary for handling the increasing stress with decreasing temperature.

For these conditions of variable stress and temperature, the following simple but unproven theoretical method may be used to estimate creep: For a given material and a given operating stress the value of the Larson-Miller parameter P corresponding to, say, 1 percent creep can be determined from a plot such as Fig. 4. For a given temperature T, the time t required to produce the selected creep can then be determined. The quotient of the selected creep to the thereby determined time t specifies the average creep rate over the time t. For this theoretical method such creep rates are assumed to be functions of only stress and temperature and to be independent of previous stress, temperature, or accumulated creep. For the varying stress and temperature of the isotope capsule, these creep rates are integrated with respect to time in order to determine the total accumulated creep. A method for accomplishing this is described in Ref. 4.

Typical creep tests conducted to date have been at constant stress and temperature; however, data are required on the behavior of the material under changing stress and temperature. Progressive-load creep tests are being conducted on T-111. In these tests, the stress is nominally zero at the start and increases at a given rate (psi/hr), until the desired creep is achieved. A typical curve from this type of test is shown in Fig. 5. Using a method similar to the Oak Ridge National Laboratory method previously discussed, Sheffler (Ref. 3), working under a NASA program, developed the following mathematical expression to determine the creep life to a given percent creep strain:

$$\ln L = \left[\frac{\ln \dot{\sigma}}{AT} - \ln \frac{AT}{AT - 1} - \frac{B}{AT - C}\right] \frac{AT}{AT - 1}$$

where

L = creep life, hr

$\dot{\sigma}$ = stress rate, psi/hr

T = temperature, ^{o}R

ABC = empirical constants dependent upon material

The constants are derived from constant-stress tests carried out to the desired percent creep strain. Predictions made using this formula for a particular heat of material have shown good agreement with the experimentally determined results in variable-stress tests up to about 4000 hours with T-111.

The progressive load-type tests have also shown that as the stress approaches approximately three-fourths of the tensile yield strength at lower temperatures, below about 1800^{o} F, the creep strain deviates from that predicted by the Larson-Miller plots. This means that the design limits for an isotope capsule would no longer be based on creep, but on criterion based on yield strength limits, when the stress approaches three-fourths of the yield strength of the strength member.

STRUCTURAL STABILITY

The material utilized for encapsulation of isotopic fuels is required to have an extremely long, useful life. Therefore, a knowledge of its long-time stability is necessary. The stability of a material can be partially determined by its ductility after long-time exposure to elevated temperature. Also, the ductility of the containment alloy is very important to allow deformation of fuel capsules on impact, rather than allow capsule rupture and subsequent fuel release occur. The ductility is also a measure of the ability of the material to withstand thermal stresses and resist thermal fatigue. T-111 alloy has been tested for long times to determine the stability of welds (Ref. 5). Fig. 6 shows the effect of long-time exposure of T-111 welds made by the tungsten-inert-gas process on the ductile-to-brittle transition temperature. The post-weld anneal of 1 hour at 2400° F was selected to impart alkali-metal corrosion resistance to the T-111. The 1t-bend-radius test utilized in this work is very severe, imparting approximately 33 percent strain in the outer fibers of the specimen, and is used for the ductile alloys since it results in a sharp delineation of transition temperature. This sharp delineation makes it possible to detect small differences in aging behavior of very ductile alloys. It is apparent from Fig. 6 that after post-weld annealing, the aging reaction is slow. Although the peak transition temperature occurs later when aging at 1800° F than when aging at 2100° F, the effect is more severe. The transition temperature after 10 000-hour aging at 2100° F is -25° F; and after 10 000-hour aging at 1800° F, it is 125° F. Specimens that were aged 5000 hours at 2100° F with no post-weld anneal exhibited a transition temperature of 80° F. This would be the case for an isotope capsule where no post-weld annealing can be accomplished.

The effect of aging reaction on ductility, i.e., total elongation and reduction in area, was determined for specimens aged 5000 hours at 2100° F with no post-weld anneal. At 32° F, smooth tensile specimens exhibited a total elongation of 25 percent and a reduction in area of 28 percent before failure. This is compared with a total elongation of 22 percent and a reduction in area of 44 percent in the as-welded

specimens. Thus, while the transition temperature of the aged material, based on the severe bend test, had increased to approximately 80° F, the "engineering" amount of ductility even below room temperature has not been affected. As a result of these data, it would appear that even without a post-weld anneal, there would not be significant loss of engineering ductility after exposure to high temperature for long times.

NEW ALLOYS

By virtue of good workability, welding characteristics, and elevated temperature strength, the tantalum-base materials appear to offer the best promise as a structural material for isotope containment. The T-111 tantalum alloy presently being pursued for the application appears adequate; however, stronger alloys are of interest. The interest is great since stronger alloys would allow a reduction in material thickness, or an increase in safety without a weight penalty. A series of fabricable, weldable tantalum alloys have been developed. The most developed advanced alloy has useful design strengths at temperatures up to 2600° F (Ref. 6).

The creep strength of this most highly developed advanced alloy, ASTAR-811C, is compared with T-111 in Fig. 7. Also shown in this figure is a preliminary plot of the strength of material from a developmental ingot containing Ta-13W-1.5Re-0.7Hf-0.025C. This heat of material is one of a series of various compositional ingots being investigated at this time. ASTAR-811C is presently commercially available in sheet form. It can be seen that advanced alloys of this type will offer significant strength advantages over the T-111 although the data shown are for a pilot plant heat of material and may not represent a final composition chosen for larger melts and more extensive examination. Therefore, it should be pointed out that the data are shown only to demonstrate that there is the potential of having significantly stronger, but still fabricable, alloys available in the future.

FABRICATION

Processing

The selection of the encapsulation materials is the first step in the construction of test systems. It is then necessary to assure the production of materials of high, consistent quality to withstand the service conditions. Stringent specifications have been written for the pruchase of refractory metal alloys for space power systems (Ref. 7).

Typical processing sequences for the quality refractory alloys normally include numerous electron-beam melts to lower the oxygen level as much as possible, a minimum of two arc melts to minimize alloy element segregation which can lead to subsequent processing difficulties, encapsulating or otherwise protecting the surface of in-process material to minimize oxygen pickup during working at elevated temperatures, heat treating in vacuums of 1×10^{-5} torr or better, as well as wrapping the material with a refractory metal foil. Other requirements during processing include proper surface conditioning by machining and/or pickling between processing sequences, as well as in-process chemical analysis checks to insure retention of starting material purity. The final quality assurance inspection should include, as a minimum, dye penetrant and ultrasonic testing, chemical analysis, and elevated-temperature strength testing of samples from each lot of material.

The processed material must be final shaped into the desired product. The T-111 material is readily fabricable and can be sheared, blanked, spun, drawn, and bent at room temperature without cracking. The requirements for cold forming are proper lubrication to prevent galling, and sufficient power. One example of T-111 fabricability applicable to isotope encapsulation is work done by Atomics International for the U.S. Atomic Energy Commission. Their work has resulted in the production of T-111 tubes with closed hemispherical ends. The finished tubes were 8 inches in length, 1.68 inches in outside diameter, and 0.127 inch in wall thickness; they were formed by deep drawing from a blank 6-1/2 inches in diameter and 0.169 inch

thick (Ref. 8).

Welding

The tantalum alloys can be welded using either the tungsten-inert-gas (TIG) or electron-beam (EB) methods. The parts to be joined must be properly prepared to avoid porosity or contamination during welding. Methods of preventing weld porosity include machining the weld joints; pickling the parts with 20 percent HNO_3, 15 percent HF, 10 percent H_2SO_4, balance H_2O; and removing any pickling residue or hydrogen formed during pickling by vacuum annealing at 2000^{o} F for 1 hour (Ref. 9).

Weld chamber atmospheres must be maintained at a high quality with acceptable levels of contaminant gases being <5 ppm oxygen, <10 ppm water vapor, and <15 ppm nitrogen. In order to achieve and maintain this purity, the chamber must be capable of being evacuated to $<1\times10^{-5}$ torr or less with a maximum leak rate resulting in a pressure rise of not more than 3×10^{-5} torr per minute. Outgassing during welding can be significantly reduced if the chamber can be heated for bake-out during evacuation. After evacuation, the chamber is backfilled with helium or argon having an oxygen plus water-vapor content of <1 ppm, and nitrogen content of <5 ppm. The most satisfactory gloves checked for use in weld chambers have been made of neoprene (Ref. 10).

Monitoring the chamber atmosphere to insure maintenance of high purity is considered necessary; welding should be discontinued when the oxygen or water-vapor content gets too high. The levels set for discontinuation of welding operations are 5 ppm oxygen and 20 ppm water vapor. The weld chamber atmosphere can be further checked by making a bead-on-plate weld on stainless steel sheet and noting the degree or absence of discoloration. This test checks the environment the weld sees, and can detect oxygen levels in argon as low as 1 to 5 ppm when performed by an experienced operator.

CONCLUSIONS

The material being extensively investigated for the strength member of isotope containment capsules is T-111. Capsules constructed of the T-111 alloy include a tungsten liner and require an outer layer of platinum alloy for protection against oxidation.

Long-term stability of T-111 welds has been investigated, and it is seen that there is an aging reaction. However, subsequent tensile testing of specimens exposed to elevated temperature has shown that adequate engineering ductility is retained in the alloy.

Limited testing of new tantalum alloys has shown that the ASTAR-811C is stronger in creep than T-111, and that other newer alloys are even stronger than the ASTAR-811C. The stronger alloys could provide an advantage for isotope containment by either increasing the safety factor or reducing the weight.

The fabricability of the T-111 has been demonstrated by construction of pressure vessels in an isotope capsule configurations. Weld fabrication studies of T-111 have been conducted and alkali-metal test facilities have been built demonstrating the capability of the alloy as a construction material (Ref. 11).

While there is much experience with the T-111 alloy, there remains the task of insuring metallurgical integrity of multilayered capsules. The work necessary to insure this integrity includes evaluation of multilayered specimens exposed for long times in the operational environment of the isotope system, refinement of strength data and methods of handling the data in designing capsules for long-time service under changing conditions, and development of techniques for constructing fueled capsules and reliably sealing the capsules.

REFERENCES

1. J. L. Klann: "2 to 10 Kilowatt Solar or Radioisotope Brayton Power System," IEEE Intersociety Energy Conversion Engineering Conference Boulder, Colo., Aug. 14-16, 1968.
2. Atomics International Report AI-AEC-12713, 1968.
3. K. D. Sheffler and E. A. Steigerwald: TRW, Inc. (NASA CR-72431), 1968.
4. J. P. Nichols and D. R. Winkler: Oak Ridge National Lab. Report ORNL-TM-1735 (NASA CR-72172), 1967.
5. G. G. Lessmann and D. R. Stoner: Westinghouse Electric Corp. Report WANL-PR-(P)-011 (NASA CR-72073), 1966.
6. R. W. Buckman, Jr. and R. C. Goodspeed: Westinghouse Electric Corp. Report WANL-PR-(Q)-016 1969.
7. D. N. Miketta and R. G. Frank: General Electric Co. (NASA CR-54761), 1965.
8. J. S. Williams and P. B. Ferry: Atomics International Report AI-AEC-12712, 1968.
9. G. G. Lessmann: Welding J., 1966, vol. 45, Res. Suppl., p. 540s.
10. G. G. Lessmann and D. R. Stoner: Westinghourse Electric Corp. Report WANL-PR-P-003 (NASA CR-54088), 1964.
11. R. W. Harrison and E. E. Hoffman: General Electric Co. Report GESP-1 (NASA CR-72383), 1968.

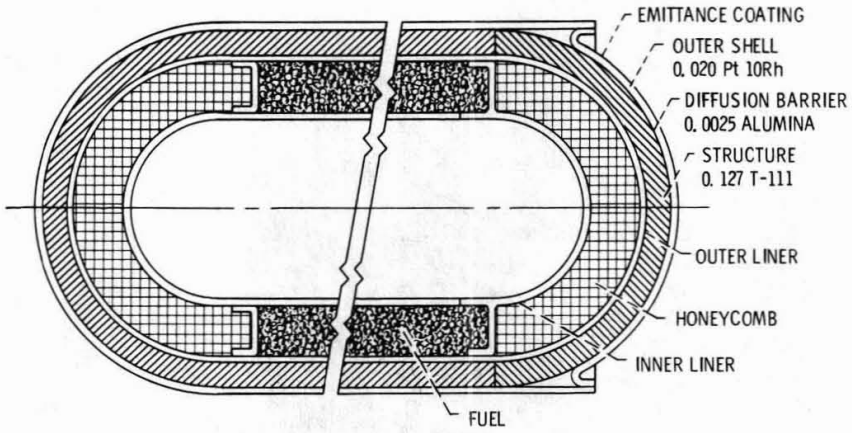

Fig. 1. - Conceptual design of isotope capsule.

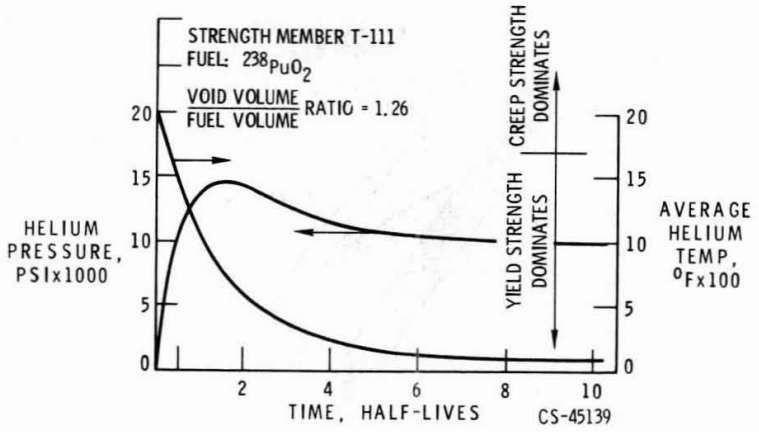

Fig. 2. - Temperature and pressure of capsule for alpha-emitting isotope.

Fig. 3. - High-temperature high-vacuum creep-test equipment. C-69-463

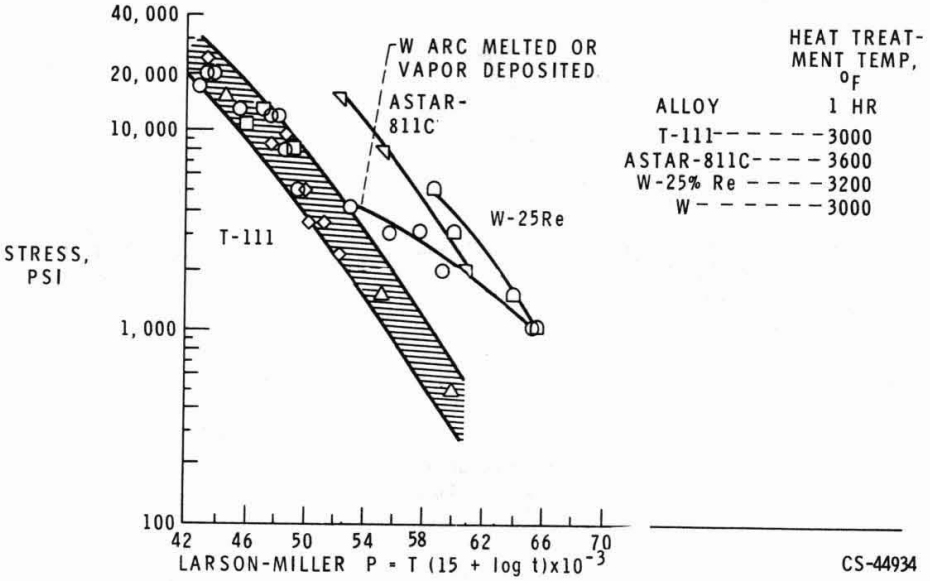

Fig. 4. - Larson-Miller plot for refractory alloys; creep, 1 percent.

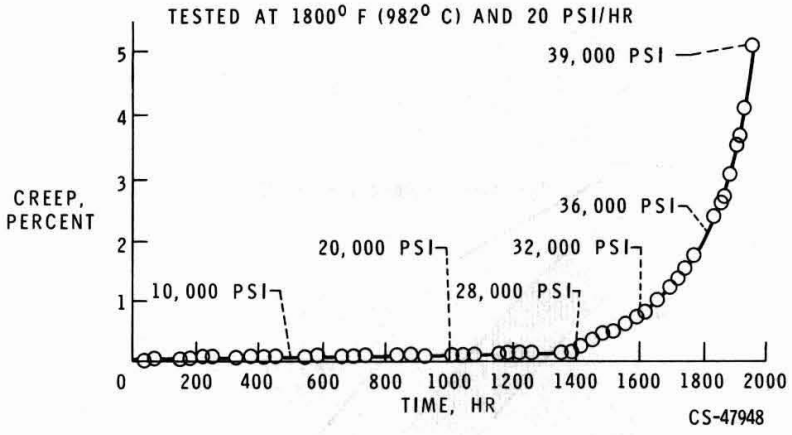

Fig. 5. - Creep curve on T-111 tantalum alloy using progressive loading.

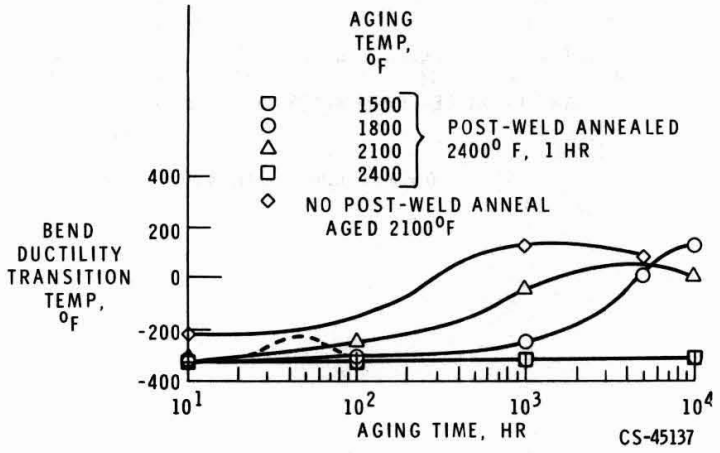

Fig. 6. - Effect of thermal aging on T-111 alloy.

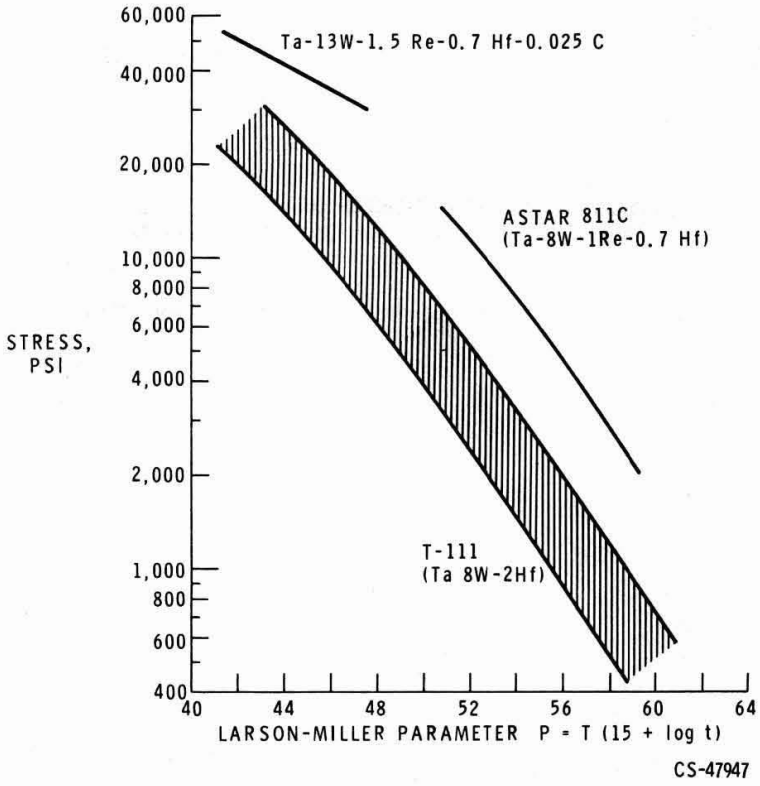

Fig. 7. - Creep strengths of tantalum alloys.

REMOTE ENCAPSULATION TECHNIQUES FOR STRONTIUM AND CURIUM FUEL FORMS*

R. G. Donnelly and R. W. Gunkel**

Abstract

The encapsulation of strontium and curium compounds for isotopic power sources requires welding by remote means in a hot cell. In the past, strontium-fueled superalloy containers have been welded by the gas tungsten-arc process. More recently, electron-beam welding has also been used. This process gives increased penetration, melts less material, provides a more inspectable weld, and is ideally suited to remote operation because the beam can be controlled electromagnetically.

Refractory alloys are the most likely materials for containing curium because of the stress buildup from helium generated by alpha decay and because of the very high temperatures for possible applications. Since helium buildup requires the container to be a pressure vessel, full-penetration welds are necessary. This presents no particular problem when the electron-beam process is used because a vacuum atmosphere is maintained, but with the gas tungsten-arc process, a vent is required to relieve pressure that would be built up by welding heat.

Examples of each of the various types of welds and in-cell welding equipment are presented.

*Research sponsored by the U.S. Atomic Energy Commission under contract with the Union Carbide Corporation.

**Metallurgists, Metals and Ceramics Division, Oak Ridge National Laboratory, Oak Ridge, Tennessee.

Introduction

At ORNL the isotopes of primary interest for power applications are ^{90}Sr and ^{244}Cm. Over the past several years ^{90}Sr compounds have been encapsulated for various power applications (1–4), and possible encapsulating techniques for ^{244}Cm fuels have been extensively developed (5,6).

Encapsulating radioisotope fuels provides an operationally reliable heat source and prevents the fuel's interaction with and ultimate dispersal into the surrounding environment. The most convenient and reliable means of encapsulation is to seal the fuel in a metal container by welding. The type of weld depends upon the fuel, container material, mission requirements, and safety requirements.

The radiation from ^{90}Sr is so intense that it must be encapsulated in a hot cell. This restricts the welding processes because the equipment must be operated and at times maintained in the hot cell.

The heat sources for the LCG [Low Cost Generator (7)] and SNAP-21 generators (8) are examples of GTA (gas tungsten-arc) and electron-beam welding, respectively. The LCG is a commercially available generator fueled with $^{90}SrTiO_3$ in a Hastelloy C container. The particular heat source described here contained 750 w(th) of fuel. The SNAP-21 generator is intended for undersea use and the 10 w(e) version is fueled with 200 w(th) of $^{90}SrTiO_3$. Again Hastelloy C is used as the container material.

Unlike strontium, curium is an alpha-emitter, and therefore helium pressure will build inside a sealed, curium-fueled capsule. Such pressure will require a high-strength container. Because of this and because operating temperatures are likely to be higher for curium-fueled generators, by virtue of their higher power density (Table 1), the refractory metals are the most promising encapsulating materials. But the feasibility of welding such capsules has not been demonstrated. For this reason a welding development program was begun.

Equipment

Because of the complications caused by filler wire, GTA fusion and electron-beam welding are used instead of GMA (gas-metal arc) or GTA welding with filler wire.

Figure 1 shows a typical GTA welding setup. The welder views the process through the cell window with a seven-power monocular and remotely operates the equipment in the cell with the master-slave manipulators. The program-controlled welding power supply is located outside the hot cell as shown. Programmed welding permits more reliable transfer of developed welding parameters to operation in the cell. Superalloy containers can be welded by the GTA process in the cell's normal air atmosphere with the very simple equipment shown in Fig. 2. A standard GTA torch is mounted over a rotating chuck with provisions for adjustment to accommodate various sized capsules. However, if a special atmosphere is required inside the capsule or if more reactive metals such as the refractory metals are being welded, a vacuum-purged inert-atmosphere chamber as shown in Fig. 3 is used. The chamber has windows in front and on top and an

auxiliary light in the side. The water-cooled electrode holder is adjustable and is mounted through the chamber wall. The chamber cover is opened by two pneumatic cylinders which lift it off its base to make the chuck accessible for positioning the capsule. The chamber can be evacuated and back-filled with an inert gas.

Modular 30-kv equipment is used for electron-beam welding. Since the equipment is modular the power supply and controls can be positioned outside the hot cell as is done with the GTA welding equipment. Only the welding chamber – with its electron-beam gun, rotating chuck and vacuum system – is placed in the cell. Figure 4 shows this equipment set up out of the cell for developmental welding. Figure 5 shows the chamber interior with a capsule in place for welding. A mirror mounted above the capsule to the left is used to help align the electron beam with the joint to be welded. Water-cooled electromagnetic focusing coils eliminate changes that could occur from coil heating.

Procedure

Strontium-Fueled Heat Sources

The encapsulation of strontium fuel forms has generally followed a five-step procedure:

1. welding development,
2. out-of-cell checkout,
3. in-cell checkout,
4. fueled capsule welding,
5. quality assurance capsule welding.

In step 1, welding development is done in the laboratory usually with short capsules having the proposed cap-to-capsule joint design. The capsules are preheated to more closely simulate a fueled capsule. This can be important since it has an effect on the weld penetration and bead contour. Metallographic examination is the primary method of determining the acceptability of welding conditions. A tentative, written welding procedure is the product of this step.

In step 2, preheated, full-sized capsules are welded to check the equipment and procedures for subsequent in-cell use. The welding equipment at this stage is the same equipment to be used in the cell, and any changes in equipment or procedure requires another full-sized capsule to be welded and examined.

In step 3, the welding equipment is transferred to the cells and tested. Again, a full-scale capsule is welded according to the written procedure and examined metallographically. If changes are found necessary, they are evaluated in another welding and examination cycle.

If a significant period of time elapses between the end of step 3 and welding the fueled capsule (step 4), another unfueled capsule is welded immediately before the fueled one. If not, the fueled capsule is welded next.

In step 5, an additional unfueled capsule is welded. This, together with the one welded immediately before the fueled capsule, is then sectioned and metallographically examined for weld quality and penetration.

This procedure is intended to give some assurance that the fueled capsule, welded under otherwise identical conditions, will have comparable weld characteristics. Obviously, this indirect inspection has shortcomings. It was recently augmented by direct ultrasonic inspection of the weld in the fueled capsule (9).

Refractory Alloy Weld Development

To demonstrate the feasibility of sealing refractory alloy capsules, weld specimens were fabricated from the molybdenum alloy TZM (Mo–0.5% Ti–0.08% Zr–0.02% C) for the GTA welding studies and from the tungsten alloy W–25% Re for the electron-beam studies. In anticipation of the heating effect of a curium fuel, weld development studies were made with a specimen preheat of 550 to 600°C. All GTA welding was performed in a high-purity argon atmosphere. Fluorescent penetrant, helium leak testing, and metallographic examination of welded specimens were used in the evaluation.

Results

Strontium-Fueled Heat Sources

Since ^{90}Sr does not produce helium by its decay, containers of these fuel compounds are not pressure vessels and therefore have not required full-penetration welds. Because of the low power density, correspondingly low application temperatures permit the use of superalloy containers. Thus, conventional GTA welds can be made in the normal cell air atmosphere with a protective inert gas supplied only through the torch. A weld was produced in this manner on an LCG heat source. This Hastelloy C capsule fueled with 750 w of $^{90}SrTiO_3$ is shown in Fig. 6 together with a schematic of the joint design and a cross section of the weld. A weld penetration requirement of 0.055 in. minimum was demonstrated on dummy capsules preheated to 250°C. The welding was done with the automatically programmed welding cycle shown in Fig. 6d.

Originally, the 200-w SNAP-21 heat source was designed for GTA welding (10). The weld penetration requirement was 0.100 in. minimum. However, as can be seen in Fig. 7, a weld penetration of only about 0.085 in. was the best that could be obtained. Later, an additional requirement made it necessary to avoid melting the top outside edge of the capsule because it was to serve as a reference mark for ultrasonic inspection of the weld. For these reasons GTA welding was discontinued in favor of electron-beam welding for this application. After a series of weld optimization studies, welds of the type shown in Fig. 8 were produced. Because of the greatly improved weld penetration capability, the capsule design was modified by eliminating the trepan and by thinning all members, to take advantage of the weld as a stress-carrying member and not just a seal. Developmental welding was done at a preheat of 300°C to simulate the fueled capsule welding conditions. Six such fueled capsules have been successfully welded.

Refractory Alloy Weld Development

The molybdenum alloy TZM was selected for the GTA welded capsule, and the tungsten alloy W–25% Re was selected for the electron-beam

welded capsule. Each alloy was considered to be the most weldable in the molybdenum and tungsten systems. Full-penetration welds were desired because fueled capsules would be helium pressure vessels.

A vent was necessary for the GTA welded capsules to relieve the pressure that would build in an enclosed capsule by the heat of welding. With no vent, the pressure would blow out the weld metal as the final seal was made. The design that evolved from the weld development program is presented in Fig. 9a together with a cross section of a weld. The small step between the cap and capsule wall (Fig. 9a) was necessary to center the cap, and the relieved area in the cap adjacent to the joint was necessary to eliminate the notch which tended to cause root cracking at the root of the weld. After several test welds, it was also obvious that when the material on the outside diameter of the cap was melted, it slumped to form a bulge around the capsule. To compensate for this, the cap diameter was reduced and the outer edge of the capsule was removed. The only unusual feature of making this weld was that it was important not to decrease the weld current too quickly. A fast initial decay was found to produce a large lump on the weld bead. This lump resulted from the highly agitated and very large weld puddle being allowed to solidify too quickly. Vents were sealed by plugging and GTA welding with a short weld cycle.

As with the GTA welded capsules, full-penetration welds were desired for the electron-beam welded tungsten alloy capsules. But, since welding would be performed in a vacuum, no vent was necessary. The much simpler joint design is shown in Fig. 9b.

One unusual facet about the welding of these capsules was that we found it necessary to defocus the electron beam. A sharply focused beam passed through the capsule wall and struck the opposite side of the capsule, causing it to crack. Despite the defocused beam, full-penetration welds could still be made. Slumping of the weld metal was also observed on these capsules, but it could be limited to 0.015 to 0.020 in., as shown in Fig. 9b.

The W–25% Re used on this portion of the program was extruded material derived from powder-product stock. As can be seen from Figs. 9b and 10a, there was severe fusion-line porosity in welds on this material. To ascertain whether this was the result of using powder-derived material, a cap was machined from arc-melted-and-extruded W–25% Re material and welded to a powder-derived sleeve. Figure 10b is a photomicrograph of this weld. It can be seen that the porosity was obtained only at the fusion line of the powder-derived sleeve. Thus, for an actual application, material fabricated from melted stock would be used.

Acknowledgments

The authors wish to acknowledge the assistance of J. D. Hudson and B. F. Early for the welding of capsules and G. M. Slaughter and R. J. Beaver for their technical guidance.

References

1. Strontium-90 Fueled Thermoelectric Generator Power Source for Five-Watt U.S. Coast Guard Light Buoy – Final Report, MND-P-2720, February 2, 1962, p. 27.

2. J. H. Gillette, Review of Radioisotopes Program, 1964, ORNL-3802, August 1964, p. 30.

3. J. H. Gillette, Review of Radioisotopes Program, 1965, ORNL-4013, August 1965, pp. 16, 17.

4. J. H. Gillette, Review of Radioisotopes Program, 1966, ORNL-4155, August 1967, pp. 33, 34.

5. R. G. Donnelly, Metals and Ceramics Division Annual Progress Report for Period Ending June 30, 1966, ORNL-3970, October 1966, pp. 225–227.

6. R. G. Donnelly, Metals and Ceramics Division Annual Progress Report for Period Ending June 30, 1967, ORNL-4170, November 1967, pp. 229, 230.

7. Trademark of the Martin-Marietta Corporation.

8. Prime contractor, 3M Company.

9. R. W. Steffens, H. N. Pedersen, and F. M. Coffman, Nondestructive Testing of Isotope Containment Capsules Phase I SNAP-21 and SNAP-23, BNWL-528, January 1968.

10. SNAP-21 Program, Phase II Quarterly Progress Rept. No. 3, MMM 3691-17, May 1967, pp. 2–10.

Table 1. Properties of Selected Strontium and Curium Fuel Compounds[a]

Fuel Compound	Radiation	Half Life	Power Density (w/cm^3)
$^{90}SrTiO_3$	β, γ	28 years	0.85
^{90}SrO	β, γ	28 years	1.4
$^{244}Cm_2O_3$	α, n, γ	18.4 years	26.4
$^{242}Cm_2O_3$	α, n, γ	163 days	1170

[a]E. D. Arnold, Handbook of Shielding Requirements and Radiation Characteristics of Isotopic Power Sources for Terrestrial, Marine, and Space Applications, ORNL-3576, April 1964.

Fig. 1. Setup at cell window for gas tungsten-arc welding.

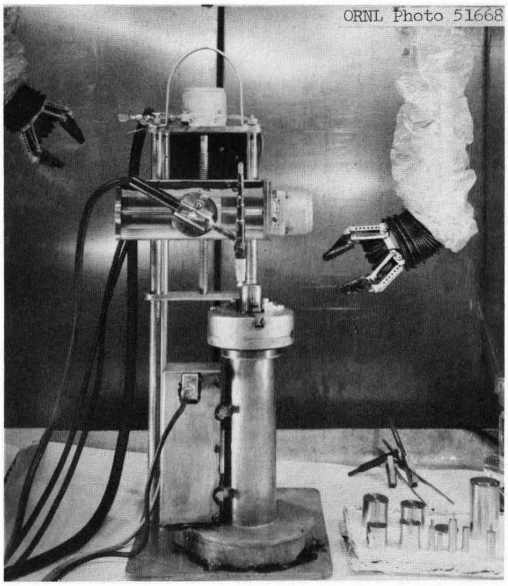

Fig. 2. In-cell, open-atmosphere equipment for gas tungsten-arc welding.

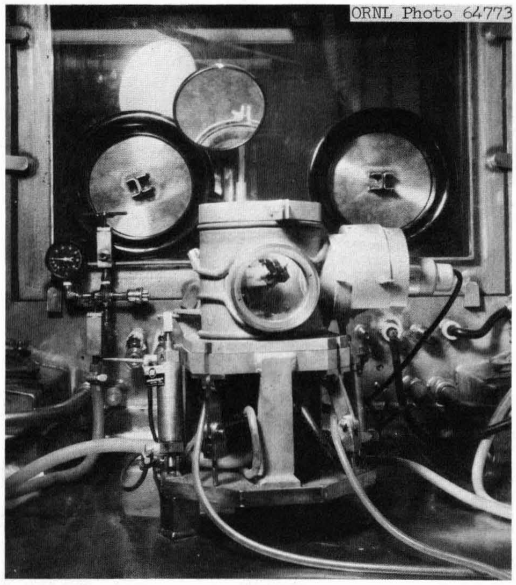

Fig. 3. In-cell, inert-atmosphere chamber for gas tungsten-arc welding.

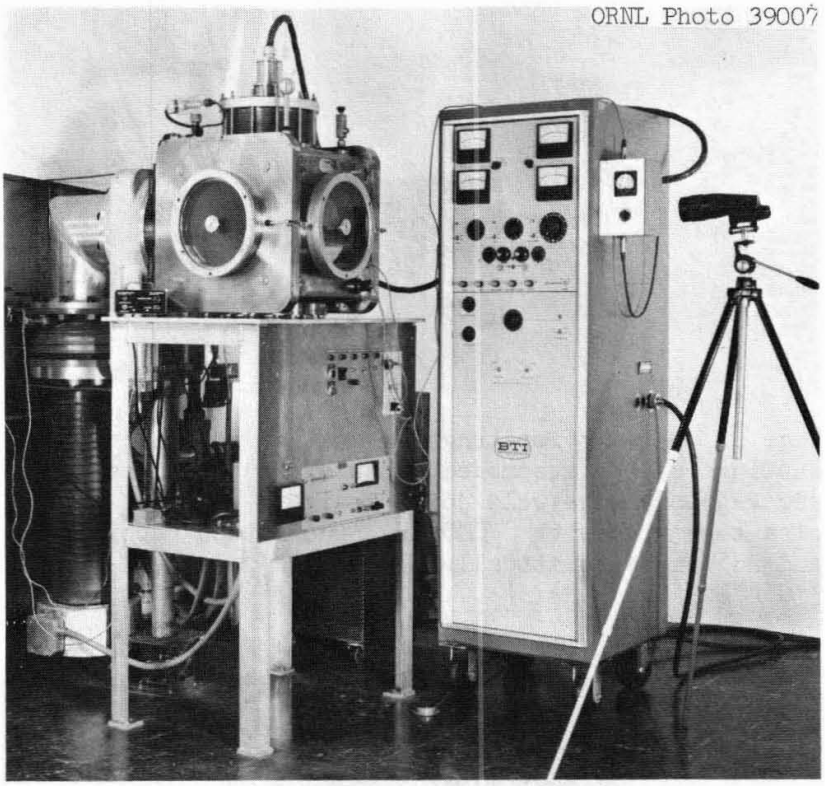

Fig. 4. Electron-beam equipment set up for developmental welding.

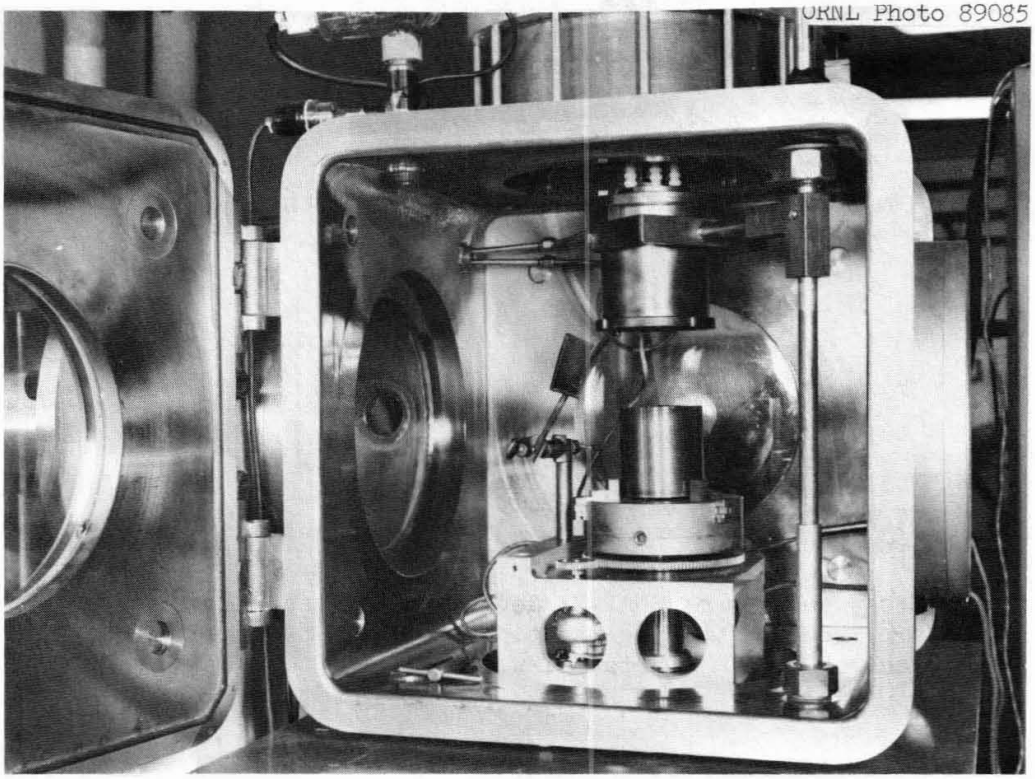

Fig. 5. Interior of electron-beam welding chamber with capsule ready for welding.

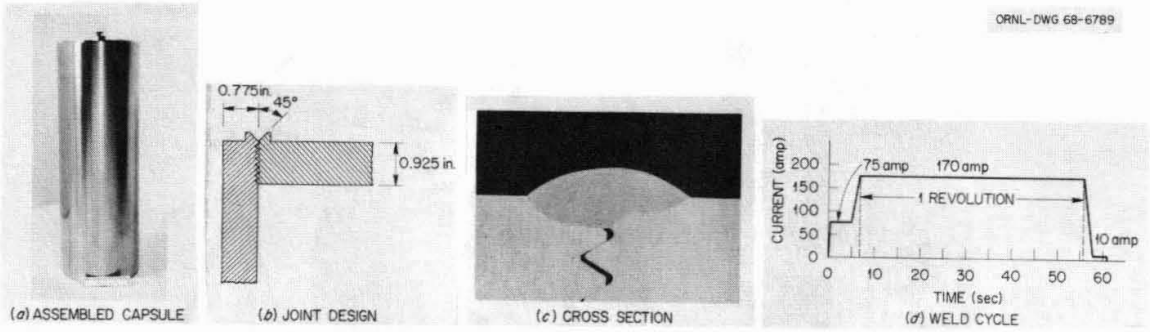

Fig. 6. Details for tungsten-arc welded LCG capsules showing (a) the assembled capsule, (b) threaded cap and V-groove edge weld joint design, (c) cross section of a test weld with 0.080-in. penetration (approx 7×), and (d) the automatically programmed weld cycle used.

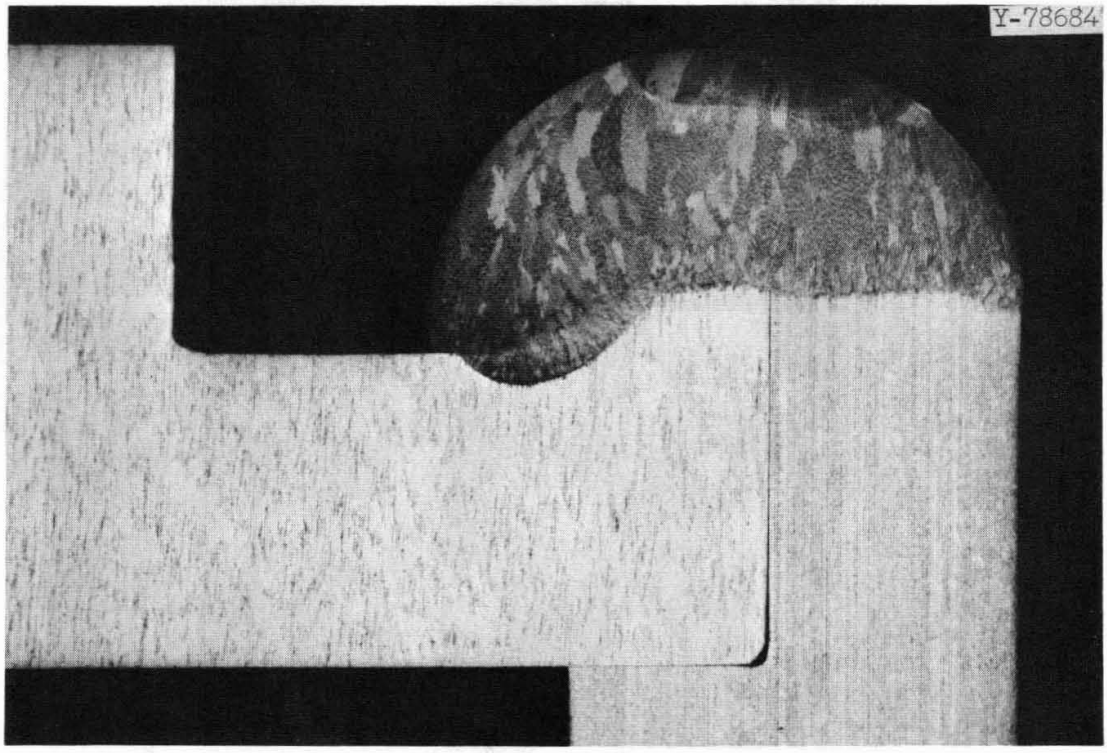

Fig. 7. Cross section of SNAP-21 developmental capsule welded by the gas tungsten-arc process; weld penetration, 0.085 in.; etchant: 38 HCl, 12 lactic acid, 10 HNO_3 (Parts); 12×.

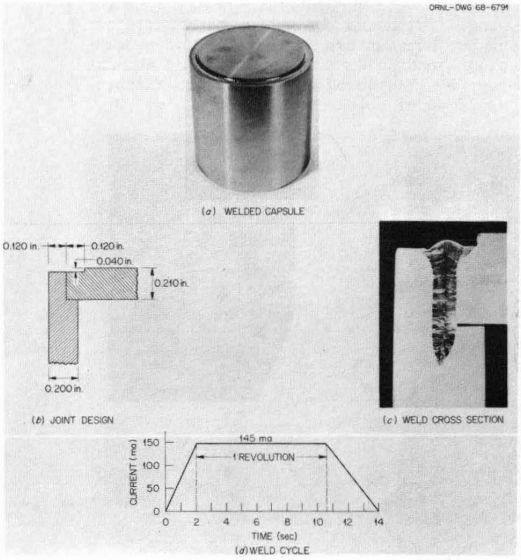

Fig. 8. Details for electron-beam welded SNAP-21 capsules showing (a) the welded capsule, (b) the butt-type joint design used, (c) a cross section of a developmental weld with penetration the full 0.170-in. depth of the cap (approx 7x), and (d) the automatically programmed weld cycle used.

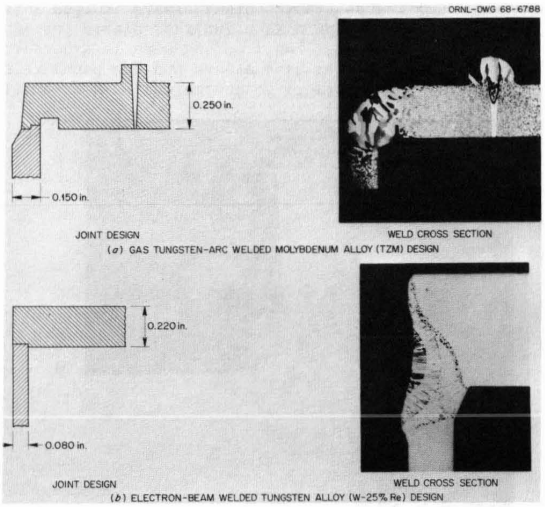

Fig. 9. Joint designs and welding results for refractory metal capsules. (a) cross section approximately 3x and (b) cross section approximately 6x.

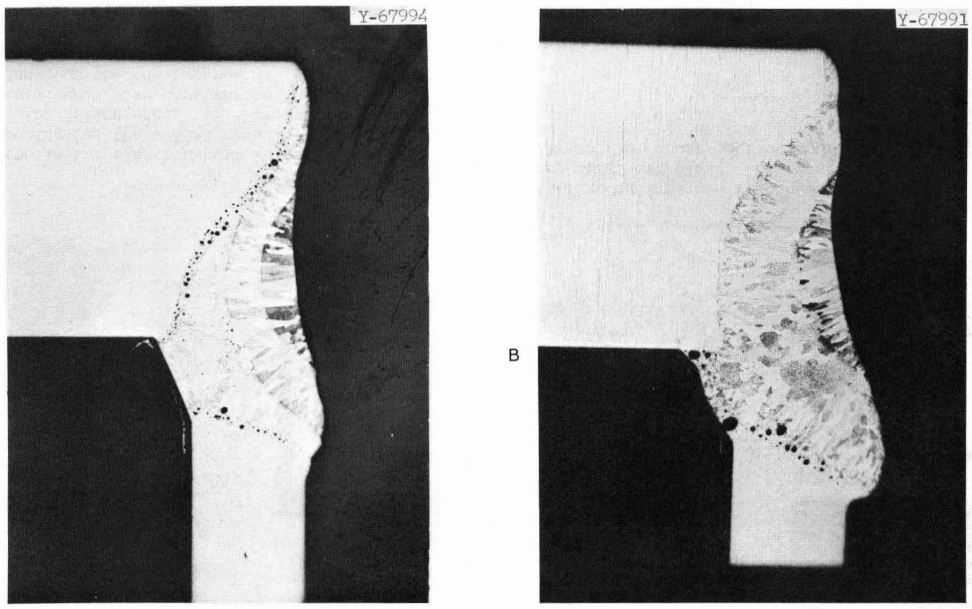

Fig. 10. Electron-beam welds in W–25% Re specimens showing the effect of fabrication history on fusion-line porosity. (a) Weld with extruded cap and sleeve both fabricated by the powder-metallurgy technique. Note porosity only at each fusion line. (b) Weld with cap fabricated by arc casting and extruding, and sleeve fabricated by powder-metallurgy technique and extruding. Note porosity only at sleeve fusion line. Approx 16x.

ULTRASONIC TEST SUPPORT FOR CONTAINER INTEGRITY ASSURANCE

R. W. Steffens

Abstract

Ultrasonic nondestructive testing techniques, when properly integrated into the capsule development program, can be used to establish the container integrity of fueled isotope capsules. The ability of ultrasound to detect close fitting cracks, and to obtain complete inspection of the container volume, advantageously supplements the information normally acquired through radiographic, dye penetrant, and metallographic analysis.

Ultrasonic test support during an isotope capsule development and fabrication program is classified into four phases with each phase having specific quality control and ultrasonic test development objectives.

The remote ultrasonic verification of the integrity of fueled SNAP-21 capsules illustrates the effectiveness of applying a cooperative approach between capsule fabrication and nondestructive testing personnel to assure capsule certification.

R. W. Steffens is an engineer with the Pacific Northwest Laboratory, Battelle Memorial Institute, Richland, Washington.

Introduction

Ultrasonic nondestructive testing (NDT) advantageously supplements the quality control tools of radiography and metallography and enhances the ability to establish the integrity of the isotope container components and closure welds. The use of ultrasound to detect close fitting cracks and to obtain complete maps of container material parameters has been particularly useful in the support of closure weld development and integrity certification.

Integration of ultrasonic testing into the design and development phases of capsule fabrication provides two quality assurance functions. First, complete ultrasonic scanning of weld volumes for weld parameter variations facilitates selective use of radiography and metallography in possible problem areas. Thus, the probability of detecting and defining undesirable weld characteristics during the development phase is enhanced, and optimum welding and testing techniques can be developed. Secondly, the correlation obtained between nondestructive and destructive data on developmental capsules is necessary to develop confidence in the ability to nondestructively establish the integrity of a fueled capsule.

General methods and philosophies of ultrasonic test development and verification have evolved which provide economical and high confidence use of ultrasound as a capsule fabrication quality control tool. The ultrasonic support is conveniently split into the four following phases:

Phase 1: Preassembled Component Inspection
Phase 2: Developmental Closure Weld Inspection
Phase 3: Ultrasonic Test Standardization and Calibration
Phase 4: Establishment of Fueled Container Integrity

The first three phases provide quality control and design feedback information to the capsule fabrication organization in addition to the ultrasonic test development considerations. Phase 4, the establishment of fueled container integrity, is the implementation of the test techniques developed in phases 2 and 3. The following discussion, through examples of recent activities in this area, illustrates the ultrasonic test support sequence and test verification techniques.

Discussion

Phase 1 - Preassembled Component Inspection

Efficient inspection of the components is obtained when ultrasonic, radiographic, dye penetrant, and metallographic analyses are used in a complementary manner. Specific objectives of the ultrasonic inspection in this phase are to supplement the radiographic and dye penetrant test by the detection of intersurface defects and tightly closed surface cracks.

The supplementary use of ultrasonics and radiography is illustrated through the results obtained during the inspection of vendor fabricated

seam welds in the rhenium cylinders procured for a promethium containment program. Two types of inner-surface weld defects, insufficient penetration, and cracks, which are ultrasonically detected in the seam welds, are shown in Figure 1. Radiographic analysis of the seam weld detected weld porosity, and, thus, consideration of both the ultrasonic and radiographic data was necessary for selecting best cylinders.

Of particular note were the severe laminar defects shown in Figure 2 which were detected in a 16 ft. long, Hastelloy-C tube initially procured for the outer clad of the SNAP-23 development capsules. Removal of the sample from the pipe caused the separation of the laminations. The high incidence of the laminations in this pipe necessitated replacement of the pipe by the vendor.

Lack of penetration and/or inner-surface cracks were ultrasonically indicated in the seam weld of a 10 ft. long section of Hastelloy-C tubing procured for the inner clad on developmental SNAP-23 capsules. Subsequent radiographic analysis of the weld verified the ultrasonic indications and, additionally, permitted differentiation between the two defect types.

Severe cracking, some entirely through the wall, was ultrasonically detected in the Tungsten-25% rhenium cylindrical cans procured for a promethium capsule developmental program. The capsule diagram in Figure 3 shows locations of the cracks. The axial cracks were detected by both ultrasonics and dye penetrant techniques and appeared to radiate from chuck marks. Galling of the surfaces during the machining operation masked the lip and circumferential defects, and they were not detected during the dye penetrant analysis. Fourteen out of 40 capsules contained defects.

The above examples illustrate the supplementary and complementary nature of different NDT methods and this interrelationship is maintained throughout the following test development phases.

Phase 2 - Developmental Closure Weld Inspection

Assurance of fueled capsule closure weld testability is acquired through test development performed on developmental welds. Quality control objectives of the ultrasonic inspection are to provide feedback information to weld development engineers concerning (a) areas where possible cracks or voids exist, (b) variations in, and extent of, weld penetration, and (c) suggestions for weld joint design changes, if necessary, to enhance weld compatability with ultrasonic testing.

The test development objective in this phase is to develop ultrasonic techniques which can be calibrated, standardized, and then reliably implemented for the inspection of a fueled capsule.

The general compatibility of the capsule design with application of ultrasonic techniques can be theoretically evaluated by the ultrasonic engineer by considering such factors as wall thickness, surface finish,

and weld joint configuration. Thus, consideration of weld testability at the initial design stage can decrease the cost of test development.

Ultrasonic indications of variances in weld properties are generally verified by radiographic and/or metallographic analysis. When close communication is maintained between the ultrasonic, radiographic, and metallographic personnel, the weld development personnel are provided with the most economic and thorough definition of the weld characteristics.

The weld closures discussed in the following examples were selected to illustrate the use of ultrasonics to define weld characteristics during the weld development phase. These examples were obtained during the early weld design stages of the SNAP-21 and AMSA (Advanced Manned Strategic Aircraft) program and they should not be construed as containing any indication whatsoever of ORNL's (Oak Ridge National Laboratory) or PNL's (Pacific Northwest Laboratory) weld design or weld performance capabilities.

Through close interlaboratory cooperation between the 3M Company, ORNL and PNL, the weld parameters of the early design, SNAP-21 developmental TIG (Tungsten Inert Gas) welds were ultrasonically evaluated and undesirable weld characteristics were found to exist. Figure 4 shows two detrimental weld characteristics--weld root cracks and lack of weld penetration. Through extensive metallographic evaluation of the ultrasonic defect indications, the weld root cracks were found to exist primarily in the inner and outer welds of the three pass weld. Excessive melt down of the outer corner was the prime cause of insufficient penetration. Due to the melt down of the outer corner, highly refined and complicated ultrasonic techniques were required to monitor the weld parameters on these developmental welds. Considering these undesirable weld characteristics and the difficult ultrasonic test procedures required to establish the integrity, the weld joint was modified and the TIG welding techniques were reevaluated.

Two other developmental welds were subsequently evaluated, a second design TIG weld and a first design electron beam (e. b.) weld. Although the redesigned TIG weld showed a significant reduction of weld root cracks, gross variances of weld penetration at the seam weld in the cylinder wall produced an area of insufficient penetration as shown in Figure 5. The penetration was maximum in the area of the seam weld and minimum to one side of the seam weld. Melt down of the outer corner continued to be a problem in the implementation of the ultrasonic tests. Additionally, variations in the amplitude of the ultrasonic signals from the unwelded joint were encountered. Metallographic analysis in the areas of reduced signal amplitude showed tightly closed joints at the weld root and at intermediate points along the joint. These variances in signal amplitude further complicated the ultrasonic testing and calibration procedure.

The photomicrographs in Figure 6 show the ultrasonically detected, metallographically verified, characteristics of the first e. b.

developmental welds. Although the .200 inch to .300 inch penetration far exceeded the .100 inch required, three undesirable characteristics--porosity, laminar voids and misaligned weld volumes were observed. The majority of the porosity and laminar defects were located in the weld root area and thus did not undermine the integrity of the weld. The end-caps of the sample welds were removed to enhance the radiographic analysis of the weld, and porosity was readily detected with the radiographic techniques. Comparison between the radiographic and ultrasonic results showed porosity to account for approximately 30% of the defects. Laminar defects accounted for the remaining 70%.

The laminar defects, porosity and unwelded joints in the e. b. welds, were optimally oriented for detection with an ultrasonic technique which could be reliably performed remotely. Due to their testability and desirable penetration, the e. b. welds were selected over the TIG welds for the fueled SNAP-21 capsules. Subsequent weld technique development and ultrasonic test optimization resulted in the establishment of high integrity of the closure weld on the fueled SNAP-21 capsules.

AMSA Weld Development Samples. The developmental weld characteristics of the e. b. closure welds in the L-605 material of the AMSA capsule closely resembled the characteristics of the SNAP-21 e. b. welds as shown in Figure 7. Note the presence of porosity and intervolume cracks. Insufficient penetration due to a misaligned weld volume was also detected. Although the weld characteristics paralleled those of the SNAP-21 welds, development of ultrasonic inspection techniques were most difficult due to the circumferential location of the weld, and two different manually performed ultrasonic tests were required to establish weld integrity.

The results of the SNAP-21 and AMSA test development programs illustrate several pertinent points. As demonstrated in the comparison of ultrasonic signals between the first and second developmental TIG welds in the SNAP-21 program, changes in weld joint design and/or the welding technique can significantly change the character of the ultrasonic signals. Thus, reevaluation of the test method is recommended when weld design parameters are changed. The melt down of the outer corners of the SNAP-21 TIG welds prevented automatic scanning of the weld parameters and the refined, manual test procedures would have been impractical for remotely measuring the penetration of a fueled capsule. The melt down of the outer corner of a peripheral weld generally complicates the test methods and should be avoided if remote and/or automatic inspection of the weld is desired.

The peripheral location of the SNAP-21 e. b. welds facilitated the development of test methods which could be performed both remotely and automatically. In comparison, the circumferentially located AMSA e. b. welds were not conducive to remote or automatic inspection even though the undesirable characteristics to be detected were the same as the SNAP-21 welds. Thus, the test requirements are a function of the location of the weld on the capsule.

The weld root cracks in the TIG, and laminar type cracks in the e. b. weld, were not detectable by radiographic techniques. Ultrasonic results could not differentiate between the porosity and cracks in the e. b. weld. Thus, both ultrasonics and radiography were necessary to completely define the undesirable weld characteristics.

Phase 3 - Ultrasonic Test Standardization and Calibration

Development of realistic weld defect standards for calibration of ultrasonic techniques and equipment are necessary if high confidence is to be obtained in the ultrasonic establishment of the weld integrity on fueled capsules. The standard must be representative of undesirable weld parameters characterized during the development period and must permit interpretation of the ultrasonic data in terms of the weld specifications. Most effective standardization of the ultrasonic test is obtained when the fabrication and nondestructive testing personnel jointly design the standard. The confidence level of the ultrasonic test techniques should be established not only by the consideration of the test performance on the standard, but also by the test performance on actual developmental weld flaws.

The test standard shown in Figure 8 was jointly developed by ORNL, the 3M Company, and PNL to assist in the calibration of the ultrasonic weld evaluation on fueled SNAP-21 capsules. Test standardization was based on the ultrasonic reflections from the bottoms of eight radially orientated drill holes. The standard cylinder was machined to the same tolerances as the actual SNAP-21 capsule clad and out of the same Hastelloy-C bar stock. The holes were machined to the average radial depth of a typical weld volume. The holes ranged in diameter from .015 inches to .070 inches as shown in Figure 9. The ultrasonic indications are shown in the graph. Seven holes, located in a circumferential plane, provided the basic standardization. The eighth hole, 0.015" dia., was located within 0.005 inch of the top and was used to evaluate the ultrasonic test in that area. The top drill hole was detectable with a slight modification of the ultrasonic test incident angle. Ultrasonic defect indications were correlated to the standard by noting the number of circumferential passes during which the indication was observed.

The X-Y recordings shown in Figure 9 illustrate a read out technique which was developed to display small, randomly located defect indications such as those observed in the SNAP-21 e. b. welds. Each line spacing represents .006 inch of axial transducer travel, with one line representing a complete circumferential scan. Thus a map of the weld area is obtained.

The X-Y recording shown in Figure 10 facilitates data interpretation when unwelded portions of the weld joint are being monitored. The line spacing and length represents the axial and circumferential positions, respectively. The recorder pen is actuated only when a signal indicating the presence of the joint is detected.

As can be noted by comparing the above examples, the read out technique depends upon the parameter that is being monitored. When these recordings are calibrated by the use of a standard, they provide a convenient data recording method.

Phase 4 - Inspection of Fueled Capsules

Three factors to be considered before applying the ultrasonic tests developed in Phases 1, 2, and 3 are: (a) radiation protection for test operators, (b) ultrasonic test equipment, and (c) thermal protection of the ultrasonic transducer.

Test facilities which provide the necessary operator radiation protection can vary from the remote, "hot cell" facilities, for inspection of strontium fueled capsules, to the "controlled area" facilities, for promethium and plutonium capsules.

The radiological, thermal, and geometrical characteristics are unique to each individual capsule, and the ultrasonic tests and equipment required to inspect the capsules are unique to that particular capsule. The equipment requirements normally increase as the isolation between the test operator and test tank increases. Thus, the ultrasonic test station developed for the inspection of the strontium fueled capsules was fully automated; whereas, standard laboratory equipment was used for the promethium capsules.

Thermal output of fueled capsules tested to date has ranged from 500 to 1500 watts. In general, the water bath temperature should be maintained below 80°F, and a constant temperature water flow should be directed on the face of the ultrasonic transducer. Precooling of the fueled capsule is recommended to prevent adding extra heat into the ultrasonic test water.

Summary

In summary, the successful ultrasonic inspection of fueled capsules is usually the result of an ultrasonic test program performed in support of the capsule development program. Integration of ultrasonic test support into the development program has a dual purpose. First, the preassembled components and development welds are inspected to assure integrity before the capsules are fueled. Secondly, certification of the ultrasonic test techniques during the development period insures the testability of a fueled capsule.

To obtain the best results from sample weld evaluation, ultrasonic, radiographic, and metallographic inspection should be closely coordinated. In particular, ultrasonic and radiographic results often supplement each other to provide a more complete inspection.

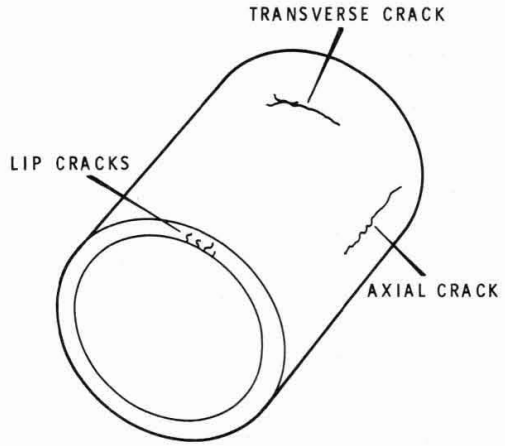

Fig. 1. Seam weld defects in rhenium cylinder

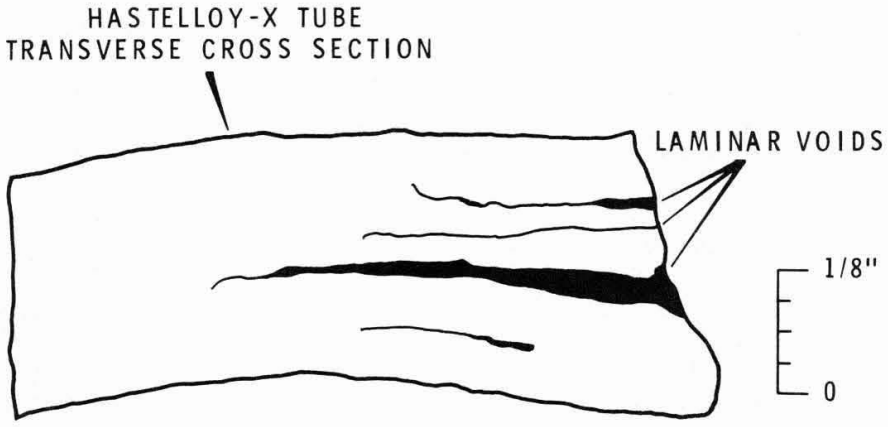

Fig. 2. Laminar voids in Hastelloy-X tubing

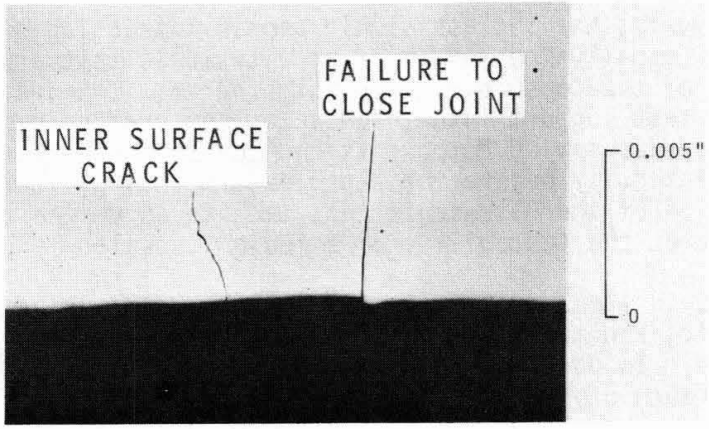

Fig. 3. Cracks in Tungsten-25% Rhenium cylindrical cans

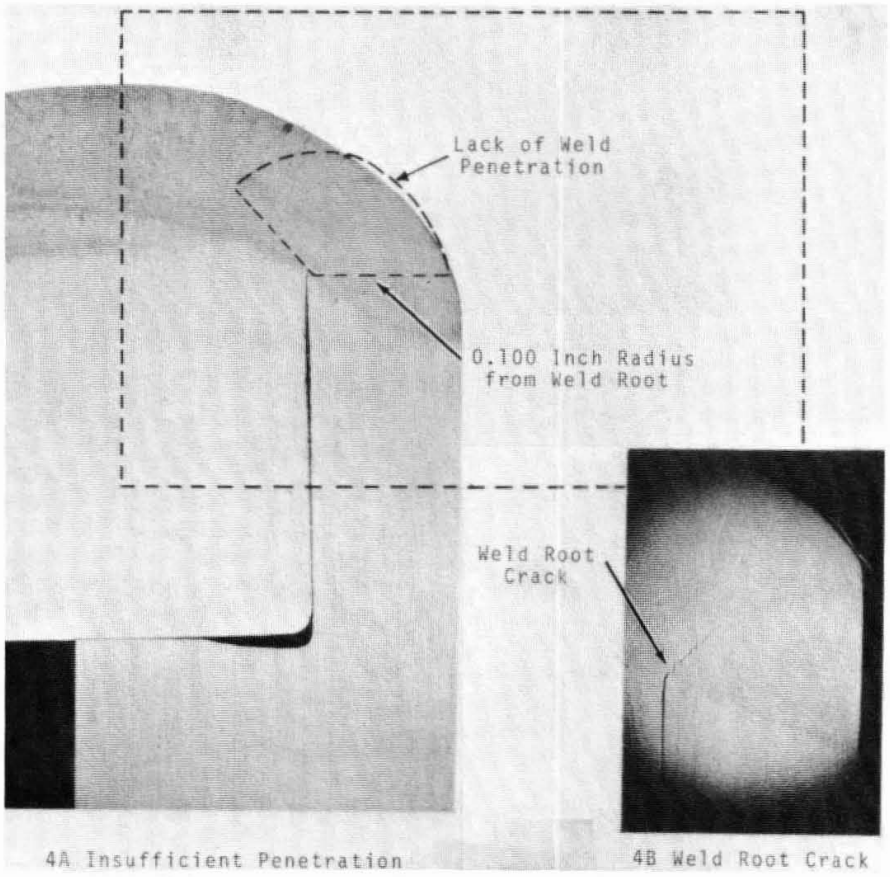

Fig. 4. Undesirable parameters in Phase I SNAP-21 welds

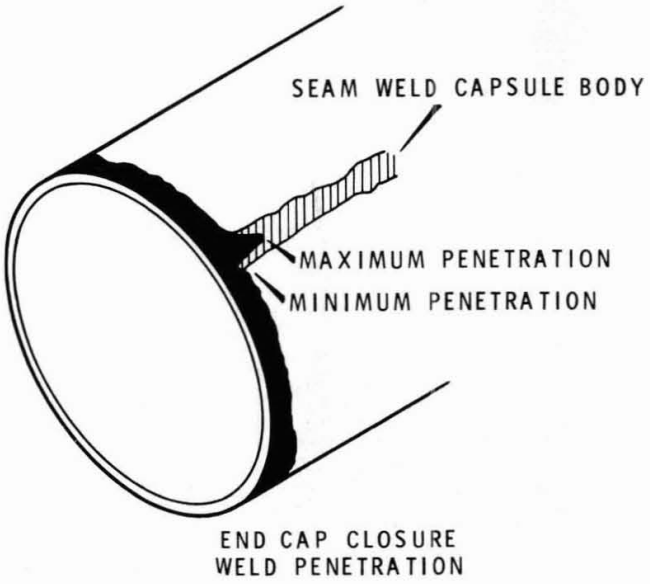

Fig. 5. Extreme closure weld penetration changes in seam weld area on Phase II SNAP-21 capsule

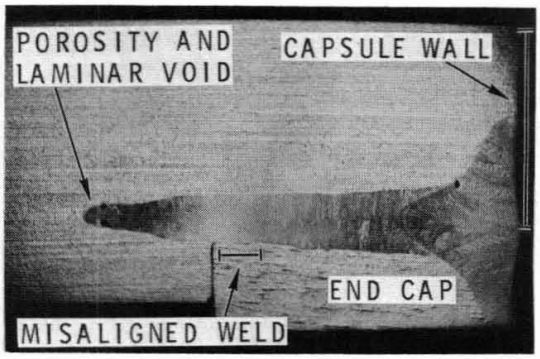

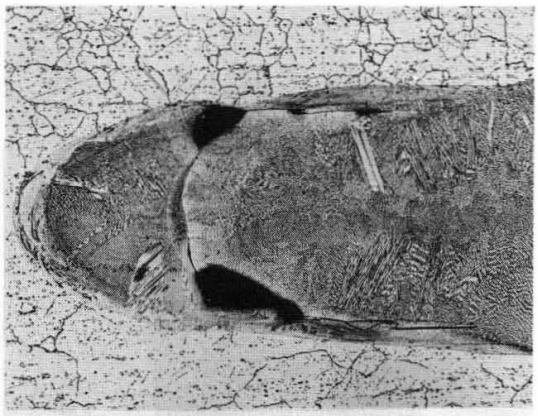

Blowup of Porosity and Laminar Void

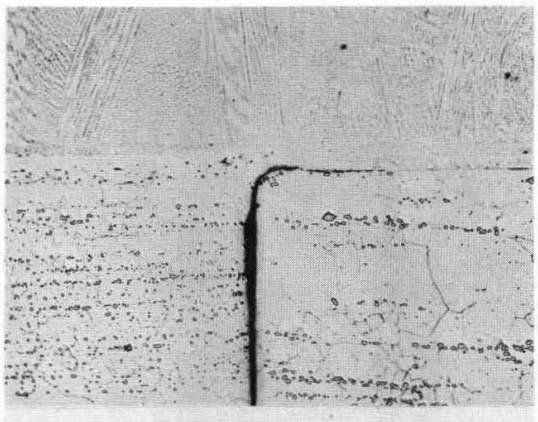

Blowup of Misaligned Weld

Fig. 6. Undesirable characteristics in SNAP-21 developmental e. b. weld

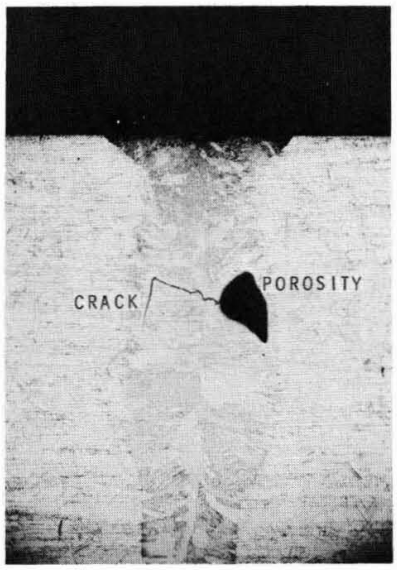

Fig. 7. Undesirable weld characteristic in AMSA e. b. weld

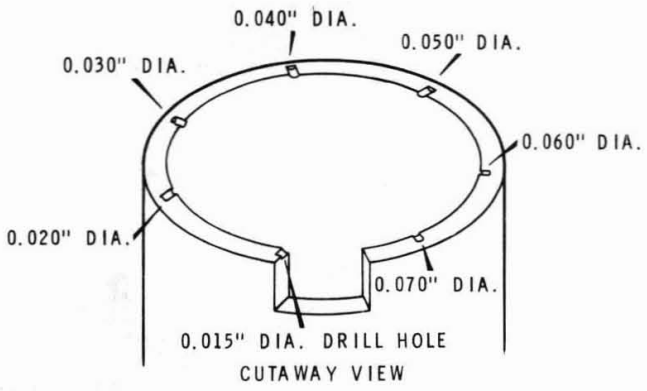

Fig. 8. SNAP-21 ultrasonic test standard flat bottom drill holes

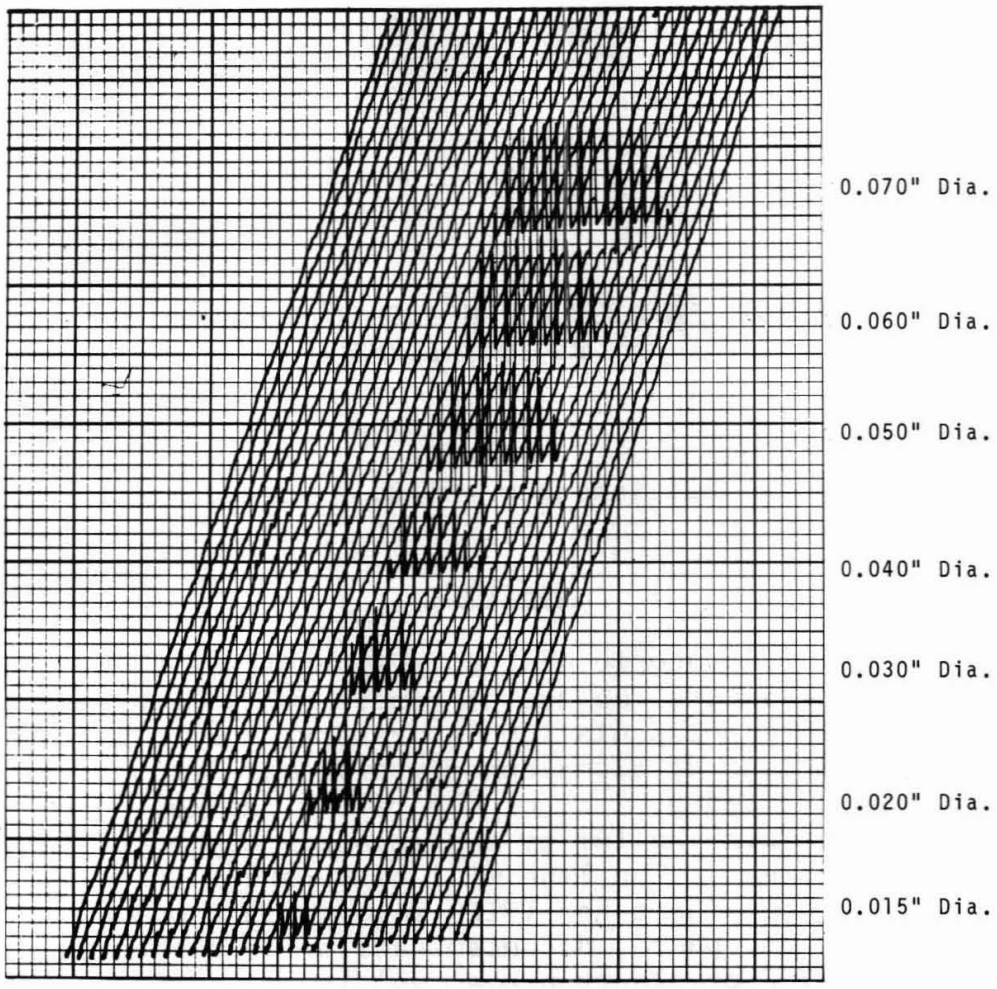

Fig. 9. X-Y Calibration recording of SNAP-21 standard

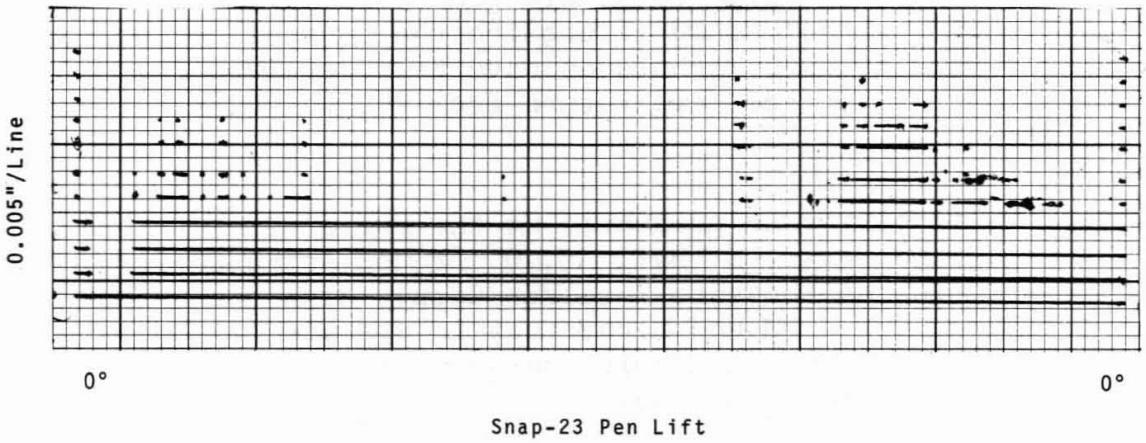

Fig.10. X-Y recording of unwelded joint in SNAP-23 developmental weld

REMOTE ENCAPSULATION TECHNIQUES FOR ^{210}Po FUEL FORMS

R. J. Baltisberger and C. O. Brewer

Abstract

Forecasted ^{210}Po isotopic heat source requirements are large enough to necessitate the use of remote manipulator equipped facilities. The encapsulation laboratory under construction consists of a line of alpha boxes approximately 60 ft in length and shielded by 2 ft of concrete. The cell area is to be supplied with helium by two separate cryogenic purification systems. The line will have capabilities for loading, tungsten-inert gas (TIG) welding in a polonium contaminated atmosphere, decontamination, leak checking, assaying and TIG or electron beam welding in uncontaminated boxes. The facility consists of boxes rather than a single cell, so that surface radioactivity can be controlled and progressively lowered as the sources move through the line to completion. A prime consideration in the encapsulation of polonium is the method of cooling the sources during the various operations. Techniques have been developed for maintaining a surface temperature from 200 to 400°F.

R. J. Baltisberger is presently at the University of North Dakota, Grand Forks, N. Dak. C. O. Brewer is Supervisor of Encapsulation at Monsanto Research Corp., Mound Laboratory, Miamisburg, Ohio. Mound Laboratory is operated by Monsanto Research Corp. for the Atomic Energy Commission under Contract No. AT-33-1-GEN-53.

Introduction

Mound Laboratory has produced ^{210}Po heat sources for a number of years. The hazardous nature of ^{210}Po makes it imperative that the sources be carefully designed and produced under strict safety regulations. The size of the source is a critical factor in determining the requirements for a safe operation. The earliest ^{210}Po source, SNAP-3, which was fabricated in late 1958, produced 2.5 W of electrical power (1). In 1964 the Poodle program required the encapsulation of approximately 300 W (thermal power) of ^{210}Po in a thruster test application. Presently a compatibility testing program is under way at Mound in which 1-5 W (thermal) of ^{210}Po is sealed in capsules. The quantities of radiation emitted from the above described sources permit operation in inert atmosphere gloveboxes without heavy shielding, other than shadow shielding. Anticipated requirements for larger heat sources, which will produce 400-500 W (electrical), or 25,000 W (thermal) of ^{210}Po, will require fabrication in remotely operated hot cells.

General Procedure

Polonium-210 heat sources consist of four basic elements: the fuel, a liner, a strength member and an oxidation barrier if a refractory metal strength member is used (Fig. 1). The preparation of the fuel is described in a separate paper by Kershner (2). The liner is fabricated of refractory metal, which contains the ^{210}Po fuel so that an uncontaminated weld can be made on the strength member; ^{210}Po contamination in the weld zone of the strength member causes cracking of the weld. This effect is eliminated by a primary encapsulation in a liner made of material easy to weld in the presence of ^{210}Po. The primary liner is decontaminated to a level between 10^4 and 10^6 counts/min. At this level of surface contamination the strength member weld can be made. The strength member is fabricated from an alloy giving the source the necessary strength to withstand the pressure buildup due to temperature and helium release of the ^{210}Po. An oxidation barrier protects the refractory metal parts from external attack.

Cell Design

The overall layout of the ^{210}Po encapsulation facility at Mound Laboratory is presented in Fig. 2. The facility is not

complete at this time, but it is under construction and will be ready for operation early in 1969. In addition to the facility there is a small cell for loading individual heat source capsules into the final fuel package. In one of our programs there will be a number of individual sources loaded and sealed in Boxes 1 through 9. The completed capsules will be stored and assembled into a fuel block in the special cell. The entire facility consists of alpha boxes constructed behind 24 in. of concrete shielding and operated by manipulators. The use of boxes allows a progressive lowering and control of the surface activity as the fabrication of a source is completed. Front-loading master slave manipulators are used in the facility.

Glove ports are available for repair work only from the rear of the cell line. The rear is shielded to 25 mrem/hr with steel doors which allow access to the glove ports. The line is designed to handle up to 1500 W of ^{210}Po per source. These sources must be removed from a box if hand repair is to be done. Access pass boxes are located at four points, two on the rear and one at either end of the line.

Two independent inert atmosphere systems are used for this facility. The helium purification systems will remove O_2, N_2 and H_2O cryogenically. One system will operate the first two boxes, which will be highly contaminated. The second system will furnish helium to the boxes for the second and third welds and for the special fuel block loading cell.

The facility is designed so that weld closures can be made at three different contamination levels. A tungsten-inert gas (TIG) weld can be made at any one of the three levels: $>10^6$ counts/min in Box 2, 10^3-10^4 counts/min in Box 5, and <10 counts/min in Box 9. Boxes 3 and 7 are decontamination areas which reduce the capsules to the necessary levels before transportation to the next closure step. Decontamination from a high level to a range of 10^4 - 10^5 counts/min is achieved by soaking with a basic permanganate solution, then ultrasonic cleaning with oxalic acid solution, in Box 3. In Box 7 oxalic acid solution is used to decontaminate to less than 10 counts/min. Leak checks of the welds are made in Boxes 4 and 8. Only the leak check chamber is located in the line. Helium leak check equipment is connected externally to the line. In addition to the TIG welding equipment, Box 6 is available for electron beam welding. The electron beam welders give the line the capability of welding the strength member either by EB or by TIG techniques.

Fig. 3 presents an outline of the major fabrication steps in each area of the facility. The final steps in fuel fabrication are completed in Box 2 followed by a gamma assay to

determine if the fuel content is correct. A rough neutron count is made on each source. A value of <200 n/Ci/sec is required for the fuel. Details of the fuel fabrication are presented in the paper by Kershner(2).

Temperature control on polonium heat sources is of prime importance. The heat flux of these sources is between 30 and 50 W/in.^{2} of capsule surface. Without external cooling the sources can rise to temperatures exceeding 300°C, which can do considerable oxidation damage to the refractory metal capsules. Two types of cooling are used. Segmented chill blocks are used in the weld fixture to reduce the surface temperature to approximately 100°C. The block can also be used to chill the sources under vacuum for the electron beam welding and leak checking. A second block of solid aluminum can be used to transport the capsules from one work station to another. The aluminum has a heat capacity adequate for a 2-min transport time. The aluminum block is chilled in a clam shell block, used as a storage block.

Windows on the box line are filled with an aqueous zinc bromide solution; the window thickness is 24 in. A typical cell cross section is shown in Fig. 4. The boxes are constructed of 304 stainless steel and are 42 in. in depth. The height of the boxes is 5 ft. to make room for the manipulators. The lengths of the boxes vary with the function being performed. The total length of the facility is approximately 60 ft.

Conclusion

The encapsulation facility was built as a development laboratory for a number of various sizes of heat sources. For this reason the line has few permanent fixtures which remain in the facility from one project to another. The experience at Mound Laboratory has been that each source project has capsules of a wide variety of shapes, sizes and welding configurations. The final thermoelectric generator packages are quite different from program to program, so the heat sources are designed to fit the size requirements of the package. This means with each new development program internal fixtures are replaced or modified.

References

1. R. T. Carpenter, U. S. Atomic Energy Commission Isotopic Power Applications, Large Scale Production and Application of Radioisotopes, USAEC Report DP-1066, du Pont de Nemours & Co., Savannah River Laboratory, Aiken, South Carolina, 1967.

2. C. J. Kershner, Properties and Fabrication of Polonium Fuel Forms, Nuclear Metallurgy Symposium on Materials for Radioisotope Heat Sources, October 2-4, 1968.

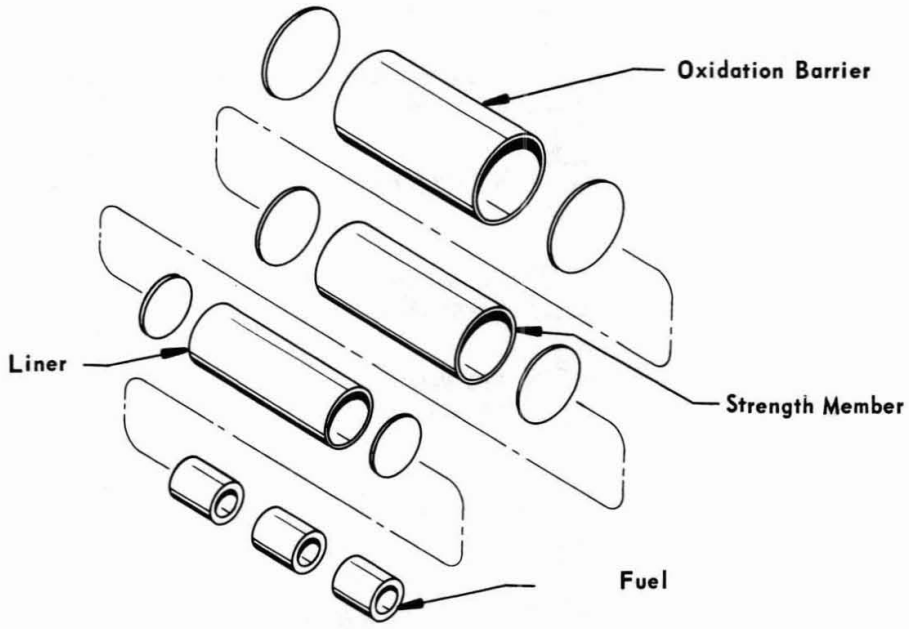

Fig. 1. Polonium-210 heat source members

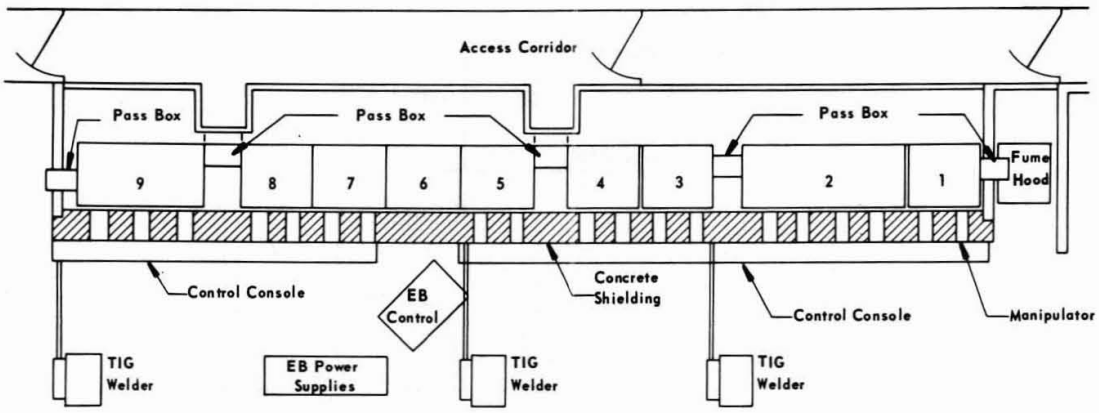

Fig. 2. Facility layout

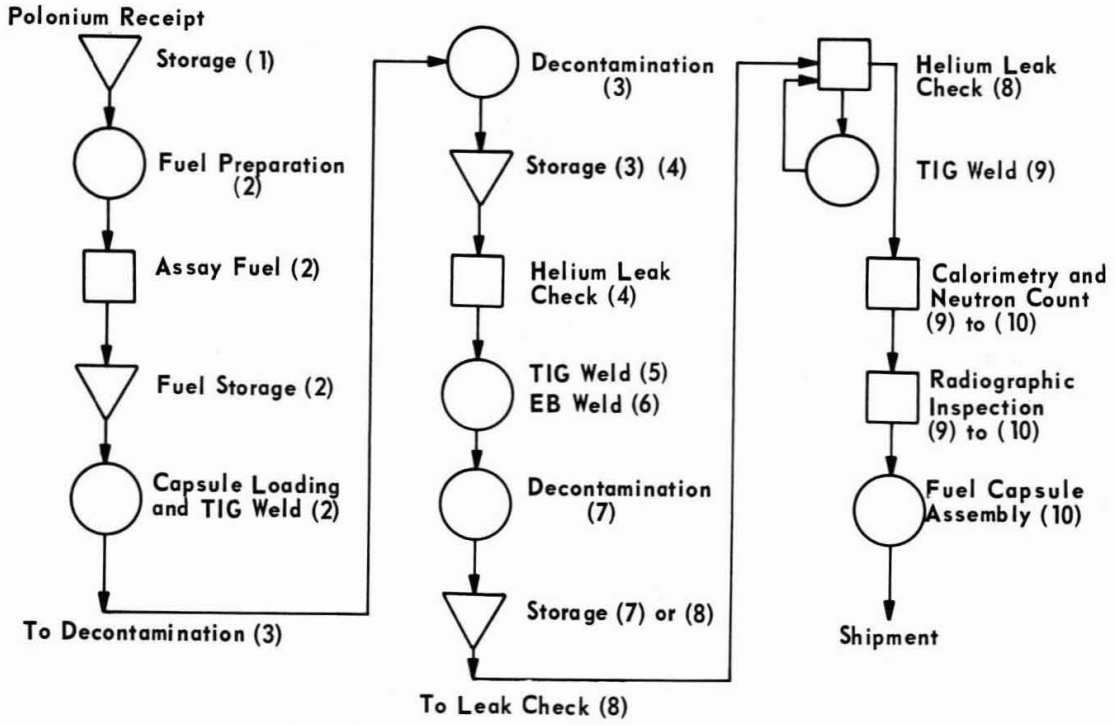

Fig. 3. Polonium encapsulation flow diagram (box numbers are shown in parentheses) Box 10 is the cell for loading heat source capsules into the final fuel package.

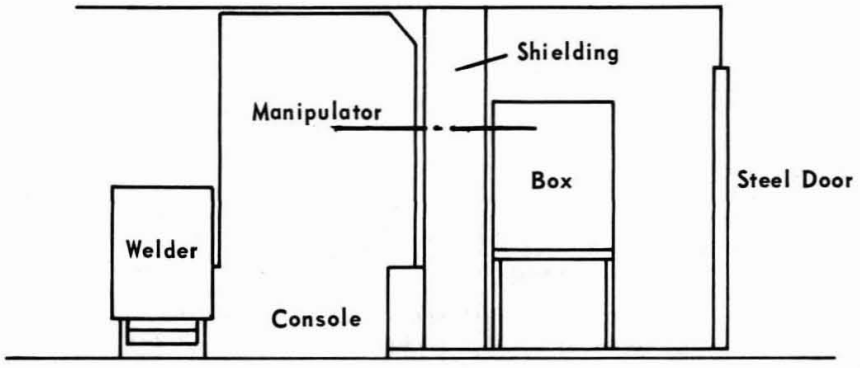

Fig. 4. Cross section of cell area

REMOTE ENCAPSULATION TECHNIQUES FOR ^{238}Pu FUEL FORMS

D. L. Coffey

Abstract

A remotely operated facility with thick radiation shielding was completed for fabrication of ^{238}Pu sources above 200 W thermal output without excessive neutron and gamma radiation exposure of the operating personnel. Nine interconnected stainless steel alpha boxes with controlled atmospheres are shielded by water. The individual operations include fuel loading, tungsten-inert gas welding, decontamination, helium leak checking, calorimetry, dimensional gaging, and alpha counting. The equipment required to perform these operations is either automatic or operated by mechanical manipulators extending through the radiation shielding. Water-cooled chill blocks control the capsule surface temperature during welding and helium leak checking.

D. L. Coffey is Group Leader of Source Development at Monsanto Research Corporation, Mound Laboratory, Miamisburg, Ohio.
Mound Laboratory is operated by Monsanto Research Corporation for the U. S. Atomic Energy Commission under Contract No. AT-33-1-GEN-53.

Introduction

A remotely operated facility for fabricating ^{238}Pu fueled heat sources was recently completed at Mound Laboratory. This heat source fabrication line consists of nine interconnected type 304L stainless steel alpha boxes which are shielded by a nominal 18 in. of water. The water acts as a radiation shield which precludes excessive exposure of the operating personnel to neutron and gamma radiation from the ^{238}Pu fuel. All operations are performed automatically or with commercially available, front-mounting master-slave manipulators.

Fabrication Line

Figure 1 is a pictorial cross section of the heat source fabrication line. The typical stainless steel alpha boxes are covered on the top, back, and partially on the front with welded carbon steel tanks which contain water and a rust inhibitor. The viewing windows in the shielding consist of stainless steel framed, tempered glass boxes, which contain distilled water and a copper sulfate solution to inhibit algae growth. All interior metal surfaces of the window housings have seven coats of an epoxy protective paint.

The steel tanks in back of the alpha boxes can be drained through a line having a quick-disconnect joint; the tanks can be moved from the boxes with a fork-lift truck. The tempered glass windows in the rear of the boxes have standard 8.5 in. glove ports fitted with lead-filled Neoprene gloves. Routine maintenance and cleaning can be performed as a normal glovebox operation when the rear shielding is removed.

Control consoles (not shown) are mounted outside the front shielding below the viewing windows on each of the boxes and contain all the necessary switches, controls, and readouts required to operate the fixtures in each box.

The enclosed mechanism shown above the fabrication line is a conveyor system which transports radioactive materials to the various processing and analytical operations in the building. Access to the conveyor is provided by a chain driven elevator in one of the boxes as shown in Fig. 2. A water-cooled incoming storage area for individual containers can be seen in front of the elevator.

Figure 3 is a layout of the encapsulation line. The stainless steel alpha boxes, exclusive of shielding, are 42 in. deep by 40 in. high and are mounted on steel legs,

which are 36 in. long. The varying lengths of the boxes are shown, with the exception of boxes 1 through 4. Boxes 1 through 4 are used for fuel form preparation and are not the subject of this paper.

The alpha boxes are designed to operate with either a dynamic air atmosphere or a recirculated dry inert gas atmosphere. The atmosphere used in a particular box is dependent upon the reactivity of the fuel form and the capsule material with the box atmosphere at temperatures encountered during fabrication. The thermal conductivity of the gas in the interfaces between capsule components is also taken into consideration. The boxes normally operate at a negative pressure of 1 to 3 in. of water.

The fabrication line is designed so that the fuel and the unassembled capsule hardware are passed into one end of the line; a complete, doubly encapsulated heat source is removed from the other end of the line.

The primary functions performed in box 5 are: 1) calorimetry and/or weighing of the fuel, 2) fuel storage, 3) loading of the fuel into the primary capsule, 4) tungsten-inert gas (TIG) welding of the closure joint of the primary capsule, and 5) disassembly of a completed heat source, when required.

Box 6 contains the elevator used to receive and insert containers into the conveyor system as shown in Fig. 2.

Box 7 contains facilities for removing alpha contamination from the outside surfaces of the welded primary container. The contamination is reduced to a level at which it will not be transferred to fixtures or secondary capsule components in subsequent operations.

The primary functions performed in box 8 are: 1) loading the primary capsule into the secondary capsule, 2) TIG welding of the closure joints of the secondary capsule, 3) helium leak checking the heat source, and 4) determining the thermal power output of the heat source by calorimetry. This box is provided with an internally mounted, electrically driven overhead hoist which is used to move the source from one operation station to another inside the box.

The functions performed in box 9 are: 1) alpha counting wipes of the external surfaces of the heat source to assure that no contamination is present, 2) gaging the external dimensions of the source, and 3) transferring the completed source from the fabrication line. The heat source is transferred from box 9 through a sealed door and a plug in the shielding into a shielded transporter, which is mated to a flange around the plug opening. The transporter is used to move the completed heat source to the shipping cask or to

other areas for additional tests or inspection.

The details of the fixturing and procedures used to fabricate a heat source are highly dependent upon the design features of a specific heat source. However, this discussion is limited to general considerations which apply to all the types of heat sources which can be fabricated in this line.

All TIG welding is fully automatic and is usually performed with a programmed welding machine. One of the most critical aspects of the welding fixturing is the chill block used to maintain a given capsule temperature during welding. A rule of thumb, based upon past metallurgical experience, has been to maintain the surface temperature in the weld zone at less than 220°F before and after welding to insure that the fuel capsule welds are adequately represented by unheated example and test welds. Figure 4 shows a typical TIG welding fixture. This fixture consists of a series of water-cooled, clam shell chill blocks. A rotary tube welding head is used with this particular fixture. A water-cooled, clam shell, capsule storage chill block and one of the vacuum pass boxes can also be seen in this photograph.

Alpha contamination is normally removed from the surface of the primary capsule by ultrasonic cleaning with an acidic solution or by mechanical scrubbing with a slightly abrasive cleanser. Also of prime concern is the removal of all cleaning material from the surface of the capsule after decontamination. This is normally done by thoroughly rinsing in distilled water. Figure 5 shows the decontamination box. The ultrasonic cleaner tank can be seen as a well in the floor of box. Primary capsule storage chill blocks can be seen also. The alpha counting equipment consists of a solid-state detector and preamplifier mounted in the box and a scaler-timer readout outside the line. The detector and preamplifier can be seen mounted on the rear wall of this box.

The calorimeters used to verify the thermal power output of the completed heat sources are either of the water bath type or the inert gas (usually helium) bath type which give results to within 1% at the 95% confidence level when the source output is in excess of about 500 thermal watts.

All leak checking of the capsules is performed with a commercially available helium mass spectrometer type detector with the test chamber mounted in the box line. A major feature of the test chamber is the chill block which must maintain the capsule at low enough temperatures to preclude excessive creep, pressure buildup, and oxidation while in a vacuum and during pump-down of the chamber.

Acknowledgment

The author acknowledges the assistance of C. P. Johnston and F. A. Traino in the preparation of this paper.

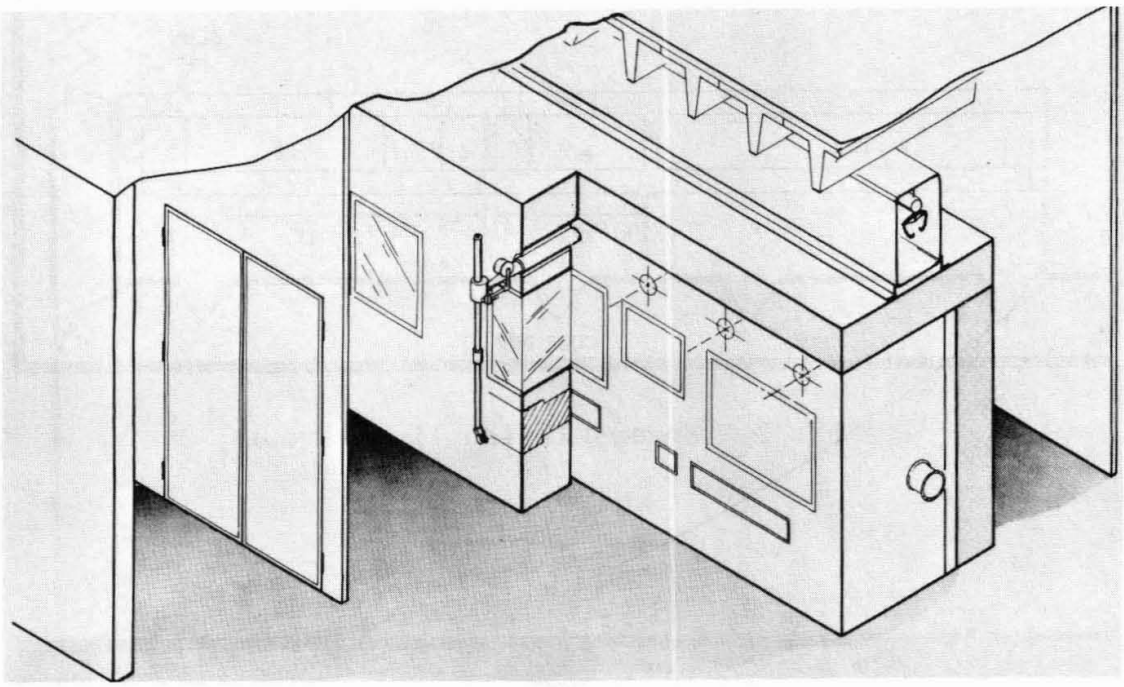

Fig. 1. Pictorial cross section of encapsulation line

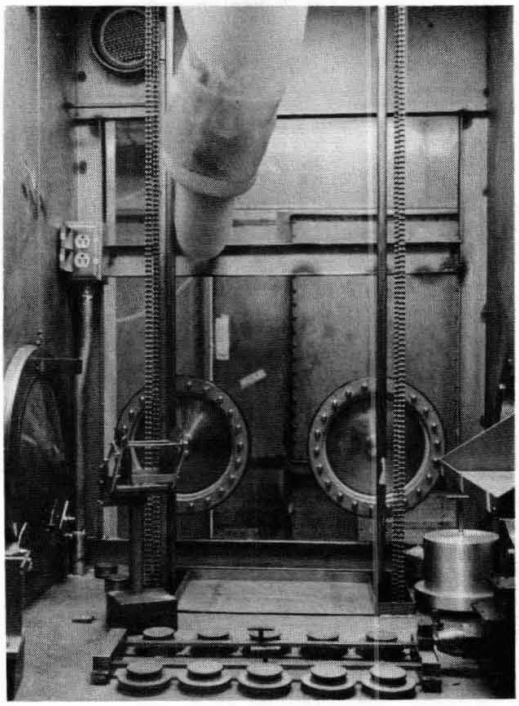

Fig. 2. Box 6 - conveyor system elevator

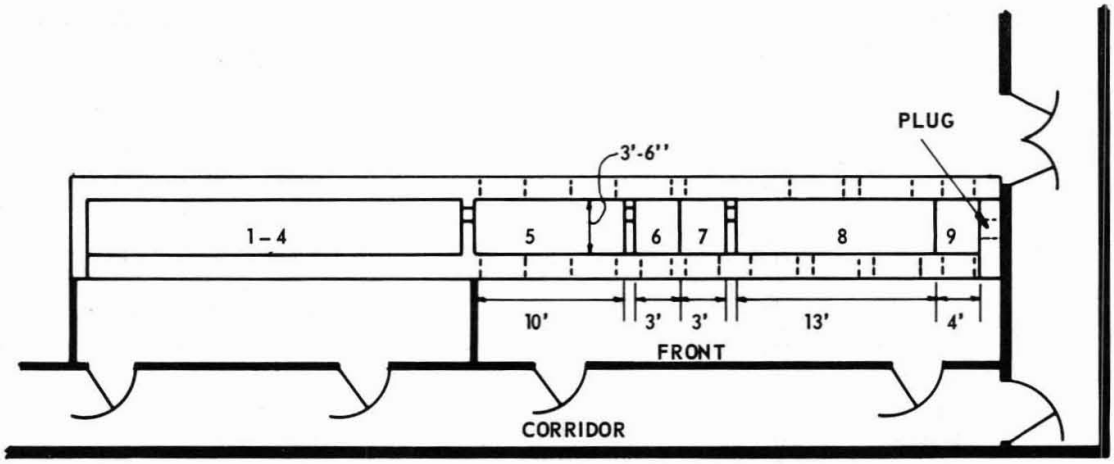

Fig. 3. Encapsulation line layout

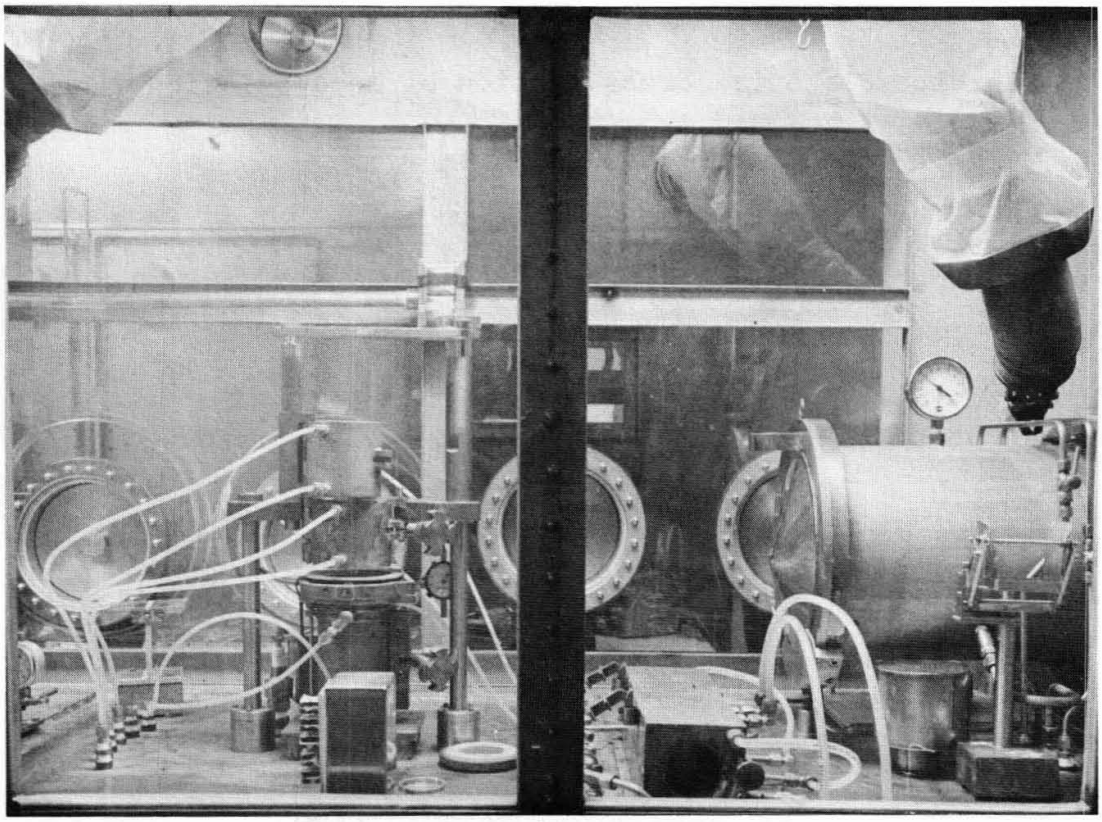

Fig. 4. Box 8 - typical TIG welding fixture

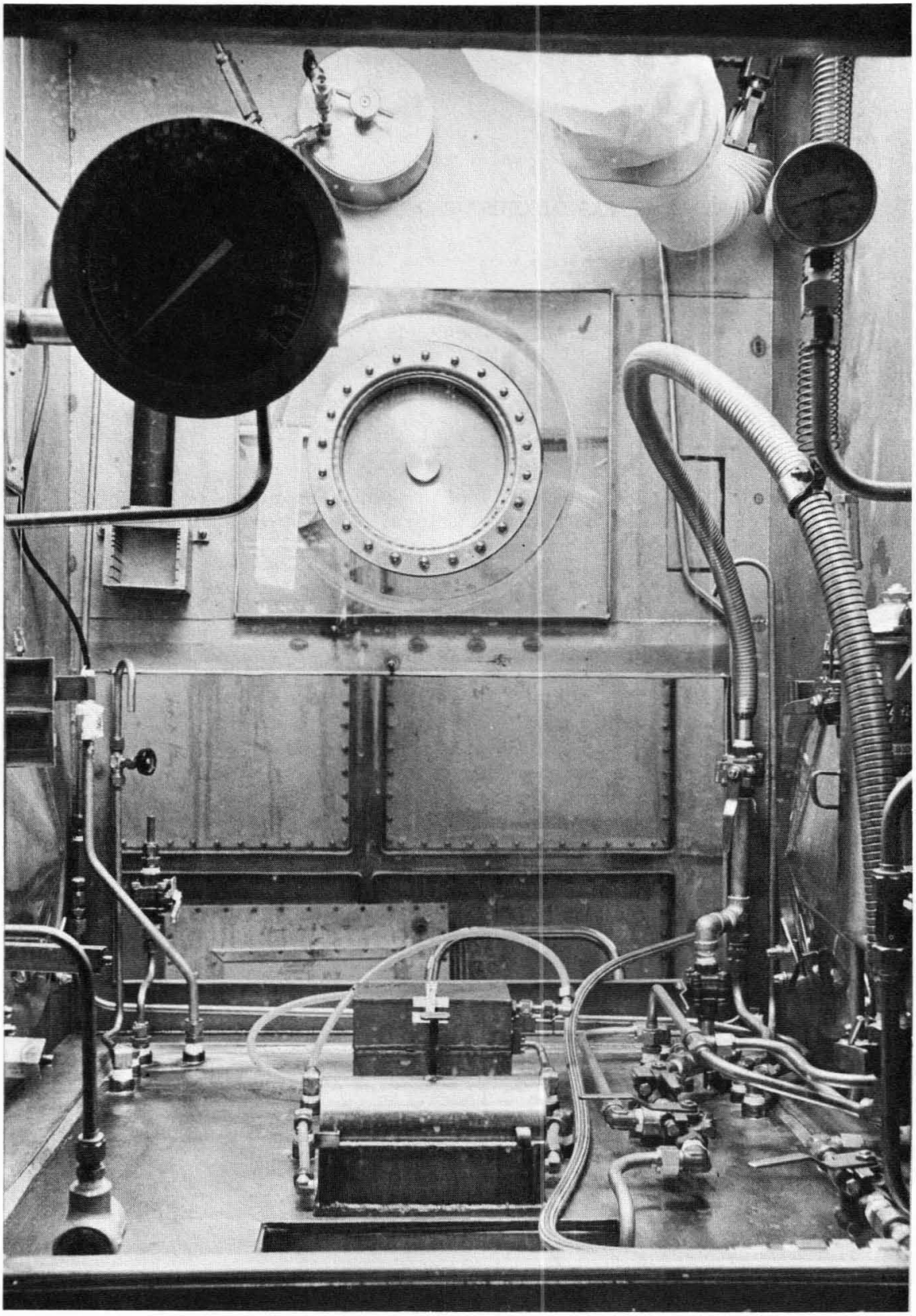

Fig. 5. Box 7 - decontamination fixtures

EVAPORATION OF RADIOISOTOPE CAPSULE MATERIALS IN VACUUM*

D. T. Bourgette**

Abstract

This paper is based on a study of evaporation behaviors of stainless steels, superalloys, and refractory alloys. Haynes-25 and type 316 stainless steel were tested at temperatures of 760 to 1150°C and pressures of 10^{-10} to 10^{-7} torr for times to 3500 hr. The role of composition was determined by comparing the evaporation results and microstructures of these alloys with 700-hr tests conducted at 870 and 980°C on Hastelloy N, Inconel, and types 304 and 446 stainless steel. Evaporation rates increased with increasing chromium and manganese concentration and temperature, but decreased with time at constant temperature.

Evaporation resulted in surface enrichment of the low vapor pressure elements and bulk changes in alloy composition. This evaporation mode resulted in subsurface void formation, concentration gradients, and changes in the microstructure of each alloy.

The creep-rupture properties of type 316 stainless steel were determined in argon after exposure to vacuums of 10^{-7} to 10^{-9} torr for times to 5000 hr at 870°C. Haynes-25 is being evaporation tested at 800°C and 10^{-8} torr while under creep stresses of 2,500 to 15,000 psi to ascertain the effect of stress on evaporation behavior.

Results of evaporation tests on tantalum- and niobium-base alloys in high vacuum at temperatures of 1200 to 1500°C showed that no serious evaporation problems exist below 1300°C.

---

*Research sponsored by the U.S. Atomic Energy Commission under contract with the Union Carbide Corporation.

**Staff metallurgist, Metals and Ceramics Division, Oak Ridge National Laboratory, Oak Ridge, Tennessee.

Introduction

Because of the importance of superalloys and refractory alloys for space applications, we have conducted experimental programs designed to determine compositional and microstructural stability of these alloys in vacuum. This paper emphasizes the more important results of four principal areas of research:

1. evaporation behavior of superalloys containing chromium with emphasis on compositional and microstructural stability in type 316 stainless steel and Haynes-25,
2. effect of evaporation losses on the creep behavior of superalloys,
3. effect of parent oxide coatings on evaporation kinetics of superalloys,
4. evaporation behavior and compositional stability of refractory alloys.

Metal loss through evaporation is a potential problem for many space applications since temperatures are often encountered at which some alloying components have significant vapor pressures. The evaporation rates (ω) of pure metals or simple compounds evaporating as monomolecular species are adequately described by the Knudsen-Langmuir equation

$$\omega = \alpha p/(2\pi RT/M)^{\frac{1}{2}} .$$

In this expression, α is the evaporation coefficient (usually taken as unity), p is the vapor pressure, M is the gram molecular weight of the vapor species, and the other symbols have their usual meaning. This equation, however, requires assumptions which are not valid for relatively complex structural alloys. Selective evaporation of the more volatile elements is quite likely, with the result that the surface composition may continually change with time; hence it is impossible by present methods to calculate the evaporation losses of complex structural alloys using the vapor pressure of the components. Therefore, such data must be derived experimentally. The selective losses of certain elements may further cause the formation or solution of phases in the alloy which could result in variations in the strength and ductility of the alloy. It is also possible that an applied stress may enhance the evaporation rate or result in appreciable materials loss at temperatures lower than those desired for service, especially in thin members. Direct experimentation is necessary to determine the existence and severity of these vacuum effects.

Experimental Procedure

The test material, the preparation of specimens, the high vacuum evaporation equipment, and the creep test equipment used in these studies have been described elsewhere (1–4).

Results and Discussion

Validity of the Experimental Technique

To verify the accuracy of our experimental technique, we first determined the vapor pressure of pure iron and nickel by the Knudsen-Langmuir equation assuming a vaporization coefficient equal to unity. Our measured vapor pressures agreed well with the published values. The experimental value of 2.25×10^{-7} torr for nickel compares with the published value (5) of 3.00×10^{-7} torr at 1038°C, while an experimental value of 1.54×10^{-7} torr for iron compares to a published value (6) of 1.77×10^{-7} torr at 872°C.

Evaporation of Polished Surfaces

Evaporation losses from types 304, 316, and 446 stainless steels, Inconel, Hastelloy N, and Haynes-25 were measured at 872 and 982°C and from 5×10^{-7} to 5×10^{-8} torr to evaluate compositional effects, especially with regard to high vapor pressure alloying elements such as chromium and manganese. Results of 700-hr tests, summarized in Table 1, showed that evaporation rates at both temperatures increased with increasing chromium and manganese concentrations. For all alloys except Hastelloy N, the evaporation rate at a given temperature decreased with time, the decrease being greater at the lower temperature.

Figure 1 compares the continuous evaporation losses of these alloys at 872 and 982°C. The evaporation rates appear nearly constant after about 50 hr, although, as shown later, longer term tests with type 316 stainless steel and Haynes-25 showed that the evaporation rates actually continue to decrease slowly with time.

The initial evaporation losses, mainly from the surfaces, severely changed surface concentrations of the high vapor pressure elements. For example, microprobe analyses showed that at 872°C severe manganese and chromium concentration gradients existed at the conclusion of many 600-hr tests, although at 982°C where diffusion rates were greater, the concentration gradients were less.

During the later stages of evaporation when loss rates approached linearity, the grain boundaries beneath the surface exhibited voids, precipitates near the surface disappeared, and grain growth resulted — probably from loss of carbon.

Chemical analysis of posttest alloy specimens revealed substantial losses of chromium, manganese, and carbon. The results of 600-hr tests of several alloys are compared in Table 2. Losses of manganese and chromium increased with increasing concentration of these elements; however, carbon losses appeared to be independent of chromium and manganese losses. This behavior and the fact that metallographic examination showed a depletion of precipitates below the specimen surface suggested a decomposition of carbides.

Evaporation of Haynes-25 and Type 316 Stainless Steel

The evaporation behavior of two potential capsule materials, Haynes-25 and type 316 stainless steel, was studied in more detail from 760 to 1150°C for times to 3500 hr. This study provided data on the chemical composition of vaporized metal deposits as a function of time, on the kinetics of the evaporation process, and on the resultant effects of evaporation losses on microstructure, creep behavior, and original alloy composition.

Identification of Evaporated Elements

Chemical analyses of vapor deposits from 500-hr tests of Haynes-25 are summarized in Table 3. Although the total amount of deposited metal increased with temperature, relative concentrations of the deposits varied significantly, but systematically. As the test temperature was increased from 872 to 1093°C, the concentration of higher vapor pressure elements, such as chromium, manganese, and iron, decreased relative to the lower vapor pressure elements, cobalt, nickel, and silicon. In tests conducted for 5 to 500 hr at 982°C the concentrations of manganese and iron in the deposited vapor decreased with increasing time, while concentrations of the remaining elements increased. The concentrations of chromium and cobalt increased at a significantly greater rate than did nickel and silicon, indicating a selective loss of alloying elements that resulted in continually changing surface compositions.

Electron probe microanalysis of specimens tested at temperatures from 872 to 1150°C for times to 3000 hr showed concentration gradients that varied with time and temperature. Typical results, as illustrated in Fig. 2 for a 1040°C test, confirmed the chemical analysis and indicated a depletion of Fe, Cr, Ni, and Mn at the specimen surfaces. The surface concentrations of tungsten and silicon increased significantly while the cobalt concentration increased only slightly. Further, losses of the higher vapor pressure elements, chromium and manganese, from the interior regions of the specimen resulted in increased cobalt, tungsten, and iron concentrations in these regions. This behavior indicated that later losses of the higher vapor pressure elements were diffusion-rate dependent.

Similar results were obtained for type 316 stainless steel. Results from variable time-constant temperature tests showed that manganese was the major contributor to the total evaporation loss from this alloy. However, the manganese concentration in the vapor deposit decreased markedly with time. The chromium content, on the other hand, increased with time in the vapor deposit. Concentrations of the remaining alloying elements in the vapor deposits were consistent with their vapor pressures and concentrations in the original alloy. Chemical analyses of the deposited metal vapors from tests conducted at 7.0×10^{-9} torr and 872°C are summarized in Table 4.

Metallography

The microstructure of Haynes-25 over the temperature range studied exhibited four major changes as a result of evaporation losses:

1. Microscopic subsurface voids formed from the coalescence of vacancies (Kirkendall effect).

2. A "honeycomb" structure formed at specimen surfaces above 1000°C.

3. Laves phase $(Co,Ni)_2(W,Cr)$ formed at specimen surfaces.

4. Laves precipitate dissolved in the subsurface regions of the specimens due to bulk compositional changes.

These microstructural changes are illustrated in Fig. 3.

Wlodek (7) reported that Haynes-25, on prolonged exposure at 650 to 1100°C, will precipitate a Laves phase, which can lead to alloy embrittlement. This aging reaction produced maximum precipitation in the vicinity of 870°C after about 1000 hr. Aging treatments at higher temperatures resulted in less Laves phase in the microstructure. Wlodek further stated that silicon stabilized the Laves phase and also the hexagonal-close-packed modification of the cobalt matrix. Other constituents such as iron and nickel tend to stabilize the face-centered cubic high-temperature structure of the cobalt matrix. Nickel also tends to decrease the stability of the Laves phase.

Slight compositional changes involving the elimination of silicon, a decrease in the tungsten level, and an increase in the iron and nickel contents may suppress the Laves phase precipitation in the temperature range 850 to 1000°C (7). This study has shown, however, that in addition to chromium and manganese, significant amounts of iron and nickel with lesser amounts of silicon were evaporated from the specimen surfaces. Loss of these elements from the surfaces of thin specimens essentially increased the concentration of tungsten and cobalt. This evaporation behavior could therefore promote the formation of the Laves phase above 850°C. Wlodek (7) also reported that Laves phase forms within 64 hr at 760 to 980°C. But evaporation tests have shown that far longer times are required to appreciably change the bulk composition of the alloy at these temperatures. Therefore the Laves phase in the microstructures shown in Fig. 3 resulted from thermal effects and not from evaporation.

X-ray diffraction analysis showed that the surfaces of all Haynes-25 specimens exposed to vacuum at 930 to 1150°C contained Laves phase. Metallographic examination further showed that the amount of Laves phase at the specimen surfaces increased with temperature or with increased evaporation losses, as illustrated in Fig. 3. The Laves phase dissolved in the subsurface regions while it was forming on the surface. This anomalous behavior is attributed to the substantial differences in composition between these regions caused by selective evaporation.

The higher evaporation losses from regions near the surface and the coalescence of voids directly beneath the surface resulted in a honeycomb structure at the specimen surfaces. Voids were less extensive in the subsurface regions but were present throughout the microstructure of the 0.015-cm-thick specimens that lost 2 mg/cm^2 or greater. The formation of these voids is attributed to the coalescence of vacancies by the Kirkendall effect.

In the case of type 316 stainless steel, grain boundary grooving became apparent after 1 hr at 1000°C and 4 hr at 800°C. After 500 hr at 872°C the microstructure exhibited subsurface void formation, grain growth, disappearance of precipitates, ferrite formation at the specimen surfaces, and widening of the grain boundaries. These phenomena are metallographically illustrated in Figs. 4 and 5. After 1000 hr, chi phase began to precipitate and large grain boundary voids began to appear.

Formation of a ferrite surface layer was verified by x-ray analysis and was apparently caused by the rapid loss of austenite stabilizers (e.g., carbon and manganese). At 872 and 982°C, ferrite precipitation began just prior to the appearance of grain boundary voids; as evaporation losses continued and the specimen thickness decreased, the ferrite precipitate disappeared. Apparently the low nickel losses coupled with high loss of chromium at longer times caused the ferrite to retransform to austenite. For example, Fig. 5 shows that the 892-hr test resulted in surface ferrite while the 3453-hr test showed no indication of ferrite. Further, Fig. 4 shows that the evaporated surface of the 3453-hr test contains annealing twins, which are usually associated with the face-centered cubic structure rather than the body-centered cubic ferrite. In addition, all short-term test specimens were ferromagnetic, while the long-term tests (> 1000 hr) were not. Also ferrite was not detected by x-ray diffraction analysis in specimens tested longer than 1000 hr.

When the surfaces of type 316 stainless steel specimens transformed to ferrite, the evaporation rate approached that for pure iron. For example, at 982°C the evaporation rate of pure iron was constant and equal to 6.2×10^{-3} mg cm^{-2} hr^{-1}, while the rate for type 316 stainless steel at the end of a 650-hr test was 6.64×10^{-3} mg cm^{-2} hr^{-1}.

Evaporation Kinetics of Polished Surfaces

Evidence of preferential depletion of higher vapor pressure elements was manifested by the existence of concentration gradients and time-dependent changes in the composition of vapor deposits. Therefore, losses of these elements are diffusion-rate controlled and their evaporation rate at any one temperature should decrease with time. Evaporation rates for Haynes-25 are plotted in Fig. 6 as a function of temperature for times to 1000 hr. Note that the curves are nearly parallel, indicating that the evaporation mechanisms or the activation energy for the evaporation process does not change significantly between 2 and 1000 hr. It is postulated that this change may be due to the formation of Laves phase on the specimen surfaces of the Haynes-25. For type 316 stainless steel, curves of this type were also parallel over the time range investigated, 2000 hr.

We should emphasize that the test specimens were only 0.015 to 0.020 cm in thickness and that greater thicknesses might yield quite different experimental results. The major differences would probably be an increase in the slope of the concentration profiles of the evaporating elements near the surfaces and a decrease in the severity of void formation within the bulk of the sample. The evaporation rates would remain relatively high, however, as long as the temperature was

sufficient for the higher vapor pressure elements to diffuse to the specimen surfaces. Greater thicknesses in effect make more material available for selective evaporation.

Oxidized Surfaces. It has been demonstrated that surface oxides can retard evaporation of pure metals (8). To ascertain how effectively oxide films retard evaporation of the alloys listed in Table 1, several specimens were oxidized in air and in wet hydrogen and subsequently evaporation tested under high vacuum at 982, 927, 872, and 760°C. The results for all of the alloys tested were nearly the same; therefore, only the results for type 316 stainless steel will be discussed.

Oxidation of specimens in air resulted in a layer of mixed oxides including αFe_2O_3, $NiO \cdot Fe_2O_3$, and $Fe_2O_3 \cdot Cr_2O_3$. After the evaporation tests, Cr_2O_3 was the only oxide still remaining on the specimen surfaces. Therefore, all subsequent oxidation tests were conducted in wet hydrogen so that only Cr_2O_3 was formed on the specimens surfaces.

The Cr_2O_3 layer formed on the specimen surfaces retarded evaporation for different periods of time, depending on evaporation temperature. At 760°C, the Cr_2O_3 film was fully protective against evaporation losses of the base metal, at least to 1142 hr. At the three higher temperatures, 982, 927, and 872°C, the Cr_2O_3 films deteriorated initially at intersections of the surface with grain boundaries. This behavior resulted in a semicontinuous network of voids within the Cr_2O_3 film. The remaining Cr_2O_3 film became progressively thinner due to evaporation and to a reaction of oxygen with carbon in the metal. As in the case of specimens without oxide films, subsurface voids appeared in the base metal and increased in size and number with increasing temperature. Simultaneous loss of austenite stabilizers resulted in the formation of surface ferrite at 982 and 927°C for short-term tests, while at 872°C no ferrite was detected in a 1456-hr test. These evaporation effects are metallographically illustrated in Fig. 7. Results of the 1000-hr evaporation tests for both polished and oxidized surfaces are compared in Fig. 8 and show that a Cr_2O_3 layer does afford a slight degree of protection against base metal evaporation. The important feature of Fig. 8, however, is the parallel behavior of the curves which indicate that the evaporation mechanisms for both polished and oxidized surfaces are the same.

We postulate that the Cr_2O_3 film is initially reduced by carbon from the substrate metal principally in the grain boundary areas. Then evaporation of the Cr_2O_3 film further reduces its thickness, and eventually small holes appear in the oxide layer and expose the metal at the grain boundaries. Metals evaporation undermines the oxide layer, and spallation exposes larger areas of the substrate. This behavior would result in greater evaporation losses, but because of the adherent Cr_2O_3 film over the remainder of the surface grains, the total evaporation rate is less than for the polished condition. The photomicrograph of an as-evaporated sample in Fig. 9 illustrates this behavior.

Effect of Evaporation on Creep

Type 316 Stainless Steel. Several tests were run to evaluate the influence of exposure to high vacuum on the creep-rupture properties of

type 316 stainless steel at 870°C. Flat creep specimens, 0.102 cm thick, were exposed to a vacuum of 10^{-8} torr for times to 5000 hr, while control specimens were heated in high-purity argon. In addition, specimens were oxidized in wet hydrogen, followed by a high vacuum evaporation treatment at 870°C. All specimens were subsequently creep tested in argon at 870°C.

These studies have shown that type 316 stainless steel undergoes considerable change in its creep properties when exposed for long periods of time at 870°C. Material initially cold worked becomes stronger when heated at 870°C prior to creep testing. If the alloy is initially heated for 1 hr at 1040°C in vacuum it grows weaker when annealed at 870°C for long times. The precipitates in the photomicrographs presented earlier have been identified as chi phase, carbides of the $M_{23}C_6$ type, and traces of sigma phase, and are believed to be responsible for the observed creep behavior. For example, the as-received material contained some residual cold work that provided nucleation sites for carbide precipitation which would improve the strength with holding time at 870°C. At some point, the carbides would all precipitate or a steady state would be reached between precipitation and agglomeration so that no further strengthening would occur. When the steel is annealed at 1040°C, the residual cold work is removed, carbides are dissolved, and grain growth occurs, but the creep strength is greater than in the as-received condition. The reason for this behavior is not known. The precipitates that are formed when the material solution annealed at 1040°C is held at 870°C during the evaporation tests may not be of the proper morphology to strengthen the alloy. This behavior may account for the lower strength values after the 870°C treatment. Further, the loss of alloying elements by evaporation would reduce the strength.

The formation of a thin surface oxide does not observably change the creep properties at 870°C. This behavior was expected, since other investigations (9) have shown that surface films on a polycrystalline specimen are not effective at elevated temperatures due to the numerous internal surfaces present.

Haynes-25. Haynes-25 was creep tested in high vacuum at 785°C and stress levels of 2,500 to 15,000 psi to correlate evaporation losses and microstructure with the observed creep behavior and stress. The results, tabulated in Table 5, indicate that evaporation losses increase with stress. Microstructural examinations showed that the amount of Laves phase precipitated in 1000 hr also increased with stress, but we think this behavior is due to the compositional change and is not directly related to stress.

Evaporation also affected the creep properties of Haynes-25. For example, a specimen tested at 10^{-8} torr and 14,500 psi ruptured in 246 hr at 785°C, but a control specimen tested in argon at 1 atm ruptured in 540 hr. These results are compared with those of other investigators (10) who found a rupture life of 2500 hr at 816°C for air-tested specimens. Also, the time to 1% plastic strain as a function of stress varied from 8 to 15 times less for the vacuum-tested samples when compared to results from air tests.

Evaporation and Stability of Refractory Alloys

Evaporation losses of T-111 (Ta–8% W–2% Hf) and five niobium-base alloys, Nb–1% Zr, FS-85 (Nb–27% Ta–10% W–1% Zr), B-66 (Nb–5% Mo–5% V–1% Zr), C-129Y (Nb–10% Hf–10% W–0.01% Y), and D-43 (Nb–10% W–1% Zr–0.1% C) were determined for various times at temperatures between 1200 and 1500°C and pressures from 7×10^{-7} to 6×10^{-10} torr. The details of this work have been reported elsewhere (11).

In general, there were no serious evaporation problems associated with these alloys, especially at temperatures of 1200 to 1300°C. The alloys exhibiting the greatest evaporation losses contained the higher vapor pressure elements such as V, Zr, Y, and Hf. For example, B-66 (the most volatile alloy studied) lost 1.70 mg/cm^2 at 1500°C and 7×10^{-9} torr in 316 hr, while at 1200°C and 6×10^{-10} torr a weight loss of 0.077 mg/cm^2 was measured in 513 hr; vanadium and zirconium losses contributed 95% of the total weight loss. Metallographic examination showed that evaporation occurred only at the surfaces; no subsurface voids were detected, nor did evaporation seem to occur at any preferential sites, such as grain boundaries or impurity inclusions at or near the surfaces.

Total weight change appeared to be pressure and composition dependent. At 1200 to 1300°C and 10^{-7} torr, the niobium-base alloys FS-80 and D-43, containing only zirconium as the evaporating element, gained weight, while at the same temperature and 10^{-9} torr weight was lost. We attribute this behavior to interstitial contamination at 10^{-7} torr and purification at 10^{-9} torr. For those alloys with more than one evaporating species, such as B-66 and C-129Y, weight was lost at both the high and low test pressures at 1500°C. The evaporation losses in these cases overshadowed the changes in the interstitial contents.

Changes in the interstitial concentrations depended upon pressure. At 1500°C and 10^{-9} torr or lower, carbon was retained while oxygen, nitrogen, and hydrogen were evolved. At a higher pressure of 10^{-7} torr and 1500°C, carbon was lost while oxygen and nitrogen contents increased. It is believed that the reaction of carbon and oxygen resulted in the loss of carbon at the higher pressures, while at 10^{-9} torr not enough oxygen was present to appreciably reduce the carbon concentrations. These results are illustrated in Figs. 10 and 11.

Conclusions

High vapor pressure elements such as Cr, Mn, Fe, Ni, Cu, and Si are preferentially lost when superalloys are exposed to a vacuum of 10^{-7} torr or greater at temperatures of 760 to 1150°C. This evaporation is characterized by an initially high rate due to the presence of the more volatile elements, chromium and manganese, at the surface. When the surface becomes depleted of these elements, further loss depends on their diffusion rates in the alloy. Compositional changes occur at every temperature investigated; in the case of type 316 stainless steel after 1000 hr, the loss of austenite stabilizers promotes ferrite precipitation, while in Haynes-25 the loss of chromium, manganese, and nickel promotes Laves phase formation at the surfaces.

Type 316 stainless steel coated with Cr_2O_3 does not initially evaporate as rapidly as when polished, but the final rates of evaporation at 870, 925, and 980°C are great enough to rule out adequate protection of the base alloy by this technique. At 760°C, however, Cr_2O_3 fully retards evaporation at least for 1150 hr.

Exposure to vacuum apparently has no significant effect on the mechanical behavior of 0.102-cm-thick specimens of type 316 stainless steel. In the case of thinner cross sections or longer vacuum exposures where the composition of the stressed section would be seriously altered, strength properties will undoubtedly be affected.

Simultaneous stressing and evaporation result in quite a different behavior in Haynes-25. Preliminary studies show that evaporation from the grain boundaries of thin specimens (0.0305 cm) results in easier grain boundary motion with reduced creep strength and rupture life. Increased stress also produces increased evaporation losses.

Evaporation of alloying elements from tantalum- and niobium-base refractory alloys is low at temperatures of 1000 to 1300°C for short-term tests at 300 to 700 hr. We conclude that within this temperature range no serious evaporation problem exists under high vacuum conditions. However, exposure for several thousand hours at 1300 to 1500°C would result in severe losses of volatile alloying elements such as hafnium and vanadium.

The interstitial instability of these refractory alloys is considered a serious problem if the control of interstitials is essential to the mechanical behavior of the alloy. At 10^{-9} to 10^{-10} torr, the instability results in a loss of oxygen, nitrogen, and hydrogen, while at 10^{-6} to 10^{-8} torr, the concentration of oxygen and nitrogen increases, and the carbon content decreases over an extended period of time. A carbon-oxygen reaction results in the loss of carbon, probably as CO.

References

1. D. T. Bourgette, Evaporation of Iron-, Nickel-, and Cobalt-Base Alloys at 760 to 980°C in High Vacuums, ORNL-3677, November 1964.

2. D. T. Bourgette and H. E. McCoy, ASM (Am. Soc. Metals) Trans. Quart. 59(2), June 1966, pp. 324–339.

3. H. E. McCoy, W. R. Martin, and J. R. Weir, 1961 Proceedings of the Institute of Environmental Sciences National Meeting, April 5, 6, 7, 1961, Washington, D. C., Institute of Environmental Sciences, Mt. Prospect, Ill., 1961, pp. 163–176.

4. D. T. Bourgette, High-Temperature Chemical Stability of Refractory-Base Alloys in High Vacuum, ORNL-TM-1431, April 1966.

5. J. F. Elliott and M. Gleiser, Thermochemistry for Steelmaking, Vol. 1, Addison-Wesley, Reading, Mass., p. 270.

6. E. A. Gulbransen and K. F. Andrew, Trans. Met. Soc. AIME 221, 1961, p. 1247.

7. S. T. Wlodek, Embrittlement of a Co-Cr-W (L-605) Alloy, R 61 FPD 538, Dec. 1, 1961.

8. W. L. Winterbottom and J. P. Hirth, Evaporation of Silver Crystals, Carnegie Institute of Technology, Metals Research Laboratory, 1962.

9. J. R. Cuthill and W. N. Harrison, Effect of Ceramics Coatings on the Creep Rate of Metallic Single Crystals and Polycrystalline Specimens, WADC Technical Rept. 56-85, April 1965.

10. R. Widmer, J. M. Dhosi, A. Mullendore, and N. J. Grant, Mechanisms Associated with Long Time Creep Phenomena, AFML-TR-65-181, June 1965.

11. D. T. Bourgette, Trans. Vacuum Met. Conf., 8th, New York, 1965, (ed. L. Bianchi), American Vacuum Society, Boston, Mass., 1965, pp. 57–73.

Table 1. Evaporation Rates from 700-hr Tests of Iron-, Nickel-, and Cobalt-Base Alloys at 5×10^{-7} to 5×10^{-8} torr

Alloy	Alloy Composition,[a] wt %									Evaporation Rate ($mg\ cm^{-2}\ hr^{-1} \times 10^{-4}$)			
										872°C		982°C	
	Fe	Ni	Mo	Co	C	W	Mn	Si	Cr	Initial[b]	Final[c]	Initial	Final
Hastelloy N	4.10	69.76	17.81	0.15	0.04		0.29	0.58	6.78	1.54	1.54	30.8	30.8
Inconel	5.84	79.62			0.04		0.54		14.29	7.57	2.89	59.7	33.5
Type 316 stainless steel	64.03	13.28	2.25		0.05		1.67	0.74	17.05	30.0	6.59	114.0	66.4
Type 304 stainless steel	68.84	10.68			0.07		1.61	0.84	18.04	53.7	6.71		
Haynes-25	1.41	10.50		49.81	0.02	15.72	1.58	0.76	19.46	58.5	5.66	140.0	69.2
Type 446 stainless steel	73.91	0.71			0.02		1.20	0.14	24.71	73.8	25.7	156.0	69.0

[a] Impurity elements not listed.

[b] Maximum rate during first 50 hr of test.

[c] Rate during last 50 hr of test.

Table 2. Elemental Losses of Iron-, Nickel-, and Cobalt-Base Alloys Evaporated at 872°C

Alloy[a]	Length of Test (hr)	Percent Decrease in Original Concentration		
		Mn	Cr	C
Hastelloy N	598	13.9	1.61	29.7
Inconel	618		3.86	28.5
Type 316 stainless steel	604	21.6	5.21	27.4
Type 304 stainless steel	608	29.4	5.96	27.1
Haynes-25	557	44.9	3.01	28.4
Type 446 stainless steel	613	54.1	4.85	12.1

[a]See Table 1 for original compositions.

Table 3. Chemical Analyses of Vapor Deposits Evaporated from Haynes-25

Test Conditions[a]	Actual Weight Loss[b] (mg)	Analyses of Vapor Deposits														Total Weight of Vapor Deposit[c] (mg)
		Cr		Mn		Co		Fe		Ni		Si		W		
		(mg)	(wt %)	(mg)	(wt %)	(mg)	(wt %)	(mg)	(wt %)	(mg)	(wt %)	(mg)	(wt %)	(mg)	(wt %)	
872°C for 504 hr	3.40	2.11	66.88	0.56	17.75	0.26	8.27	0.18	5.70	0.03	1.01	0.001	0.03	0.01	0.35	3.155
927°C for 507 hr	4.70	3.08	66.31	0.68	14.64	0.48	10.33	0.17	3.66	0.21	4.52	0.001	0.02	0.024	0.52	4.645
982°C for 509 hr	11.80	7.63	66.58	1.24	10.82	1.75	15.27	0.38	3.32	0.28	2.41	0.15	1.31	0.03	0.29	11.46
1038°C for 505 hr	23.6	14.90	64.50	2.18	9.44	4.43	19.18	0.79	3.42	0.65	2.81	0.08	0.35	0.07	0.30	23.10
1093°C for 503 hr	303.90	146.50	47.79	17.10	5.58	106.0	34.58	9.00	2.94	26.60	8.68	0.94	0.30	0.41	0.13	306.55

[a] At 1×10^{-9} torr.

[b] Initial sample weight minus final sample weight.

[c] Weight of deposit determined by analytical chemistry methods.

Table 4. Chemical Analyses of Deposits Evaporated from Type 316 Stainless Steel at 872°C and 7×10^{-9} torr

Element	Vapor Pressure of Element (torr)	Analyses[a] of Original Alloy (wt %)	Analyses in Weight Percent of Vapor Deposit at Various Times in Hours					
			6	12	25	50	150	480
Mn	8×10^{-4}	1.67	77.72	71.24	70.2	68.1	59.85	50.88
Cr	2.5×10^{-6}	17.05	3.18	3.84	4.40	7.91	19.95	29.4
Si	7×10^{-7}	0.74	0.712	0.971	1.31	1.45	1.51	1.70
Fe	1.5×10^{-8}	64.03	1.29	1.33	2.39	4.86	9.03	12.27
Ni	4×10^{-9}	13.28	1.01	1.4	1.62	1.71	1.83	1.95
C	5×10^{-19}	0.05	7.53	4.32	3.93	2.11	1.70	1.41
Mo	3×10^{-14}	2.25	b	b	b	b	b	b

[a] See Table 1 for original composition.

[b] Not detected.

Table 5. Effect of Stress on the Evaporation Losses of Haynes-25 at 785°C after 1000 hr

Stress (psi)	Weight Loss (mg/cm^2)
0	0.06
2,100	0.1477
4,500	0.1864
6,900	0.2014
9,500	0.2236
14,500	0.04[a]

[a]Specimen ruptured in 246 hr.

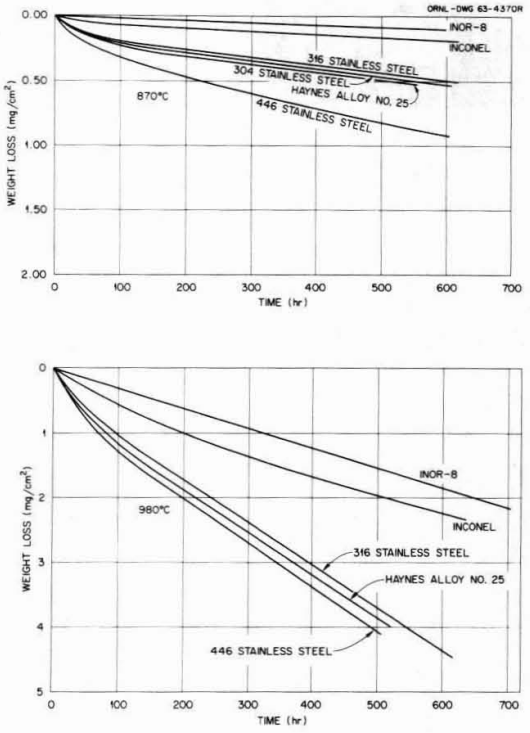

Fig. 1. Evaporation losses of iron-, nickel-, and cobalt-base alloys at 870 and 980°C and approximately 5×10^{-7} to 5×10^{-9} torr.

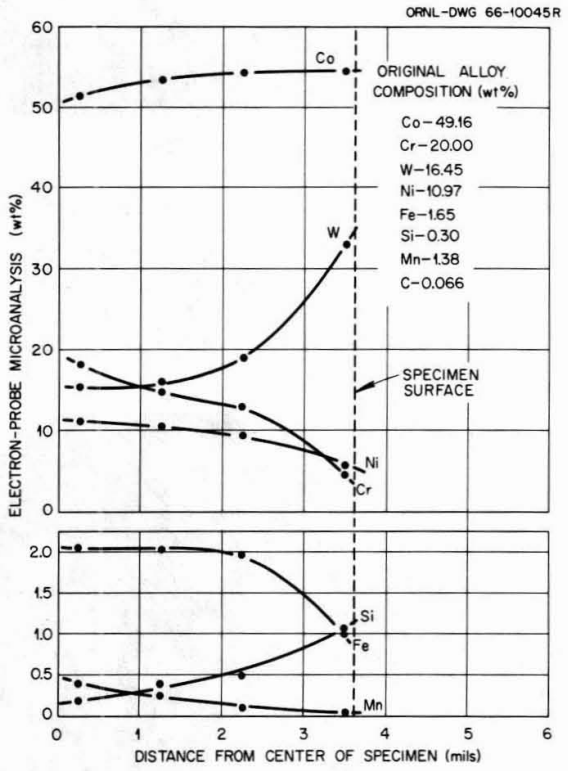

Fig. 2. Composition profile of a Haynes-25 specimen evaporation tested at 1040°C for 2672 hr.

PHOTO 84997

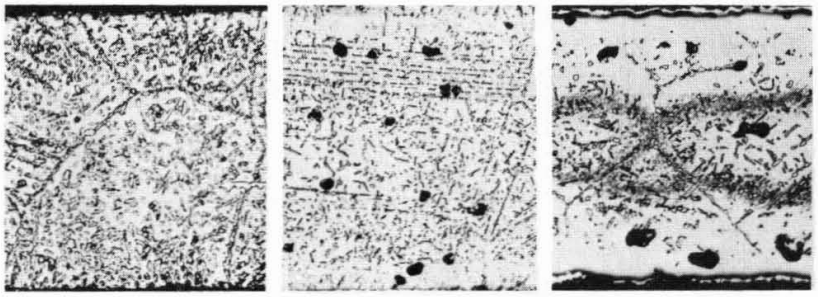

870°C Y-70344 930°C Y-70339 980°C Y-70338
1142 hr 2043 hr 2157 hr
WT. LOSS – 0.68 mg/cm^2 WT. LOSS – 3.41 mg/cm^2 WT. LOSS – 8.73 mg/cm^2

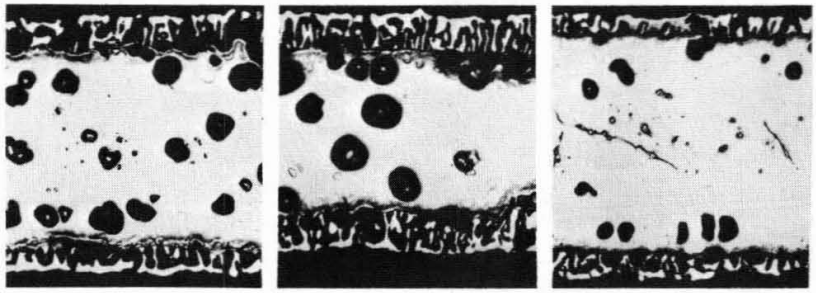

1040°C Y-70343 1090°C Y-70342 1150°C Y-70341
2672 hr 670 hr 164 hr
WT. LOSS – 22.6 mg/cm^2 WT. LOSS – 27.5 mg/cm^2 WT. LOSS – 25.2 mg/cm^2

Fig. 3. The effect of evaporation losses on the microstructure of Haynes-25. Original magnification, 500×. Etchant: electrolytically polished and etched using a platinum cathode in a solution of 100 cm^3 H_2O + 40 cm^3 $HC_2H_3O_2$ + 40 cm^3 HCl + 15 cm^3 H_2SO_4 + 40 cm^3 HNO_3 + 25 g $FeCl_3$.

PHOTO 67325

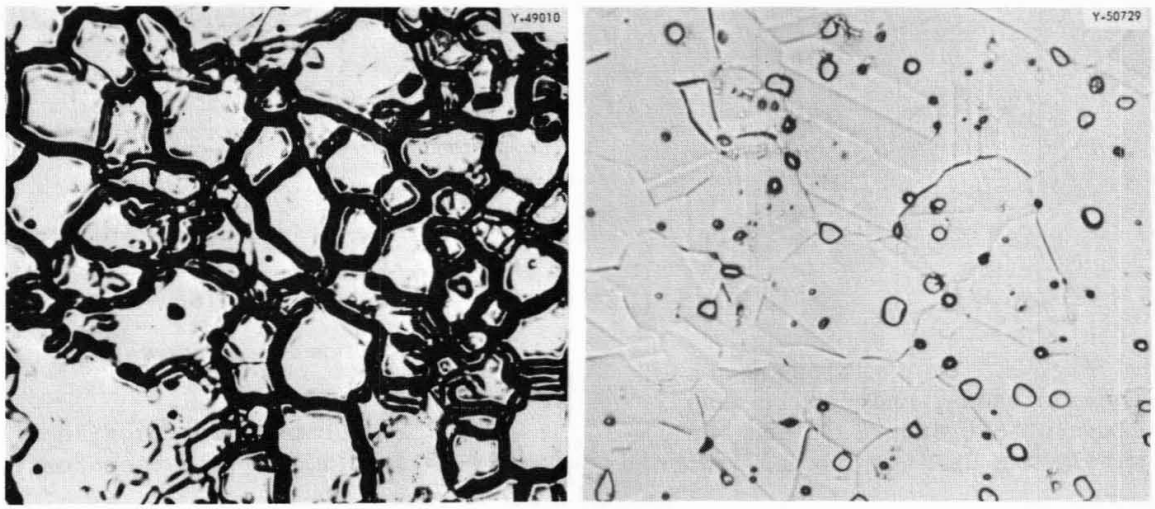

613 hr 6.59×10^{-4} mg/cm^2/hr 3453 hr 3.90×10^{-4} mg/cm^2/hr

Fig. 4. As-evaporated surfaces of type 316 stainless steel tested at 870°C and 8×10^{-9} torr for 613 and 3453 hr, Respectively. Original magnification, 200×.

PHOTO-62803

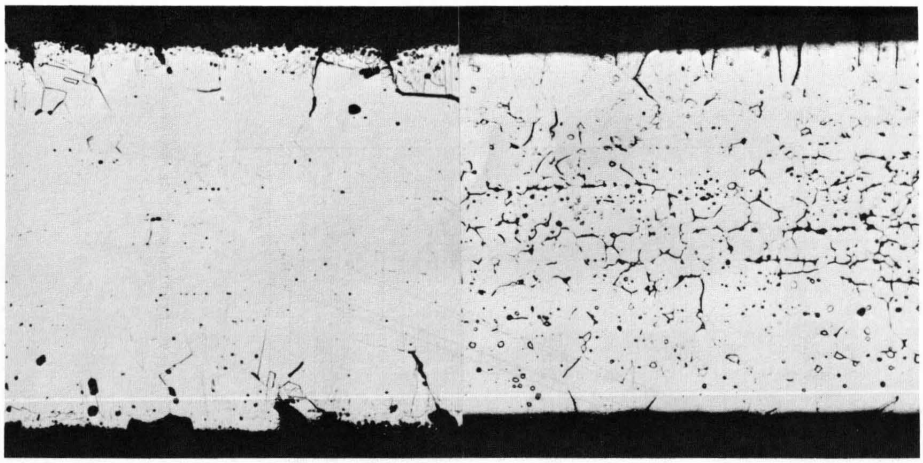

892 hr (Y-49174) 3453 hr (Y-50726)

Fig. 5. Cross section of type 316 stainless steel tested at 870°C and 8×10^{-9} torr for 892 and 3453 hr, respectively. Etchant: glyceria regia.

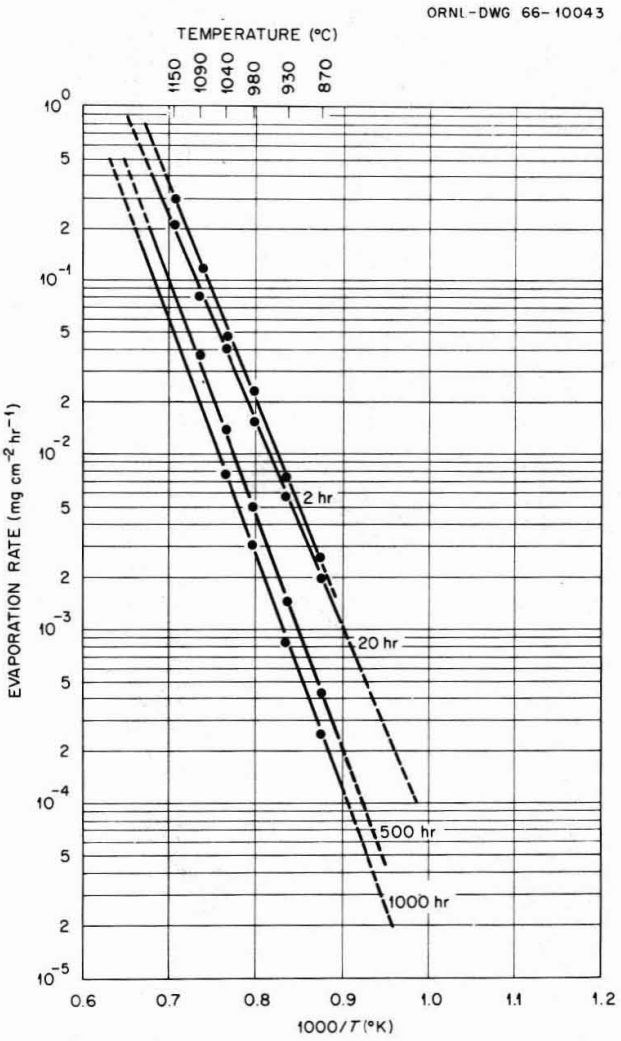

Fig. 6. Variations in the evaporation rate of Haynes-25 with time and temperature.

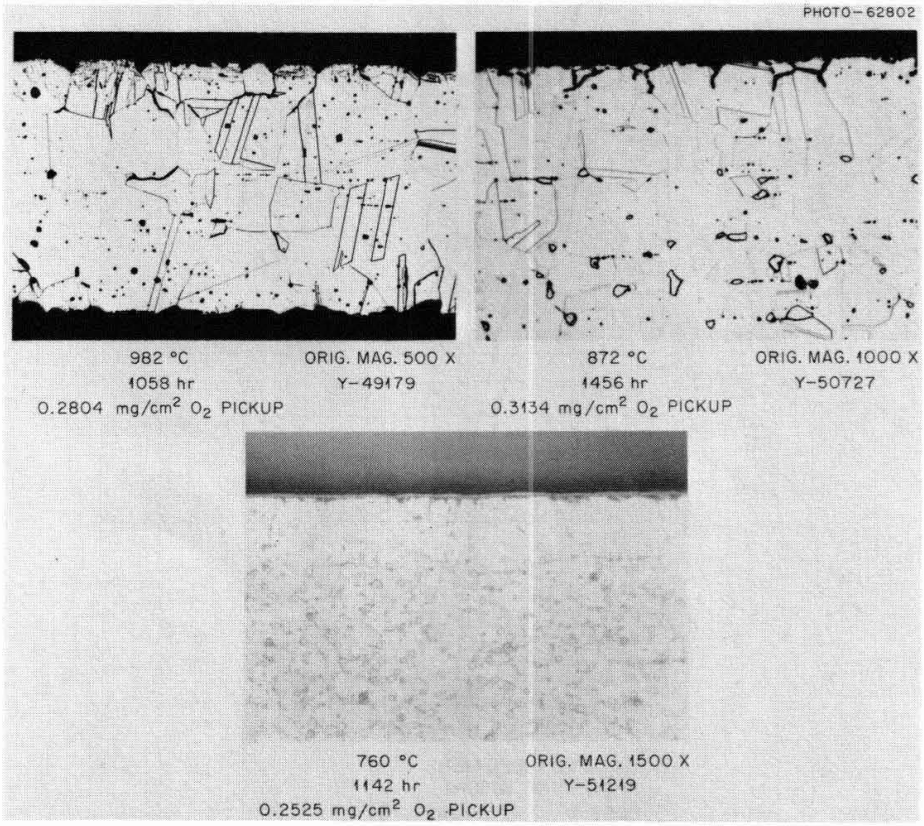

Fig. 7. Type 316 stainless steel oxidized in wet hydrogen and subsequently evaporation tested in high vacua.

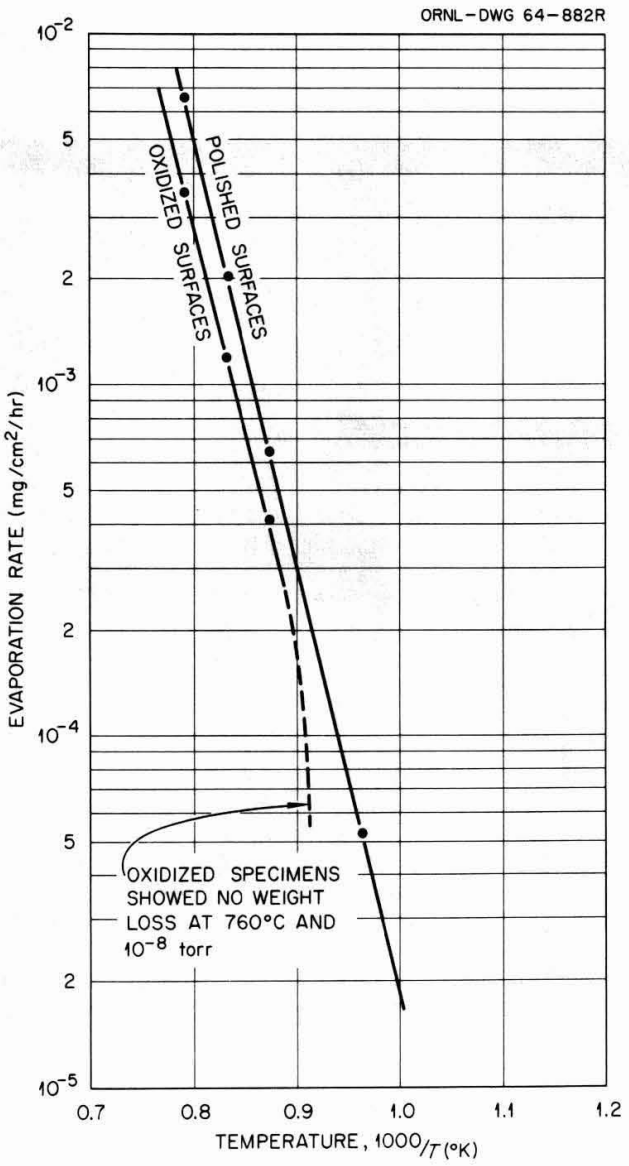

Fig. 8. Comparison of the final evaporation rates of type 316 stainless steel in both the polished and oxidized conditions.

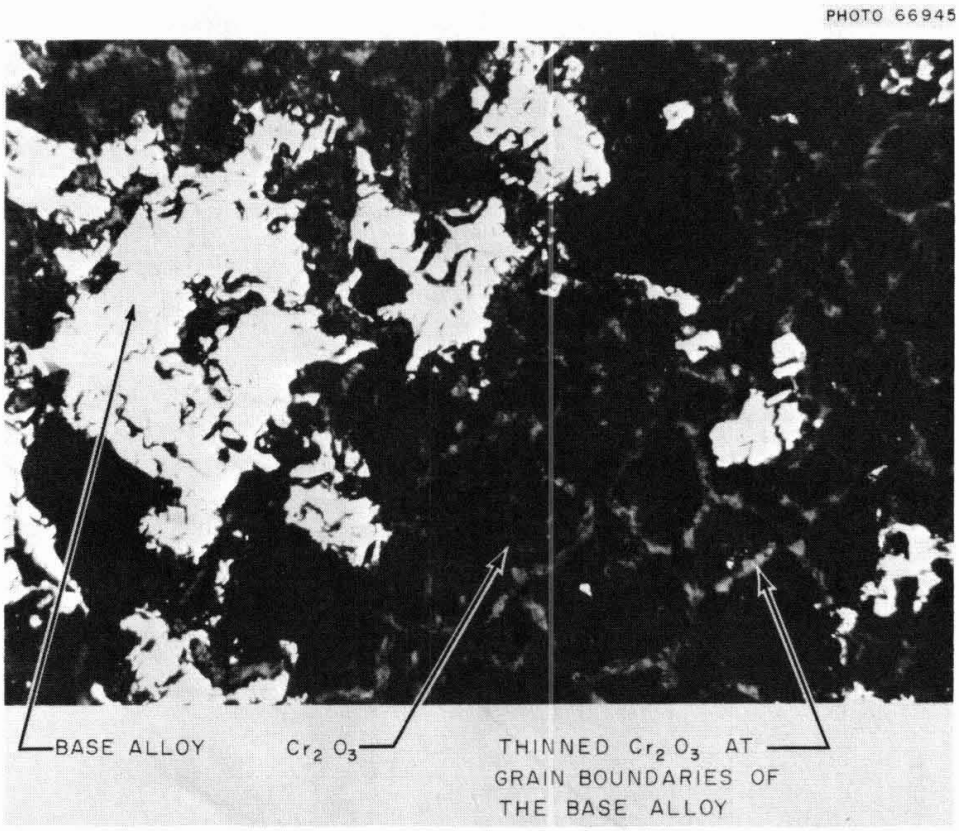

Fig. 9. As-evaporated surface of type 316 stainless steel oxidized in wet hydrogen and subsequently tested at 872°C and 2×10^{-8} torr for 2900 hr. 1500×.

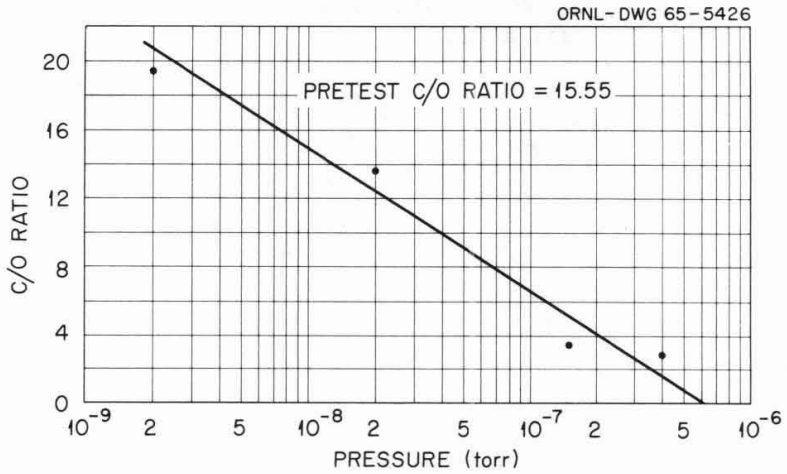

Fig. 10. Variation of the carbon-oxygen ratio in D-43 as a function of pressure at 1500°C.

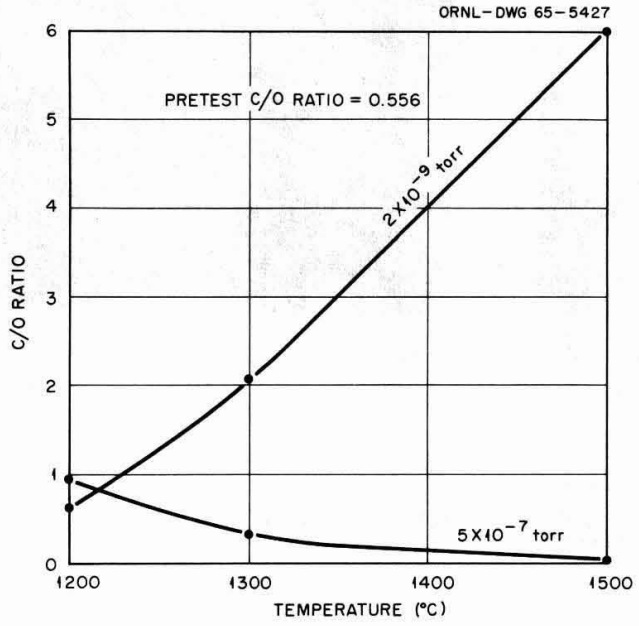

Fig. 11. Variation in the carbon-oxygen ratio in FS-80 as a function of temperature.

LAUNCH-PAD ACCIDENT ENVIRONMENTS*

S. L. Jeffers and F. D. Kite

Abstract

A determination of the effects of a launch-pad accident requires that the principal environments be well characterized. This paper discusses the environments of explosion and fire resulting from a missile abort on or near the launch pad.

Sandia Laboratories, Albuquerque, New Mexico

*This work was supported by the U. S. Atomic Energy Commission.

Introduction

The Aerospace Nuclear Safety Department, which has been in existence at the Sandia Laboratories for the past six years, is vitally concerned with all aspects of the safety of space nuclear systems.

All space nuclear systems are launched on chemical rockets which contain a tremendous inventory of highly combustible and explosive propellants. There is easily enough stored energy on board to completely disintegrate the nuclear system and its radioactive fuel if a mishap occurs on or near the launch pad. Our job is to determine if there is any way in which the destructive forces of a missile abort can be directed toward the nuclear system with sufficient energy to release the radioactive fuel to the biosphere. If such an event can happen, then we must determine its probability and the subsequent hazard.

The first step in assessing the overall hazard from a launch pad accident is to describe the environment to which the nuclear system would be exposed if a launch pad accident occurred. Since these accidents are all random events that vary from one extreme to another it is very difficult to arrive at an exact definition. We will describe here the environmental models which we have developed or are developing. Although they are not exact they are indispensable for a hazards analysis.

Our considerations of the hazards problems indicate that the on-pad abort of a space vehicle is a prime event for the potential release of radioactive material. The hostile environment of the on-pad accident is a compound of mechanical, thermal, and thermo-chemical forces. They may either independently or in combination rupture the primary fuel container of a radioisotopic generator.

Discussion

Safety analyses require quantitative definition of the launch-abort environment. Because very little quantitative information was available when we started this work, we had to learn about the environment of a launch-abort. Our present knowledge of the launch-abort environment has been gained through four principal activities: (1) Review of the literature; (2) review of launch accident reports; (3) monitoring of launches; and (4) testing programs.

Relatively straightforward analytical techniques are used once environment parameters associated with stress analysis for blast loading and heat-transfer analysis for fireball are defined. Experience has been that engineering judgment must be relied on heavily because of the uncertainty of some of the values assigned to the near-field on-pad accident environment.

Literature Review

The literature review for information concerning the blast and fire hazards of propellant systems was not very productive. The small amount of work that had been done was principally concerned with facilities siting problems. It had little or no relation to near-field environments such as a nuclear power supply would experience in the event of a catastrophic accident.

Review of Launch Accident Reports

Through the cooperation of the Office of Range Safety at Eastern Test Range we had the opportunity to review accident reports and motion picture films of aborts that had occurred on the Cape Kennedy launch sites. These reviews furnished some appreciation for the severity of a launch-abort as well as some quantitative data of explosive strength based on post-accident evaluations.

Monitoring of Launches

In order to improve the data from on-pad accidents, a system (Fig. 1) was designed and built to monitor launches from Eastern Test Range. This Pad-Abort Measuring System (PAMS) is designed to record twelve channels each of explosion and fire data. The Office of Range Safety at Eastern Test Range has been monitoring launches with PAMS since July, 1964 and has retrieved data from one accident in that time, the Atlas-Centaur abort of March 2, 1965.[1]

Testing Programs

The greatest single source of data concerning the hazards potential of an on-pad abort has been Project PYRO. We have participated in this program along with the USAF and NASA during the past four years. The overall objective of the study was to develop a reliable philosophy for predicting the credible damage potential which may be experienced from the accidental explosion of liquid propellants during launch or test operation of military missiles or space vehicles.

Three propellant combinations were chosen for this test program. The combination of nitrogen tetroxide (N_2O_4)/50% unsymmetrical dimethyl hydrazine (UDMH) plus 50% hydrazine (N_2H_4) was selected as representative of hypergolic propellants. (Hypergolic propellants are self-igniting when the fuel and oxidizer make contact.) The other two propellant combinations are the commonly used liquid oxygen (LO_2)/kerosene (RP-1) and the liquid hydrogen (LH_2)/liquid oxygen systems. The propellant combinations of N_2O_4/50% UDMH - 50% N_2H_4, LO_2/RP-1, and LO_2/LH_2 were tested in tanks of 200, 1000, and 25,000 pounds total propellant weight. We have taken advantage of the testing programs of others through the previously mentioned literature review.

The purpose of all these activities is and has been to develop an accurate description of the composite hostile environment of an on-pad accident including the mechanical forces from an explosion and the thermal forces from the fireball and residual fire.

The most frequently used measure for the explosive yield from liquid rocket propellants is percent TNT weight equivalence. This is a relatively easy way of characterizing the propellant's explosive yield because a large amount of work has been documented concerning the blast phenomena from TNT. The principal shortcoming of this method of characterizing liquid propellant explosions lies in the fact that, at short radii, different values for percent TNT weight equivalence are found between the peak overpressure and the pressure impulse data.

Essentially all aborts of liquid fueled missiles on or near the launch pad result in explosions. The severity (or yield) of the explosion is principally controlled by the amount of fuel and oxidizer that become mixed before detonation takes place. The amount mixed is definitely a random event and must be treated probabilistically. The explosive yield is also a function of the total propellant weight. In order to account for these two variables we define a yield-probability curve for a nominal weight and then ratio that curve up or down depending on the specific system under consideration.

To date we have defined a yield-probability curve for the LOX/LH_2 combination only. The yield-weight relation in this case is given approximately by

$$Y_2 = Y_1\left(\frac{W_1}{W_2}\right)^{1/3}$$

where Y_1 and Y_2 are explosive yields in percent TNT, and W_1 and W_2 are total propellant weights.

Fig. 2 shows a frequency vs yield plot of the 25,000 pound LH_2/LO_2 PYRO test data and a yield-probability curve scaled to 250,000 pounds. It should be pointed out that the data we used came from a controlled test program and not from a series of random aborts. As a consequence, the precise shape of the yield-probability curves and the scaling from one weight to another cannot be fully substantiated. We do feel, however, that as more abort data become available the refined curves will not be substantially different from the ones presented in Fig. 2.

Test results from the propellant combination of LO_2/RP-1 did not follow a smooth curve as did the LH_2/LO_2 but will still serve as an index of the expected frequency of a given yield. Yields are expected to be greater for liquid propellants in this ascending order: the hypergolic propellants, LH_2/LO_2, and LO_2/RP-1. The application of these yield values in the analysis of a specific launch vehicle requires the careful exercise of engineering judgment since we have virtually no data from tests of more than one propellant combination.

Solid rocket propellant vehicles or launch vehicles with solid components are not expected to contribute significantly to the probability of accidents or to increase the magnitude of the overall hazard.

The most frequent abort of solid vehicles has been loss of guidance after launch, with command destruct initiated by the range safety officer. Command destruct of a solid propellant vehicle does not generate a large homogeneous fireball like the liquid but separates into relatively small chunks of free-burning propellants.

Tests have shown that it takes a very high-order explosion (of the order of 150,000 pounds per square inch) to initiate detonation of most solid rocket propellants. Explosions of this strength are not available from the liquid propellants so we do not expect detonation of the solids.

The thermal environment from liquid propellants does not seem to vary as widely as the explosion environment. The thermal energy from an abort will be instantaneously very high as the initial explosion occurs, diminishing as the fireball grows and lifts off to the lower energy level of the residual fire from atmospheric combustion of the remaining fuel. We have developed a model of the thermal environment (Fig. 3) which can be applied to any liquid-propellant launch vehicle. The abscissa, time, has been normalized to the cube root of total propellant weight.

Following fireball liftoff, a stem develops connecting the rising fireball to the pad surface (Fig. 4). From observation of pad aborts, the duration of this "hot" stem is about 50 percent of liftoff time. The sharp break shown on the thermal model graph represents the transition from the payload being engulfed in the stem combustion zone to the payload receiving radiant energy from the rising fireball, which by the end of the stem duration already is a considerable distance above the pad surface.

The heat flux, shown as the left-hand ordinate in Figure 3, is the flux incident on the surface of an object enveloped by the fireball. The right-hand ordinate is the corresponding effective black body radiating temperature of the fireball. After the fireball has lifted and no longer provides significant radiation to the pad surface, the residual fire will provide a heat flux of about 13 BTU/sec-ft^2. Residual fire duration can easily be as long as an hour.

The model is considered to be applicable to all liquid propellant combinations. Theory indicates that fireball temperatures should not vary appreciably for liquid hydrocarbon fuels, and measurements of fireballs from both cryogenic and hypergolic propellants have consistently indicated surface temperatures of 4400 to 4600° F.

The high thermal energies in the fireball environment of an abort may have the potential to start significant corrosive or erosive reactions to containment materials. To evaluate potentially hazardous reactions, TRW Systems investigated for us the chemical integrity of radioisotope containment materials in launch-abort environments.[3,4] The duration of the thermal pulse is too short in most cases to initiate thermochemical reactions which would be considered hazardous--i. e., cause significant loss of containment material. There are four

situations which may be hazardous under certain conditions: beryllium burns with a "breakaway" reaction at 2400°F in a water vapor environment, the cobalt-based super-alloy Haynes 25 forms a eutectic with carbon at 2100°F, tantalum-tungsten alloys will not survive long in an oxidizer-rich combustion environment, and graphitic materials burn rapidly in oxygen-rich environments.

Future Plans

Our efforts will continue to be directed toward gaining more knowledge and increased confidence in our description and modeling of the on-pad accident environment. The explosive yields of the propellants will be modeled so they can be used as inputs to existing computer codes for stress analysis to determine the survivability of a radioisotope power source. The thermal environment model will also be used for inputs to heat transfer codes to determine if melt of the various engineering materials will occur. Thermochemical effects will probably continue to be evaluated on a "by hand" basis from examination of the outputs from thermal analysis.

Summary

Blast modeling is currently done on a system-to-system basis and considers the type and weight of propellants aboard the launch vehicle. Percent TNT weight equivalents of the propellants are used as a basis for blast modeling and these are used in conjunction with classical explosion shock-wave formulae to analyze the effect on system components.

A model of the on-pad abort thermal environment from liquid rocket propellants has been developed. This model considers the heat flux to which the payload from an aborted vehicle would be exposed as that payload falls through a growing fireball and comes to rest near the center of the launch area. Tests have shown that the intensity of the heat flux from different propellant combinations is approximately the same for all with the fireball duration dependent on a cube root function of propellant weight.

The magnitude of the effects of these environments varies from negligible to catastrophic and the compound analysis of a specific system requires careful consideration of the possible sequences of the hostile environments.

REFERENCES

1. F. D. Kite, B. E. Bader, and D. M. Webb, Sandia Corporation, and C. N. Golub, Pan-American Airways, Launch Hazards Assessment Program, Report on Atlas-Centaur Abort, SC-RR-65-333, October 1965.
2. L. J. Van Nice and H. J. Carpenter, Thermal Radiation from Saturn Fireballs, TRW Systems, Inc., Task ASPO-24, Contract No. NAS9-4810, December 1965.
3. J. L. Blumenthal and M. J. Santy, An Experimental Investigation of the Behavior of Beryllium in Simulated Launch Abort Environments, TRW Systems for Sandia Corporation, SC-DC-65-1637, July 1965.
4. J. L. Blumenthal, J. D. Kuenzly, and M. J. Santy, Study of the Chemical Integrity of Radioisotope Containment Materials in Launch Abort Environments, TRW Systems for Sandia Corporation, SC-CR-66-2044, April 1966.

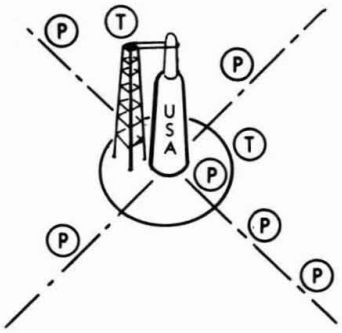

SIGNAL CONDITIONING & MAGNETIC TAPE RECORDING STATION IN BLOCKHOUSE

(T) THERMAL SENSOR STATIONS (2)

- 4 THERMOCOUPLES
- 1 RADIOMETER
- 1 CALORIMETER

(P) PRESSURE TRANSDUCERS (12)

Figure 1. Diagram of Pad-Abort Measuring System

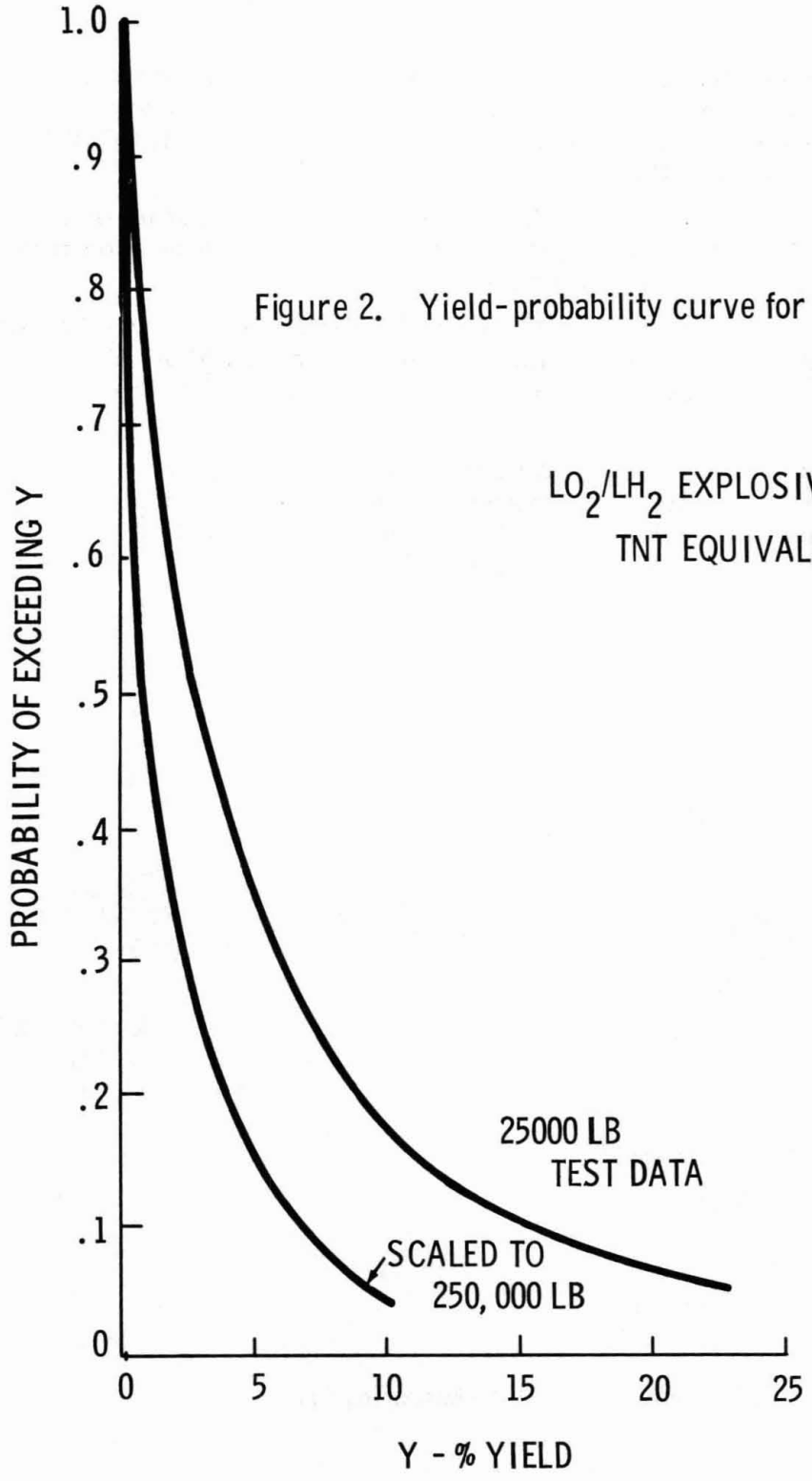

Figure 2. Yield-probability curve for LO_2/LH_2

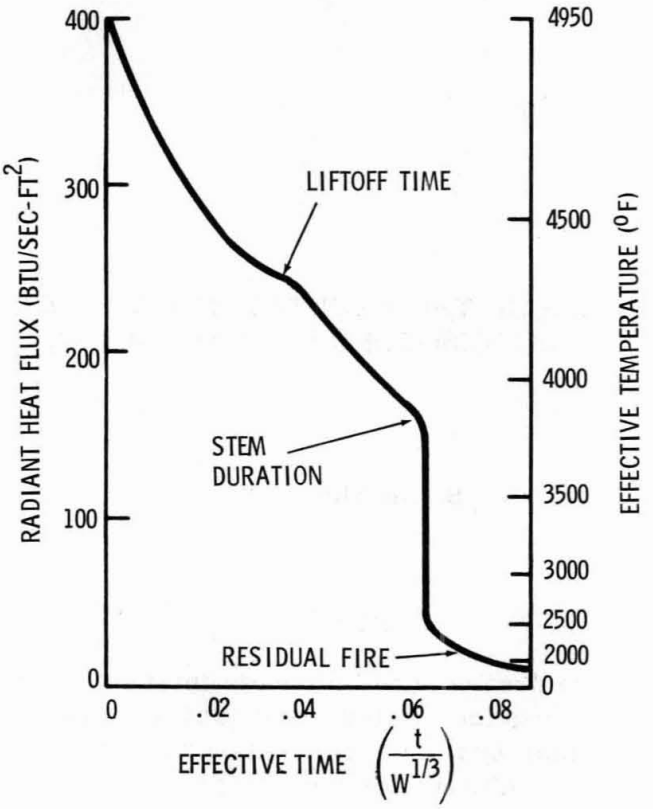

Figure 3. Predicted pad abort thermal environment

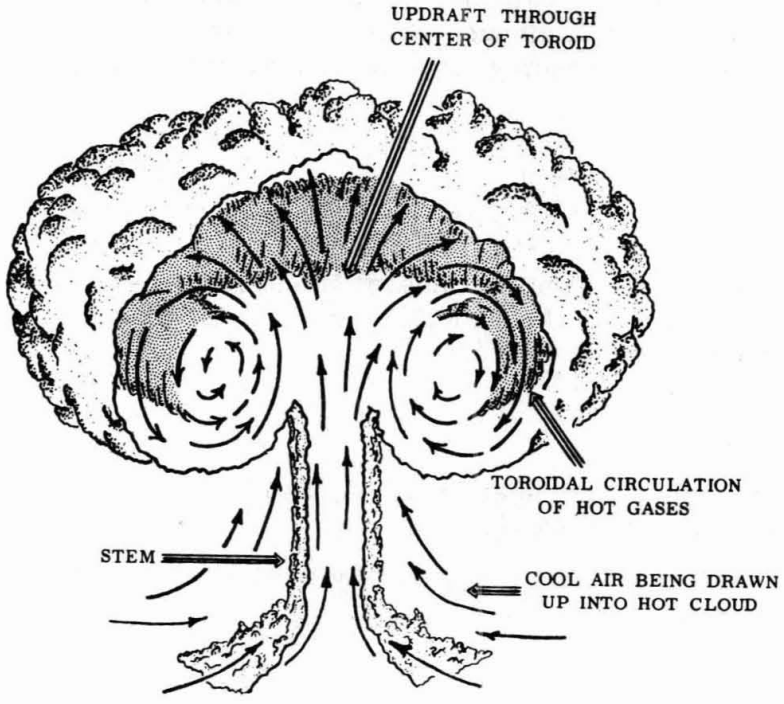

Figure 4. Artist's conception of explosion fireball

EFFECTS OF THE REENTRY ENVIRONMENT ON RADIOISOTOPE HEAT SOURCES*

S. McAlees, Jr.

Abstract

Use of radioisotope heat sources in space missions requires that adequate safety be provided in the event that mission aborts lead to reentry of the nuclear system. The initial reentry conditions, along with the spacecraft configuration resulting from the abort, define the environment to which the nuclear system is exposed.

A typical program conducted jointly by the system contractor, government agencies, and Sandia Laboratories to define the environment and system response is discussed. Materials and design concepts selected to provide intact reentry for a particular system are presented.

Acknowledgment

The author is indebted to General Electric Company for Table IV and Figs. 8, 9, and 14 through 19, and for some ideas expressed in Reference 1.

Reentry & Space Sciences Division, Sandia Laboratories, Albuquerque, New Mexico.

*This work was supported by the United States Atomic Energy Commission.

Introduction

Safe reentry of radioactive power sources is of prime concern for spacecraft missions. A nuclear fuel capsule produces power continuously for long periods of time, so that, normally, reentry and fuel release sooner than 10 times the isotope half-life may present a radiation hazard to the populace.[1] The major hazard is the introduction of the isotopes into the bodies of persons inhaling or ingesting the released material, either directly or at the end of an ecological chain. Early SNAP (Systems for Nuclear Auxiliary Power) systems employing system burn-up and high altitude fuel release have been accepted as nonhazardous. However, the probability of aborts which could prevent attainment of high altitude orbits and the expected increase in number of flights and quantities of radioactive fuel restrict the early approach and emphasize the desirability of intact reentry.

Abort situations that produce the reentry environments which impose problems for intact reentry stem from three conditions: (1) Malfunction of the system at high velocity but prior to achieving orbit; (2) natural decay from either short- or long-lived orbit; and (3) super-orbital return from lunar or planetary missions. Other environments that challenge fuel capsule integrity include: pad abort fireballs and after-fire, booster explosion and flying debris. These challenges must be considered in addition to the natural reentry environment.

Evaluation of the Reentry Environment

Perhaps the single most important parameter which determines the reentry environment is the ballistic coefficient $\left(\frac{W}{C_D A}\right)$. The influence of the ballistic coefficient on various trajectory parameters is shown in the simplified equations[2] of Table I. The relation between the ballistic coefficient and reference convective heating rate $(\dot{q}\sqrt{R})^*$ is shown graphically in Fig. 1. For a fixed reentry velocity and angle, an increase in ballistic coefficient produces higher heating rates and increased total integrated heat.

Typical mission requirements and potential abort situations for current SNAP systems produce the trajectory velocity and altitude versus time histories[3] shown in Figs. 2, 3, and 4. The reference cold wall convective heating rates for selected pre-orbital abort, earth orbital decay and lunar return trajectories are shown in Figs. 5, 6, and 7. In addition to the reentry heating environment, deceleration and pressure loads pose specific problems to intact heat source design. Reentry environmental parameters are summarized in Table II.

---

* $\dot{q}$ ≡ convective heating rate, Btu/ft^2-sec
R = spherical radius, ft.

Reentry Vehicle Concepts

The problems of intact reentry of radioactive heat sources are significantly different from those of the typical ICBM reentry: (1) The orbital decay reentry can be several orders of magnitude longer in time duration. (2) The shallow reentry angle provides little aid to vehicle aerodynamic stability through rapidly increasing dynamic pressure. (3) Since provision must be made for rejection of internally generated heat, intact reentry cannot be assured by the mere addition of insulation and ablation materials. (4) Planned SNAP missions require consideration of orbital decay and high angle lunar return trajectories so that either high heating rates or high total integrated heat may be expected. (5) The reentry vehicle which protects the fuel source may be attached to or contained in other spacecraft components. (6) In an abort situation, the R/V (reentry vehicle) may be constrained by or separated from the parent vehicle in an adverse manner, leading to stagnation heating conditions or high angular vehicle rates at low altitudes.

To meet the problems of intact reentry of radioactive heat sources, two vehicle design concepts have been applied in recent SNAP programs. Aerodynamically oriented vehicle and omnidirectional vehicle designs are shown in Figs 8 and 9, respectively. The aerodynamic vehicle uses a low-density ablation material, ESM (elastomeric shield material), heat protection system on the nose and flare. The radioisotope capsule, located within a beryllium cylindrical section, transfers heat to the cylinder by radiation. The cylinder is located in a separated flow region where, for low angles of attack, a minimum of aerodynamic heating is experienced. Vehicle stability is provided by the flare. The reentry cask design is predicated on free flight prior to onset of aerodynamic heating in an orbital decay trajectory.

Based on the orbital decay trajectory and reference heating rates previously discussed, an aerothermodynamic analysis was conducted to determine the temperature response of the beryllium cylindrical section and the Haynes 25 fuel capsule. Vehicle angle-of-attack decay[3] is shown in Fig. 10. The average heating rate ratios,[4] which relate local heating rates on the rotating cylinder to the trajectory reference rates, are shown for angles-of-attack from 0 to 20 degrees in Fig. 11. These inputs, when applied to the thermal model shown in Fig. 12 and Table III, generated the temperatures reached on the beryllium cylinder and capsule wall. If a particular node on the beryllium cylinder reached the melt temperature (solidus - 2345°F), that location on the cylinder was assumed to fail and the node was removed, allowing the aerodynamic heating to be applied directly to the Haynes 25 on the fuel capsule wall. Results of this analysis, revealing maximum cylinder and fuel capsule temperatures of near 1740°F and adequate earth orbital decay reentry capabilities, are shown in Fig. 13.

The omnidirectional vehicle concept, applied to both superorbital and earth orbital reentries, is an outgrowth of the original aerodynamic design. The reinforced graphitic material around the cask provides thermal protection by reradiation and ablation for any vehicle attitude during reentry. This concept, using a columbium/silver/silicon-dioxide secondary heat shield thermal switch system, was studied for reentries involving vehicle spin, tumble and stable orientations. The silver conductors carry away the internal heat generated prior to reentry; during reentry the conductors melt and thus prevent the external aerodynamic heating from being conducted inward and raising the temperature of the fuel capsule. Later analyses indicated that capsule temperature could be improved (300°F lower) by replacing the columbium/silver/silicon-dioxide system with a beryllium heat sink. Results of the thermal analysis[5] for the lateral spin and planar tumble cases are summarized in Figs 14, 15, and 16, and Table IV. Results of the oriented reentry analyses for the orbital decay case are shown in Figs. 17, 18, and 19.

For the oriented reentry at high-angle superorbital conditions, cask surface temperatures of 5000°F may be expected.

Conclusions

Many vehicle configurations, materials and heat protection systems have been used to successfully reenter nonradioactive payloads. But unique problems associated with use of radioactive payloads limits use of this proven reentry technology. Several heat protection systems, involving combinations of ablation, separated flow, reradiation, thermal switch and heat sink concepts have been demonstrated theoretically to provide fuel capsule protection against SNAP reentry environments. These concepts have been applied to aerodynamic and omnidirectional vehicle designs. Of these, systems that combine the omnidirectional vehicle with ablation/reradiation/heat sink concepts to protect the fuel directly appear most attractive in view of today's technology.

Additional safety may be afforded future SNAP systems through active or passive transpiration cooling, development of new fuel forms (matrix, solid solution, etc.) and aerodynamic shaping of fuel forms. Safety may also be enhanced by providing system redundancy through sequential packaging of "intact" or "safe" components. For example, one could contain an intact fuel form in an intact capsule, in turn contained in an intact reentry vehicle.

Ultimately, for economic and "absolute" safety considerations, controlled-intact vehicles allowing fuel recovery and re-use at end of space life would be desirable.

REFERENCES

1. M. J. Brunner, C. V. Dohner, and R. L. Lawit, Re-Entry of Radioactive Power Sources, Journal of Spacecraft and Rockets, 5 (4), April 1968, pp. 448-453.
2. H. Julian Allen and A. J. Eggers, Jr., A Study of the Motion and Aerodynamic Heating of Missiles Entering the Earth's Atmosphere at High Supersonic Speeds, NACA TN 4047, October 1957.
3. S. McAlees, et al., Aerothermodynamic Analysis of the SNAP 27 Fuel Cask, SC-RR-66-611, September 1966.
4. R. E. Berry, R. D. Klett, D. W. Larson, and H. R. Spahr, Aerothermodynamic and Structural Analyses of the SNAP 27 Fuel Cask, SC-RR-66-2651, January 1967.
5. SNAP 27 Quarterly Report No. 10, Contract No. AT(30-1)-3535, January 1, 1968 to March 31, 1968, General Electric Missiles and Space Division.

TABLE I

INFLUENCE OF BALLISTIC COEFFICIENT ON VARIOUS TRAJECTORY PARAMETERS

EQUATIONS OF MOTION	$\begin{cases} \frac{d^2y}{dt^2} = -g + \frac{C_D \rho V^2 A}{2M} \sin\theta \\ \frac{d^2x}{dt^2} = \frac{C_D \rho V^2 A}{2M} \cos\theta \end{cases}$
VELOCITY	$V = V_E e^{-\frac{C_D \rho_o A}{2\beta M} e^{-\beta y}}$
ALTITUDE OF MAX. DECELERATION	$y_1 = \frac{1}{\beta} \ell n \frac{C_D \rho_o A}{\beta M \sin\theta_E}$
MAXIMUM DECELERATION	$-\left(\frac{\frac{dV}{dt}}{g}\right)_{Max} = -\left(\frac{\frac{dV}{dt}}{g}\right)_1 = \frac{\beta V_E^2 \sin\theta_E}{2ge}$
ALTITUDE OF MAX HEATING RATE	$y_3 = \frac{1}{\beta} \ell n \left(\frac{3C_D \rho_o A}{\beta M \sin\theta_E}\right)$
MAXIMUM HEATING RATE	$\left(\frac{dH_s}{dt}\right)_{Max} = 6.8 \times 10^{-6} \sqrt{\frac{\beta M \sin\theta_E}{3eC_D \sigma A}} V^3$

TABLE II

REENTRY ENVIRONMENTAL PARAMETERS FOR SNAP VEHICLES
ENTERING THE EARTH'S ATMOSPHERE

SYSTEM	$\dot{q}\sqrt{R}_{max}$	$\int \dot{q}\sqrt{R}$	P_{T_2} (Atm)	DECELERATION (g)
SNAP 38° Lunar Return	1672	9108	5.4	206.0
SNAP 20° Lunar Return	1350	13500	3.0	115.0
SNAP 6.25° Lunar Return	454	25091	0.37	14.2
SNAP EARTH ORBITAL DECAY	90	42070	0.17	6.98
SNAP PRE-ORBITAL ABORT	303	8487	1.43	25.2

$\dot{q}$ ≡ Convective heating rate, Btu/ft^2-sec

R ≡ Spherical radius, ft

$\dot{q}\sqrt{R}$ ≡ Reference convective heating rate, Btu/ft$^{3/2}$-sec

P_{T_2} ≡ Vehicle total pressure, ATM

g ≡ Acceleration due to gravity (Note: Deceleration is measured in g's.)

TABLE III

FUEL CASK THERMAL MODEL

Node	Material	Node Weight (lb)	Radial Location (in.)
1	Beryllium	0.103	1.9
2	Beryllium	0.162	1.9
3	Beryllium	0.162	1.9
4	Beryllium	0.162	1.9
5	Beryllium	0.162	1.9
6	Beryllium	0.162	1.9
7	Beryllium	0.140	1.9
8	Haynes 25	0.091	1.17
9	Haynes foam	0.103	0.981
10	Haynes foam	0.103	0.711
11	Haynes foam	0.103	0.516
12	Haynes 25	0.394	1.17
13	Fuel	--	0.976
14	Fuel	--	0.7325
15	Haynes 25	0.394	1.17
16	Fuel	--	0.976
17	Fuel	--	0.7325
18	Haynes 25	0.394	1.17
19	Fuel	--	0.976
20	Fuel	--	0.7325
21	Fuel	--	0.976
22	Fuel	--	0.7325
23	Haynes 25	0.394	1.17
24	Haynes foam	0.1128	0.981
25	Haynes foam	0.1128	0.711
26	Haynes foam	0.1128	0.516
27	Fuel	--	0.976
28	Fuel	--	0.7325
29	Haynes 25	0.394	1.17
30	Fuel	--	0.976
31	Fuel	--	0.7325
32	Haynes 25	0.394	1.17
33	Fuel	--	0.976
34	Fuel	--	0.7325
35	Haynes 25	0.394	1.17
36	Fuel	--	0.976
37	Fuel	--	0.7325
38	Haynes 25	0.098	1.17
39	Haynes foam	0.103	0.981
40	Haynes foam	0.103	0.711
41	Haynes foam	0.103	0.516

TABLE IV

OMNIDIRECTIONAL FUEL CASK PEAK TEMPERATURES FOR ORBITAL DECAY AND LUNAR RETURN TRAJECTORIES

	EARTH ORBITAL LATERAL SPIN	6.25° S.O.PL.* TUMBLE SIDE HEAT	38° S.O.PL.* TUMBLE SIDE HEAT
GRAPHITE O.D.	2543°F @ 6260 sec.	3700°F @ 82 sec.	4750°F @ 12 sec.
GRAPHITE I.D.	2451°F @ 6260 sec.	3004°F @ 90 sec.	2794°F @ 18 sec.
Be O.D.	2027°F @ 6300 sec.	1822°F @ 160 sec.	1349°F @ 185 sec.
Be I.D.	2021°F @ 6310 sec.	1816°F @ 170 sec.	1351°F @ 185 sec.
CAPSULE O.D.	2008°F @ 6370 sec.	1784°F @ 284 sec.	1498°F @ 201 sec.
LINER I.D.	2158°F @ 6560 sec.	1937°F @ 404 sec.	1680°F @ 201 sec.
MAX. Δ T from Be O.D. to I.D.	28°F @ 6270 sec.	52°F @ 100 sec.	30°F @ 20 sec.

*S. O. PL. ≡ Superorbital planar

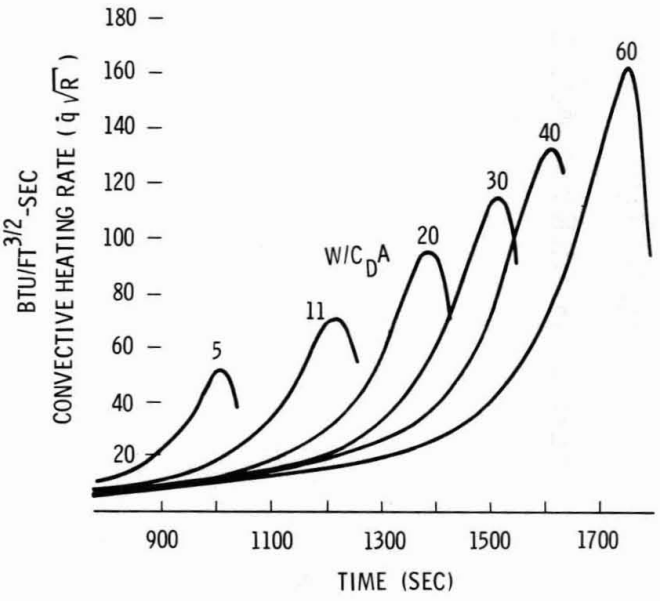

Figure 1. Reference convective heating rates for earth orbital decay — constant ballistic coefficient

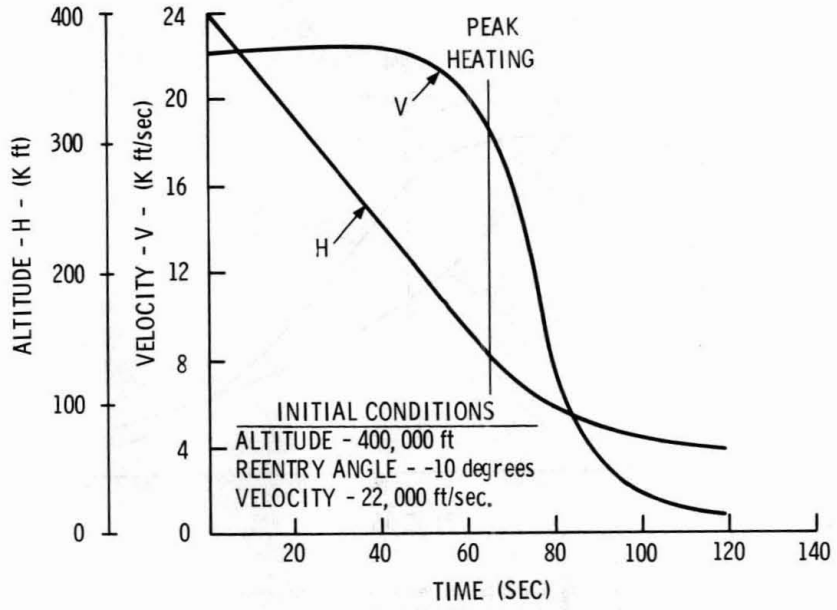

Figure 2. Velocity and altitude versus time for pre-orbital abort of a SNAP fuel cask

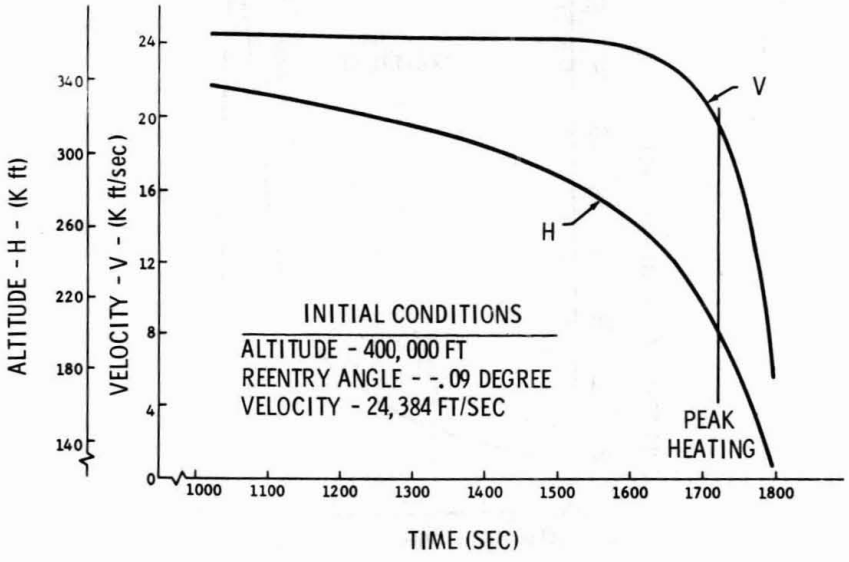

Figure 3. Velocity and altitude versus time for earth orbit reentry of a SNAP fuel cask

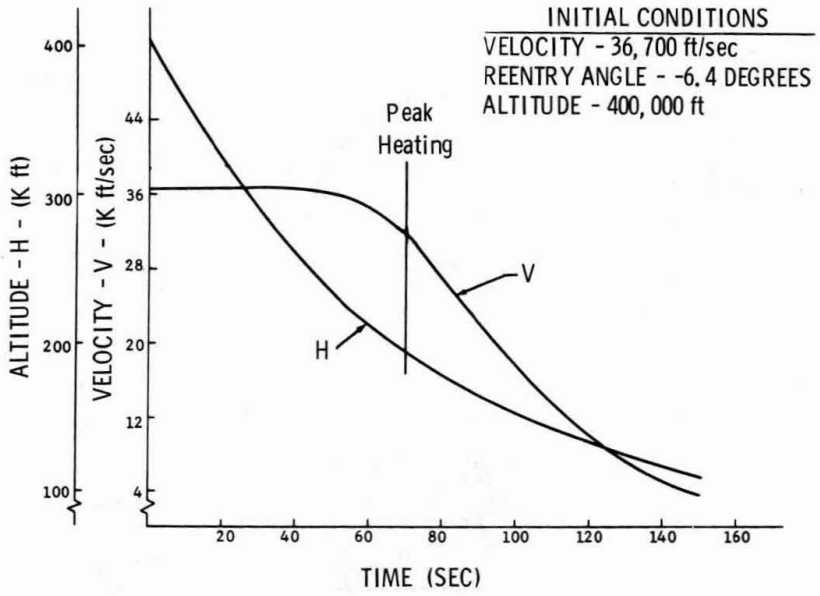

Figure 4. Velocity and altitude versus time for supercircular reentry (γ_ϵ = -6.4°) of a SNAP fuel cask

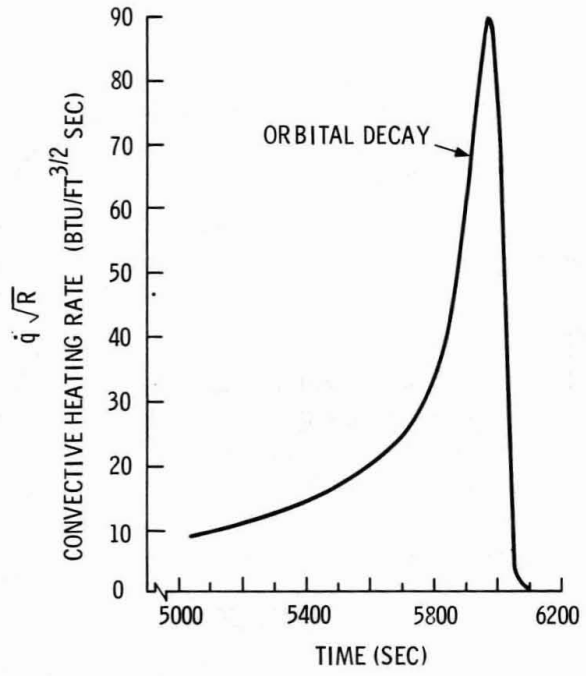

Figure 5. Reference convective heating rate for SNAP vehicle in earth orbital decay trajectory

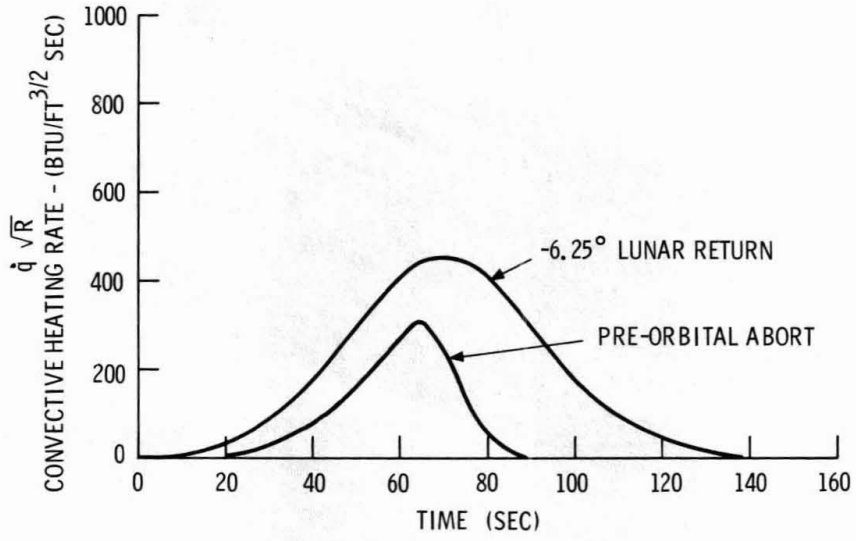

Figure 6. Reference convective heating rates for SNAP vehicle in pre-orbital abort and shallow angle lunar return trajectories

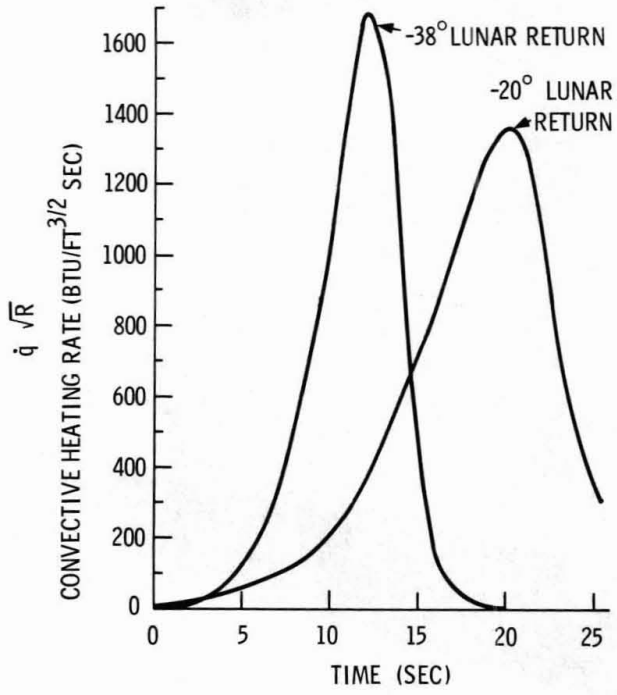

Figure 7. Reference convective heating rates for SNAP vehicle in high angle lunar return trajectories

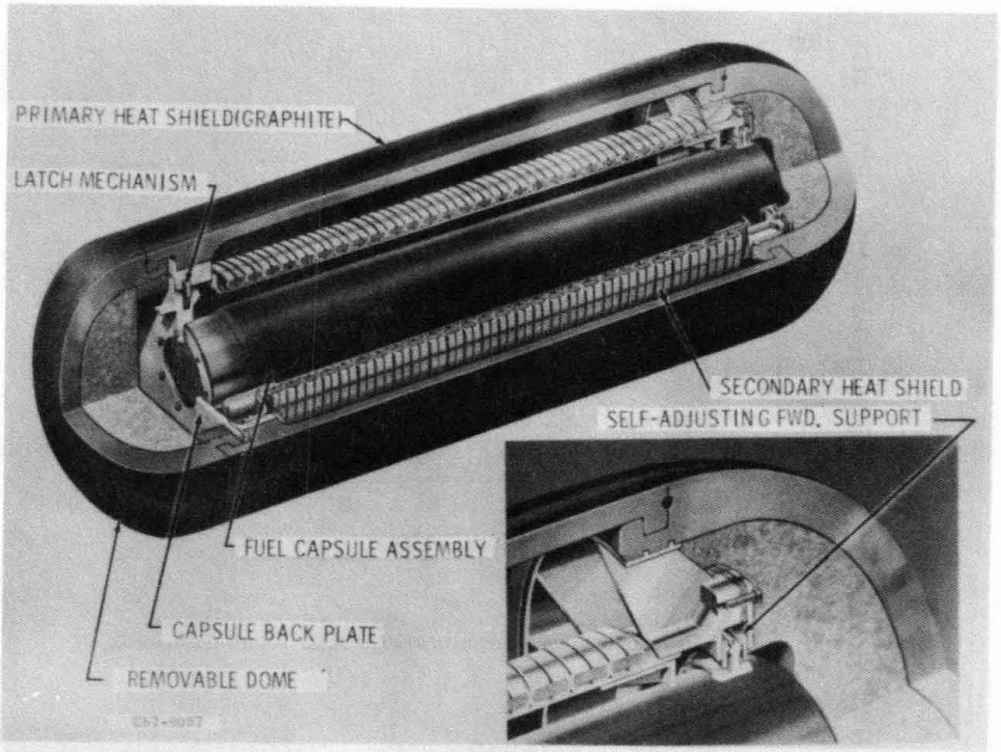

Figure 9. Omnidirectional reentry vehicle

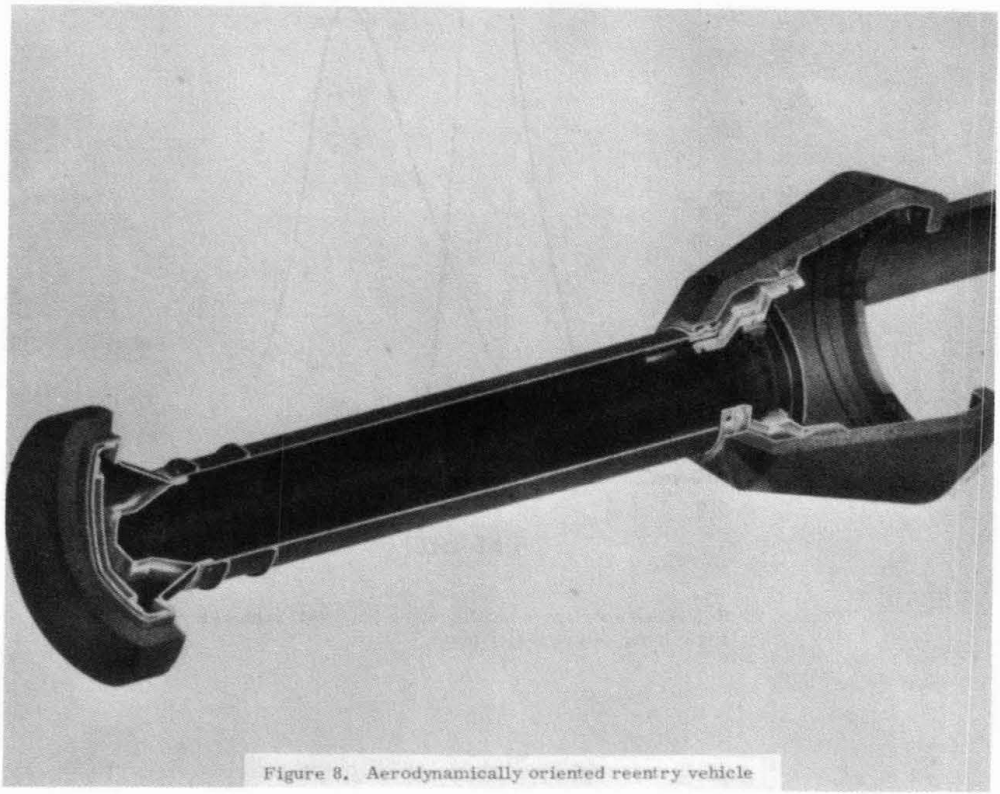

Figure 8. Aerodynamically oriented reentry vehicle

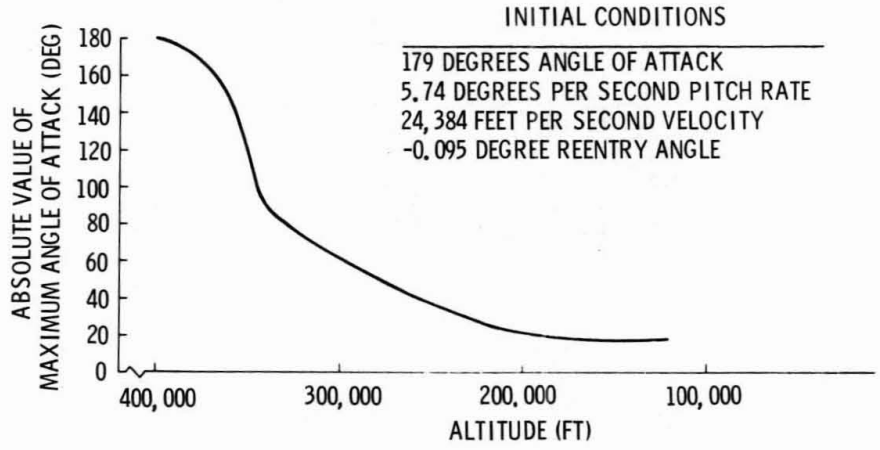

Figure 10. Maximum angle of attack as a function of altitude for the SNAP fuel cask – orbital decay reentry

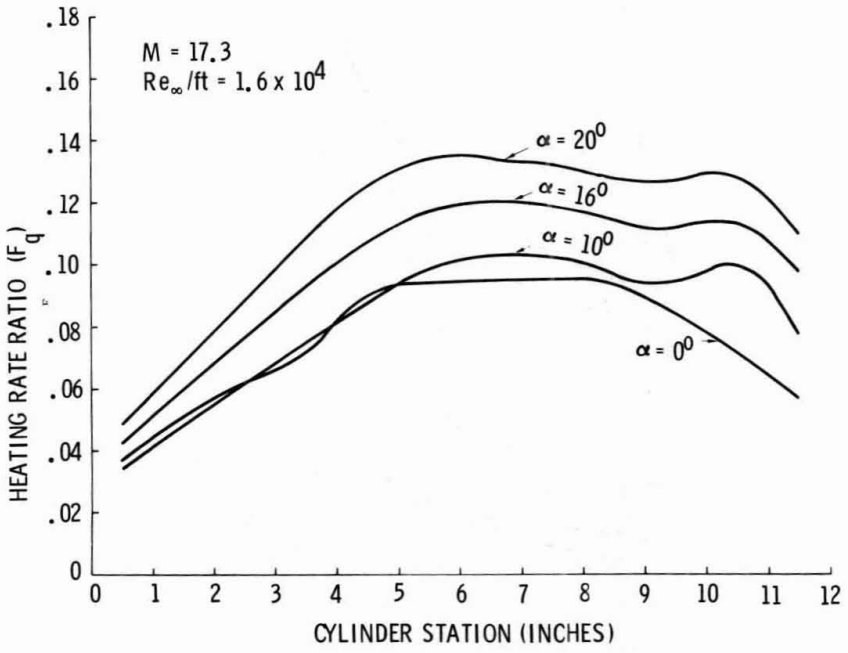

Figure 11. Average heating ratios for a rotating SNAP fuel cask

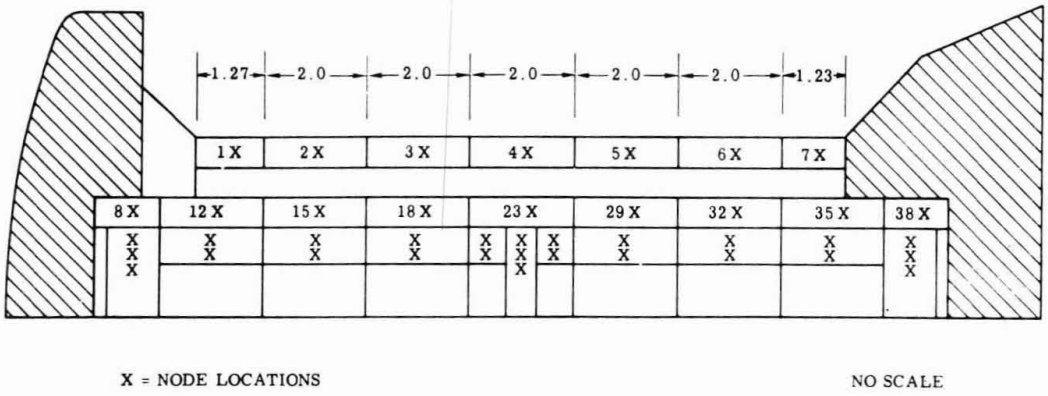

Figure 12. Thermal model of fuel cask — centerbody

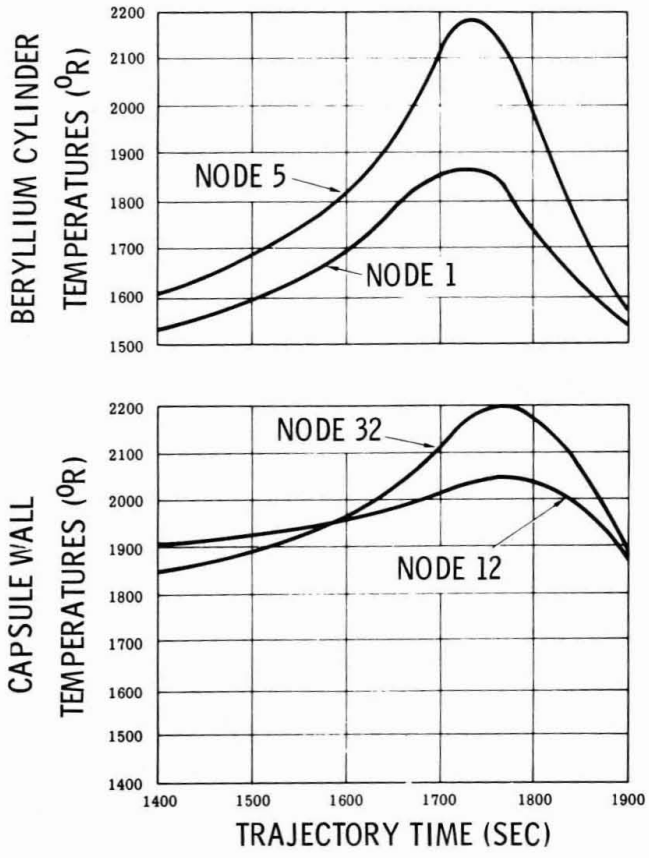

Figure 13. Temperature ranges for orbital decay — nominal heating

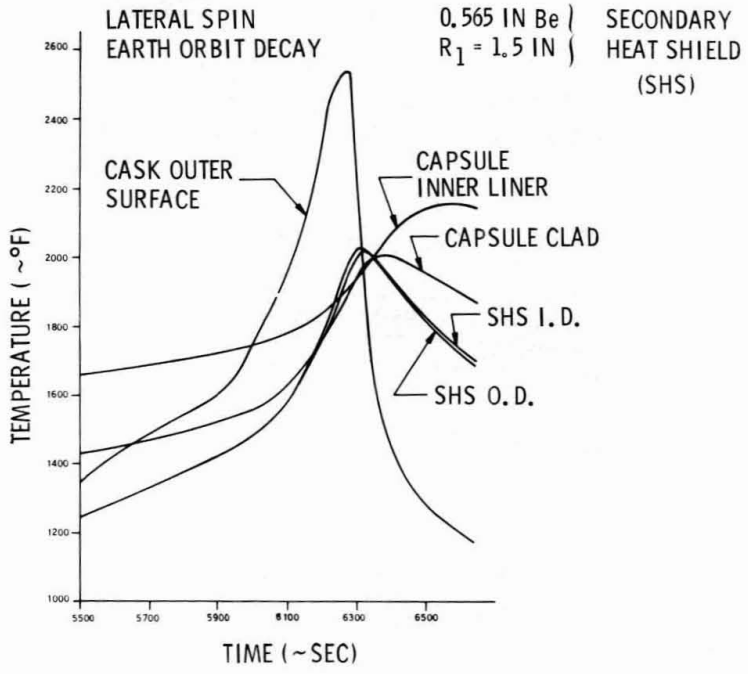

Figure 14. Omnidirectional fuel cask temperature response for orbital decay reentry

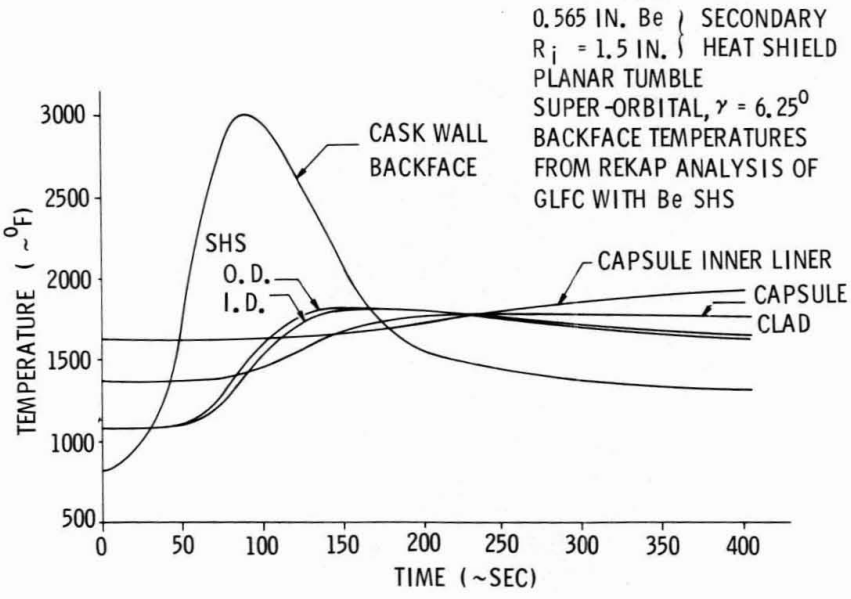

Figure 15. Omnidirectional fuel cask temperature response for shallow angle lunar return trajectory

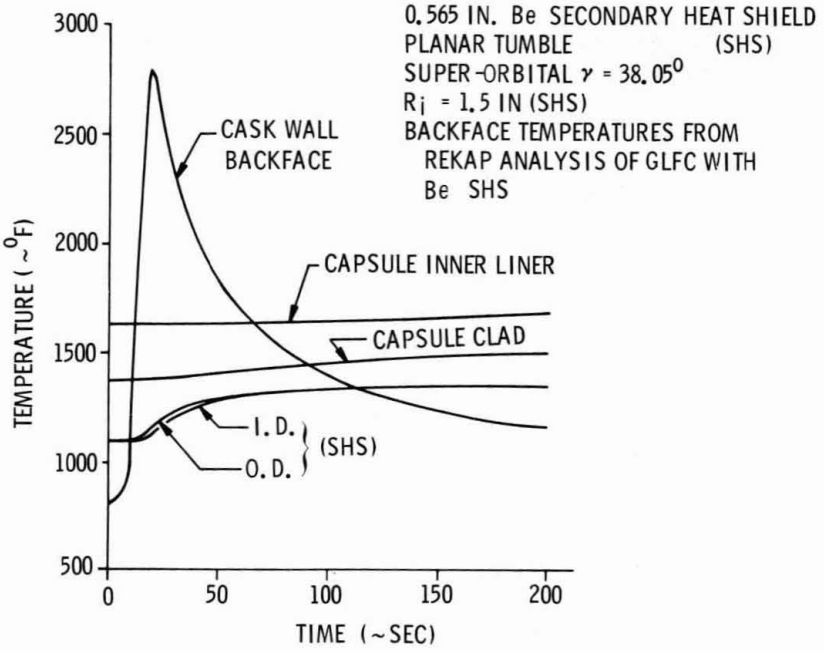

Figure 16. Omnidirectional fuel cask temperature response for high angle lunar return trajectory

MAXIMUM CASK WALL RADIAL GRADIENT

EARTH ORBIT DECAY
ORIENTED CASK
LM SHIELD REMOVED AT 300K FT (5900 SEC)

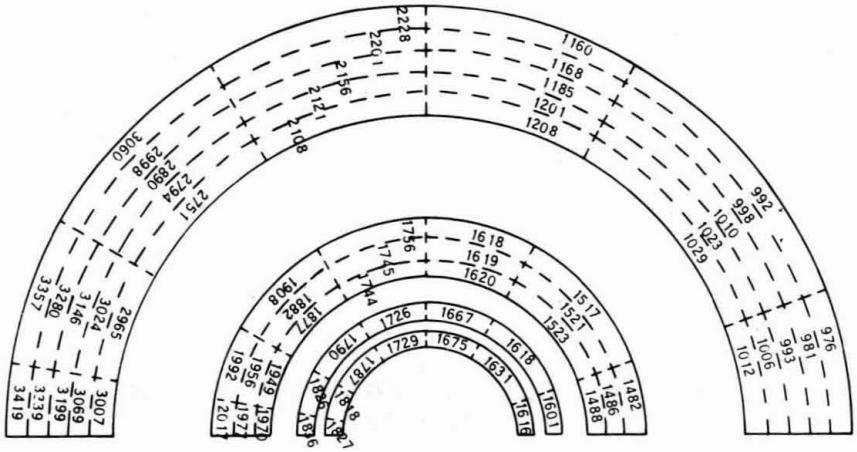

Figure 17. Fuel cask temperature response for oriented earth orbital decay — maximum radial gradient

MAXIMUM CASK WALL TEMPERATURE
MAXIMUM CASK WALL CIRCUMFERENTIAL GRADIENT

EARTH ORBIT DECAY
ORIENTED CASK
LM SHIELD REMOVED AT 300K FT (5900 SEC)

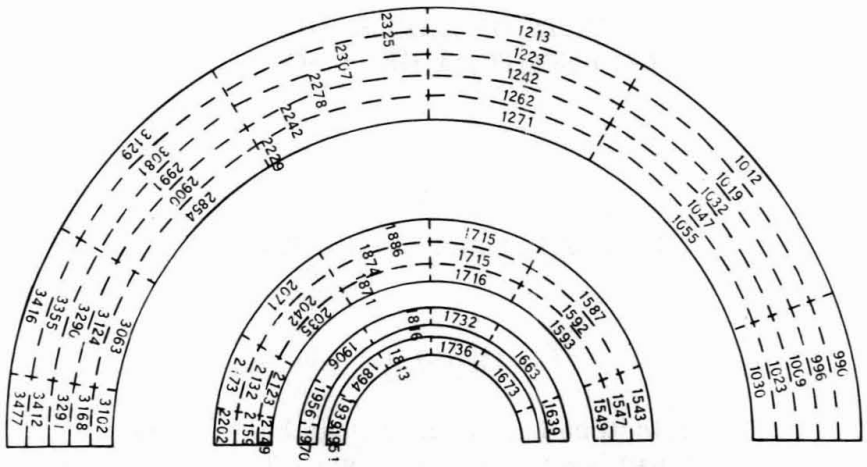

Figure 18. Fuel cask temperature response for oriented earth orbital decay – maximum circumferential gradient

MAXIMUM CAPSULE CLAD TEMPERATURE

EARTH ORBIT DECAY
ORIENTED CASK
LM SHIELD REMOVED AT 300K FT (5900 SEC)

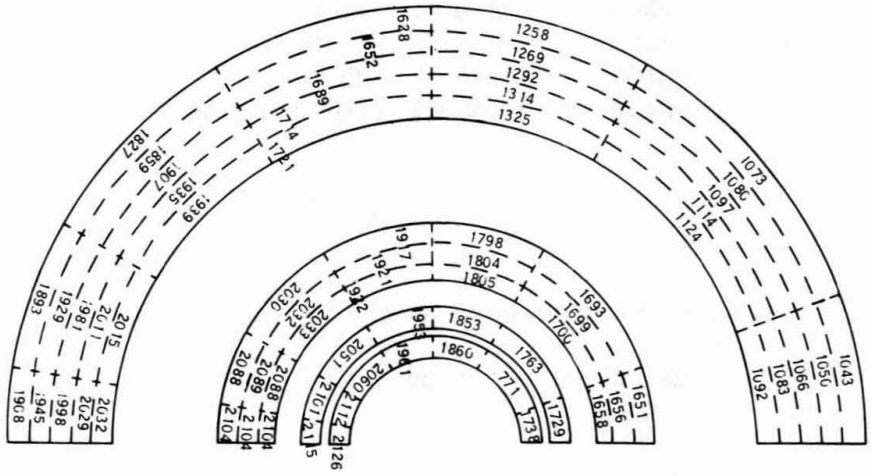

Figure 19. Fuel cask temperature response for oriented earth orbital decay – maximum capsule temperature

EFFECTS OF EARTH BURIAL OF RADIOISOTOPE HEAT SOURCES*

S. L. Jeffers and F. L. Baker

Abstract

Earth burial of radioisotope heat sources has been of interest because increased emphasis has been placed on disposal by intact reentry. With an intact system, the heat source may penetrate the earth during initial impact, or be buried by blowing sand or shifting soil over a period of time. Once buried, the heat source's temperature will rise, causing several reactions occurring singly or in combination: corrosion or chemical attack by the soil; melting of the container; melting of the soil; or fuel property degradation.

Our studies have been directed toward a better definition of high-temperature soil properties and the inclusion of these properties in our heat transfer models. We also have under way a series of actual burial tests using electrical heaters both in the laboratory and in the field. It may be possible to dispose of radioisotope heat sources by adjusting their geometry so that they will melt their way deep into the earth.

Sandia Laboratories, Albuquerque, New Mexico.

*This work was supported by the United States Atomic Energy Commission.

Introduction

For the past six years the Aerospace Nuclear Safety Department at Sandia has been vitally concerned with all aspects of the safety of space nuclear systems. For the past two and a half years we have been investigating the problems of earth burial of radioisotopes. This is the result of an increased interest in disposal by intact reentry.

With an intact system it is quite possible that the radioisotope heat source will penetrate the surface of the earth during the initial impact. If not, it is still quite possible that blowing sand or shifting soil will gradually cover the heat source over a period of time.

Once the heat source is buried, its temperature will rise because of the insulating properties of the surrounding soil. As the temperature increases, corrosive action or chemical attack by the soil will be accelerated and the container may melt. These reactions working singly or in combination can result in loss of capsule integrity. In addition the soil may melt and the fuel may degrade. If capsule integrity is lost and the radioisotope is released, a formerly safe situation must now be evaluated for its possible hazardous biological consequences.

Our approach to understanding the problem has been to conduct burial experiments in the laboratory and the field, to measure high temperature thermal properties of soils, and to analytically correlate the information available so that predictions of burial results can be made. We want now to discuss and evaluate our approach in some detail.

Theory

When a heat source is buried in soil the steady state heat transfer can be expressed by the familiar equation

$$q = - KA\, dT/dx \qquad (1)$$

where

q = heat flow

K = conductivity

A = area

T = temperature

x = distance.

As a complication in this case, K is not a constant but is some unknown function of T.

We can simplify the discussion by solving the equation for a spherical heat source. In this case $A = 4\pi r^2$ and the equation is:

$$q = -K(T)\, 4\pi r^2\, dT/dr \qquad (2)$$

or

$$\frac{q}{4\pi}\int_{r_1}^{r_2}\frac{dr}{r^2} = -\int_{T_1}^{T_2} K(T)\,dT \qquad (3)$$

where

r_1 = radius of the sphere

r_2 = distance from center of sphere

T_1 = surface temperature of sphere

T_2 = ambient soil temperature.

Integrating from r_1 to infinity, we obtain

$$\frac{q}{4\pi r_1} = -\int_{T_1}^{T_2} K(T)\,dT. \qquad (4)$$

The key then is to evaluate K(T) so that the equations can be solved manually for spheres or long cylinders, or by computer for more complicated shapes. A literature survey early in the study revealed that low temperature thermal conductivity data existed for some soils but that essentially no high temperature (above 500°F) conductivity data existed. Since the high temperature conductivity is the controlling element in the problem, we set out to generate our own data.

Results and Discussion

One of the first difficulties encountered was soil selection. Since there is an infinite variety of soils, which one or ones should be selected for testing? Although the answer to this question is not at all simple, it is extremely important. We solicited help in the area from Dr. J. L. Post,* a research geologist working for the University of New Mexico. Through use of a USGS document[2] and other sources he selected nine test soils to represent the predominant and extreme soil types of the world. In Table I the soils are tabulated and reasons are given for selection.

We are currently using two approaches to determine conductances of soils--obtaining data from both laboratory tests and in situ tests. The National Bureau of Standards, under contract to Sandia, is determining from laboratory generated data the steady state effective conductances of these soils up to their melt temperature. The NBS Laboratory

*See Reference 1.

set-up is shown in Figures 1 and 2.[3] Preliminary data are shown in Figure 3.

We are gathering data for determining conductances from field testing both in relatively undisturbed soils and in reconstituted soils. The reconstituted soils used were selected to represent these extreme conditions:

1. Ottawa Sand - high thermal conductivity
2. Bentonite - low thermal conductivity
3. Mixture (1/3 bentonite, 1/3 Ottawa sand, 1/3 crushed feldspar) - low melt point

Table 1. Representative Soils

Soil Type	Reason for Selection
1. Calcareous	Common to arid and semi-arid regions of world. CaO, one of 12 most plentiful oxides of the earth's crust, tends to have a very high melting range.
2. Coastal Clayey	Typical of well-weathered soils, representative of about 15% of total land area of world.
3. Magnesian	Representative of soils derived from gabbros, basalts, and dolomites.
4. Granitic Detrital	These soils with a high alkali feldspar content have a low melting range. They are typical of many detrital soils, which comprise about a quarter of total land area of world.
5. Lateritic	Representative of tropical humid regions, comprising more than 10% of total land area of world. FeO and Fe_2O_3 are two of most plentiful oxides of the earth's crust.
6. Podzol	Leached organic soils of woodland regions of temperate zones, which comprise about a quarter of total land area of world.
7. Dune Sand	Typical of barchan sand dunes of world, representative of about 7% of total land area of world. Consists largely of SiO_2 which comprises nearly 60% of the oxides in the earth's crust.
8. Playa Salt	Typical of very saline bolson playas of the world; most extreme chemical corrosive action upon heating.
9. Ottawa Sand	A standard material that has been previously investigated.

One method we use is to bury an electrically heated capsule and control the power input so the temperature of the capsule surface is near 2500°F. During the experiment we monitor and record the capsule surface temperature and the soil temperature at several locations near the capsule. Using a three dimensional heat transfer program (Herman) with a detailed model of the system, we feed the necessary inputs (i.e., power, burial depth, heater dimensions, etc.), and an assumed conductance into the computer. We compare the computer temperature output to the measured temperature data and then modify the assumed conductance until the computed and measured data closely match. Preliminary conductance curves derived in this manner are shown in Figure 4. Further work is required to refine these curves.

We also make more direct measurements by burying a long slender heater, again making temperature measurements at several locations near the heater.

Again using the basic steady state conduction equation

$$q = - KA \, dT/dx \tag{1}$$

and solving for a cylinder where

$$A = 2\pi rL$$

we obtain

$$K = - \frac{q}{2\pi rL} \frac{1}{dT/dr} . \tag{5}$$

The scheme then is to measure the slope (dT/dr) of the temperature-distance data, plug it into the equation and solve for K as a function of distance. A simple cross plot gives us K as a function of T, which is the form we want. This method is convenient and straightforward. Preliminary data developed with this technique are shown in Fig. 5.

Knowing the effective thermal conductance of soils gives us a partial but by no means the total answer to what happens in a burial situation. One of our first discoveries was that the soil does not remain in close contact with the capsule as the capsule gets hot. The soil gradually starts to melt and shrink away from the capsule (Fig. 6). This change in configuration causes a change in the heat transfer and makes it much more difficult to calculate. Other interesting reactions such as sintering of the soil (Fig. 7) add to the complexity of the problem.

One of our major problems, which is not yet solved, has been to find an electrical heater that would operate continuously at high temperatures in a burial situation. The only resistance element we have found that will perform satisfactorily is self-bonded silicon carbide. We have been using a mullite or alumina tube to represent a capsule with a bayonet type globar element (manufactured by Carborundum) inserted for the heater element. This technique works reasonably well but it is restricted to cylindrical shapes.

We feel that under certain conditions the fuel capsule or its inventory of fuel will actually melt its way downward into the soil. If true, this could hold out the promise of being a safe disposal technique. In any event we need to know what will happen to a buried radioisotope heat source.

In order to melt most soils we have to reach capsule surface temperatures of approximately 3000°F. Our difficulty has been in developing a heated capsule that will reach 3000°F over its entire surface. Any "cold" spots will cause the capsule to hang up and not sink. We now believe we have a spherical capsule with a cylindrical globar heater that will do the job (Fig. 8). To date we have checked out the hardware only at low temperatures (1500°F), but it looks very promising. Another problem area which we recognize but have not explored is the rate of high temperature corrosion of the capsule surface; knowledge in this area would, of course, help us estimate the burial life of a capsule.

Future Work

We feel we have only scratched the surface of this problem and now must dig deeper. We expect to do more testing in situ rather than in reconstituted soils; we expect to pursue the phenomenon of melting soils and sinking capsules; and, we expect to study what happens to an uncontained radioisotope buried in the soil. It may be that the fuel will provide its own protective cocoon of molten and sintered soil and thus remove itself from the biological chain of effects.

Conclusion

To us, a full understanding of what happens to a buried radioisotope heat source is extremely important. We must be able to establish the degree of hazard. Right now that hazard could range from severe for a soluble radioisotope fuel released in ground water to zero if protected by its own cocoon or sunk to great depths in the soil by its own melting action.

REFERENCES

1. J. L. Post, University of New Mexico, The Fusion of Soils, SC-CR-67-2688, Sandia Corporation, 1967.
2. Jerald M. Goldberg, F. Raymond Fosberg, Marie-Helene Sachet, Allen Reimer, World Distribution of Soil, Rocks, and Vegetation, U. S. Dept. of the Interior, Geol. Survey TEI-865, 1965.
3. D. R. Flynn and T. W. Watson, Thermal Conductance of Soils, National Bureau of Standards Report No. 9665, SC-CR-68-3422, Sandia Corporation, 1968.

Figure 1. Vertical cross section of NBS apparatus for measuring thermal conductance of soil

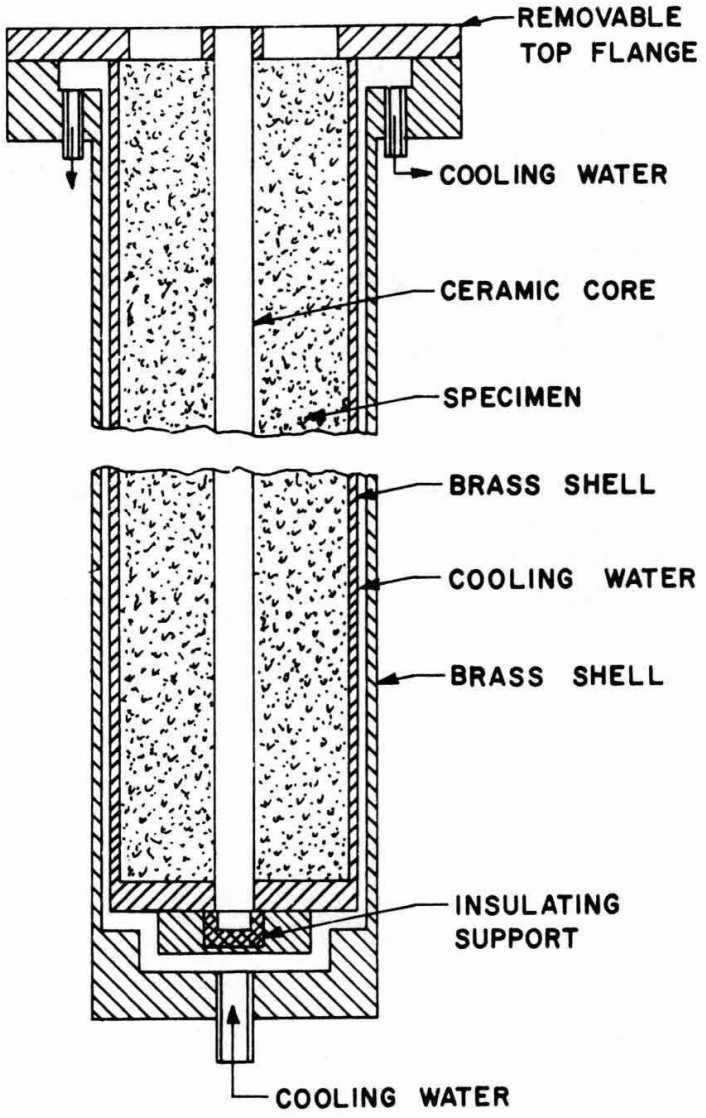

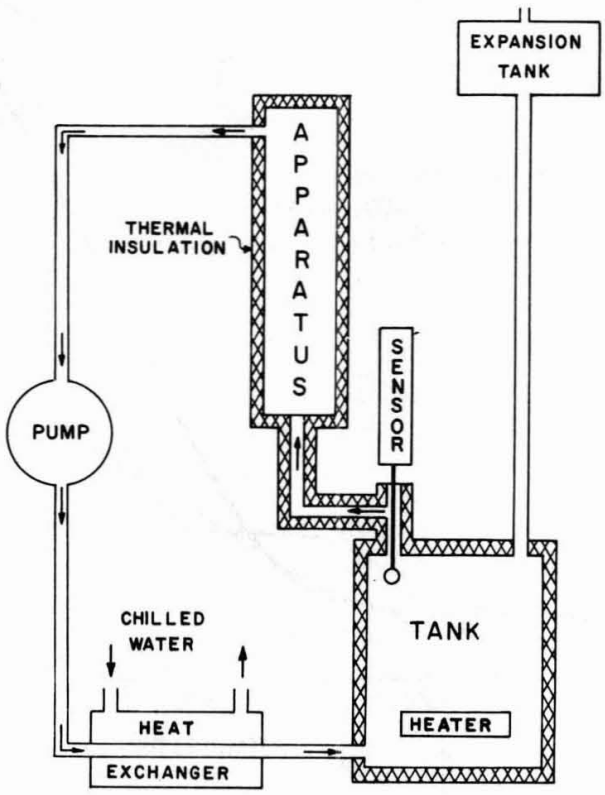

Figure 2. Circulating system used to cool NBS apparatus

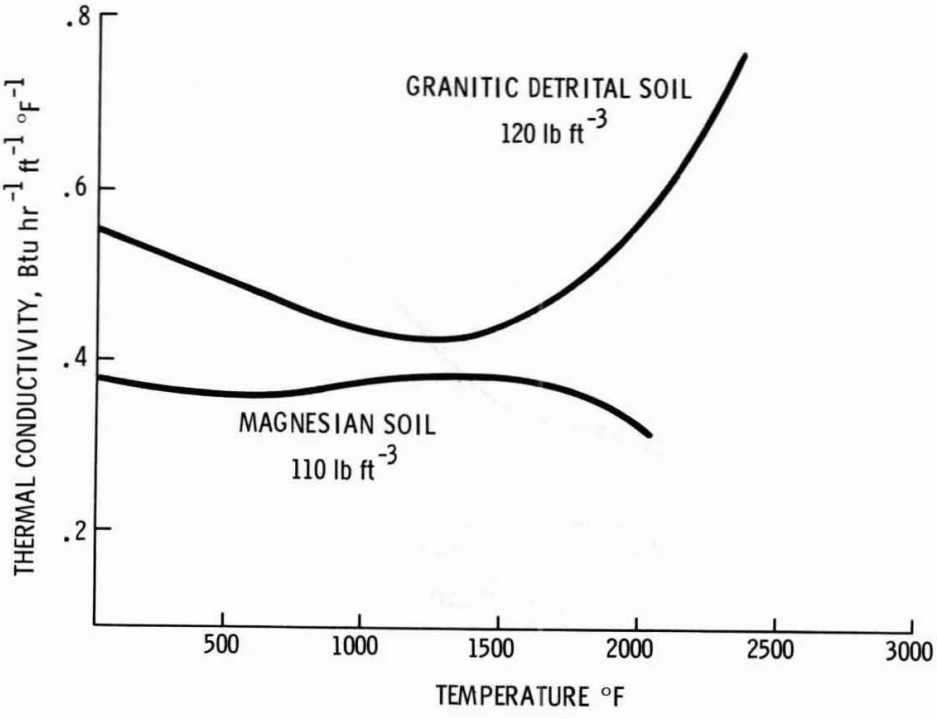

Figure 3. NBS preliminary data on two soils

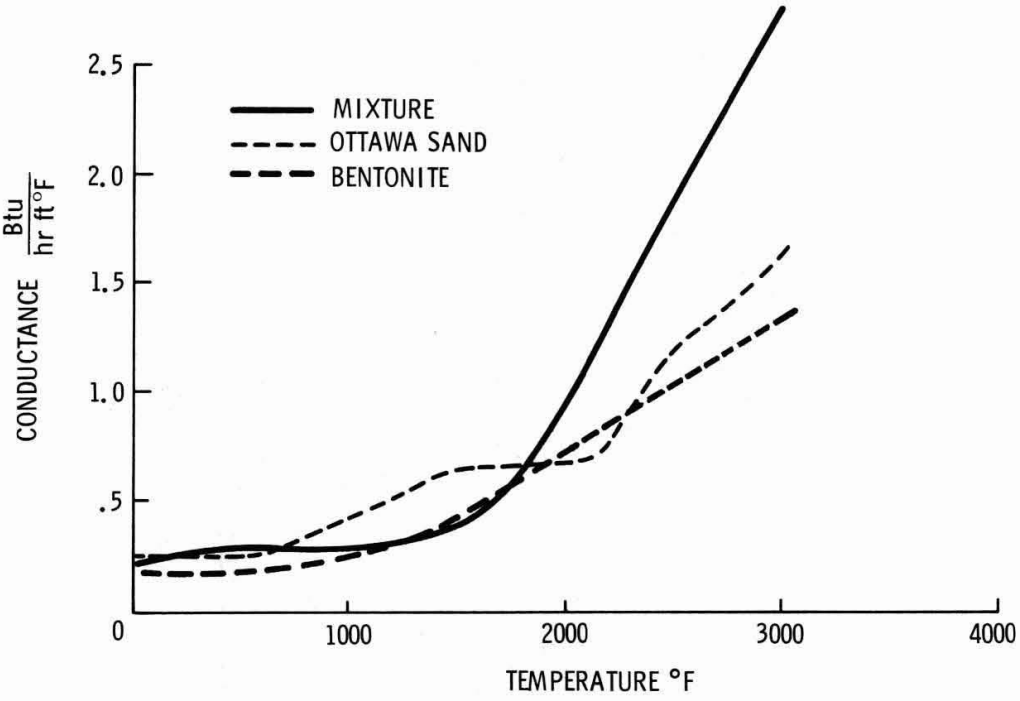

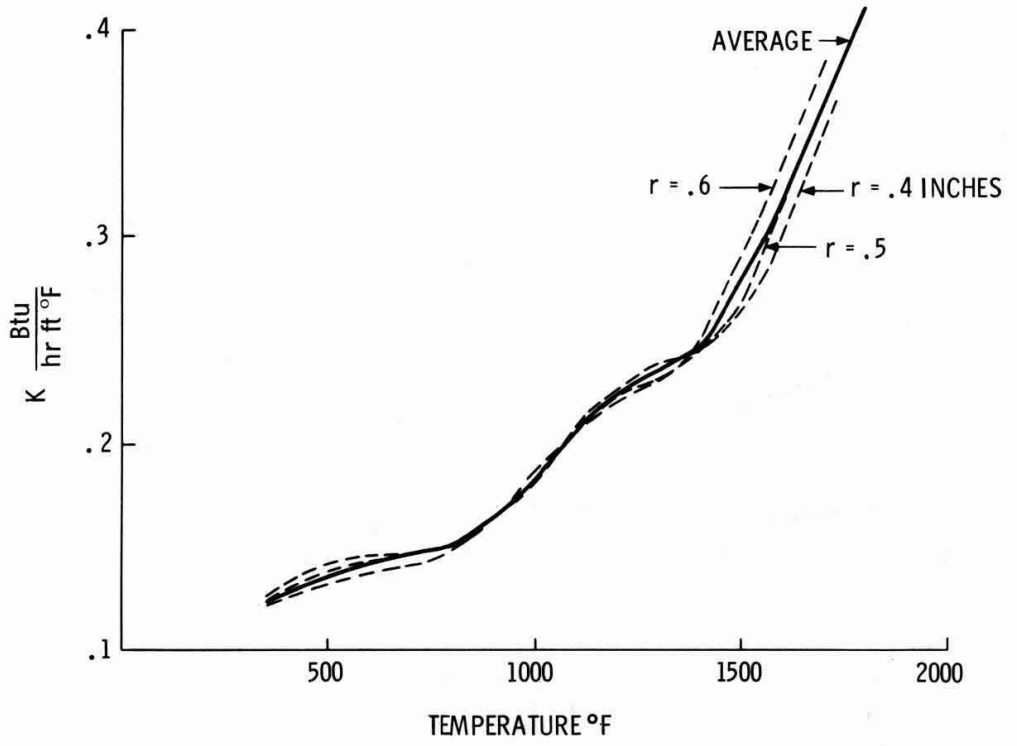

Figure 5. Preliminary data on conductivity of Ottawa sand as a function of temperature

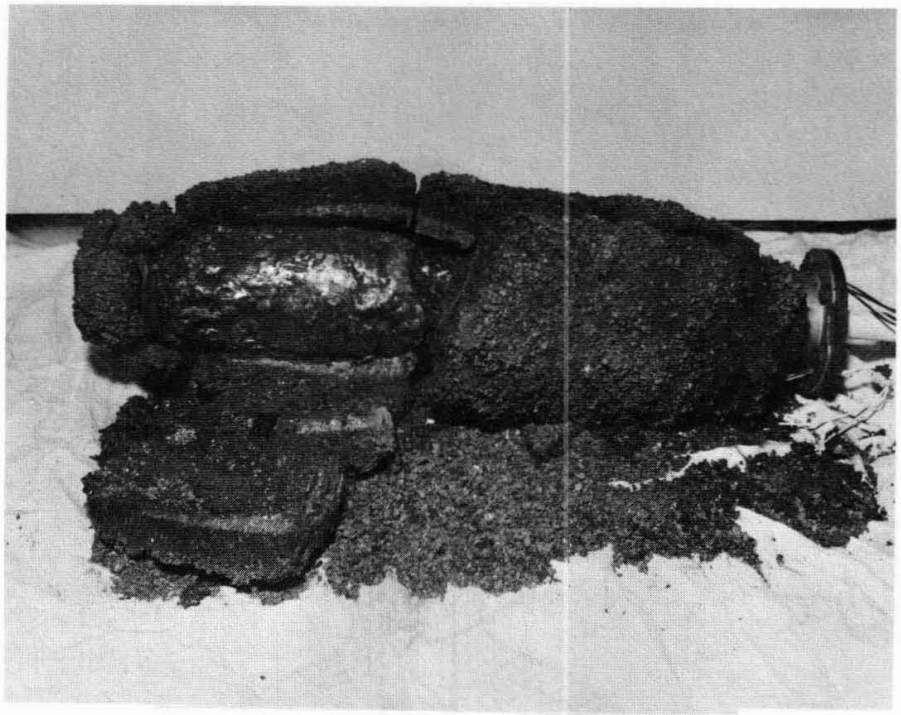

Figure 6. Melted soil shrinking from capsule buried in bentonite for several days

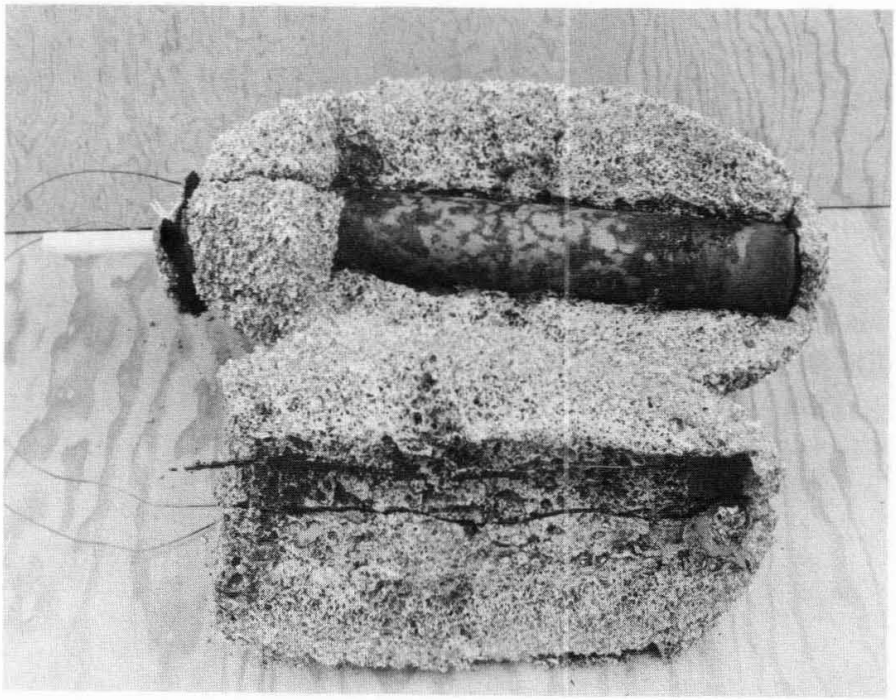

Figure 7. Sintered soil around a capsule buried in a mixture of 1/3 bentonite, 1/3 Ottawa sand, and 1/3 crushed feldspar for several days

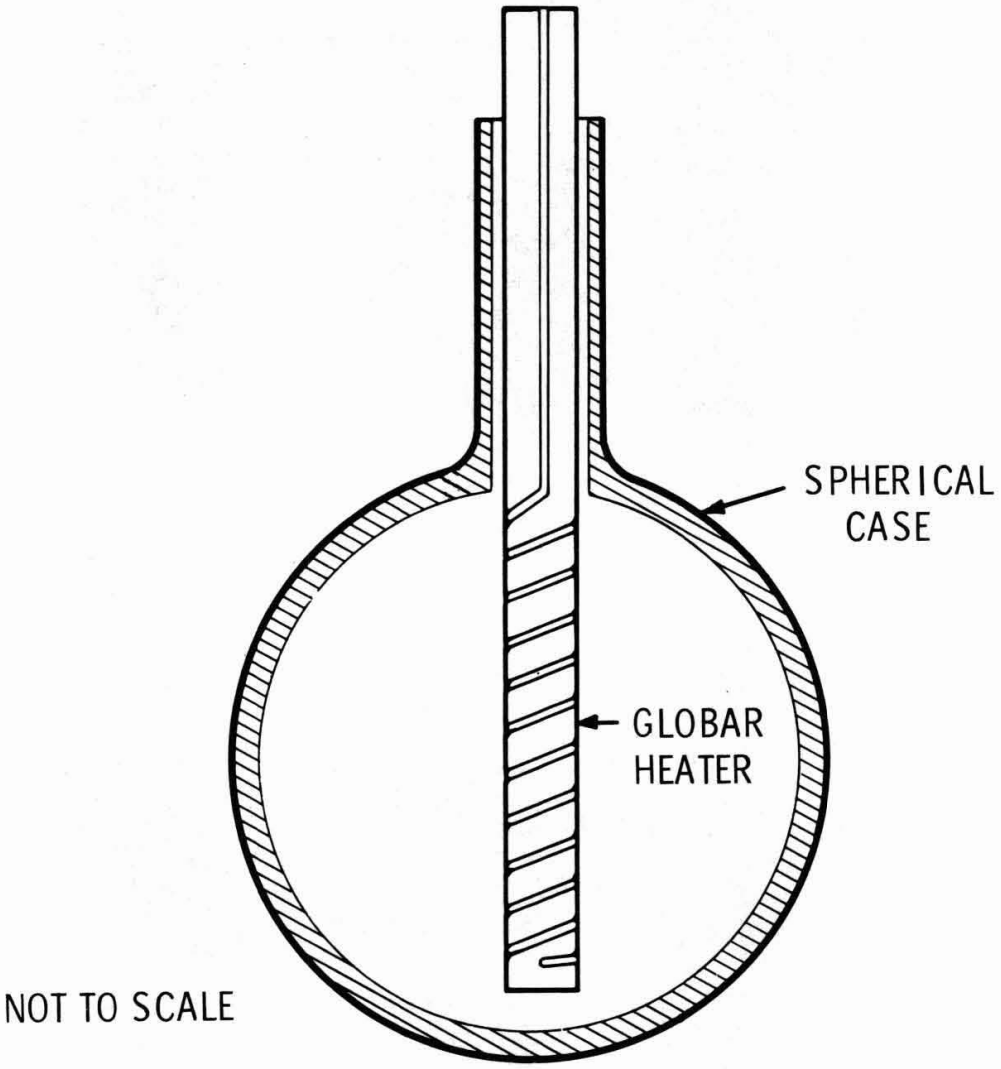

Figure 8. Spherical heater configuration

HEATING TESTS OF ENCAPSULATED COBALT HEAT SOURCES

C. L. Angerman and J. P. Faraci

Abstract

Capsules of nickel- and cobalt-based alloys that contained unirradiated or irradiated cobalt metal wafers performed satisfactorily during heating tests at typical heat source conditions, 10,000 hr in air at 850° to 1000°C. Typical capsules are 1 to 3 in. long and 0.94 in. in diameter with 0.05- to 0.10-in.-thick walls. Cobalt wafers, 0.040 in. thick, are cleaned, measured, and stacked in capsules that are sealed by TIG welding.

The best capsule materials, Haynes-25, Hastelloy-X, Hastelloy-C, and Inconel-600, were selected from screening tests that were designed to measure the kinetics of the three most important factors affecting the integrity of the heat source capsule. The results are listed below.

(1) Reaction between the cobalt and the capsule.

Interdiffusion at the cobalt-capsule interface formed a solid-solution zone that terminated in a band of Kirkendall voids in the capsule material.

C. L. Angerman, a Senior Research Metallurgist, and J. P. Faraci, a metallurgical engineer, are at the Savannah River Laboratory, E. I. du Pont de Nemours and Co., Aiken, S. C. 29801

(2) Diffusion of ^{60}Co through the capsule wall.

Radiotracer measurements of diffusion showed that ^{60}Co penetrated significantly along the grain boundaries of the capsule materials.

(3) Oxidation of the exterior capsule surface.

Intergranular penetration and depletion of alloy constituents underneath the continuous oxide scale contributed significantly to the total depth affected by oxidation.

Extrapolation of results from these short-term tests indicates that capsule performance would be satisfactory up to 1000°C for service times out to 50,000 hr. Capsule heating tests are continuing to confirm predicted performance to 5 yr.

Introduction

Irradiated cobalt metal (^{60}Co) has properties that make it attractive for use with thermoelectric converters or Rankine and Brayton engines in applications requiring powers of 2 kw(th) (1-3). Cobalt-60, with a half-life of 5-1/4 yr, is readily available (hundreds of megacuries per year) and at a low cost (<25¢/Ci or $16/w). It is produced by the direct irradiation of commercially available cobalt metal with little change in properties except for an expected increase in hardness. High specific activities, up to 450 Ci/g (62 w/cm^3), can be achieved by irradiation in Savannah River Plant reactors.

Cobalt-60 must be encapsulated prior to use in a heat source to prevent the spread of contamination and to provide a convenient means for handling. The nickel- and cobalt-based superalloys are promising encapsulation materials since the capsule temperature in many heat sources will not exceed 1000°C (4). The importance and preliminary assessment of the compatibility of the capsule materials with cobalt and the oxidation resistance of the capsule materials have been discussed previously (5). This paper describes additional screening tests that led to the selection of Haynes-25, Hastelloy-X, Hastelloy-C, and Inconel-600 as the most promising capsule materials, and the results of heating tests to demonstrate capsule performance at typical heat source conditions (through 10,000 hr at 850°C and 5000 hr at 1000°C). Demonstration tests are continuing to the 5-yr exposure times expected of heat sources. Screening tests to select suitable refractory metals and heating tests of capsules at 1200°C, or above, will be initiated in the near future.

Results and Discussion

Properties of Superalloy Capsule Materials

The four performance requirements of a capsule material are compatibility with the cobalt, relatively low diffusivity of the cobalt, resistance to corrosion by heat transfer media, and adequate strength. The reactions involved in compatibility and corrosion must be slow enough so that the unaffected capsule wall provides sufficient strength to prevent excessive creep or rupture. To select the most promising capsule materials, each reaction was evaluated using appropriate laboratory-scale tests with unirradiated cobalt.

Compatibility

During service, the capsule must not react with the cobalt to cause eutectic melting or rapid growth of intermetallic compounds. Published binary phase diagrams were reviewed to establish that no eutectics that melt below 1300°C form between cobalt and the principal components of the superalloys (6). Cobalt does form intermetallic compounds with chromium, molybdenum, and tungsten, which are present in several of the superalloys. To investigate possible formation of these compounds and any higher order reactions with cobalt, multilayer diffusion couples were heated for 1 week at 800° to 1200°C and then examined metallographically.

Of fourteen superalloy candidates tested, the six most compatible with cobalt were TD Nickel, Inconel-600, Haynes developmental alloy No. 188, Hastelloy-C, TD Nickel Chromium, and Haynes-25 (5). None of the couples melted. Metallographic examinations and microprobe analyses of the diffusion couples showed that the capsule alloys reacted with cobalt to form a solid solution that terminated in the superalloy with a band of Kirkendall voids. Based on extrapolation of the 168-hr data, compatibility (cobalt-superalloy reaction) zones up to 0.060-in. wide would be expected after 5 yr (one ^{60}Co half-life) at 1000°C.

A similar review of the published phase diagrams between cobalt and the refractory metals indicated that only tungsten and rhenium are suitable for encapsulating cobalt metal. Preliminary diffusion-couple tests showed that the two intermetallic compounds that form between cobalt and tungsten grow at an acceptably slow rate. A solid-solution zone formed with rhenium; no Kirkendall voids were observed in either tungsten or rhenium.

Diffusion of ^{60}Co

Diffusion of ^{60}Co through the capsule wall is a potential mechanism for releasing ^{60}Co in heat sources where the capsule is exposed directly to the heat transfer media. Significant amounts of radioactivity could be introduced into the corrosion product on the capsule surface and transported outside the shielding by the primary coolant. This consideration leads to an estimate of 1 ppm as the maximum allowable concentration of ^{60}Co at the capsule surface (4).

Both volume and grain boundary diffusion coefficients were calculated from the measured ^{60}Co concentrations in samples that were plated with cobalt containing ^{60}Co and heated for 100 hr at 800° to 1200°C. The ^{60}Co concentration in the samples was measured by the residual activity technique (7). The diffusion coefficients were calculated using both instant-source and constant-source models for diffusion (8). The instant-source model assumes that a small, finite amount of the diffusing species is present initially and is conserved during diffusion; the constant-source model assumes that an infinite supply of the diffusing species is available at all times. Extrapolations of short-term data from both models are being compared with long-term data to determine which model provides the best extrapolation. These two techniques were selected to measure grain boundary diffusion because it accounts for the deepest penetrations.

Results from the short-term tests were extrapolated to predict the depth at which the ^{60}Co concentration would be 1 ppm after 1 and 5 yr at 800° to 1000°C. Predicted depths for the three alloys with the least diffusion, Hastelloy-X, Haynes-25, and Hastelloy-C, are shown in Table 1 along with predicted depths in Inconel-600. Diffusion was assumed to occur in a wall of infinite thickness. This assumption leads to predicted penetrations of ^{60}Co that are slightly lower than for capsule walls of finite thickness, but which are satisfactory for ranking the candidate alloys. Typical predictions of concentration profiles after 5 yr of service are shown in Fig. 1.

Hastelloy-X was heated for 5000 hr at 1000°C to confirm the extrapolation of the short-term data to give data for typical operating times. As shown in Fig. 2, the measured penetration with Hastelloy-X was less than that predicted by either the instant- or constant-source models for diffusion, but greater than that predicted on the basis of volume diffusion alone.

Oxidation Resistance

Oxidation by air is the most likely type of corrosion for many heat sources because the capsules would be exposed to air during fabrication and loading. Other gases used as heat transfer media might contain enough oxygen impurity to produce oxidation during the life of the source. Although liquid-metal corrosion was not considered specifically, one of the alloys selected on the basis of oxidation resistance, Haynes-25, is also resistant to attack by mercury (9).

Of twenty alloys tested, the five most resistant to oxidation were TD Nickel Chromium, Hastelloy-X, Haynes-25, Hastelloy-C, and Inconel-600. Coupons of the candidate alloys were exposed to still air at 1000°C for 1000, 5000, and 10,000 hr. The total depth affected by oxidation was measured metallographically. This depth included the thickness of the oxide scale and the depths of intergranular penetration, internal oxidation, and alloy depletion (caused by alloy constituents diffusing to the oxide scale, which acted as a sink), as shown in Fig. 3. The scale spalled some during testing. Extrapolation of these laboratory screening tests indicates that less than 0.030 in. of the four best alloys would be affected by oxidation during service for 5 yr at 1000°C. The variation in oxidation with temperature was measured by 500-hr tests in still air at 850° to 1150°C.

Strength

Since no gas is generated during the decay of cobalt, the major source of pressure in a heat source capsule fueled with ^{60}Co is the expansion of the fill gas and the release of sorbed gas inside the capsule. With proper capsule design, the stress in the capsule wall from differences in the thermal expansion between capsule and cobalt is negligible. The estimated stress in the wall of a typical capsule (1.0-in.-diam. by 0.1-in. wall) is less than 300 psi at 1000°C. Because of this low stress, ^{60}Co can be encapsulated in nickel- and cobalt-based superalloys at temperatures above those normally considered appropriate for these alloys.

Extrapolations of literature data indicate that capsules made with TD Nickel, TD Nickel Chromium, or Haynes-25 will require wall thicknesses less than 0.020 in. to prevent 0.5% creep in 5 yr at 1000°C; other alloys, such as Hastelloy-X and Inconel-600 will require greater than 0.050 in. (1,10). These extrapolations will be confirmed by capsule heating tests at typical heat source conditions and by creep tests of pressurized capsules. Changes in strength and ductility of the alloys during heating tests will be

assessed by mechanical burst tests of ring sections cut from capsules after test.

Selection of Best Capsule Alloys

Based on the above tests, Haynes-25, Hastelloy-X, Hastelloy-C, and Inconel-600 were selected for further testing in capsule heating tests. Fig. 4 shows the parts of an assumed 0.100-in.-thick wall affected by each reaction after 50,000 hr at 1000°C. The sum of the thicknesses affected by the compatibility and oxidation reactions in each of these four alloys was less than that in any of the other alloys tested; the depth of ^{60}Co penetration was also smaller. Hastelloy-X was included because the small depth affected by oxidation compensated for its moderately wide compatibility zone. Conversely, Haynes-188, which had a relatively small compatibility reaction zone, was not included because of the large depth affected by oxidation. Although the two TD-series alloys were among the strongest and most compatible, they were not included for further testing because of the large depth of ^{60}Co penetration. With compatibility, oxidation, and diffusion reactions minimized, the four alloys selected would be expected to have the longest possible service lives, perhaps up to 5 yr, and would be least affected by any temperature excrusion resulting from abnormal operation of the heat source.

Ultimate selection of capsule material and wall thickness depends on the design of the particular heat source and its expected operating conditions. All of the factors considered above may not be of equal importance. The controlling factors will depend, for example, on the desired capsule life and the location of the capsule relative to the shielding and heat transfer media. For example, Inconel-600 or Hastelloy-C would be selected if compatibility was the major requirement of the capsule; Hastelloy-X would be selected if oxidation resistance was most important. Haynes-25 would be selected under the requirement that the sum of the incremental thicknesses of capsule wall required for compatibility, oxidation, and strength be minimized and yet be sufficient to prevent ^{60}Co release by diffusion (Fig. 4). This requirement is conservative because the fractions of the wall affected by the compatibility and oxidation reactions are assumed to have no strength.

Capsule Heating Tests

Experimental capsules containing either unirradiated or irradiated cobalt (inactive and active capsules, respectively), are being heated for up to 10,000 hr in still air at 850° to 1000°C to demonstrate capsule performance and to measure the effects of the radiation field. The operating

limits for capsules will be defined by other tests extending beyond 10,000 hr. The effects of abnormal operating conditions on capsule performance will be measured by tests of shorter duration. Satisfactory performance of several capsules through 1000 hr at 850° to 1000°C was reported previously (4).

The experimental capsules, 1 to 3 in. long and 0.94 in. in diameter with 0.05- to 0.10-in.-thick walls, Fig. 5, were fabricated from the four selected alloys for heating tests at typical heat source conditions. The capsules were filled with cobalt wafers 0.745 in. in diameter and 0.04-in. thick, which had been nickel plated prior to irradiation to minimize the spread of contamination; the capsules were then sealed by TIG welding (11). A void volume equivalent to about 5% of the wafer volume was left at the top of each capsule to accommodate release of adsorbed gas from the cobalt and differential thermal expansion between the components. The active capsules being tested contain 5000 to 40,000 Ci of ^{60}Co, depending on the capsule length and the specific activity of the cobalt (100 to 300 Ci/g).

Demonstration Tests

At 850°C. Inconel 600 has performed satisfactorily through 10,000 hr at 850°C with inactive capsules and through 10,000 hr at about 900°C with active capsules. Dimensional measurements indicated negligible changes, and helium leak tests indicated no loss of integrity. The compatibility and oxidation zones in the capsule were about as wide as expected. During the test, the cobalt wafers bonded to each other and to the capsule walls. Haynes-25, Hastelloy-X, and Hastelloy-C, the other three most promising alloys, are also expected to perform satisfactorily at these temperatures, based on the relative rates of the compatibility, oxidation, and diffusion reactions found in screening tests. Representative structures in the Inconel-600 capsule heated for 10,000 hr are shown in Fig. 6.

The radiation field from the ^{60}Co apparently did not affect the performance of the capsule. The compatibility and oxidation observed in the capsule tests fit the expected parabolic relationship with time, as shown in Fig. 7. Curves with slopes of 1/2 were drawn through the data points. The widths of the compatibility and oxidation reaction zones predicted for 900°C from Arrhenius plots of data from the screening tests with inactive cobalt agree with the widths found with active capsules. This agreement suggests that the effect of the radiation field on capsule oxidation and capsule-cobalt interaction is negligible.

At 1000°C. Inactive capsules of Haynes-25, Hastelloy-C, Hastelloy-X, and Inconel-600 have performed satisfactorily through 5000 hr at 1000°C. The thicknesses of the capsule walls affected by compatibility and oxidation generally agreed with the values predicted from the laboratory screening tests, as shown in Fig. 8. In some instances the compatibility zone in the capsules was thinner than expected, probably because of the less intimate contact between the capsule wall and the cobalt wafers.

Safety Tests

Two series of capsule tests were conducted to give preliminary indications of capsule performance under abnormal operating conditions. One series simulated the effects of transient overheating that might occur if the heat transfer media was lost. The other series characterized the performance of defective capsules operating at normal temperatures.

Two inactive capsules of Inconel-600 were heated for 100 hr at 850°C and then heated for 24 hr at successively higher temperatures in 50°C increments up to 1300°C. No loss of integrity was detected by helium leak tests; however, spalling of the oxide scale during the temperature cycles caused decreases in capsule diameters (up to 0.010 inch) that masked any increases that might have occurred from swelling or creep.

Cobalt oxidation inside capsules of Inconel-600, TD Nickel, or TD Nickel Chromium that were intentionally defected was minor or negligible during heating for 1000 hr at 1000°C. One capsule of each material had an 0.008-in.-diameter hole drilled through the capsule wall; the cap of a second capsule of each material was inserted with a press fit but was not welded. The cobalt oxidation was negligible in the pinholed Inconel-600 and TD Nickel capsules, apparently because the holes became plugged with the oxide scales from the capsules themselves. In contrast, an 0.008-in.-thick oxide scale formed on the cobalt in the vicinity of the pinhole in the TD Nickel Chromium capsule, because the TD Nickel Chromium did not oxidize enough to plug the pinhole. The cobalt oxide scale apparently did not spall. In the unwelded capsules neither the cobalt nor the interior capsule walls oxidized; this indicated that the press fit of the cap formed a reasonably tight seal. Additional tests will measure the potential release of minute quantities of ^{60}Co.

Acknowledgment

The information contained in this article was developed during the course of work under Contract AT(07-2)-1 with the U. S. Atomic Energy Commission.

REFERENCES

1. C. P. Ross. Isotopes and Radiation Technology, 5(3), 185 (1968).

2. W. C. Windley, Jr. Properties of ^{60}Co and Cobalt Metal Fuel Forms. USAEC Report DP-1051 (Rev. 2), Savannah River Laboratory (1968).

3. C. L. Angerman. Trans. Amer. Nucl. Soc., 10, 114 (1967).

4. C. L. Angerman, F. D. R. King, J. P. Faraci, and A. E. Symonds. Nucl. Appl., 4, 88 (1968).

5. C. P. Ross, C. L. Angerman, and F. D. R. King. Development of ^{60}Co Capsules for Heat Sources. USAEC Report DP-1096, Savannah River Laboratory (1967).

6. F. R. Morral. Cobalt and Its Alloys. Cobalt Information Center, Columbus, Ohio (1958).

7. P. L. Gruzin. Akademii Nauk. SSSR. Doklady, 86, 289 (1952).

8. T. Suzuoka. J. Phys. Soc. Japan, 19, 839 (1964).

9. J. J. Owens, J. F. Nejedlik, and J. W. Vogt. The SNAP II Power Conversion System Topical Report No. 7 — Mercury Materials Evaluation and Selection. USAEC Report ER-4103, Thompson Ramo Wooldridge, Inc. (1960).

10. Alloy Digest, published by Engineering Alloys Digest, Inc., Upper Montclair, N. J.

11. J. P. Faraci. Experimental ^{60}Co Heat Source Capsules. USAEC Report DP-1145, Savannah River Laboratory (1968).

Table 1. Calculated Diffusion of ^{60}Co in Capsule Materials

Material	Depth at which ^{60}Co concentration is ~1 ppm, mils			
	800°C		1000°C	
	1 yr	5 yr	1 yr	5 yr
Hastelloy-X	8	12	35	77
Haynes-25	12	18	37	67
Hastelloy-C	12	18	45	76
Inconel-600	20	38	~100	>100

FIG. 1 ^{60}Co CONCENTRATION PROFILES EXPECTED AFTER FIVE YEARS OPERATION AT 800° AND 1000°C

Predictions were made with constant - source model and based on coefficients calculated from experimental data using instant - source model.

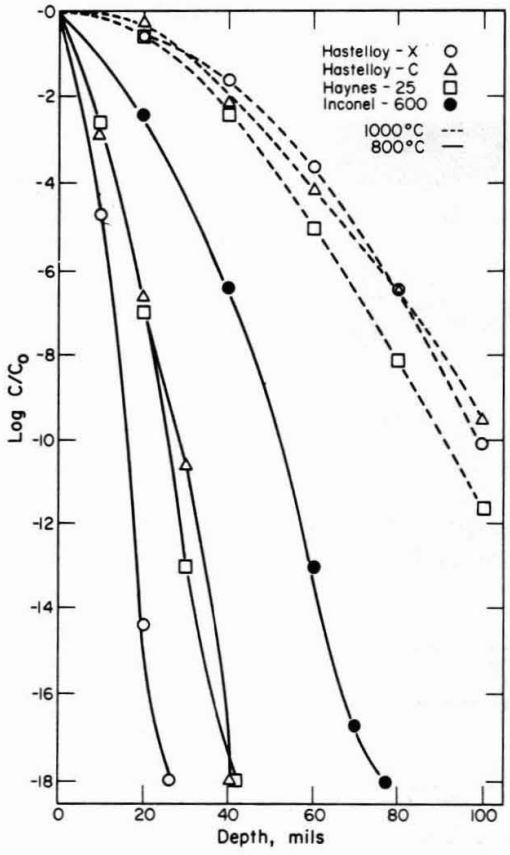

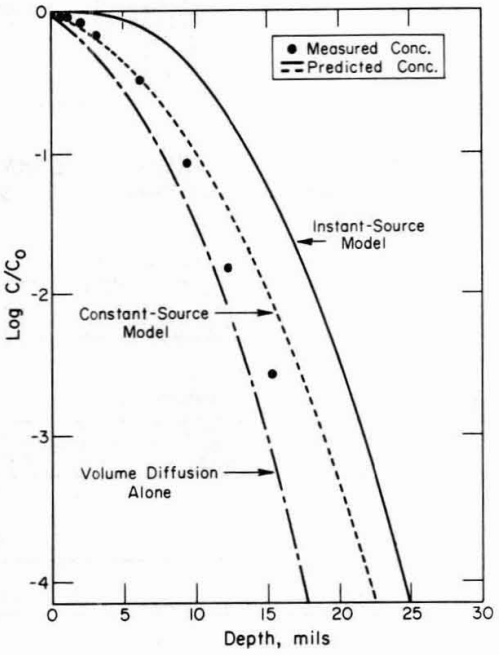

FIG. 2 COMPARISON OF MEASURED AND CALCULATED ^{60}Co CONCENTRATIONS IN HASTELLOY- X HEATED 5000 HOURS AT 1000°C

Predictions were based on diffusion coefficients calculated from 40 - hour data using the instant - source model.

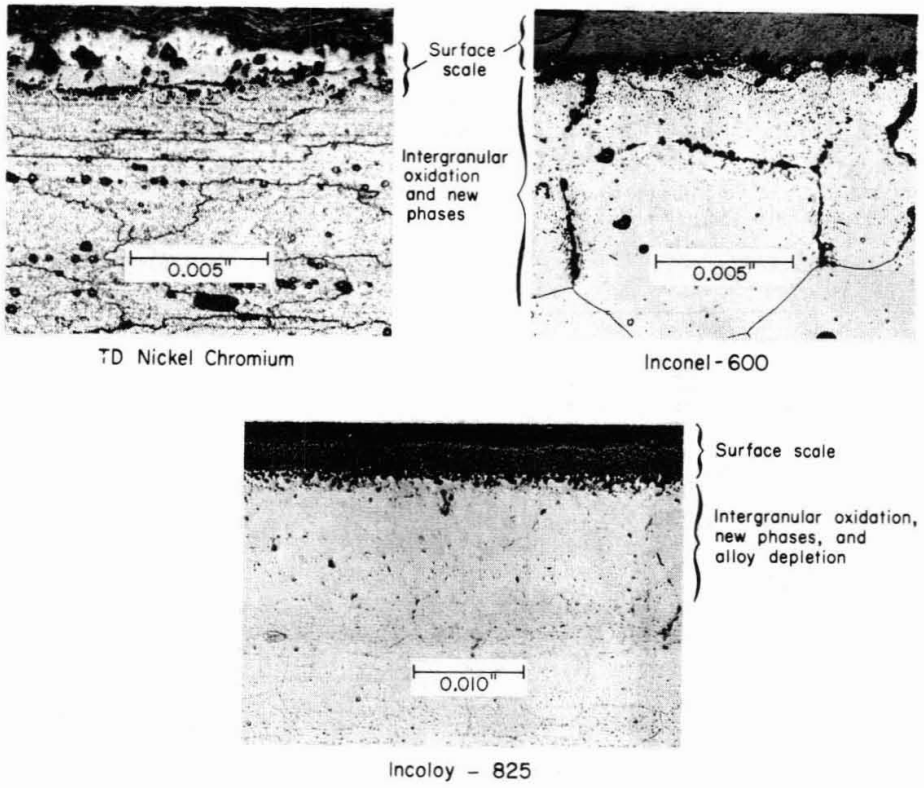

FIG. 3 EXAMPLES OF OXIDATION BEHAVIOR OF CANDIDATE CAPSULE MATERIALS
Specimens Exposed 9400 Hours in Still Air at 1000°C

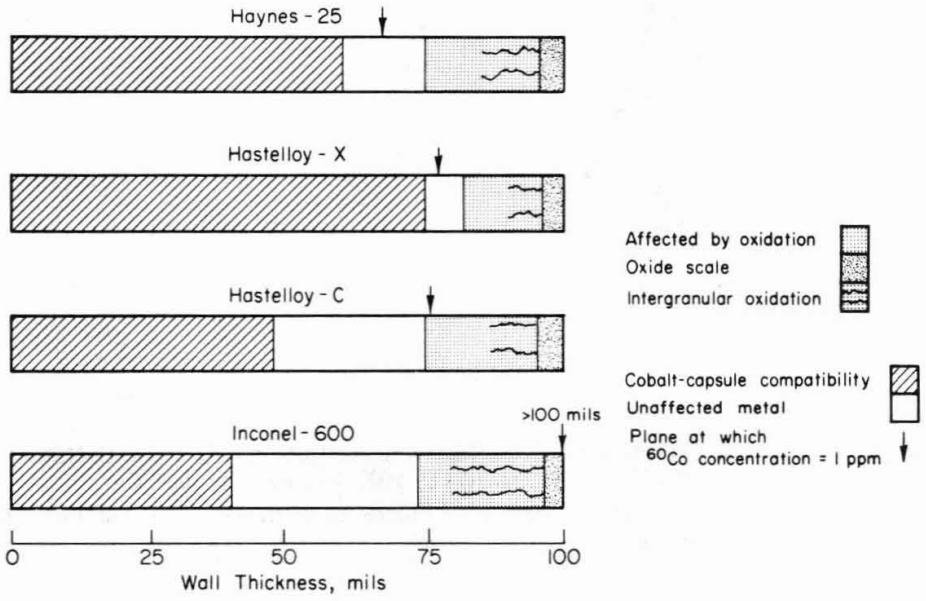

FIG. 4 PREDICTED REACTION ZONES IN CAPSULE WALL
AFTER 50,000 HOURS AT 1000°C

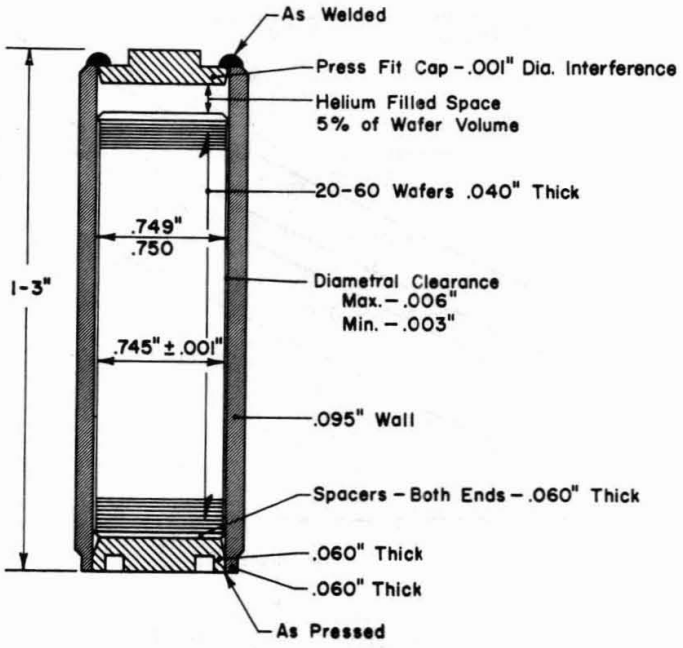

FIG. 5 EXPERIMENTAL CAPSULE

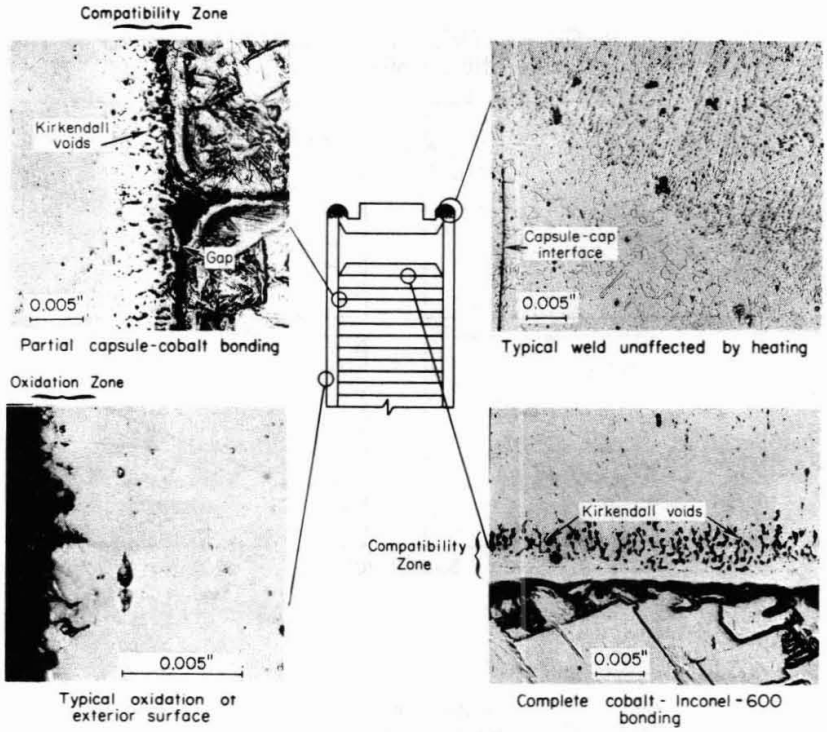

FIG. 6 STRUCTURE OF INACTIVE INCONEL - 600 CAPSULE HEATED 10,000 HOURS AT 850°C

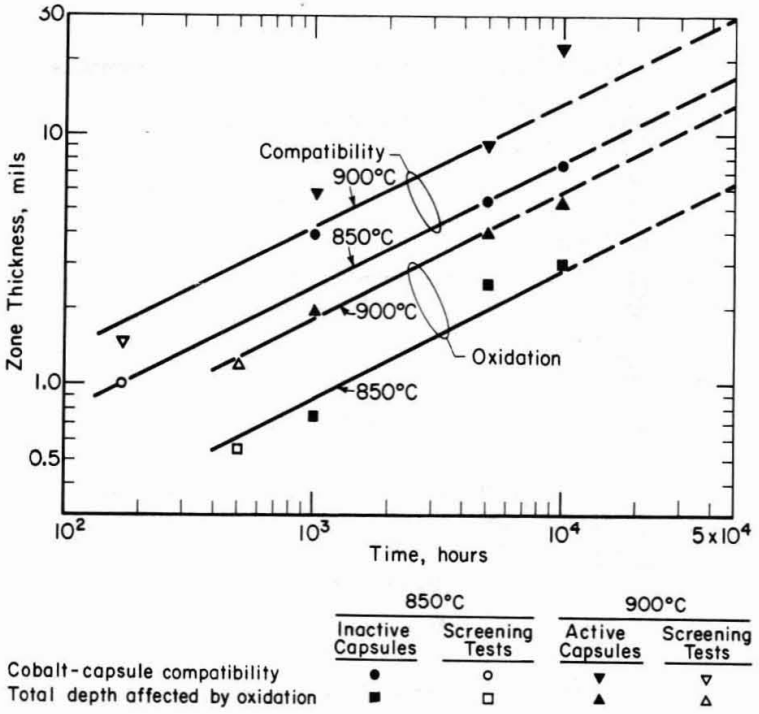

FIG. 7 COMPARISON OF HEATING TESTS ON INACTIVE AND ACTIVE CAPSULES OF INCONEL - 600

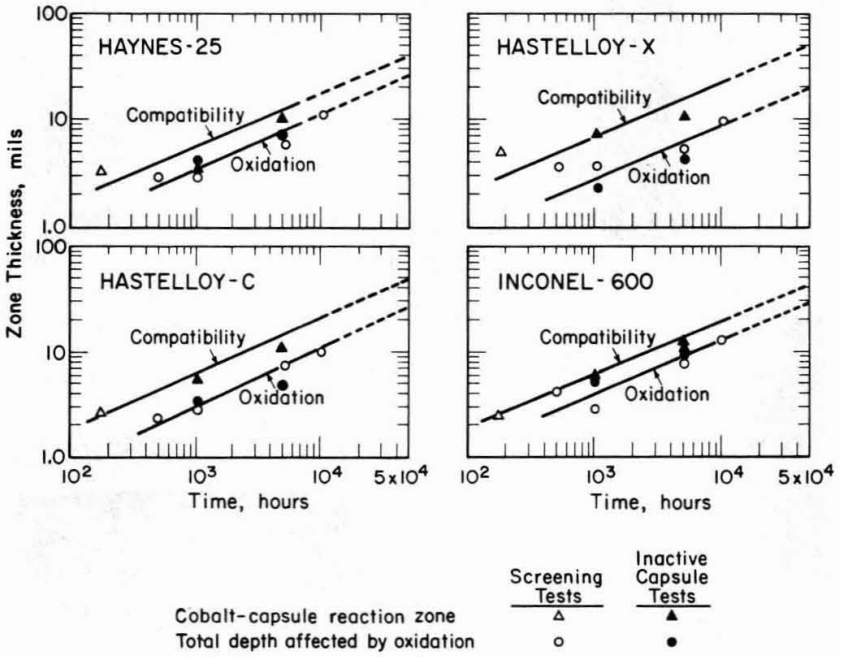

FIG. 8 GROWTH OF COBALT-CAPSULE COMPATIBILITY AND CAPSULE OXIDATION ZONES
Comparison of Screening and Capsule Heating Tests

CORROSION OF FUEL CAPSULES BY AND RELEASE OF RADIONUCLIDE FUELS TO SEAWATER

S. Z. Mikhail and D. A. Kubose

Abstract

Under the sponsorship of the Atomic Energy Commission NRDL is studying the release of radionuclides from radioisotope heat sources to the ocean environment. Both laboratory and in situ ocean tests are carried out on the fuels as well as on encapsulant materials. Seawater corrosion and corrosion-erosion rates of the encapsulants are measured in the laboratory using electrochemical and radioactive tracer techniques. Corrosion data obtained to date are summarized. In situ ocean testing utilizes electrically heated and radioisotopic fuel-loaded capsules. Fuel dissolution rates are measured in the laboratory under different conditions. Plutonium dioxide fuel was exposed in the ocean for 5 months. Results of the post-exposure examinations are reported. The ocean tests are conducted at NRDL's test site, San Clemente Island.

S. Z. Mikhail is Head, Nuclear Systems Technical Group
D. A. Kubose is Head, Isotope Release Program, Nuclear Applications Branch, both with the Naval Radiological Defense Laboratory, San Francisco, California 94135

I. INTRODUCTION

Under the sponsorship of the Divisions of Space Nuclear Systems and Reactor Development and Technology of the U. S. Atomic Energy Commission, the Naval Radiological Defense Laboratory (NRDL) has been conducting a program to examine the environmental effects on both operational and proposed space and marine/terrestrial radioisotope generators. One of the main aspects of the program has been the investigation of the behavior of fuel-containment materials in the ocean environment. Determination of the solubility in and modes of interaction of the fuels with seawater constitutes another essential and complementary portion of the program.

The corrosion rates in seawater are affected by its salinity, oxygen content, biological organisms, temperature and velocity. The populations of micro- and macro-organisms, and plants inhabiting seawater have great effects on the deterioration of metals by electrochemical, chemical, and mechanical actions. These effects invalidated corrosion data collected in sodium chloride or synthetic seawater solutions in most cases. Such a situation occurred when identical samples of flat bar specimens of several metals subjected to erosion/corrosion action test using the U. S. Naval Engineering Experiment Station's (EES) apparatus to simulate the conditions experienced on the leading edge of ship propellers (1). The results showed that the use of synthetic seawater solution not only failed to disclose the possible intensity of the corrosive effect of natural seawater but also failed to indicate the proper order of merit of the alloys investigated.

In the case of fuel dissolution rate determinations the results obtained in a natural seawater environment can be expected to be quite different than those obtained in other test media such as distilled water. These differences can be in both the nature and extent of the dissolution behavior and in the direct interaction of marine organisms with the fuel material.

This Laboratory's program to explore the nature and impact of the ocean environment on capsule materials and fuels includes both controlled laboratory examination in seawater, and in situ ocean evaluations at NRDL's test station at San Clemente Island where unperturbed long-term test locations are available. The laboratory tests are designed to:

1. develop immediate answers which can be used temporarily in design calculations until long-term marine testing results are available.

2. establish the conditions under which certain ocean environment effects could be predicted by laboratory measurements.

3. develop methodologies which can be used for in situ ocean examinations.

Concurrent with the laboratory examinations, marine testing is carried out with fuel subsystem simulations which are electrically heated, with fuel subsystems containing radionuclide fuels and with bare fuels.

Testing with electrically heated mockups will provide data on:

1. effect of marine fouling at different water depths,

2. effect of the ocean-bottom-water interface which may create unique problems,

3. effect of partial burial in the bottom material.

Testing with the fuel subsystems containing radioactive material will provide maximum information on the effects due to release of ionizing energy into the water. Finally, oceanic evaluation of bare fuel exposures will investigate fuel degradation and radioactivity release phenomena.

The present document discusses the testing procedures followed in the above studies and summarizes some of the results obtained to date.

II. LABORATORY TESTS

II.1 Corrosion of Encapsulants

Two independent methods were employed for the determination of the corrosion rate of the various encapsule alloys in seawater: 1. tracer techniques in which neutron irradiated specimens of the metals were immersed in seawater and the seawater analyzed for radioactive corrosion products; 2. electrochemical techniques in which the corrosion current density was measured, and the corrosion rate calculated by application of Faraday's Law.

II.1.1 Radioactive Tracer Studies (2-5)

II.1.1.1 Experimental Procedures*

a. Test Specimens

Test specimens were machine-cut, polished and cleaned with benzene and ethanol in an ultrasonic cleaner. Surface profile measurements were made using a Proficorder before and after exposure to seawater. Some Haynes 25 specimens were grit blasted with #20 grit then covered with an emissive coating by the Missile and Space Division of the General Electric Co., Valley Forge, Pa. The coating had the following composition: 60% iron titanate, 30% calcium titanate and 10% silica.

The specimens and appropriate standards were then irradiated in a nuclear reactor. Of the elements present in the specimens, only cobalt and chromium and (marginally) nickel were activated in sufficient amounts and with sufficiently long product half-lives to be useful as tracers in these studies.

*For detailed description of the procedures and the testing apparatus reference (6) should be consulted.

b. Standard Specimen Exposure Tests

The specimens were exposed to seawater in a twenty-unit apparatus each designed to expose one specimen at a time. The apparatus was designed to provide control of the seawater temperature, oxygen content and the velocity of seawater past the specimen. All components of the apparatus in contact with the seawater were nonmetallic. Sampling was accomplished by draining of the seawater solution and analysis of an aliquot of the collected sample.

For standard series experiments a metal sample was immersed in a liter of filtered natural seawater contained in a pyrex vessel and maintained either at 6±2°C (to approximate the water temperatures observed in the basins off the southern California coast) or at room temperature. The sample was mounted (off axis) on a holder, rotated at a speed such that water flow rate past the specimen face was 0.7 ft/sec. Air was continuously bubbled through the solution by means of a fritted pyrex bubbler. The flow rate, kept at approximately 50 cc/min, was enough to air-saturate the seawater and provide an oxygen concentration of about 6.5 ml/l the highest concentration of oxygen normally expected in seawater (7). In certain experiments the standard exposure conditions were changed: nitrogen gas, instead of air was bubbled through the solution or the sample rotation was discontinued.

c. Erosion-Corrosion Tests

These studies were conducted to determine the combined effect of erosion and corrosion on the release rates of encapsulant alloys. Since many alloys owe their corrosion resistance to protective films or layers of corrosion products, erosive removal of these films lead to significantly increased corrosion rates.

In these experiments, a metal specimen was mounted in a square cavity at the bottom of a teflon-coated stainless steel vessel, and held in place with a silicone rubber adhesive. The specimen's exposed surface, Fig. 1, was flush with the bottom surface of the chamber. The top of the chamber had a removable pyrex window assembly to permit placement of the specimen and addition and removal of the seawater/bottom-material mixture. A mixture of 500 ml seawater with 50 g of ocean-bottom material was placed in the vessel. The vessel was tilted from side to side to allow the seawater/bottom-material to wash over the specimen at an approximate velocity of 0.9 ft per sec. Water temperature was maintained at 22-25°C. Periodically the seawater/bottom-material mixture was removed and analyzed for ^{60}Co activity. Fresh seawater/bottom-material mixture was added and the experiment continued.

Three specimens of the metal were studied at one time, each in a separate test chamber. The three chambers were mounted on a platform which was in turn mounted on a drive mechanism and the entire apparatus enclosed in a lead shield, Fig. 2.

d. Gamma Radiation Effects Experiments

The sample was exposed for the whole duration of the experiment to the 1500-curie NRDL ^{60}Co source. Dose rate to the water was approximately 2×10^5 rads/hr. Conditions were the same as those of the standard exposure experiments described above except that no temperature control or sample rotation was provided.

e. Hot Vapor Exposure Tests

Inasmuch as radioisotope capsules could be subjected to hot seawater vapor environments when accidentally buried in the ocean bottom it was decided to conduct experiments to determine the corrosion rates of the encapsulants under such conditions.

The apparatus used to expose test specimens to hot seawater vapor, Fig. 3, consists of an inner pyrex tube and an outer stainless steel container. The pyrex tube had a circumferential indentation on which the specimen rested, the seawater level being below this indentation. The assembled exposure apparatus was placed in a cylindrical electrically heated oven kept nominally at 200°C. The temperature and pressure within the S.S. vessel were monitored. After an exposure period was completed the pyrex tube was opened, the radioactive specimen removed and placed into a new pyrex tube to start another exposure period, and the seawater contained in the open tube assayed for radioactivity.

II.1.2 Electrochemical Techniques (3,8,9)

II.1.2.1 Determination of Corrosion Rates of Uncoupled Samples

Measurements of the anodic and cathodic polarization of a metal electrode by an externally applied current or potential provide the basic electrochemical data for the study of the corrosion behavior of the metal in a corrosive medium. Polarization data can be obtained by two methods depending on whether the current or the potential is allowed to be the independent variable. When current is the independent variable the term galvanostatic polarization applies; when potential is the independent variable the term potentiostatic polarization applies.

Galvanostatic polarization has been used here for the determination of corrosion rates. The theory behind the application of this technique has been adequately described (10). In essence the technique is to (in turn) cathodically and anodically polarize the test electrode by applying an external current. The degree of polarization, measured as an over-voltage E, is plotted against the logarithm of the applied current density, i. For values of E greater than about 50 mv such a plot should yield a straight line, with slope β_c for cathodic polarization and β_a for anodic polarization. Values of the corrosion current density, i_{corr} can be obtained from such measurements in two ways. One consists of extrapolating the line of slope β_c to the open-circuit potential of the test electrode. The current density at the intersection represents the dissolution rate of the electrode and hence its corrosion rate in terms of current density. The other method of obtaining i_{corr} consists of applying the relation (11-12)

$$\Delta E/\Delta i = \frac{\beta_a \beta_c}{(2.3)(i_{corr})(\beta_a + \beta_c)}$$

where $\Delta E/\Delta i$ is the slope (on a Cartesian-coordinate plot) near the region of the open circuit potential (i.e., E less than about 50 mv); in this region the change of E with i is linear.

Test electrodes were fabricated from bar stock. They were machined into right circular cylinders 0.5 inch in height and 0.25 inch in diameter. Each electrode was polished, mounted on an electrode holder and ultrasonically cleaned before immersion in seawater.

Fig. 4 shows the circuit used for galvanostatic polarization of test electrodes. The current was measured by determination of the voltage drop across a precision 10 megohm or 1 megohm resistance with a Keithley 610BR electrometer. The potential of the sample electrode versus a saturated calomel electrode (S.C.E.) was measured with a high-input-impedance John Fluke differential voltmeter, model 803B.

The polarization cell, Fig. 5, was a standard 1-liter, 4-neck, round bottom pyrex flask modified by a ball socket on one side to provide access for a Luggin-capillary-probe and saturated-calomel-electrode (S.C.E.) assembly. Two Beckman #39271 platinum thimble electrodes were used as the auxiliary electrodes, Fig. 4. Seawater aeration or deaeration was achieved by continuous purging with either air or nitrogen, respectively.

After being rinsed in distilled water the test electrode was placed in the polarization cell, which contained seawater previously saturated with either air or nitrogen. Electrical connections were made from the test electrode and the S.C.E. to the voltmeter and the potential measured. After this open-circuit potential had stabilized (less than about 5 mv change per hour) the remainder of the circuit shown in Fig. 4 was connected (power supply at zero output). Polarization measurements were then started by application of current from the power supply in increasing increments at regular time intervals, usually about 5 min. For each current value the corresponding potential of the test electrode versus S.C.E. was noted.

The measured values of E and i, for cathodic and anodic polarization (separately), were plotted on a semi-logarithmic scale, E being the linear ordinate. Values of β_c and β_a were determined from these plots. Values of $\Delta E/\Delta i$ were obtained from linear plots of E against i for values of E less than about 50 mv (the open-circuit potential being taken as zero volts). Values of the corrosion-current densities were obtained from these quantities by either of the two methods outlined above. The corrosion-current density was then converted to a corrosion rate by application of Faraday's Law.

II.1.2.2 Determination of Corrosion Rates of Galvanically Coupled Samples

The open-circuit potential of each test electrode was measured with respect to the saturated calomel reference electrode in aerated and in deaerated seawater. All of the test electrodes were immersed in a common container while the measurements were made. These potentials were the basis for determining a galvanic series of the SNAP 21 materials.

The galvanic currents between each of the materials in turn and all the others, as a group, when short-circuited (i.e., galvanically coupled) to each other, were measured, in aerated and deaerated seawater, in the following manner. After the open-circuit potentials were determined, all but one, say Hastelloy X, of the test electrodes were short-circuited to each other. The connection between the shorted group of electrodes and Hastelloy X was made via a zero resistance ammeter circuit (ZRA) described by Greene (13). Now, in effect, all of the other electrodes were shorted to each other so that the galvanic current between Hastelloy X and the shorted group of electrodes could be measured. After measurement of this galvanic current, the ZRA was disconnected from the Hastelloy X, the Hastelloy X shorted (now directly) to the shorted group of electrodes, and a different electrode disconnected from the shorted group (which now included Hastelloy X) and re-connected to the shorted group via the ZRA. The galvanic current between this new single electrode and the new shorted group was measured. The procedure was followed until the galvanic current between each electrode and the shorted group had been measured (the shorted group being different for each measurement); these currents were denoted as the first set. Examination of this first set of galvanic currents revealed, by their direction, which electrode (or electrodes) was the anode in reference to the other electrodes. This electrode (or electrodes) was disconnected entirely and the above procedure repeated to obtain a second set of galvanic currents. This second set revealed another anodic electrode(s). It was disconnected entirely (so that now two electrodes had been removed) and the entire procedure repeated again to obtain a third set of galvanic currents. This procedure was follwed until only two electrodes remained, the galvanic current (the last set) between them also being measured by the ZRA. This technique, in addition to providing the galvanic currents, provides an independent determination of the galvanic series. The anodic electrode in the first set of galvanic currents is the most active and the remaining electrode after the last set is the most noble.

In both the normal and the galvanic corrosion rate determinations the electrochemical equivalents of the corrosion rate, i.e., the corrosion current and the galvanic current in terms of current density (μ amp/cm^2), were measured. Faraday's Law was then used to translate these values of current density into a more immediately useful quantity such as mil per year (mpy).

II.2 Fuel Solubility (14-15)

II.2.1 Experimental Procedures*

Test procedures and results reported below pertain to PuO_2 fuel. Other fuels such as $SrTiO_3$, Pm_2O_3, Tm_2O_3 are currently being tested at NRDL and results obtained will be reported in future publications.

a. Standard Series Experiments

A weighed quantity of fuel sample was immersed in a liter of natural filtered seawater contained in a pyrex vessel and maintained at 22-25°C. The solution was stirred by gentle swirling once a day. The solution was kept out of contact with the atmosphere except during sampling.

For sampling an aliquot was filtered through a 0.45-μ membrane filter (Millipore). All the plutonium passing through this filter was defined as being in "solution". This filtering procedure gave reproducible sampling of the Pu-seawater mixture.

b. Solubility in Presence of Ocean Bottom Material

Two types of experiments were conducted in this series. In the first, varying amounts of ocean bottom material were added to solutions of PuO_2 in seawater. The mixtures were shaken once a day, and also before sampling. Aliquots of the mixture were centrifuged prior to plutonium assay. In the second type of experiments PuO_2 microspheres were added to seawater containing ocean-bottom material. The seawater was agitated once a day by bubbling air through it. Aliquots of the solution were centrifuged before assay.

c. High Temperature/Pressure Tests

Plutonium dioxide microspheres were immersed in natural seawater in a pyrex capsule and heated to 120°C (30 psi) and 190°C (180 psi) after placement of the sealed capsule in a pressure vessel.

Assay of seawater for plutonium activity was performed by liquid scintillation counting. In the high temperature/pressure tests, however, it was noticed that a crystalline precipitate was formed during the exposure period and scavenged almost all the plutonium activity from solution. The insoluble nature of this precipitate made it difficult to perform reliable liquid scintillation counting. Hence, plutonium activity was determined by γ-ray scintillation counting.

II.3 Results and Discussion

II.3.1 Corrosion of Encapsulants

*For detailed description of the procedures and the testing equipment reference (6) should be consulted.

II.3.1.1 Corrosion Rates Determined by Tracer Techniques

a. Standard Specimen Exposure Tests

Table 1 shows a comparison between corrosion rates of Haynes-25 based on cobalt and chromium analysis. It is noted that the rate agree within a factor of less than two. Table 2 gives the corrosion rates for uncoated, half- and completely-emissively coated Haynes-25 after 160 days immersion in seawater. The observed increase in the corrosion rate of the coated specimens was not due to release of the coating itself to seawater as determined by γ-pulse height analysis of the seawater for its corrosion products. There are two possible causes for the higher corrosion rate of the completely-coated specimens. One, the emissive coating-Haynes 25 system functions as a galvanic couple with the Haynes 25 being the anode; and two, the higher corrosion rate is a surface area effect. The surface area effect is felt to be the more important of the two since the emissive coating has a relatively low electrical conductivity. As stated before, prior to the application of the emissive coating the surface of the specimen is grit blasted with #20 grit (for the half-coated specimens only the half to be coated was grit-blasted) and hence its surface area is much greater than the surface area of the uncoated specimens, whose surface has been polished with #600 grit paper. Since the corrosion rates reported here are based on the geometric surface area of the specimens, the reported corrosion rates of the half- and completely-coated specimens are much higher than if their actual surface areas were used in the calculation of their corrosion rates. This explanation is based on the assumption that the emissive coating does not affect the transport of cobalt and chromium ions from the Haynes 25 to the seawater.

Fig. 6 displays corrosion rates of Hastelloy X and C at room temperature in aerated and deaerated seawater. The rates are seen to decrease with time and approach constant values after about 100 days of exposure.

b. Erosion-Corrosion Tests

Erosion-corrosion data determined for Haynes-25 in seawater-ocean bottom material mixture under different exposure conditions, are included in Table 3. The release rates are noted to be higher by four orders of magnitude than the corresponding values obtained in the absence of erosion by ocean bottom material, determined by tracer techniques.

A combination of three possible effects is responsible for the increased rate of metal deterioration in the seawater-bottom material erosion-corrosion system. The first is the increase in the surface area of the specimens (corrosion rates reported here are based upon geometric surface area). The surface profile of the specimens before and after exposure to the seawater-bottom material system is shown in Fig. 7. It can be seen that the surface profile is significantly rougher after exposure. The surface area effect was found to account for a factor-of-10 increase in the corrosion rate (see a and c in Table 3). The second effect is the removal of any corrosion-protective surface film from the specimen by the erosive action of the seawater-bottom material system.

This exposes a continuously fresh metal surface to the seawater; hence an increase in the corrosion rate would be expected. The third effect is the "wearing away" of the metal by physical abrasion by the seawater-bottom material system.

c. Gamma Radiation Effects Experiments

Fig. 8 shows the corrosion rate of Hastelloy C in aerated and deaerated seawater under a ^{60}Co radiation field of 2×10^5 rads/hr. Corrosion rates obtained after about 100 days for both the aerated and deaerated cases compare well with those obtained in the absence of radiation fields.

d. Hot Vapor Exposure Experiments

Table 4 includes corrosion rates of Haynes-25 and Hastelloy C in hot water vapor environment. The rates are between one and two orders of magnitude higher than the corresponding values under standard exposure conditions.

II.3.1.2 Corrosion Rates Determined by Electrochemical Techniques

Table 5 presents the normal and galvanic corrosion rates for the SNAP 21 materials in aerated and deaerated seawater. It should be noted that the galvanic corrosion rates listed in Table 5 were measured with unequal areas of anode and cathode. The effect of the surface area ratio is dependent upon the polarization behavior of the anodic and cathodic members of the galvanic couple.*

II.3.2 Fuel Solubility

a. Standard Series Experiments

The shaded area in Fig. 9 represents the range of dissolution rates of PuO_2 fuel in natural seawater obtained from a series of 5 experiments conducted at room temperature using 4-10 mg of fuel in each case. Included in the same figure are the dissolution rates at 5°C, in diluted seawater (1:1 distilled to seawater), in seawater solutions containing twice the normal concentrations of carbonate and sulphate and 1.2 times the normal amount of chloride anions. It is noted that in every case the initial dissolution rates decrease with time then level off.

The dissolution rates shown in Fig. 9 are expressed in terms of unit weight of PuO_2. Studies have also been made in which the dissolution rate has been expressed in terms of unit surface area of the microspheres. This rate is 3.7×10^{-4} $\mu g/mm^2/day$.

*For further discussion on this point refer to reference (16).

b. Solubility in Presence of Ocean-Bottom Material (14)

When varying amounts of ocean-bottom material were added to solutions of PuO_2 in seawater a very rapid initial absorption of the plutonium activity was observed, followed by a relatively less rapid approach to quantitative removal from the seawater (Table 6).

Results obtained in the second type experiments, where PuO_2 microspheres were added to seawater-ocean bottom mixtures (14), are shown in Fig. 10. The unexpected peak in the curve indicates that initially the rate of release of plutonium dioxide was greater than the rate of adsorption of the plutonium activity by the bottom material. After about 15 days the adsorption rate overtook the release rate and became greater until about 100 days when the two rates became approximately equal. The following is a qualitative interpretation of the shape of the curve.

At the start of the experiment, when the beads were on the surface of the bottom material, the release rate was greater than the adsorption rate and hence the net amount of plutonium activity released to the seawater kept increasing. During the initial period of 15 days the release rate gradually decreased due to settling of the beads into the bottom material (the density of plutonium dioxide is about three times that of the bottom material). Concurrently, the rate of adsorption gradually increased due to the chance for more efficient adsorption when the beads are buried in the bottom material. At about 15 days the rates of release and adsorption became equal. At this time the net amount of plutonium activity released to the seawater began to decrease. At longer times (> 100 days) the layer of bottom material at the seawater-bottom-material interface became saturated with the adsorbed plutonium activity and hence could not remove the activity from the seawater. An equilibrium situation was then established, the rates of release and adsorption being equal. The plutonium dioxide beads continued to release activity but this released activity was now being adsorbed by the inner bulk of the bottom material after diffusion of the activity through the surface.

The effectiveness of plutonium activity removal by the bottom material is emphasized by the fact that if the bottom material had not been present in this experiment, the total plutonium activity released (based upon the average room-temperature release rate of 4×10^{-3} $\mu g/mg/day^5$) after 160 days would have been 6.4×10^{-1} $\mu g/mg$ instead of 10^{-3} $\mu g/mg$ as indicated in Fig. 10.

It should be noted that in a true ocean situation the effectiveness of the bottom material in absorbing released activity will depend primarily on the contact time of the seawater containing the activity with the bottom material. The best situation with respect to most efficient adsorption of the released activity would be if the fuel beads were buried. If the beads were not buried, the released activity will diffuse away from the beads and have little contact time with the bottom material. Other factors such as current velocity and bottom terrain would further modify the degree of adsorption in the case of unburied beads.

c. High Temperature/Pressure Tests (15)

Fig. 11 shows the dissolution rate data as a function of exposure time at room temperature as well as at 120° and 190°C. It can be seen that the room temperature release rate has remained essentially constant at about 4×10^{-3} μg/mg/day up to 280 days of exposure.

The initial release rate at 190°C was about an order of magnitude above the average room temperature rate. After about 20 to 30 days of exposure at 190°C the rate abruptly decreased to about a factor of five below the average room temperature rate. After this sharp decrease the rate changed relatively slowly, decreasing from 1×10^{-3} to 5×10^{-4} μg/mg/day over a period of 140 days. After 90 days of rate measurements at 190°C the temperature of one of the duplicate samples was reduced to room temperature for all subsequent rate measurements. After this temperature change, the release rate initially decreased from 5×10^{-4} to about 1×10^{-4} μg/mg/day and then began to increase, ultimately approaching the average room temperature rate of 4×10^{-3} μg/mg/day.

As a tentative explanation of the dissolution behavior at 190°C it is suggested that the relatively insoluble salt which precipitated from the seawater during exposure, and which was identified by x-ray diffraction analysis as calcium sulfate, forms a coating on the plutonium dioxide beads. This coating acts as a diffusion barrier to the plutonium activity, thereby lowering the release rate. In the sample where the release rate was measured at room temperature following measurements at 190°C, the initial decrease at room temperature was due to the lower diffusion rate of the plutonium activity through the coating at room temperature. The subsequent increase in the release rate at room temperature was due to the slow dissolution of the calcium sulfate coating (calcium sulfate has a negative solubility temperature coefficient).

In contrast to the results at 190°C the release rate at 120°C decreased steadily and rapidly from a factor of two above the average room temperature rate to a relatively constant value of 1.5×10^{-4} μg/mg/day. Apparently, the mode of formation of the calcium sulfate coating is dependent on the temperature and/or pressure of the seawater. At 190°C the coating forms rather suddenly after a period of 3 to 4 weeks whereas at 120°C the coating begins to form immediately and continues to build up over a long time period.

The "peak" in the release rate curve of one of the samples exposed at 120°C is thought to be caused by a breaking up or fracturing of some of the plutonium dioxide beads. This would expose uncoated surfaces to the seawater and cause an initial increase in the release rate. As the calcium sulfate coating builds up on the fresh surfaces, the release rate would start to slow down and ultimately decrease to the value for a completely coated sample.

Indications of fracturing were observed during the retrieval of the plutonium dioxide beads from the calcium sulfate precipitate and seawater. Previous to the time when the release rate began to increase the retrieval process was fairly easy and could be performed quickly.

When the release rate began to increase the retrieval process became much more difficult because of the presence of extremely minute particles of plutonium dioxide. These particles were much smaller than the average bead diameter of approximately 150 microns. Since a large fraction of the beads comprising the sample were irregular in shape, it is not unreasonable to expect small fragments to break off from some of the more irregular beads.

It is obvious that the increase in rate cannot be entirely due to an increase in fresh surface area. It may be that these fresh surfaces, caused by the postulated fracturing, have a larger inherent release rate than that of the normal outside surface.

III. IN SITU OCEAN TESTS

III.1 Test Facility

The NRDL test facility at San Clemente Island (SCI) consists of two primary parts, the underwater test rig and the shore control station. The general configuration of the underwater test rig is shown in Fig. 12.

The island is one of the Channel Islands and the waters surrounding it are typical of the group as a whole. The island is oriented geographically to form a protected shore on its east side. The water there is clear and smooth, being sheltered from both the prevailing summer sea and swell as well as storm-generated sea conditions during the winter months. Because it is located in close proximity to the southern California coast, the entire island environment has come under study, particularly from the standpoint of meteorology and oceanography.

III.2 Tests in Progress

On-going tests at SCI include heated capsules and mockups designed to investigate the true ocean environmental behavior of the encapsulant and other SNAP materials. SNAP fuels are also under examination in specially designed exposure chambers. A summary of the tests in progress follows.

III.2.1 SNAP Materials

III.2.1.1 SNAP 19 (17)

Five electrically heated capsules instrumented with thermocouples and pressure transducers have been under water for the past 15 months. Table 7 lists their locations and their current temperatures and internal pressures.

III.2.1.2 SNAP 21 (18)

a. Electrically heated capsules: Four electrically heated capsules have been under water for the past 9 months. Their locations are as follows: 50 ft below water surface (130 ft water), 10 ft above the bottom, on the bottom and buried under 3" of ocean bottom. A schematic diagram of an electrically heated SNAP 21 capsule is shown in Fig. 13.

b. Electrically heated mockups: An electrically heated mockup designed to examine the galvanic behavior of the 21 materials is under test. A diagram of the mockup is presented in Fig. 14. A similar test mockup to determine the extent of marine fouling is also under test.

c. Radioisotope-loaded capsules (19): Two fully-fueled SNAP 21 capsules will be very shortly implanted in the ocean at the test site. The exposure system will be composed of the following functional components: 1) an exposure shield chamber, 2) a seawater circulation system, and 3) a monitoring and control apparatus.

In operation, the exposure shield, Fig. 15, is suspended from a buoy at a depth of 75 feet in water 130 feet deep. Seawater flows into the exposure shield chamber from the bottom port, passes over the test specimen maintaining it at a relatively low temperature, and passes out through the top port. The exposure shield chamber is designed to be watertight if the inlet and outlet ports are sealed. Temperature sensors are provided to measure water temperature in the exposure shield chamber at the inlet and outlet ports and at two locations near the test specimen. The test specimen is held in place by alumina standoff pieces which are attached to lugs provided on the inner cylinder wall and the inside surface of the top cap. These standoff pieces provide electrical insulation of the test specimen from the exposure shield chamber and so minimize the possibility of galvanic coupling with the chamber materials.

III.2.1.3 On-Going and Post-Ocean Exposure Evaluations of SNAP Materials

It should be noted that in situ ocean exposure tests are qualitative in nature. However, valuable information regarding the long-term behavior of the test systems in their true environment are being obtained by means of visual observation (i.e. underwater photography) and temperature and pressure data collection. Post-ocean exposure evaluation will be achieved by detailed visual and photographic examination, dimension and surface roughness measurements, helium pressurization and leak testing, liquid dye penetrant inspection, eddy current testing, and radiographic and ultrasonic examinations. Correlation between laboratory predictions and in situ results are expected to be very helpful in assessing the performance of current as well as projected SNAP capsules and other components in the ocean environment.

III.2.2 SNAP Fuels (20)

III.2.2.1 Plutonium Dioxide Tests

A current program involves exposure of uncontained $^{238}PuO_2$ fuel to the ocean. In this test, an exposure chamber located on the ocean floor contains the plutonium dioxide fuel and ocean-bottom material; a water circulation system maintains the interior of the exposure chamber in equilibrium with continuously refreshed ocean-bottom water. The same circulation system provides pumping of effluent water from the exposure chamber to a shore station for radioactivity monitoring.

Fig. 16 shows a sketch of the exposure chamber. Ocean-bottom material was taken from a pre-selected ocean-bottom location for the test (six inch depth) and placed in the lower section of the exposure chamber. Plutonium dioxide microspheres (4.18 mg ≡ 238 microspheres) were placed on the surface of the bottom material at the center of the exposure chamber. After placement of the microspheres, the top section of the exposure chamber was bolted on and the chamber lowered into the ocean to a depth of 50 ft. The influx of fresh ocean-bottom water into the exposure chamber was such that there was a complete change of water volume every 1.7 min. The average ambient water temperature was approximately 15°C.

A total of four exposure chambers have been placed on the ocean-bottom. The first chamber was recovered after a period of approximately 5 months (140 days). The other three chambers will be recovered at later dates.

After recovery over a third of the fuel beads were retrieved by isolation from large amounts (about 50 liters) of ocean-bottom material. A combination of microscopic examination and radioactivity detection by a probe was necessary during the final stages of the isolation process. Several post-exposure tests were run on both the microspheres and the surrounding material. The most important results can be summarized as follows:

a. About 70% of the recovered PuO_2 microspheres were encrusted with marine organisms. Fig. 17 shows photomicrographs of two of them.

b. Microscopic examination of several of the encrusted microspheres revealed the following (21):

1. Numerous small diatoms were adherent to the uniformly smooth surface of the Pu^{238} sphere. The aggregates were composed of sand grains (quartz or silica) and organic detritus, which was lightly cemented around the microsphere by a dense matrix of mucilage and small diatoms. Areas of the broken aggregate most densely populated by the diatoms appeared yellow-brown in color, due most likely to a characteristic organic pigment manufactured by these cells.

2. The predominant organism present was tentatively identified as Nilzschia sps. This is a relatively small cell measuring 2-10 μ and it is motile when not existing in colonial or epiphytic form. It is widely distributed, occurring most frequently as a dense mat. The cells were connected in various patterns by means of a mucilaginous secretion.

3. Appearing in the layer aggregates were several centric diatoms, measuring 24-40 μ. These were circular in form, with radial markings. A few elongate, pennate cells were also observed and identified as Navicula sps. Occurring in one preparation were 2 clusters of elongate, tapering, tube structures, yellow-brown in color, estimated to be 200 μ in length. These were of biological origin, and probably represented a colonial coelenterate or a bryozoan.

4. Bacteria were present in all preparations, and in at least two of the sedimentary aggregates, small unicells were present, 2-5 μ in size. The unicells were definitely yellow-green in color and showed active mobility by means of a single flagellum. These latter forms may be the unicellular chlorophyte, Nannochloris sps., but positive identification could not be made at this time.

5. There seems to be little question that the Pu^{238} particle had been surrounded by an organic layer, which seems to have cemented sand grains to its surface. However, it is not clear from these preliminary observations that most of the organisms found are typically found in sediment. Centric diatoms for example are usually found in upper water layers.

6. An examination of the photomicrograph showing a gastropod shell (Fig. 17b) with a similar aggregate attached to it indicated this was adventitious: The shell had many small holes bored through it, clearly showing that its host had long since died.

c. Post-exposure dissolution rates, determined for both clean and encrusted microspheres, were less than pre-exposure rates. Table 8 presents the results obtained. The release rate for the clean microspheres is slightly less than that of the control sample while the rate for the encrusted microspheres is about a factor-of-two less.

d. Results of crush strength tests (22) on recovered microspheres were inconclusive due to the absence of a statistically satisfactory number of samples.

III.2.2.2 Other Fuels

Future plans call for in situ testing of other fuels. Strontium titanate is expected to have the first priority.

REFERENCES

1. F. L. LaQue and W. C. Stewart, Some Methods for Studying the Behavior of Alloys in Seawater at High Velocity, Meteaux et Corrosion, 23 No. 274, 1948, p. 147.

2. D. A. Kubose, et al., Measurement of Seawater Corrosion of SNAP Container Alloys Using Radioactive Tracer Techniques, U. S. Naval Radiological Defense Laboratory, USNRDL-TR-1092, 10 October 1966.

3. D. A. Kubose, Basic Test Plan for Laboratory Corrosion Testing of SNAP-21 Materials, U. S. Naval Radiological Defense Laboratory, USNRDL-LR-67-9, 10 March 1967.

4. D. A. Kubose, et al., Seawater Corrosion Studies of Emissively Coated Haynes-25: Radioactive Tracer Techniques, U. S. Naval Radiological Defense Laboratory, USNRDL-TR-67-109, 19 August 1967.

5. H. I. Cordova and D. A. Kubose, Erosion-Corrosion of Haynes-25 Alloy: Radioactive Tracer Techniques, U. S. Naval Radiological Defense Laboratory, USNRDL-TR-67-142, 21 August 1967.

6. H. A. Goya, et al., SNAP Fuels and Capsule Materials: A Compendium of USNRDL Laboratory Procedures for Their Study, U. S. Naval Radiological Defense Laboratory, USNRDL-TR-68-55, 16 February 1968.

7. K. O. Emery, The Sea Off Southern California, New York, Johy Wiley and Sons, Inc., 1960.

8. D. A. Kubose and H. I. Cordova, Electrochemical Corrosion Studies of SNAP Container Materials, U. S. Naval Radiological Defense Laboratory, USNRDL-TR-1036, 7 June 1966.

9. D. A. Kubose and H. I. Cordova, Corrosion Studies of Haynes-25 Alloy in Seawater Using Electrochemical Techniques, U. S. Naval Radiological Defense Laboratory, USNRDL-TR-67-64, 16 May 1967.

10. See, for example, M. G. Fontana and N. D. Greene, Corrosion Engineering, New York, McGraw Hill Book Company, 1967, Chapters 9 and 10.

11. M. Stern and A. L. Geary, Electrochemical Polarization. A Theoretical Analysis of the Shape of Polarization Curves, J. Electrochem. Soc., 104, 1957, p. 56.

12. M. Stern, A Method for Determining Corrosion Rates from Linear Polarization Data, Corrosion 14, 1958, p. 440.

13. N. D. Greene, Experimental Electrode Kinetics, Troy, New York, Rensselaer Polytechnic Institute, 1965, p. 31.

14. D. A. Kubose, et al., Radioactivity Release from Radionuclide Power Sources. VI. Release from Plutonium Dioxide to Seawater in the Presence of Ocean-Bottom Material, U. S. Naval Radiological Defense Laboratory, USNRDL-TR-67-71, 31 May 1967.

15. D. A. Kubose, et al., Radioactivity Release from Radionuclide Power Sources. V. Release from Plutonium Dioxide to Seawater at High Temperatures and Pressures, U. S. Naval Radiological Defense Laboratory, USNRDL-TR-67-32, 27 March 1967.

16. D. A. Kubose and H. I. Cordova, Electrochemical Corrosion Studies of Galvanically Coupled SNAP-21 Materials, U. S. Naval Radiological Defense Laboratory, USNRDL-TR-68-26, 15 January 1968.

17. J. L. Mackin, et al., Basic Test Plan for Ocean Corrosion Studies of SNAP-19 Test Specimens, U. S. Naval Radiological Defense Laboratory, USNRDL-LR-164, 10 February 1966.

18. L. W. Weisbecker, SNAP-21 Safety Test Program: Basic Test Plan for Ocean Exposure Studies of SNAP-21 Electrically Heated Fuel Capsule Test Systems, U. S. Naval Radiological Defense Laboratory, USNRDL-TRC-67-15, March 1967.

19. L. W. Weisbecker and S. Z. Mikhail, SNAP Environmental Test and Radiological Effects Program: Basic Test Plan for Ocean Exposure Studies of SNAP-21 Radioisotope-Loaded Fuel Capsule, U. S. Naval Radiological Defense Laboratory, USNRDL-LR-67-96, 27 November 1967.

20. D. A. Kubose, et al., Radioactivity Release from Radionuclide Power Sources. VIIa. Dissolution Studies of Plutonium Dioxide in the Ocean-5-Months Exposure, U. S. Naval Radiological Defense Laboratory, USNRDL-TR-68-74, 16 April 1968.

21. Private Communication, Dr. B. E. Vaughan, USNRDL, Sept. 1967.

22. Private Communication from Mound Laboratory; Inter-Office Correspondence from Gary N. Huffman to Dr. Richard E. Vallee, 8 Feb. 1968.

Table 1. Comparison of Corrosion Rates of Haynes 25 Based on Cobalt and Chromium Analyses

	mpy (based on Co)	mpy (based on Cr)	Exposure Time Days*
Haynes 25 #1	3.4×10^{-5}	1.8×10^{-5}	7
Haynes 25 #2	1.4×10^{-5}	9.7×10^{-6}	7
Haynes 25 #1	1.1×10^{-5}	9.2×10^{-6}	22
Haynes 25 #2	9.2×10^{-6}	5.9×10^{-6}	22

*Seawater sampled and changed at end of 7 days followed by additional exposure period of 15 days.

Table 2. Corrosion Rate Data for Uncoated, Half- and Completely Emissively Coated Haynes 25 After 160 Days Immersion in Seawater

Specimen	Exposure Parameter	Corrosion Rate (mpy)
uncoated	aerated	3.4×10^{-6}
uncoated	deaerated	2.8×10^{-6}
uncoated	aerated, stirred	4.6×10^{-6}
half-coated	aerated	9.1×10^{-5}
half-coated	deaerated	7.6×10^{-5}
half-coated	aerated, stirred	9.1×10^{-4}
completely coated	aerated	3.0×10^{-4}
completely coated	deaerated	0.51×10^{-4}
completely coated	aerated, stirred	1.4×10^{-4}

Table 3. Comparison of Haynes-25 Corrosion Rates in Seawater

Exposure Conditions	Method	Corrosion Rate (mpy)	Reference
6°C	Radioactive tracer	1×10^{-6}	2
6°C	Radioactive tracer	3×10^{-6}	4
a. Room temperature, seawater washing over specimen	Radioactive tracer	4×10^{-6}	5
b. Room temperature, seawater and bottom material washing over specimen	Radioactive tracer	1×10^{-2}	5
c. Room temperature, seawater washing over specimen which had previously been exposed to both seawater and bottom material washing over specimen	Radioactive tracer	4×10^{-5}	5

Table 4. Corrosion Rates of Haynes 25 and Hastelloy C in a Hot Seawater Vapor Environment

Corrosion Rate (mpy)		Total Exposure Time
Haynes 25	Hastelloy C	(days)
9.2×10^{-5}	6.1×10^{-4}	14
1.5×10^{-4}	3.8×10^{-4}	29
*	4.3×10^{-4}	46
3.5×10^{-5}	-	76
5.8×10^{-5}	-	117
-	-	153
1.8×10^{-4}	7.3×10^{-4}	200

*Indicates lost sample

Table 5. Normal and Galvanic Corrosion Rate of SNAP 21 Materials in Seawater

Material	Seawater Condition	Normal Corrosion Rate (mpy)	Corrosion Galvanic Effect* (mpy)
Al	A	9.6×10^{-2}	1.1×10^{2}
Al	D	3.1×10^{-2}	1.1
Cu	A	2.9	1.4
Cu	D	8.3×10^{-2}	9.7×10^{-2}
Hastelloy C	A	4.3×10^{-3}	3.8×10^{-1}
Hastelloy C	D	4.2×10^{-4}	8.0×10^{-5}
Hastelloy X	A	8.0×10^{-3}	
Hastelloy X	D	4.0×10^{-4}	
Nickel	A	9.8×10^{-3}	2.8×10^{-3}
Nickel	D	2.2×10^{-3}	1.6×10^{-4}
304ss	A	2.3×10^{-3}	5.7×10^{-1}
304ss	D	4.0×10^{-3}	1.9×10^{-5}
Ta	A	9.6×10^{-4}	6.2×10^{-3}
Ta	D	4.8×10^{-3}	1.6×10^{-4}
Ti 621	A	7.5×10^{-4}	5.0×10^{-4}
Ti 621	D	7.1×10^{-3}	2.0×10^{-4}
U-8 % Mo	A	1.2	7.7
U-8 % Mo	D	6.8×10^{-1}	6.4×10^{-3}

*Measured with unequal areas of anode and cathode - see text.

Table 6. Adsorption of Plutonium Activity by Ocean-Bottom Material

	PLUTONIUM ACTIVITY ADSORBED (%)			
	Weight of Bottom Material (gm/20 ml seawater)			
Time (days)	0	0.16	1.11	5.26
0.15	0	8.7	35.1	68.3
1.0	0	48.6	83.7	96.3
3.0	0	84.0	98.0	99.8
7.0	0	97.1	99.5	100
17.0	0	99.5	100	100

Table 7. Electrically Heated Capsule Test Data

Unit Number	Location	Conditions
1	At 50 feet depth	Temperature: $180^{\circ}F \pm 2^{\circ}F$ Pressure: Unchanged
2	At 125 feet depth	Temperature: $200^{\circ}F \pm 2^{\circ}F$ Pressure: Unchanged
3	Buried in ocean bottom at 130 feet water depth	Temperature: $360^{\circ}F \pm 4^{\circ}F$ Pressure: Unchanged
4	On the ocean bottom at 130 feet water depth	Temperature: $320^{\circ}F \pm 3^{\circ}F$ Pressure: Unchanged
5	Inter-tidal zone	Temperature: Sinusoidal pattern maximum $600^{\circ}F + 6^{\circ}F$ minimum $150^{\circ}F \pm 2^{\circ}F$ Pressure: Sinusoidal due to temperature variation but maximum and minimum values have not changed

Table 8. Dissolution Rate of Clean and Encrusted Microspheres

	Dissolution Rate - 10^{-3} µg/mg/day							
Sample	0-20d*	20-60d	60-100d	100-140d	140-160d	160-200d	200-240d	240-280d
Control	1.33	1.35	1.35	1.48	1.60	1.60	1.60	1.60
Clean	——— in ocean ———				1.20	1.30	1.33	1.43
Encrusted	——— in ocean ———				0.48	0.61	0.65	0.76

*d = days

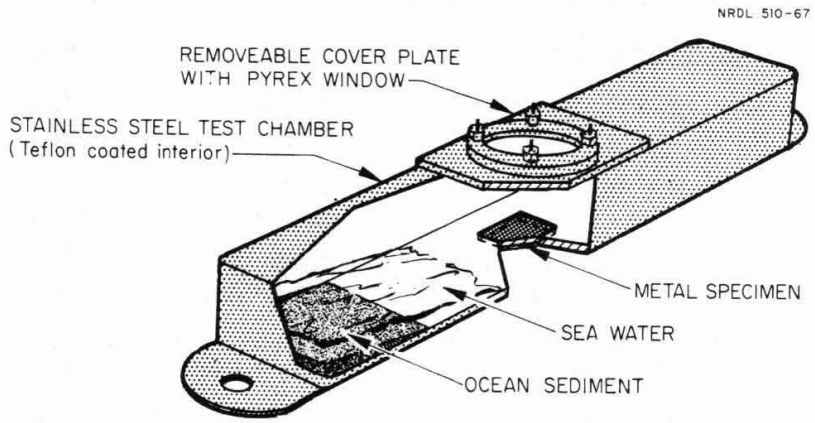

Fig. 1. Exposure Chamber for Erosion-Corrosion Experiments

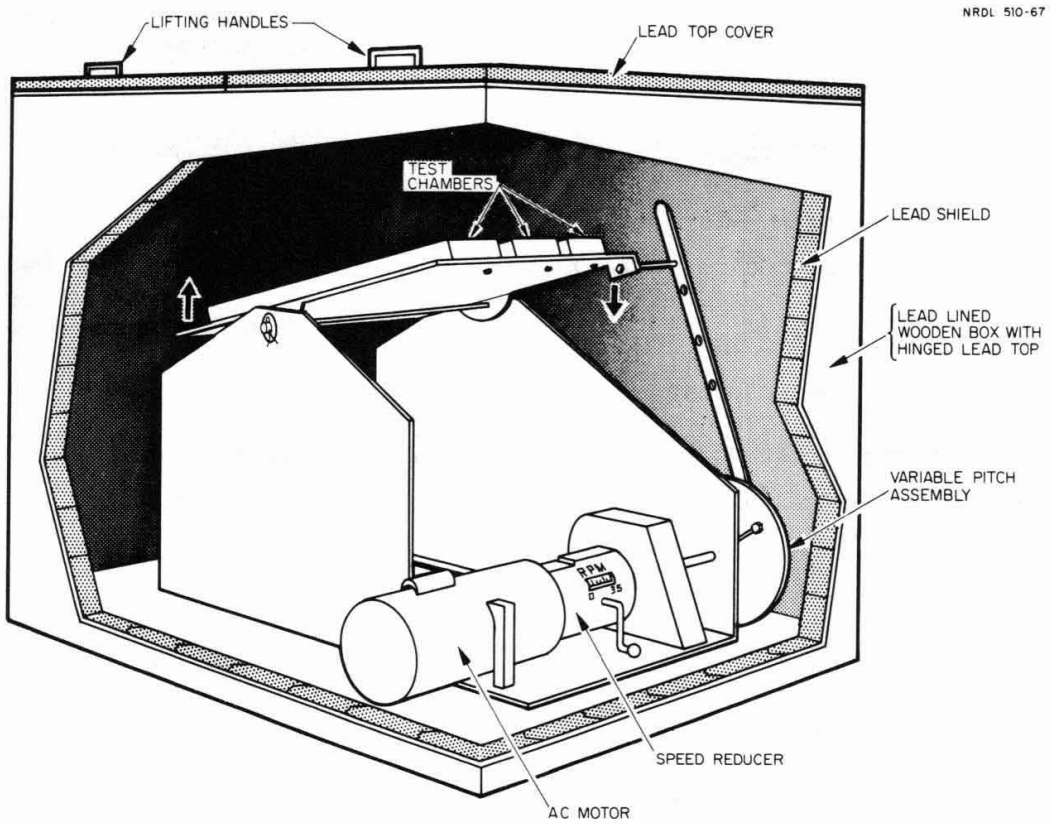

Fig. 2. Erosion-Corrosion Exposure Apparatus

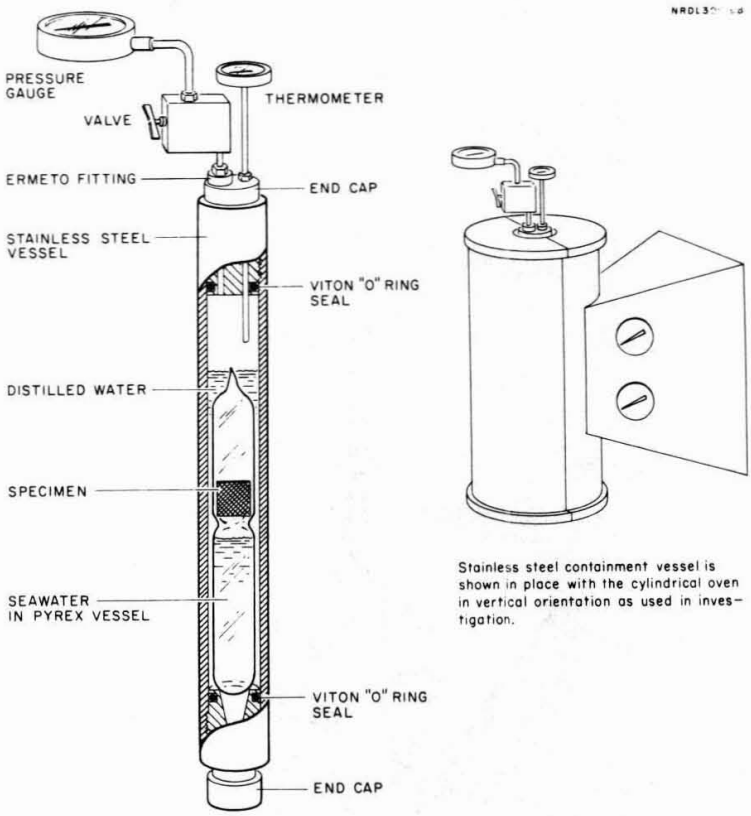

Fig. 3. Hot Seawater Vapor Exposure Apparatus

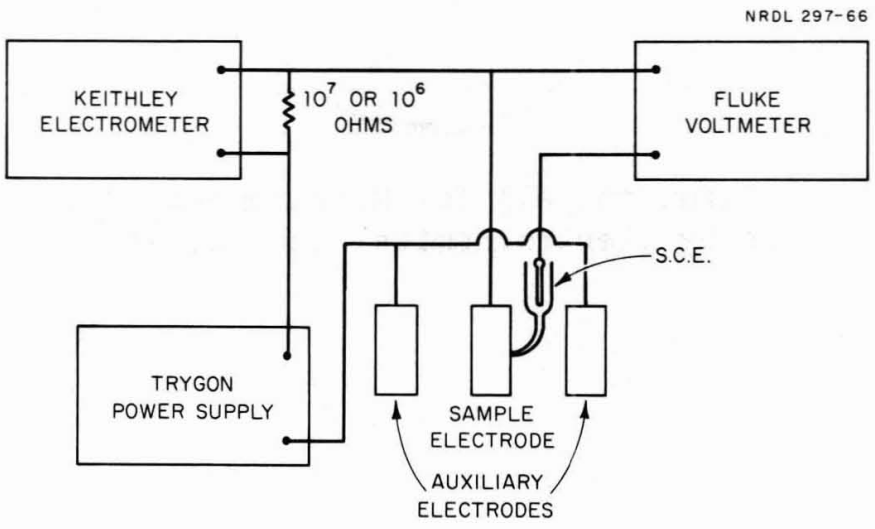

Fig. 4. Diagram of the Galvanostatic Polarization Circuit

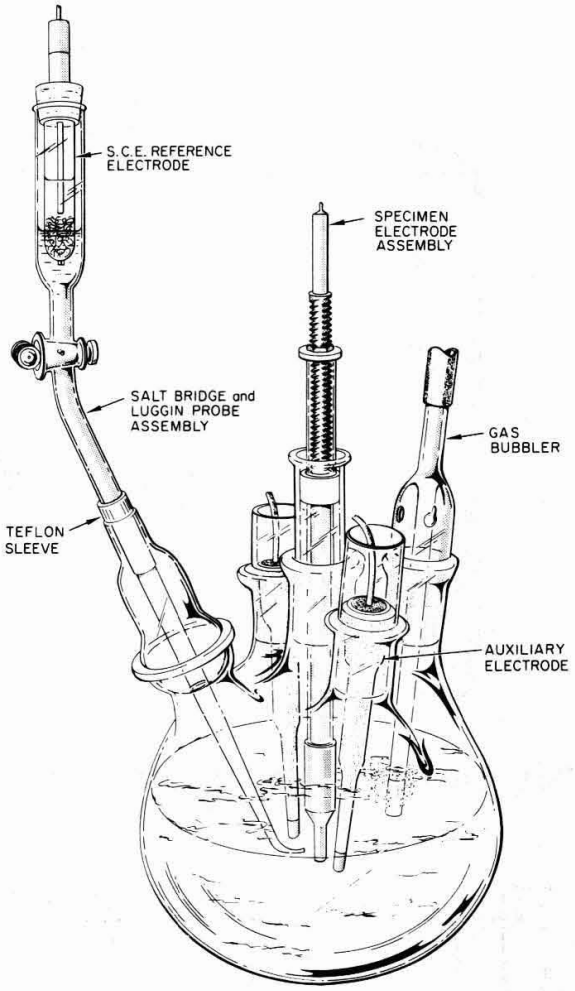

Fig. 5. Polarization Cell for Measurement of Corrosion Rates by Electrochemical Techniques

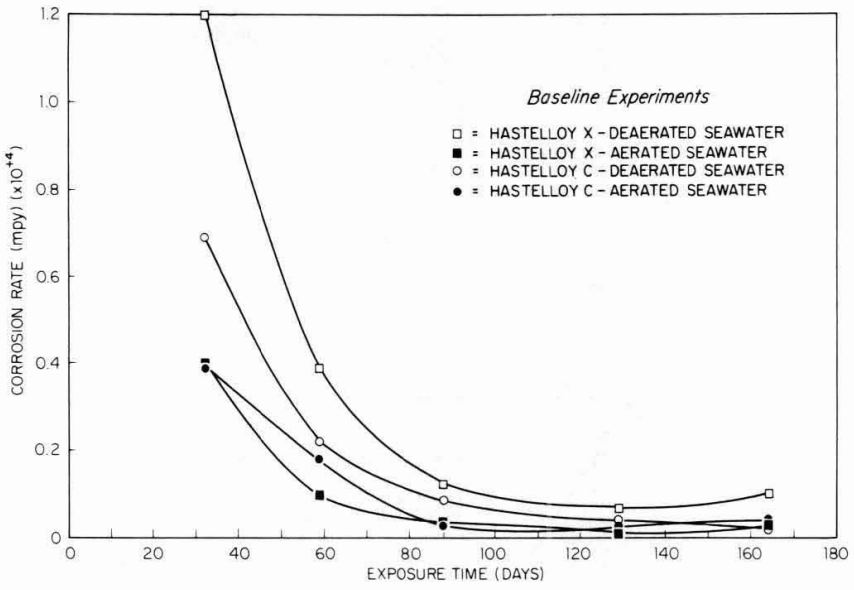

Fig. 6. Corrosion Rates of Hastelloy X and Hastelloy C at Room Temperature (Determined by tracer techniques)

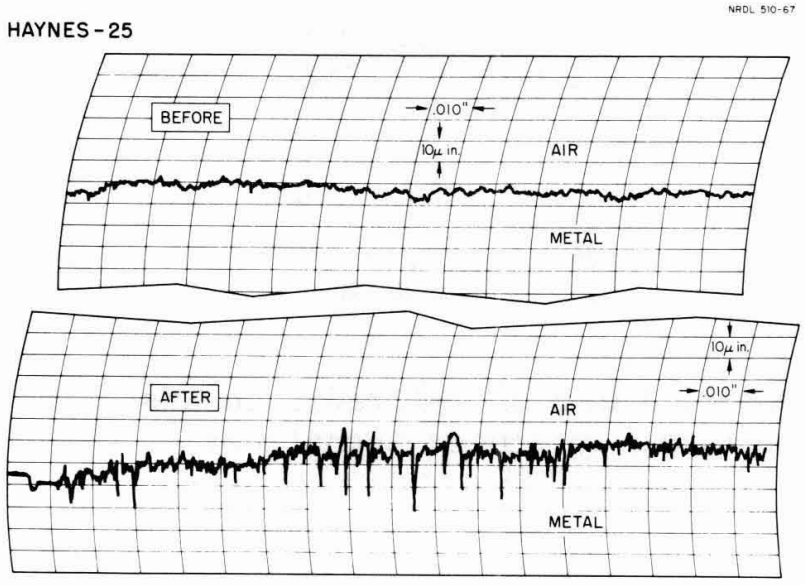

Fig. 7. Surface Profiles of a Haynes-25 Sample Before and After an Erosion-Corrosion Experiment

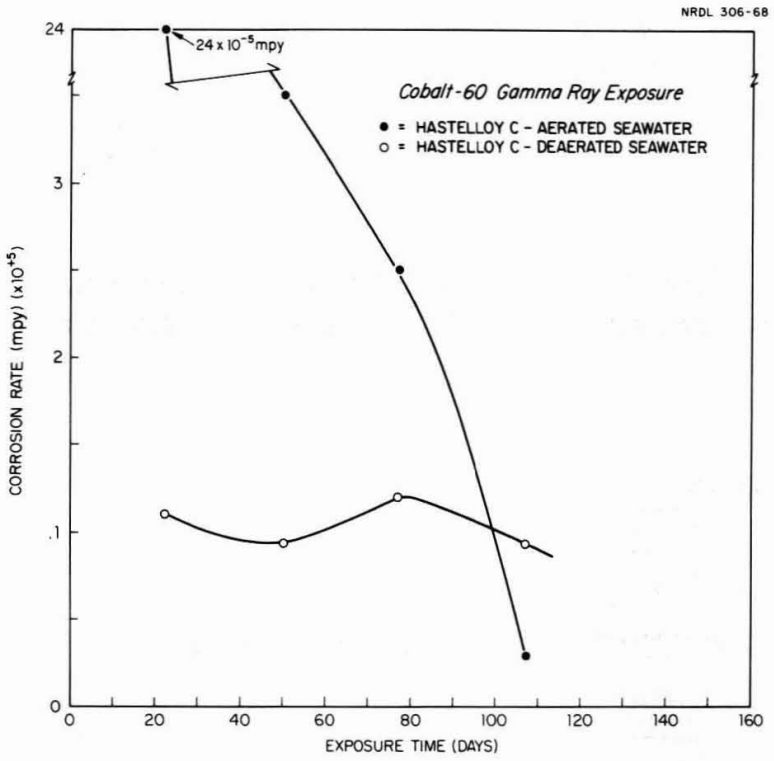

Fig. 8. Corrosion Rates of γ-Irradiated Hastelloy C (Determined by tracer techniques)

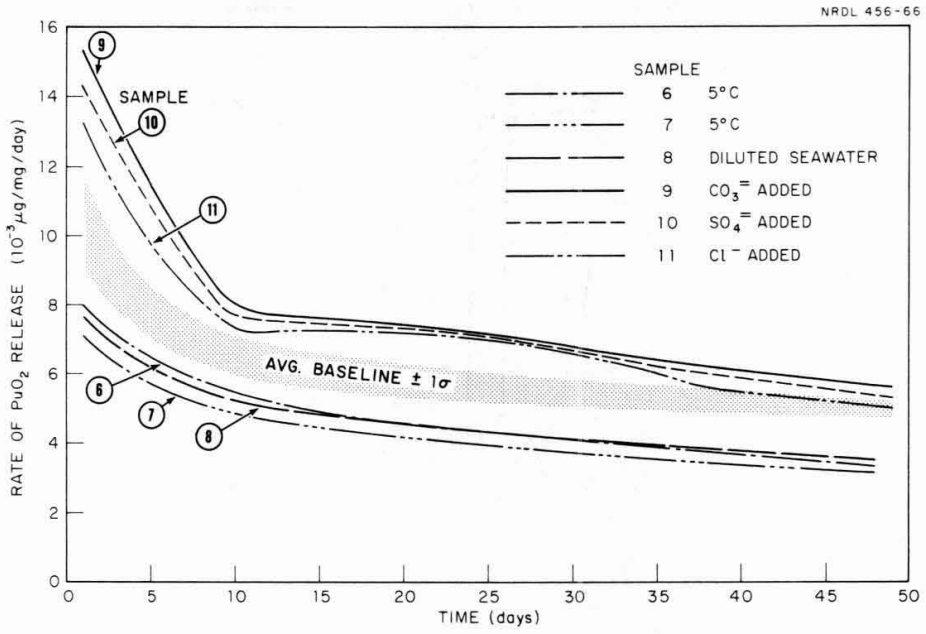

Fig. 9. Dissolution Rate of Multibead PuO_2 Samples in Seawater under Various Applied Conditions

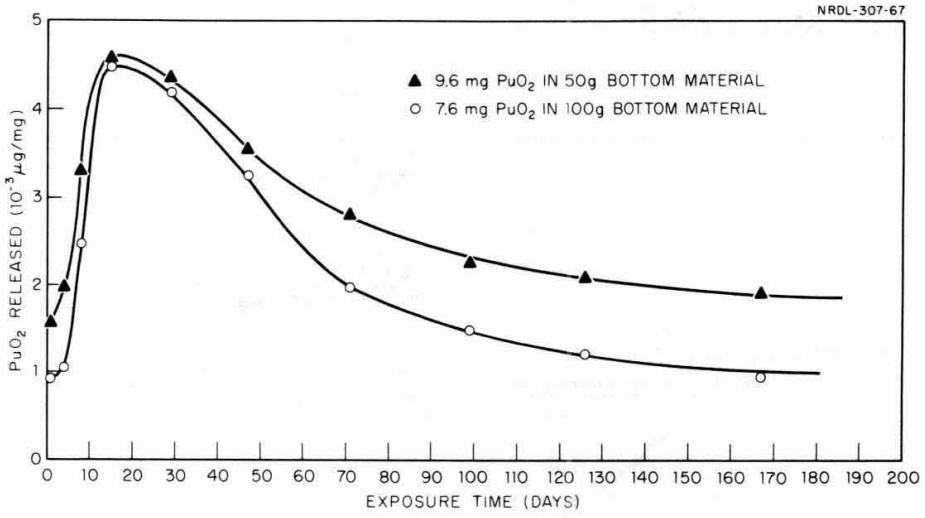

Fig. 10. Total Amount of Plutonium Dioxide Released to Seawater in the Precence of Ocean-Bottom Material as a Function of Time

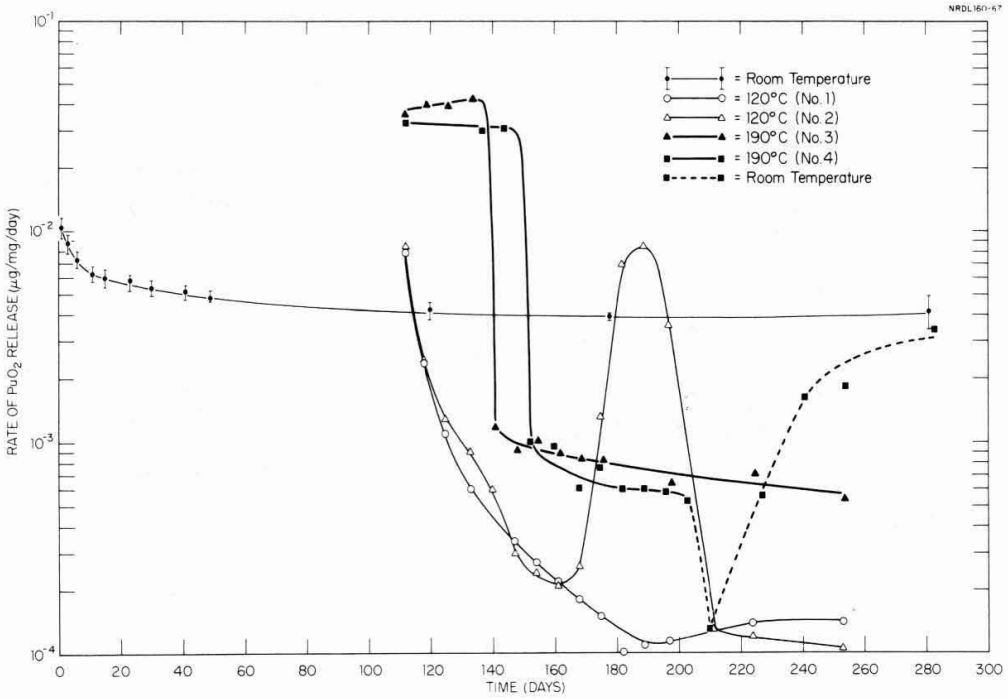

Fig. 11. Solubility Rate of Plutonium Dioxide in Seawater as a Function of Exposure Time at Room Temperature, 120 and 190°C

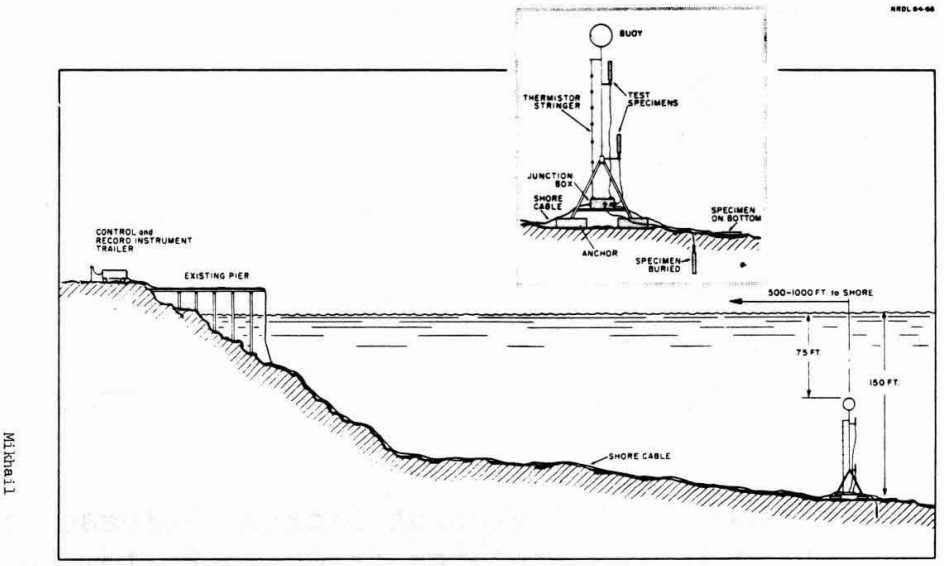

Fig. 12. A Schematic Diagram of the Underwater Test Facility at San Clemente Island

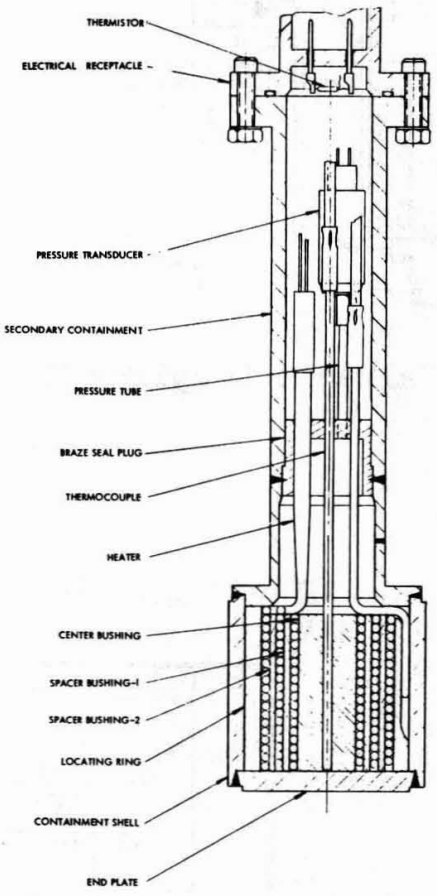

Fig. 13. Electrically Heated SNAP-21 Test Capsule

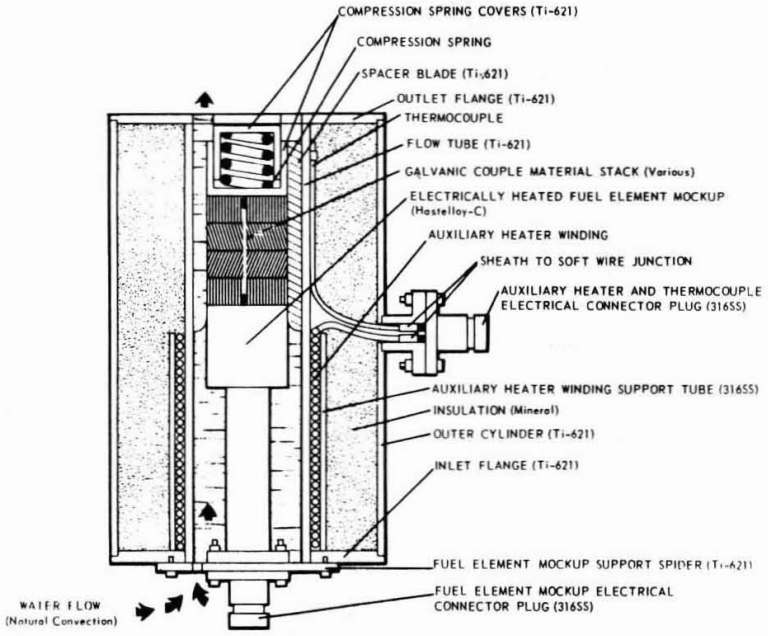

Fig. 14. Galvanic Coupling Mockup

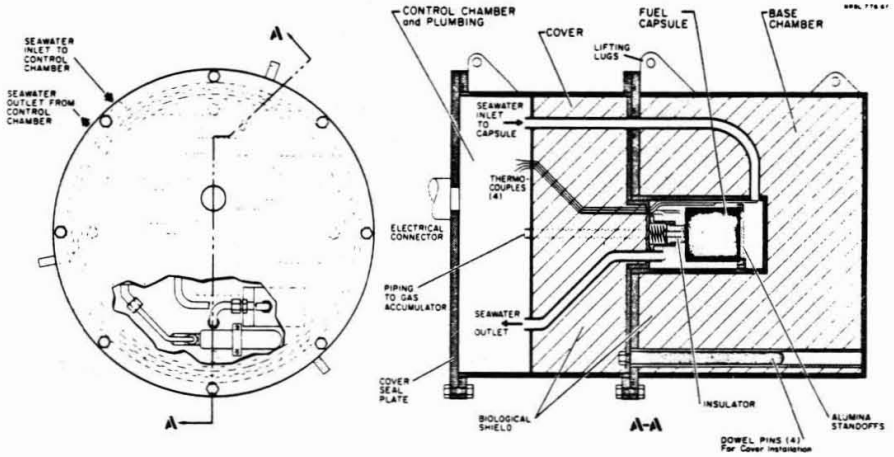

Fig. 15. Schematic Diagram of Exposure Shield Chamber Concept

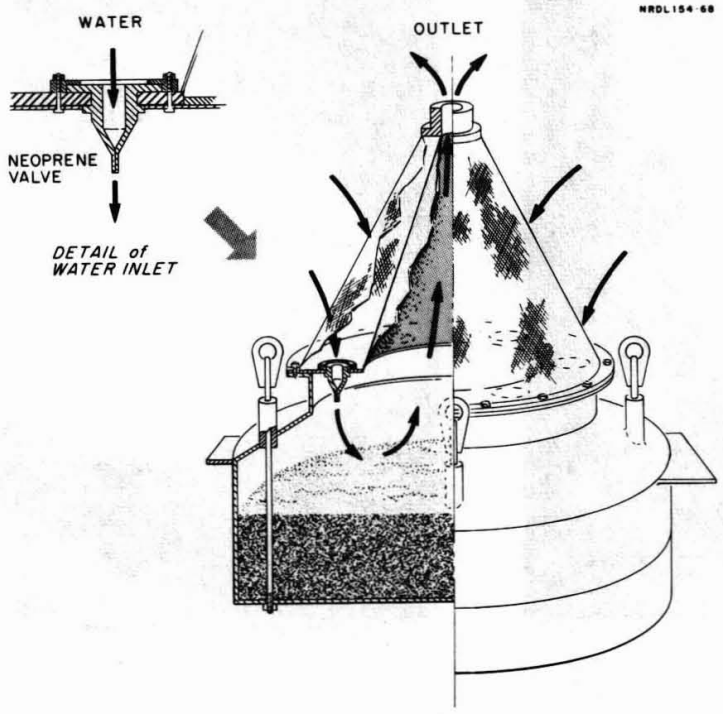

Fig. 16. $^{238}PuO_2$ Fuel Exposure Chamber

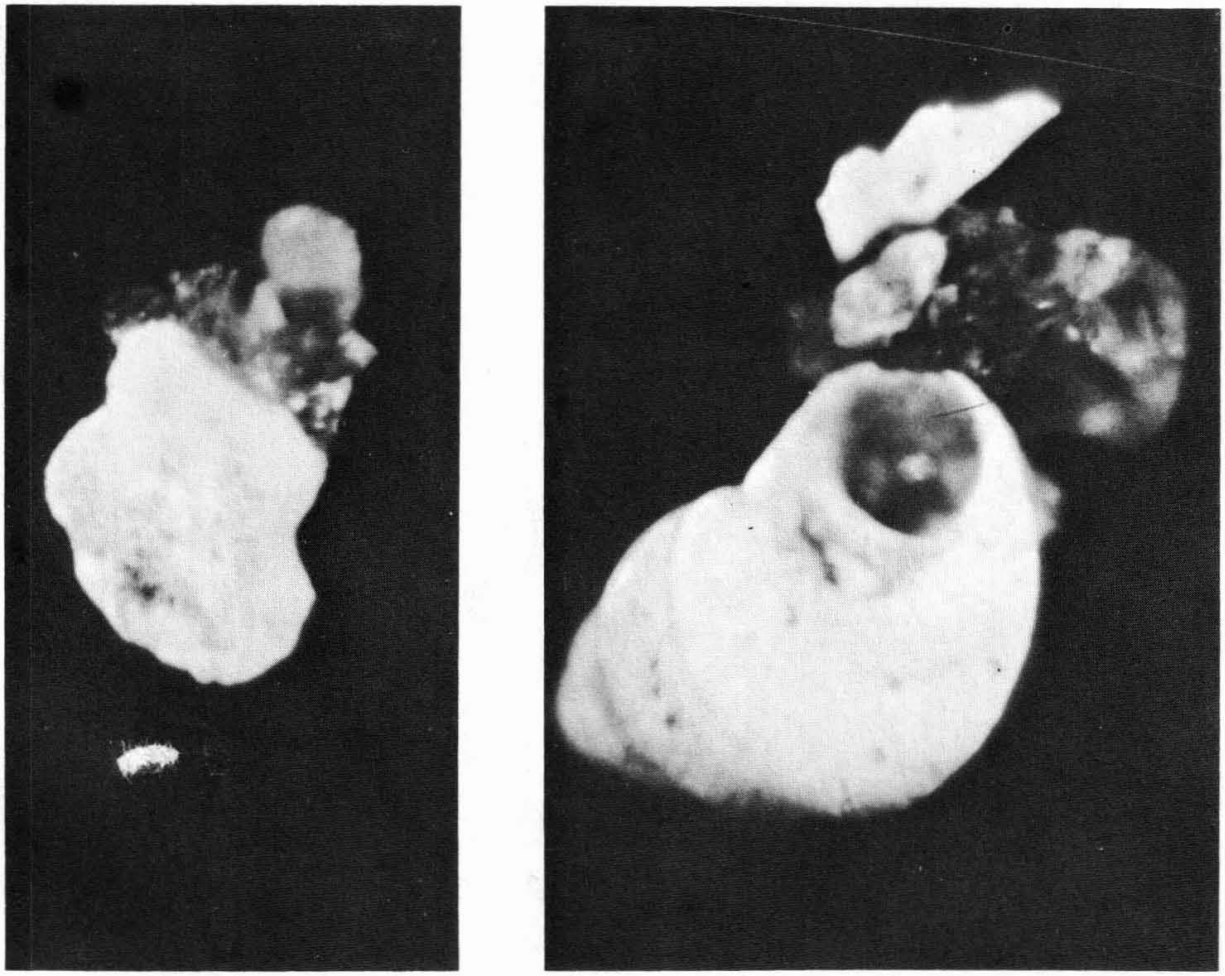

(a) (b)

Fig. 17. Photomicrograph of Some Encrusted Microspheres